UNIVERSITY
of
GLASGOW

Structural behaviour and design of adhesive bonded thick adherends steel beams in bending

Danny Loke Kah Lei, B. Eng

Submitted in fulfilment of the requirements for the degree of Doctor of Philosophy at

the University of Glasgow

Feb 2007

DEPARTMENT OF MECHANICAL ENGINEERING

University of Glasgow

Glasgow G12 8QQ

ABSTRACT

There is an increasing potential for the use structural epoxy adhesives in steel fabrications, especially where thermal distortion from fusion welding causes production difficulties. Applications may include grillage panels for ships and similar construction, especially where stiffeners are welded to relatively thin plating, using fillet joints. Substituting welding with adhesive bonding requires designers to have a good knowledge of bonded beams in term of their structural behaviours under lateral loadings and in comparison to equivalent welded beams. The bending shear in bonded beams causes large strains in the adhesives bondline, which could result in increased stresses and deflection. This research aims to provide a fundamental design guide to determine levels of stresses and deflection of such beams.

This developmental research programme was largely experimental work, which was supported by numerical and analytical methodologies. Large number of small-scale stiffened beam models were designed and manufactured to represent beams with plate stiffener connections; both welded (solid) and bonded. The stiffeners include various profiles, such as T, L, Z, flat beam and inverted T sections with various spans. The models were tested under monotonic loading in a simply supported boundary condition, within both elastic and plastic limits. In addition, the variation of adhesive bondline thickness was also considered to study its effect on bonded beam behaviour. The thesis presents the methodology for evaluating and comparing these models. Besides the mechanical testing; analytical methods based on beam and sandwich theory and finite element techniques were used.

The research work shows that

(i) Bonded beams behave quite differently to the solid/welded beams in terms of stresses and deflection. When compared to solid beams, bonded beams tend to exhibit higher bending stresses and deflections

(ii) Different beam sections were compared and evaluated in the research, and it was found that a bonded T section being most suitable to resist bending.

(iii) An elastic-plastic experimentation was necessary to demonstrate failure of the bonded beams under high bending loads. The bending behaviour of the bonded beam under gross deformation was analysed

(iv) The effect of varying the adhesive thickness reflected through interface coefficients may be extended to full scale bonded panel analysis through suitable techniques allowing the behaviour extrapolation to the real scale.

CONTENTS

LIST OF FIGURES

LIST OF TABLES

NOMENCLATURE

a^b: thickness of test piece

b: width of beam / test specimen

c: adhesive thickness

D: structural rigidity

d: distance from neutral axis from section centroids

G: shear modulus of elasticity

E: young's modulus

E_f: modulus of elasticity of adherends

E_a: modulus of elasticity of adhesive

L_c parallel length of test specimen

L_o gauge length of test specimen

M bending moment

P: three point bending load

Q: first moment of area

S: shear stress in the adhesive

τ: transverse shear stress in beam

σ^0: residual stress at origin

σ^*: ultimate stress in material

σ_n: bending/tensile stress in the

ε^0: residual strain at origin

ε^*: ultimate strain in material

V^*: transverse shear force

ν: poisson's ratio

w_1: deflection in beam (adherend)

w_2: deflection in beam (adhesive)

w_{TOT}: total deflection in beam

ACKNOWLEDGEMENTS

The author would like express his most sincere gratitude Dr Safa Hashim of the Department of Mechanical Engineering for his active supervision and endless encouragement throughout the study. I would also like to thank the technicians, Alex Torry, Denis Kerns, Alan Birbeck and John Davidson for their assistance in the experimental work.

The work was supported in funding by the ORS award by UK Universities. Such support is gratefully acknowledged.

Finally, the author wishes to thank his wife Mavis Choong and parents Larry & Christine Loke for their constant support and encouragement throughout this study.

CHAPTER ONE

INTRODUCTION

It is only in recent years that engineers have become practically interested in adhesive bonding for structural joints as an alternative to more traditional methods of attachment. Particular interest in the bonding of metals has been steadily growing ever since the gluing of load-bearing parts in metal aircraft was introduced 65 years ago. The bonding process was used initially in the bonding of name plates and or be used in conjunction with decorative surfaces in non-critical aerospace applications. Nowadays adhesive bonding has grown to include fabrication of primary aerospace structural components without mechanical fasteners. The successful development in aerospace has inspired the use of structural adhesives in marine industries. There is a potential in structural adhesives to replace or used in conjunction with traditional joining techniques such as welding, riveting and bolting, which are normally the primary joining process for ship structures. The lack of research in adhesive applications in the fabrication of thick steel structures using adhesives was the motivation of the study.

Structural adhesives produces bonds capable of bearing an appreciable and sustained load for the period of service, without significant creep or other loss of performance. These bonds are likely to be comparatively rigid, though not necessarily to the point of becoming completely hard and brittle. The performance of structural adhesives has progressed to such a point that it is possible to consider the opportunity of novel constructions or a different structural topology for structures used in the demanding marine and offshore environment. Research in structural adhesives focused mainly on the development of new bonded constructions used in various industries. Glasgow Marine Technology Centre itself has over fifteen years research experience in adhesive bonding for marine structural applications and has demonstrated the distinct practical applications and benefits which structural adhesives can offer.

The aerospace industry uses structural adhesives to a great advantage in the construction of many components. Figure 1.1 is a diagram of a Fokker F-100

passenger aircraft, indicating the areas which are adhesively bonded. It is easy to see that much of the fuselage, the wing structure, and the engine housing are at least partially adhesively bonded. What is not apparent from the figure is that many of the internal components of the aircraft cabin are also adhesively bonded. For example, floor panels are a special construction of a material known as Nomex honeycomb core adhesively bonded to fibreglass panels. As materials such as carbon and glass fibres were introduced in the fabrication of flooring, extensive testing on these joints was required for a comparison with previous models [126]. The overhead compartments are made in a similar way. These constructions are not only lightweight but they are also stiff.

The automobile industry also uses adhesives extensively. Figure 1.2 shows the location of an automobile where adhesives are used. For example, automobile hoods are typically constructed of a top panel and a stiffener. The stiffener is joined to the top panel by "anti-flutter" adhesives which allow the hood to maintain its shape even under high stresses and wind shear. Structural adhesives were used for bonding materials such as fibre-reinforced plastic (FRP) to itself and to steel in such applications [127]. In newer automobiles, the windshield is part of the overall structure of the roof and is fastened by adhesives to the frame.

The use of adhesive bonding in ship structures has been slow compared to the other industries. However, there is an increasing trend towards combining dissimilar materials in a single ship structure, particularly for high-speed craft, where weight reduction is critical. Examples include vessels built with steel hulls and aluminium superstructures, and vessels having aluminium hulls and superstructures, but with parts such as mast, control surfaces and even bilge keels constructed in fibre composites. The introduction of fibre-reinforced composites has been mainly confined to pleasure craft, yachts, high performance racing craft, rescue and patrol vessels. For high-speed craft, adhesives have also been used to bond panes, seat rails, and the rudder bearings in the housing and propulsion shafts.

Adhesives can also be found in marine structures as sealants. Marine sealants form a durable, elastomeric waterproof seal for marine applications above and below the waterline. Sealants are often used for permanent sealing or for service and repair

applications including sealing of deck hardware and hatches, around doors and portholes, deck-to-hull assembly, through-hull fittings and seams and keel joints.

1.1 The adhesive bonding process

Adhesion is a phenomenon which allows the adhesive to transfer a load from the adherend to the adhesive joint. Since adhesion is a surface phenomenon, it follows that the physical properties of the adhesive joint depend strongly on the character of the surface of the adherend and how the adhesive interacts with that surface. The adhesive refer to a material used to join two solids together by forming between them a thin layer and resist separation. At some stage in an application the adhesive must be liquid or at least plastic. When the bond is formed it is solid, though it may or may not be flexible. The actual strength of an adhesive joint is primarily determined by the mechanical properties of the adherends and the adhesive.

Adhesive bonding is an alternative to more traditional mechanical methods of joining materials, such as nails, rivets, screws, etc. One major differentiation between an adhesive joint and a mechanical joint is that in the second, the adherend, in general, must be pierced by a mechanical fastener to execute the assembly. When an adherend is pierced by a mechanical fastener, a hole is created in the adherend. Stress concentration which result from the edges of the hole can cause a decrease in many physical properties of the adherend as well as of the mechanical joint such as stress singularities and galvanic corrosion. Adhesives also display several other advantages over mechanical fastening. The main reason for the widespread use of adhesives in the aerospace industry is the ability of adhesives to not only form a joint but also to seal the assembly in one step. Mechanical fastening often require a separate sealing procedure to create a pressurisable assembly. Adhesives also allow galvanically dissimilar materials to adhere to one another without leading to accelerated corrosion. For example, the mechanical joining of steel and aluminium would be a disaster in the making. Aluminium would act as an anode to steel and corrode rapidly in corrosive environments. Since most polymeric adhesives are non-ionic and electrical insulators, a properly effected adhesive bond would electrically separate the members of the galvanic couple while still joining them structurally. Adhesive bonding, when executed in a properly designed adhesive joint, does not exhibit high concentrations, so the properties of the adherends can be fully utilised. However, adhesive joints do

require a much larger area of contact between the adherends and the adhesive in order to carry the same load as a mechanical fastener. The major advantages of adhesive bonding for steel applications are [3,13];

- the elimination of thermal distortion associated with welding. The absence of material removal does not introduce much distortion into the adherends of the beam joints being considered in this study
- for joints where one of both of the adherends are thin as in the case of a lap shear joint, other methods of joining such as welding or riveting, may not be possible; the thinner the gauge the more difficult and the more inefficient these methods become.
- For a joint with thick adherends, adhesive bonding as compared with welding takes place over the whole surface and thus gives continuity of strength with increased stiffness, reduces stress concentration and lessens the risk of fatigue
- the reduction of pitting corrosion due to the absence of weld defects and the additional benefit of the adhesive acting as a sealant within the joint, thus minimising crevice corrosion. A correctly chosen adhesive will not itself corrode the metal and may also serve to prevent galvanic action between dissimilar adherends
- adhesive bonding may save weight, particularly when it enables a thinner gauge of metal to be used in stressed skin construction. Mechanical fastening methods tend to introduce additional weight considerations such as riveting or welding.
- in some cases it is valuable to use adhesive bonding in association with bolts or rivets to resist initiation of a peel or cleavage failure. Besides the extra strength and greatly increased fatigue resistance obtained, there are secondary advantages in corrosion protection and fluid-tightness
- the ability to create efficient complex joints, such as sandwich structures
- frequently the use of adhesives can reduce cost

However, mechanical fastening does have a number of advantages over adhesive bonding. Mechanical fasteners are relatively obvious once applied in a joining application. Adhesives, by their nature, are internal to the joint. In most cases, it is thus not easy to determine (without destructive testing) whether the adhesive was properly applied.

Another limitation of adhesive bonding is its sensitivity to heat. Limited heat resistance is inevitable, since high strength adhesives are made from organic compounds. Other significant limitations include poor heat and electrical conductivity, high thermal expansion and limited resistance to chemicals for certain applications..

In summary, the major disadvantages of the use of the adhesives are [3,13];

- pretreatment of joint's surfaces is necessary in adhesive joining which is required to obtain strong and durable joints. The significance of a cleaned surface is higher for a bonded joint than a mechanically fastened joint.
- for bonded joints, a flexible adhesive tend to have good impact resistance while a rigid adhesive tend to have good elevated temperature resistance. Hence it would be difficult to obtain the properties of good impact resistance and elevated temperature resistances through a single adhesive joint.
- the long term durability in wet/humid conditions needs further investigation due to a shortage of test data at present as compared to other mechanical fastening methods.
- a high temperature sensitivity when compare with metals
- load bearing joints require new design skills and may require optimum beam section designs, in the case of structural panels

1.2 Aims and Objectives

There is a potential for introducing structural adhesives into the steel fabrication of stiffened panels in order to avoid the thermal distortion associated with welding. Welded steel panels/beams may be designed to resist bending and associated shear stresses and deflection. The aim of the study is to assess the strength and behaviours of bonded steel beams under three-point bending within both elastic and plastic limits under static loading. This thesis essentially deals with the feasibility of using the adhesive on its own for joining steel to steel for relatively thick adherends. The research work represented here is concerned with steel/steel joints bonded with a single part epoxy adhesive. Both solid and bonded beam models were studied under various methodologies. To validate thick beam section parameters such as beam

profiles and spans; experimentation, finite element analysis and theoretical work were employed. The other aim was to produce a design guide for stresses and deflection in bonded beams fabricated from steel adherends and epoxy adhesive. The effects of varying adhesive thickness on beams behaviour were also considered.

The overall objectives are as follows;

- to consider representative beam models and establish practical bonding and fabrication processes
- to assess the static strength performance and limitations of adhesively bonded structural joints
- to investigate numerical and analytical methods for the prediction of static or failure strength in structural joint configurations
- to determine the behaviour of adhesively bonded beam elements in comparison with the welded equivalent and therefore to compare the strength of such configurations
- to compare the bending behaviour of bonded beams with different adhesive thickness
- to assess the behaviours of solid and bonded beams under elastic-plastic loading conditions

1.3 The stiffened beam/panel

The study concentrates on the adhesive bonding of stiffeners to relatively thin (6–8 mm) plating in configurations typical to ship-like structures which may include a variety of marine and land based fabrications. Similar stiffened skin structural applications are shown in Figure 1.3. The plating-stiffener combination is a fundamental element in most ship structure designs. Stiffeners supporting the plating constitute a grillage with unidirectional stiffening. The stiffened grillage plating will have to resist various loading that will result in deflection, bending and shear stresses that may be in the elastic and elastic-plastic range. The main motivation for this study was to avoid the thermal distortion associated with fillet welded stiffeners and the costly rectification often required during fabrication. Reworking steel components that have been distorted by conventional welding can involve thousands of man-hours. As such, certain marine agencies have focused their work on reducing weld distortion during fabrication of Navy ships and other vehicle types. The development

of finite element analysis tools as well as practical welding procedures has been beneficial in the reduction of welding distortion.

The structure studied is a subcomponent of the stiffened panel/beams where the panels use T, L, Z, flat and inverted T stiffeners. The dimensions of structural components in the case of marine and similar construction affect overall weight and fabrication cost considerations. Figure 1.4 illustrates schematic designs for welded steel panel, of the same flexural rigidity, D, which result in different weight and fabrication cost. The first design in Figure 1.4 is based on using thick plates (normally greater than 8 mm), large stiffeners, and wide spacing between stiffeners. The second design in Figure 1.4 however uses thinner plates, smaller stiffeners and closer spacing. The choice between the two depends on the main design requirement, (i.e. low cost with minimum weight). The fabrication cost of minimum weight design is high and is largely associated with controlling thermal distortion of thin steel plates, typically 6-8 mm. The effects of weight reduction for superstructure construction can mean higher speeds and increased stability due to reduced top weight. Further distinct potential benefits include possible increased fatigue performance of the components due to the lower stress distribution.

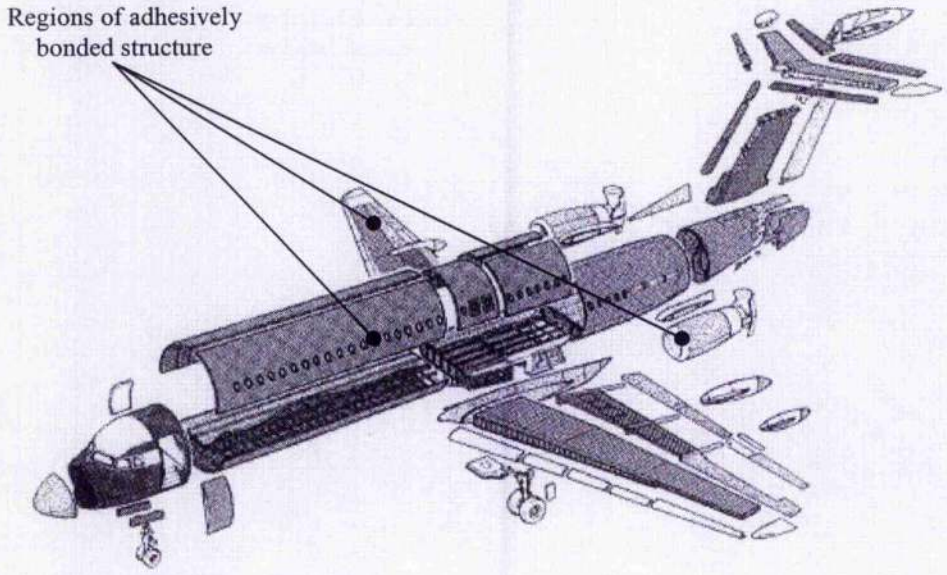

Figure 1.1 Diagram of a Fokker F-100 aircraft showing the sections of the aircraft that are adhesively bonded [3]

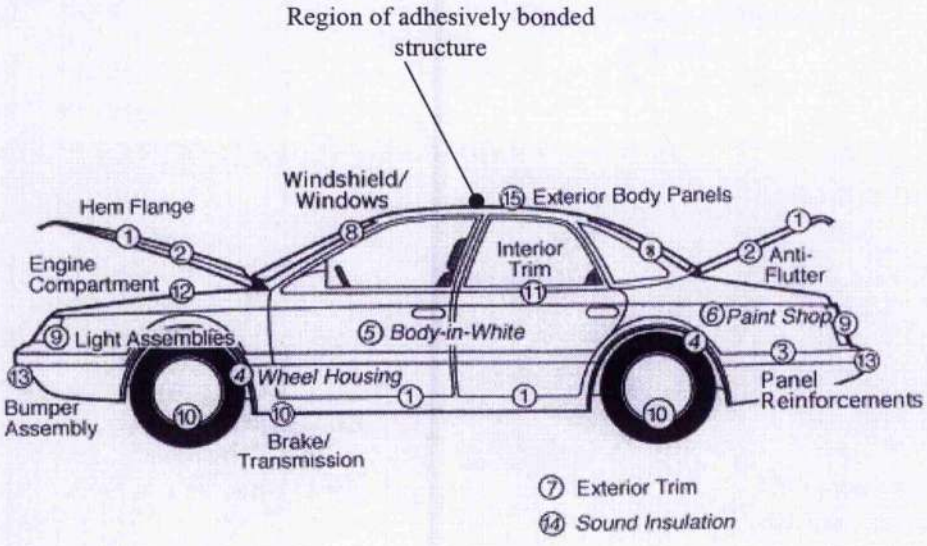

Figure 1.2 Diagram of an automobile showing locations in which adhesive and sealants could be used or are being used [3]

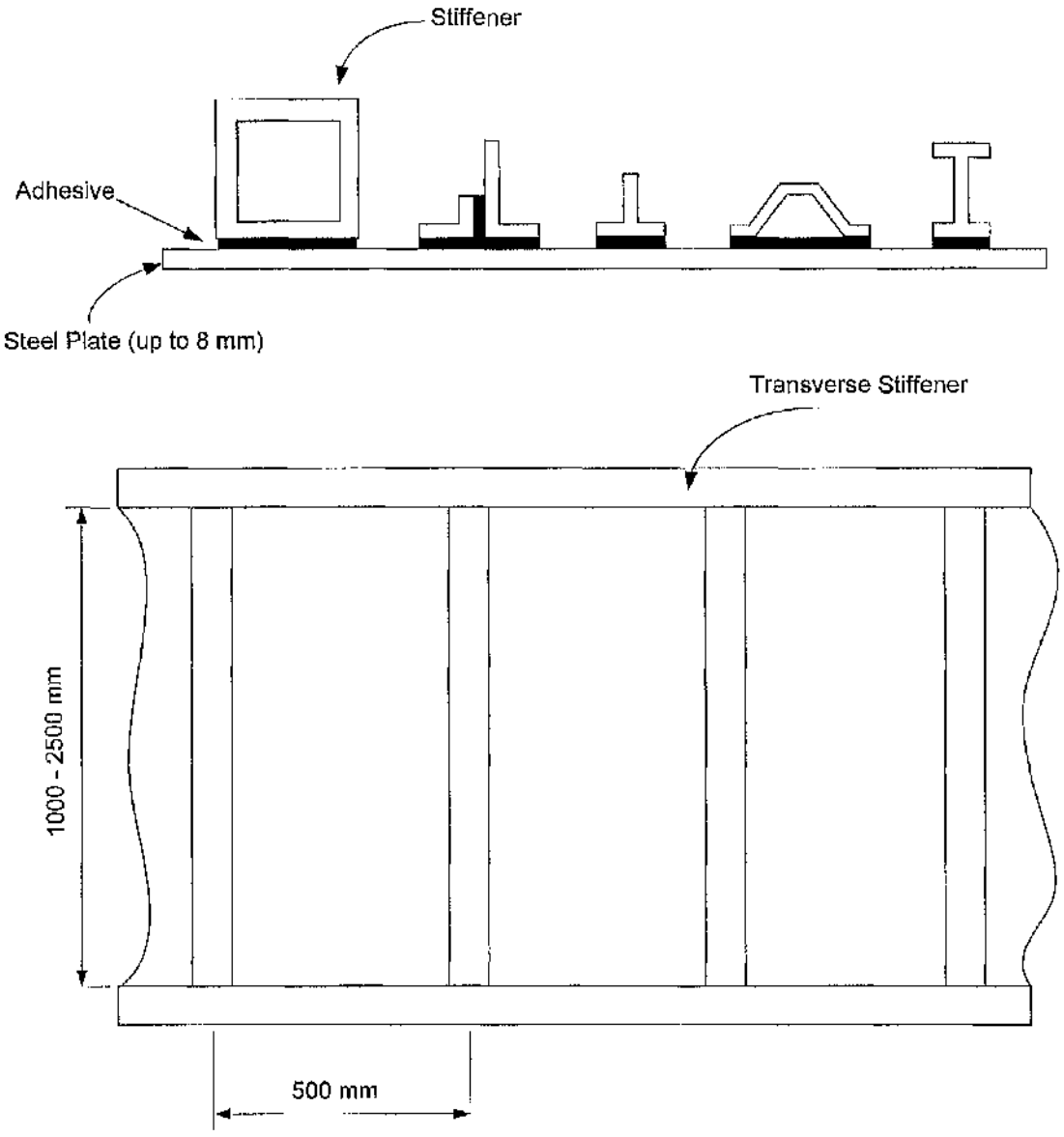

Figure 1.3 Possible bonded stiffeners for structural panel.

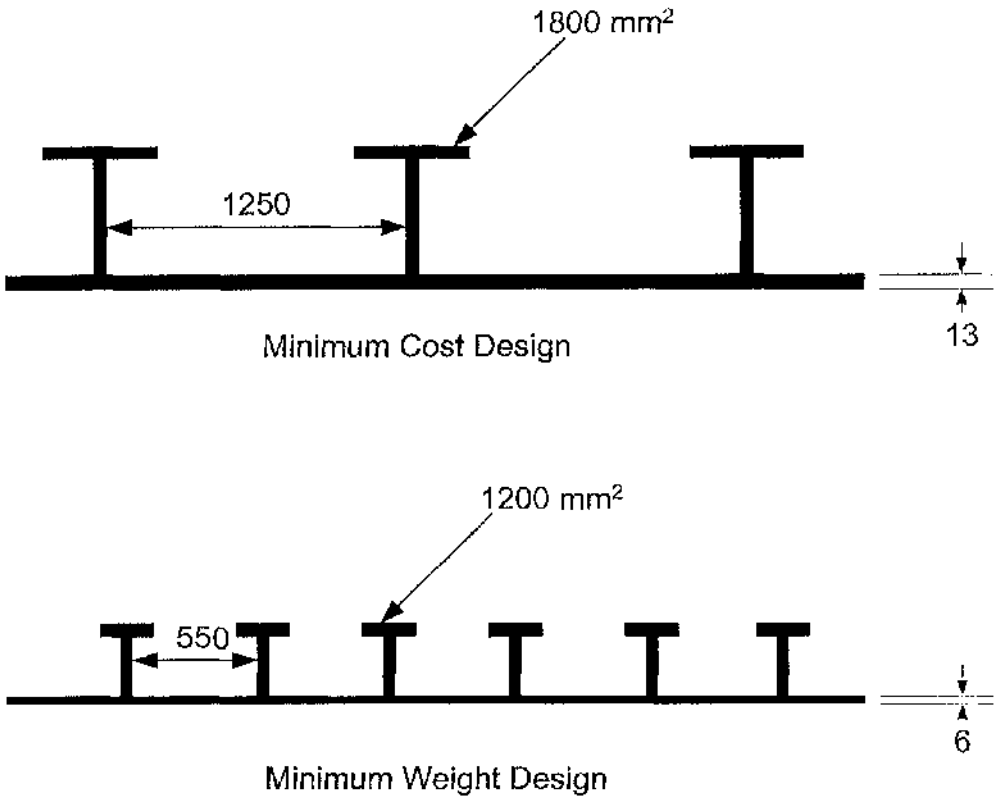

Figure 1.4 Comparison between two design concepts of grillage panels. a) minimum cost design, b) minimum weight design.

CHAPTER TWO

LITERATURE REVIEW

2.1 Structural adhesives and joining processes

In general, structural adhesives are high-performance adhesives capable of producing rigid, high strength, almost permanent bonds between substrates in continuously stressed assemblies under relatively severe service conditions for relatively long periods of time. The use of structural adhesives has increased dramatically in the last few decades due to the continual improvements of the adhesives and its applications. Besides providing good adhesion to a variety of substrates and allowing a quick application process, structural adhesives have excellent material properties and can provide a cost-effective method of joining. In the sheet metal industry, adhesive bonding has the advantage of requiring less operator skill and less post weld finishing as compared to welding. As a result, higher manufacturing efficiency, more extensive stress distribution and cleaner product surfaces could be obtained as compared to welding.

The two most important metal-bonding structural adhesives are the epoxy resins and acrylic adhesives. The epoxy adhesive represented in this study constitutes as one of the most versatile class of adhesives and is widely used in metal/metal bonding. It should be noted that the shear modulus of most structural adhesives is only a fraction of that of any commonly used engineering metal and their cohesive strength is low. However, when strained to failure structural adhesives display enormous accommodation compared to metal fastening.

Structural adhesives provide numerous manufacturing advantages to designers. Modern epoxy adhesive can offer designers flexibility to achieve economical and technical advantage for offshore and ship construction, especially in grillage connections between plates and steel stiffeners [86,93]. Bonded structures have been shown to be far more fatigue resistant than equivalent mechanically fastened structures, and when designed correctly, can sustain higher load levels than equivalent

mechanically fastened joints [119]. Bonded joints are also lighter due to the absence of the fasteners and are easily inspected using non-destructive inspection procedures (NDI), commonly implemented in the inspection of aerospace structures. However, designers have been reticent towards its application due to the limited research published on the reliability of using adhesives in marine applications. Further research into potential adhesive structural applications is needed in order to enhance the knowledge of this technology and reinforce its use in the industry.

A typical structural adhesive such as a high performance toughened epoxy adhesive offers the relative ease of application together with high joint strength and good resistance to corrosion, fatigue and impact loading in marine structures. In 2004, a study carried out QinetiQ (UK) on behalf of the Health and Safety Executive showed potential in the non-metallic repair method of using structural adhesives [79]. They compared the feasibility of adhesive/composite-based emergency repairs with the more conventional welded steel-type approach. Although initial results have been positive, the requirement to predict the useful lifetime of the non-metallic repair would however require considerable experimental work and as hence been submitted for further work. Structural adhesives also have the advantage of minimising the structural weight of marine and offshore structures. The shipbuilding company VT Group (UK) has implemented the successful use of adhesives on secondary structures and attachments of their fast patrol and strike craft range [86]. The aim of their research was to develop a philosophy and proper bonding procedures for aluminium structures that would enable lighter scantlings and practicability as compared to welding, but at a similar cost.

New material systems present potential solutions to meet the advanced performance and economic requirements in building more efficient marine structures. Presently the material that is considered for building most commercial vessels is still steel because it is economical. However composite materials such as fiberglass reinforced plastics (GRPs), fiberglass reinforced composites (FRCs) and aluminium are suitable alternatives that will reduce the weight and loss of speed associated with steel fabrications. The use of new material combinations generates the need for new joining technologies for the fabrication of more complex joints, especially in sandwich design that could be adopted in ship structures. A range of structural

adhesives were examined in recent studies for bonding steel to steel, steel to GRP and GRP to GRP in marine structures [80,81,82]. A similar study carried out by the Navy Joining Centre (US) focused on developing and implementing producible and cost effective steel to composite adhesive joining technology. The approach met requirements applicable to the US Navy destroyers [77].

Existing structural designs could also benefit from the introduction of using adhesive bonding. An example of a typical structural element could be found in a study carried out by Earl et al., where the authors analysed the tee joint connection between a bulkhead and the hull by using thermoelastic stress analysis [128]. The authors have used XE900/Ampreg 26 web bonding laminate to bond the web to the flange inner skin. In order to study the detrimental effects of air gaps, a 2 mm unfilled gap at the based of the web was created to represent air gaps that occur in vessel manufacture in the test specimen manufacture. In the manufacture of such joints, a thixotropic filled adhesive is usually used and any gaps are normally filled.

Structural adhesives have been used in joining materials in aircraft/aerospace, automotive, electrical/electronics, building/construction, and consumer/appliance applications. The feasibility of using structural adhesives in fully structural automotive body applications has been studied extensively. The automotive industry has investigated the use of structural adhesives in semi-structural applications particular for the attachment of stiffeners to bonnets and boot lids. As well as providing a uniform load distribution, adhesive bonding provides a smooth surface finish and thus eliminates the need for expensive secondary operations prior to painting the vehicle. Box sections and "top hat" beam section configurations were envisaged to feature prominently in fully stressed body shells or other forms of structural elements in vehicle construction. However, in order to reduce vehicle weight, more car body structures developed are made from lightweight materials such as composites, plastics and aluminium alloys. Fabrication of these materials in automotive applications using traditional welding techniques is not feasible and adhesive bonding is a potential assembly method. Previous research have also found the flexural and torsional stiffness and strength properties of bonded thin-sheet box-section beams to be higher than for similar beams formed by riveting or spot welding [117,118].

The bonding technology has been gradually introduced and transferred to the construction industry recently. Structural adhesives could be used in the strengthening of beams and columns by bonding plates to their surfaces in order to extend the life of ageing infrastructure. The plate bonding was achieved with the use of lightweight fiberglass-reinforced-polymer (FRP) composite plates. Plate bonding relies critically on the strength of the adhesive joint, which must be designed to have an adequate strength. A study on this joint was carried out by Stratford & Cadei, who presented an elastic bond stress analysis suitable for design [to be updated].

Understanding the adhesives properties and its limitation is an important aspect in the analysis of joints. This is especially crucial in marine structures where joints must be able to sustain difficult operating conditions. A study carried by Hashim investigated the potential of adhesively bonded steel-steel joints used in marine structures [78]. An experimental program based on large and small bonded models concluded that the cleavage and shear strength of the adhesive provides a good indication of the overall strength of adhesive and the bond. Another similar study was carried out on thick adherend steel-composite joints for offshore platforms and superstructure for ships [87]. In this paper, Hashim & Knox have assessed the strength of the bonded steel-composite structure using representative macrostructural joints under lateral loading conditions. The strength of the shell to frame joint was evaluated and the effects of the laminate thickness were also studied. They have found that increasing the laminate thickness led to a significant increase in the joint strength. The other alternative in increasing the joint's strength was found by a reduction of the frame-stiffener spacing. This approach assists in resisting a bending moment subjected between the two stiffeners. Examples of other potential adhesive applications for bonding metals in marine construction include the repair of ship superstructure, structural elements in low stress regions (lightly loaded bulkheads, fire doors, watertight doors, instrument casings and ventilation ducts, underwater repair of offshore tubular structures and bathyscaphes).

Conventional materials such as steel can be found in many marine structural applications. Welding is the commonly adopted method of joining steel members in the fabrication of steel panels (stiffeners to plates). Most structural stiffening is attached by a double continuous fillet welding procedure to a thin plate of shell, decks

and bulkheads. The ultimate compressive strength of stiffened panels is very important from the design and safety viewpoint. However, the ultimate strength of these panels depends quite significantly on the associated welding distortions and residual stresses during fabrication [130]. The welding creates tensile residual stress, on the order of the yield stress of the steel within the vicinity of the stiffeners, and lower-level compressive stress in the plating between the stiffeners. These built in stresses and strains in the components result from uneven cooling after the welding process. Besides this, the high heat input associated with welding tends causes structural distortion during fabrication. Hence it is difficult to accurately quantify the integrity of the structure and further requirements are normally included. Such requirements include post-weld operations from straightening to size reduction through cutting. As a result, a large number of man-hours may be involved in the reworking of those steel components that will increase production cost.

Due to the demanding nature of the service conditions in which vessel operate, welded components and structures are subjected to a high level of fatigue loads, which cause structural degradation and finally lead to complete failure for structural components. When cracks occur in the vicinity of weldments in structures, weld repairs are frequently considered for crack repair and in most cases mainly to extend service life of the component. When a section of a welded joint fails to pass inspection, it is common practice to repair the weld by gouging out the initial weldments in the sub-standard sections and re-welding them. However, the effectiveness of weld-repairing cracks in an already welded joint is unclear due to the increase in residual stresses, distortion in geometry and the deterioration of the microstructure caused by the additional weld process. Shankar & Wu carried out research comparing as-welded plates and weld-repaired plates in marine structures [135]. It was found that the residual life of the weld-repaired joints is even lower than that of the as-welded plates. This was attributed to the significantly larger size and greater number of defects introduced by the secondary welding process. This led to the conclusion that the repair of cracks by subsequent welding is a poor means of enhancing fatigue life.

Research has also been conducted on the welding methodologies available to the industry now. Research carried out by Joint Institute de Soudure (France) and TWI

(UK) assessed the potential of using CO_2 laser welding of thick section steel structure instead of current arc welding in shipbuilding [83]. There is a need to build confidence in such a technology which involves an investment of high capital cost. Comparison between laser welded and adhesive bonded steel sandwich structural elements showed a better fatigue performance of the latter [82].

The amount of pitting and corrosion to a welded joint in a marine environment is also an issue of concern with designers. The life of the joint could significantly deteriorate due to the exposure to chemical reaction with the seawater or other organisms that will corrode the joint area. As a result, engineers will have to conduct damage analysis in order to substantiate the integrity of the structure to prevent making significant repair to existing structures. Dong & Zhang studied stress corrosion cracking cases in detail and analysed the effects of weld strength mismatch on welding residual stresses with a butt-welded plate joint configuration [32]. This mismatch is often referred to as an inhomogeneous strength distribution across a welded joint resulting from the use of the weld metal of either a higher or lower strength than the base metal.

A single joining technology can sometimes prove insufficient to attain the required joint properties and an alternative could be found in hybrid joining processes. Hybrid joining techniques such as weld-bonding, riv-bonding, and adhesive bonding with bolts or screws were introduced in automotive and aerospace structures to take advantage of the technical and economic benefits associated with each joining process [16,17,24,28,31,84]. The key attribute of combining adhesive and mechanical assembly technologies is that a variety of benefits that can be achieved, which exceed the sum of the individual properties of the components in the holding process. The use of combination joining takes advantage of the individual components, resulting in an improved joint quality and durability while minimising production cost. However engineers must carefully consider how the processes will react with or against each other. The adhesive material used in a combination joint is capable of reducing the unsightly effects of distortion by joining aluminium panels together. In fast ferry design, adhesives were found useful combining with riveting to joint panels. Panels are very large and in many cases need assembling vertically, so rivets are required in any case just to hold the surfaces together while the glue dries.

2.2 Design and behaviour of stiffened panels and beams

The plate-stiffener combination forms one of the basic structural units of a ship. In its simplest form it is made up of a beam that is attached to a plate. Many parallel beams supporting plating constitute a grillage with unidirectional stiffening. Such stiffened panels are usually subjected to a combination of lateral bending and in-plane loads. The extremity of such load components may not occur simultaneously, and more than one component may normally exist and interact. In-plane loads include biaxial compression/tension and edge shear, which are mainly induced by overall hull girder bending or torsion of the vessel. The current study focuses on the local lateral pressure loads in the form of sea pressure, wind, concentrated weights, personnel load, and cargo pressure.

The advanced design of marine structures requires the better understanding of the ship plating under the combined loads. The combined loads have been implemented in a research carried out by Judd et al. to assess the effectiveness of adhesively bonded aluminium marine superstructures [86]. In their stress analysis of the adhesively bonded stiffened panel butt joint, the joint was subjected to a complex mix of both shear and peeling stresses resulting from both simultaneous in-plane hull bending and lateral hydrostatic pressure loads. The in-plane applied load consists of a uniform compression that causes a uniform shortening of the panel. The lateral loads represented the static and dynamic forces on the superstructure and determines the scantlings requirements. These loads can be classified into three basic types of loads:

1. Lateral load that cause negative bending of the plate-stiffener combination
2. Lateral load causing positive bending of the panel
3. In plane compression

In a separate study carried out by Shenoi & Hawkins, out-of-plane loading was subjected to top-hat stiffeners and shell plating joints [85]. These joints are typically found in fibre-reinforced plastic (FRP) ships and boats. Such out-of-plane joints are susceptible to failure by peel and delamination well before the ultimate in-plane material stress is reached. Furthermore, their dependence on interlaminar properties make them somewhat sensitive to material imperfections such as voids. The authors identified the key variables that control and govern the transfer of load from the panel to the stiffener and vice versa.

To determine the ultimate strength of the stiffened plates, the stiffened panel is normally treated as a series of disconnected struts, where each strut represents a combination of a stiffener and an associated width of plate. Such an analysis was adopted in this study using theoretical, numerical and experimental work to determine the load-deflection characteristics up to the specified collapse load. Similarly, previous work carried out at the Glasgow Marine Technology Centre involved a preliminary investigation into the adhesive bonding of stiffeners to thin plating with both single and multi-stiffened panel configurations typical of marine structures [87,88,91]. The stiffened panels were tested to plastic collapse in four-point loading under simply supported boundary conditions. Two panels were tested under a negative bending moment and the third under a positive moment. The main objective of the test was to demonstrate the efficiency of the adhesive bonds under panel bending loads and to determine the level of adhesive shear stress due to bending. It was concluded that existing beam theories for calculating stresses and deflection in bonded steel beams require some modification and further study was recommended.

The research presented in this study focused mainly on the negative bending of the panel (plate-stiffener combination). A total of five different stiffener beam cross sections were being considered in this research. The determination of the resulting deflection and strains in the adhesive or adherend as a result of bending will characterise the mechanical behaviour of the beam and in turn influences the scantling requirements in grillage structures. A similar approach was adopted in the research on the design of aluminium hull panel for high-speed craft by Herrington & Latorre [89]. A static analysis of the stiffened panel was performed to determine the displacements, stresses and strains under various pressure conditions. However, an initial experimentation on a prototype hull panel involved stresses below the yield limit that caused yielding, and hence only linear elastic behaviour was assumed.

A popular approach of assessing the ultimate strength of welded stiffened panels involves studying the load-carrying characteristics of each individual stiffened plate unit of various beam section. Normally this involves the measure of the joint's deformation subjected to a given load such as bending or tensile forces. Such experimentation allows to determine the failure load or the ultimate load for the joint being studied. Testing of welded stiffened steel plate panels in compression have

been carried out by many investigators [20,21,29,91,92]. A recent study carried out by Grondin et al. assessed the structural strength and stiffness of welded T shaped stiffeners required to resist compressive forces [90]. Part of their research involved experimental and numerical work on specimens that were loaded with 25 kN three-point lateral loads. Large deformation and finite strain analysis was performed using the finite element code ABAQUS®. The finite element analysis was found to predict quite accurately both the behaviour and the capacity of the stiffened steel plate panels.

It is also common to use 'top-hat' stiffeners to stiffen the plate panels in FRP marine structures. The stiffness of large unsupported panels constructed of FRP materials is inherently low. Stiffened panel joints are normally bonded with welding, riveting or adhesive bonding. Research carried out by Philips & Shenoi focused on the assessment of damage tolerance of such stiffeners to plate connection in FRP marine structures [18,85]. A systematic study was carried out to understand the behaviour of the top-hat stiffener under static loading and mechanism of load transfer and failure. The authors have adopted using the three-point and reverse bend test to simulate gross panel deformation and its effect on the top-hat connection.

Bulkheads in ships are normally required to withstand water pressures only and often are constructed as elastic membranes of very small thickness. An optimum design could be obtained with very light plating, efficiently joined at the seams and butts and supported by a close network of light stiffeners, well connected at the boundaries. A good water-tightness might be secured with such a bulkhead on a small weight, but the deflection would be great, since the bulkhead would have to resist the pressures entirely in virtue of tension. Great deflections are, however undesirable because, where pipes and leads pass through a bulkhead where doors are found, excessive strains was produced causing local leakages and other difficulties. Moreover, the requirement that those bulkheads shall serve as strength members of the hull render it necessary to endow them with considerable stiffness. It is for these reasons preferable to base the strength of bulkheads primarily on the stiffeners, which are capable of resisting the water pressures.

2.3 Scantling requirements of stiffened panels

Research into the optimum scantling requirements has been a subject of interest for many years, especially in developing a preliminary design stage optimisation tools for designers [94,95]. Much of the literature on optimisation of stiffened plates was concerned with minimising the weight of the plate/stiffener assemblies with manipulation of certain design variables. Design variables that are normally considered include the plate thickness, spacing between stiffeners and the geometric properties of the stiffener. A more elaborate emphasis can be found in the paper by Hughes et al., which list the detailed scantlings of the T stiffened panels used as part of an ongoing research on ultimate strength of stiffened panels at Virginia Tech [96]. However most of these researches tend to focus on a single beam section, and fail to address the efficiency of stiffeners of different cross sectional properties. M.M Alinia studied different type of stiffeners in order to obtain an optimised design procedure [97]. By using finite element method of analysis, the author found that the critical shear stress that leads to shear buckling of the panel depends on the type and the number of stiffeners. All plates which have a similar aspect ratio and number of tranverse stiffeners, have an optimal value of the flexural stiffness ratio for which the critical shear stress is at the highest possible value. The optimal value of the flexural stiffness ratio was determined for the T, L and flat beam stiffened panels. The research presented here will similarly involve studying the effects of cross sectional properties of using various types of beam sections as stiffeners for stiffening the panels.

In the preliminary design stage, designers must be careful to ensure that the ratio of stiffener spacing to plate weight is such that the required strength is obtained with the least weight. Shell bulkhead and deck plating design are all based partly on this principle. Research carried out by Kang et al. addressed the minimum weight design of compressively loaded stiffened composite panels under constrained post-buckling strength [98]. Using design variables such as size and stiffener spacing, the optimal design resulted in a weight reduction of 15.4% compared to the reference design. However, the optimised shape of the stiffeners seemed unconventional and was attributed to the fact that the stiffener spacing was too close and the upper portion of the web being too large. Such a design will be inappropriate in a real structure, as the decrease of the stiffener spacing induces a weight increase because the total number

of stiffeners will increase as well. A different approach to define stiffener spacing was found in the finite strip (FS) method. Research conducted by Wang & Rammerstorfer used the FS method to derive the effective width between stiffened plates under uniform bending [100].

2.4 Analytical method

The stress distribution in an adhesive joint is of primary importance for the designer to minimise stress concentration and assess safety factors. Early theoretical studies of the stresses in adhesive joints were directed towards the single-lap joint. Volkersen carried out the earliest analysis on a single lap shear joint under tension [120]. Assuming a linear elastic adhesive and a stiff adherend, he analysed the shear stress distribution in the adhesive layer and found that the stresses are at their maximum at both ends of the overlap. Volkersen however did not consider the peel stresses in the bond line due to the associated bending moment in the joint cause by non-collinear applied forces, and rotation in the joint due to bending of the adherend that in turn makes the problem geometrically non-linear. Golan & Reissner [121] considered the shortcomings in Volkersen's analysis by incorporating the bending effects of the adherends. This is carried out by creating a bending moment factor, relating the moment at the adherend ends to the applied load. Goland and Reissner considered the bending deformation of the adherends as well as the transverse strains in the adhesive and the associated cleavage stress. They assumed a very thin layer of adhesive compared to the adherend, so that its effect on the flexibility of the joint is negligible and the flexibility of the joint arises mainly from the adhesive layer.

The early work on joint mechanics by Volkersen and Golland & Reissner laid the foundation for a closed form solution of the stresses in bonded joints. Their analysis of single lap shear joints, based on classical theory of structures, was supported by mathematical solutions, assuming only linear elastic material properties. The two methods of analysis take a simplistic approach toward joint geometry and deformation under load. The most obvious geometric difference between these models and actual bonded joints is the presence of fillets. Many contributions have followed in their approach to attempt to avoid conservative stress distribution in a lap shear joint. Perhaps the most recent modelling which accounts for bending, shear and normal stresses has been produced by the Allman theory [139]. In this theory the adhesive

stresses have been set to zero at the overlap ends and allowed for a linear variation of the normal stresses across the adhesive thickness. This analysis is also based on a single lap joint but unlike the previous theories, it accounts for dissimilar materials and different adherend thickness and is therefore considered as less conservative. Studies has shown that Allman theory for elastic stresses in lap shear joints is suitable for linear, rigorous analysis and can be modified for non-linear adhesive behaviour. The study shows a comparison between Allman's analysis and the finite element method with the differences in peak strain level as little as 5 %.

Hart-Smith extended the analysis of bonded joints to allow for plastic behaviour in the adhesive [119]. He treated both adherends in the overlap as individual beams by adding the effects of adhesive shear strains only and then applied compatibility conditions to adherends whilst adhesive thickness deformation were not included. Several issues were investigated concerning not only elastic-plastic adhesives but also failure modes, thermal effects and the influence of adherend stiffness unbalance. The analysis by Hart-Smith assumes that the adhesive behaves ideally elastic-perfectly plastic with the data for design being obtained from a thick adherend test as specified by ASTM D3983-93. The analysis shows that, within certain limits of overlap length and adherend thickness, bonded joints can be designed such that the load capacity of the bond is greater than the unnotched strength of the parent material. This simplifies joint design procedures dramatically.

The issue with the theories mentioned is such that they are limited to the simple lap shear joints. A modified form of the elementary bending equation, derived by Allen is suitable for joints which are represented with low density core [13]. These joints are made up of a much stiffer upper and lower adherends, with commonly use beam sections such as the T and L beams. Pye and Ledbetter have incorporated this sandwich beam theory for their analysis of composite glass-adhesive T beams which are used in wall, roof and canopy structure construction [11,33]. A comparison between the experimental and calculated results show good agreement. The slightly higher stresses and deflection found in the experiments were attributed to the missing shear lag effects not being accounted for in the applied theory.

To enable designers to obtain a good qualitative stress distribution for the normal tensile stresses associated with the peel effect, a variety of practical configurations attempts were developed for general solutions. Good correlation, from generalised solutions with average stress distributions obtained from finite element analysis is claimed with reference bonded joints made up of thin gauge metal skins and T or L shape stiffeners. There seems to be no analytical technique that can effectively assess the stress level in a long continuous bonded joint (e.g. beam structure). The shear stresses, which are developed in elastic beams of solid cross section due to lateral transverse shear loads that induce bending, are examined in most 'strength of materials' text books [80,112,113]. The significance of the transverse shear stress component (generated by the transverse shear force) along a beam subjected to a flexural loading lies in the control of bending stresses and bending deflections of the beam.

2.5 Numerical method

The finite element method can be a useful aid in the design of adhesively bonded joints. The increased application of the finite element method on adhesive joints was accompanied by the development of finite element mathematical models to analyse the behaviour of those joints. Both analytical and numerical models have since been developed and extensively used in engineering with success. The finite element method was developed more by engineers using physical insight than by mathematicians using abstract methods. It was first applied to problems of stress analysis and has since been applied to other more complicated problems of continua. Adams and his co-workers are renowned for their work on failure analysis of adhesively bonded joints [3,34]. In general, their approach to joint failure prediction is to use a plane strain, geometric and material nonlinear finite element analysis with either a principle stress or maximum principal strain failure criterion.

Most engineering problems solved by the finite element method resulted in cost reduction by replacing the physical testing with the less expensive digital simulation. These problems were solved by means of computational work carried out on commercial finite element programs. These pieces of softwares have the capability to undertake static stress analysis; structural dynamics, vibration and heat transfer problems. Commonly used softwares include MSC.Nastran®, MSC.Patran®,

ABAQUS/CAE®, IDEAS®, DYNA 3D®, ANSYS® and FEMAP®. With effective simulation, these programs can drive down fabrication costs, reduce development time, and increase product quality. The MSC.Patran® and ABAQUS/Viewer® programs were used in the finite element analysis carried out in this research. These programs were chosen mainly for its comprehensive interface and ease of use. They are useful tools in the solution of problems marine, aerospace and automotive structures.

One of the most common structural elements studied using Finite Element method in aerospace structures is the stiffened panel. It is often the case that appropriate geometry and dimensional requirements are determined through study, resulting in their high efficiency in terms of stiffness to weight and strength to weight ratios. In Lanzi's study of the structural behaviour of composite stiffened flat panels under compression, the author worked on panels stiffened with L section beams used in aerospace structures [44]. An optimisation procedure was formulated in order to minimise the panel weight while fixing the width and height of the panels. The stiffened panel was modelled using the commercial program ABAQUS®. As foreseen by the numerical analyses, experimental results validated the ability of the panels designed to work in the post-buckling field until collapse, which takes place due to the failure of the stiffener blades.

For marine structures, the finite element method has been use for a wide range of analysis of offshore structures, surface and underwater naval vessels and equipment, merchant vessels and recreational vessels. The more common analyses include linear and nonlinear static and dynamic analysis of entire vessels, sub-assemblies, or individual components. The local buckling of stiffened panels in offshore structures is a common example of a sub-assembly finite element analysis. Shanmugam & Arockiasamy carried out ultimate strength test on stiffened plates that were simply supported and subjected to the combined action of axial and lateral loads [30]. A series of ten stiffened plates were experimentally tested and analysed using an elastic-plastic finite element package to determine the behaviour and the ultimate load capacity of stiffened panels. The authors concluded that the finite element modelling

procedure proposed was capable of predicting the behaviour and the ultimate load capacity of the panels with reasonable accuracy.

The finite element method is also often used in the analysis of structural adhesive joints, where the program is able to account for more sophisticated non-linear material properties, complex geometric configurations, boundary conditions and load cases. It is especially used in the fundamental study of the single lap joint [103]. Goncalves et al. introduced a new three-dimensional model, which considers geometric and material nonlinearities of the lap joint studied [46]. The finite element model introduced uses solid brick elements as well as specially developed interface elements. The main objective of the study was to calculate the stresses at the interfaces between the adherend and adhesive using the ABAQUS® software, as these regions were considered critical in lap joint structure. The finite element method is also capable of modelling complex geometric functions of adhesive joints. Gaofeng & Crocombe have presented a simplified finite element modelling approach for the design analysis of structural adhesive joints [38]. The commercial finite element program ANSYS® was used to investigate joints such as the single lap joint, double lap joint and a T section joint. They have propose a hybrid version of the modelling technique for a complex joint such as the T section joint with sharp substrate corners, as it was necessary to use a combination of beam and quadrilateral elements to obtain reliable results.

The finite element method is often used for comparison with experiments carried out in research work [45,90,96,89,102]. Feih & Shercliff used MSC/PATRAN® and ABAQUS® for the simulation of the single-L composite peel joints under tensile loading [39]. The numerical solution helped to determine the order of occurrence of different failure modes during catastrophic failure or failure taking place within the interface that cannot be observed outside through experiments. The combined numerical and experimental interpretation improves the understanding of complex failure mechanism as encountered for the peel joint failure. The ability for the finite element program to define the mechanical behaviour in specific regions will prove useful for generating data in regions, which would have otherwise be too tedious to

measure in experimental work. This function could be adapted in the investigation of the stresses/strains within the adhesive and the interface region of adhesive joints.

The low strain behaviour of structural adhesives can normally be modelled through linear elastic functions. Modelling of linear elastic behaviour is well understood and materials can be fully characterised by their Young's modulus and Poisson's ratio. These parameters are normally determined from experiments according to specified standard test methods and procedures. Linear elastic models can fully describe the performance of the more brittle adhesives that rupture before yielding. In the stiffness analysis of adhesively bonded T joints, Li et al. assumed linear elastic material properties for both adhesive and adherend materials [15]. The joints were subjected to linear loads in order to determine the stiffness of the joints and provide reference for suitable joint dimensions.

However, modern adhesive are tough materials that can sustain large strains before failure, and their deformation behaviour is highly non-linear and involves plastic deformation and flow with glassy adhesives. Such behaviour is described in finite element systems by using a non-linear structural analysis. Non-linear structural analysis normally consists of the following three types; geometrical nonlinearity, material nonlinearity or combined geometrical and material nonlinearity. Material non-linearity causes the behaviour of the material of which a structure is made to have a nonlinear stress-strain relation. A rubber-toughened adhesive is an example of a ductile material that exhibits extensive non-linear deformation before failure. An elastic-plastic model is often used in finite element analysis for describing this type of behaviour in rigid materials. In the work carried out by Dean et al. on the prediction of deformation and failure of rubber-toughened adhesive joints, different elastic-plastic finite element models were assessed for describing the non-linear deformation behaviour of a toughened adhesive [52]. Results obtained from experiments were compared to assess the predictive accuracies of the models and to explore the validity of criteria for the onset of failure in the adhesive. Their results indicate that the exponent Drucker-Prager model produces higher predictive accuracy in finite elements than the linear Drucker-Prager or the von Mises material models.

The effects of a large deflection will cause the geometry of the structure to change even when it is behaving elastically, such that linear elastic theory breaks down. The concept of geometrical nonlinearity is thus introduced in the formulation of such finite element models. Andruet et al. presented a paper on the formulations of two-dimensional and three-dimensional finite element analyses of adhesive joints, where geometrical nonlinearity was introduced in the finite element models [53]. Special 2-D and 3-D adhesive elements were developed for stress and displacement analyses for the single lap joint. The inclusion of geometrical nonlinearities was found necessary to account for large displacements, which are often observed in joints of such nature.

Edlund and Klarbring presented a general analysis method for determining the adhesive and adherend stresses and deformations in the adhesively bonded joints evaluated as three-dimensional structures by considering geometrical non-linearity and non-linear material properties of both the adhesive and plates [107]. This paper is an example of a combination of both geometrical and material nonlinearity. Both nonlinearities are important factors affecting the deformation and stress states of adhesively bonded joints. This is especially found in adhesive joints with unbalanced geometry such as corner or tee joints that can exhibit these types of non-linearities.

The mesh arrangement of the model analysed is a significant factor in determining the amount of computation work required to run the simulation. There are many different methods to develop the mesh, however the most suited for discussion includes submodelling, mesh refinement and symmetry. The finite element method is not effective for calculating the peak stress in specific areas of an assembly. In the analysis of adhesive joints, the submodelling approach provides an efficient computational tool for enhancing stress analysis in the regions of high stress gradients. For lap joints, the local stress variations near the ends of the overlap are characterised by very high gradients of stress and submodelling is normally introduced [104].

Submodelling is normally done after a uniform coarse mesh model have already been implemented, which may be effective but does not place emphasis on stress/strains prediction at a localised area. Submodelling is adopted to analyse key stress concentrations within the original global configuration with a consequent reduction in

the amount of computation. This is a more effective approach rather than adopting low order elements for finite element analyses of engineering components. The submodelling concept is also known as the cut boundary displacement method. The cut boundary is the boundary of the submodel, which represents a cut through the coarse model. Displacements calculated on the cut boundary of the coarse model are then specified as boundary conditions for the submodel. Wahab & Ashcroft used the submodelling concept to a good effect in their finite element analysis of composite beams under three-point and four-point bending [75]. The submodel contained detail of a semi-circular crack in the centre of the adhesive layer.

Another efficient method of meshing is obtained by exploiting the planes of symmetry in a joint being analysed. In modelling symmetry, we need only to model a portion of the actual structure in a finite element model. That portion, which is normally half or a quarter of the actual model, can be simulated by providing proper restraints to the associated symmetrical faces or edges. To model symmetry, the geometry, loads and the restraints must by symmetric about a plane. The use of symmetry in the analysis of adhesive joints has been exploited by various authors [75,105,106]. As a result of implementing symmetry in the modelling, the analyst could reduce the size of the analysis domain, at least by a factor of two. The reduction in the analysis domain could introduce a finer mesh, resulting in a more accurate analysis than a coarsely meshed full model with a comparable node and element count.

2.6 Effects of varying adhesive thickness in joints

The adhesive thickness is an important aspect to the integrity of a bonded joint. The influence of the adhesive thickness has been studied to a great extent in many bonded applications. Most of the research has focused on the effect of adhesive thickness on the failure load/integrity of bonded joints when subjected to tensile loads, as in the case of the simple lap shear joint test. An example of this is found in a paper by Taib studying the epoxy bonded L section joint subjected to tension forces [136]. The author found that the average failure load as well as the corresponding displacement decreases as a result of the adhesive thickness being increased. Examination of the fracture surfaces reveals that in joints with the thin adhesive layer, the fracture involves the interfaces of other adherends. However, in thick adhesive layers the

crack propagates only in one interface and does propagate to the other interfaces as it does for the thin adhesive layers.

The effects of adhesive thickness could be measured by thermal stresses in a joint subjected to fixed loading conditions. A study by Samhan and Darkish addressed the effects of varying the adhesive thickness in bonded cutting tools as a potential replacement to mechanically clamped or brazed tools [137]. The aim of the research was to assess the effect of different measures used to dissipate the heat found in bonded tools, and on the thermal and thermo-mechanical stresses developed in these tools. A comparison between two models made with adhesive thickness of 0.3 mm and 0.5 mm respectively, were subjected to specified cutting conditions. Results obtained from finite element analysis show that the 0.3 mm bonded model experiences higher thermal stress as compared to the 0.5 mm model. Both authors conclude that the thermal stresses of bonded tools will decrease as long as the adhesive thickness is increased.

The thickness of the adhesive in bonded joints has an effect on bondline integrity of the joint. Bondline integrity is influenced by debonds and the weak bondlines on the load transfer of the joint. The area of bondline integrity has been a significant "Achilles heel" in the outright acceptance of adhesive bonding in aerospace structures. These microscopic forms of separation (debonds) include voids, porosity and micro-cracking in the adhesive. Such effects are associated with poor surface treatment, moisture penetration and overheating during cure. The presence of such defects tends to result in the joint design being adhesive thickness limited. Apart from unaided visual inspection of the adhesive material after debonding of the joint, a simple magnification can identify quite small surface defects.

According to research studies, debonds directly affect the load transfer and durability of the adhesive joint, because the influence of load transfer depends on the stiffness of the bondline [129]. This was found especially true in bonded joints where the bondline is subject to pure axial tension or shear forces [131]. As a result, debonds are especially a problem associated during the manufacture of adhesive joints used in aircraft structures, which normally uses bismaleimides or polymides that are supplied in films. Research have been carried out to understand the origin of the voids and to

develop techniques to eliminate and minimise their formation [132]. However, most research studies on adhesive bondline defects tend to focus on experimentation of single and double lap shear joints or similar joints subjected to pure shear. The influence of such defects has not yet been explored thoroughly in joints subjected to a high bending moment.

A good strategy to determine the effects of debonds is a direct comparison with a defect-free joint with a joint with defects, both subjected to similar loading conditions. This technique was explored in an experimental study on the adhesively bonding stainless steel joints carried out by Pereira & Morais [27]. Single lap and double lap test specimens with and without defects were tested with the corresponding joint strengths being expressed in terms of effective overlaps. However according to results obtained, the joints strengths were generally insensitive to the presence of defects created near the overlap ends. The authors suspected that the bluntness of the defects, generated by the relatively thick film, could have played a relevant role.

The effect of debonds could be explained by analysing the associated elastic-plastic shear stress/strain curve of the material. Deformations in brittle structural adhesives are to a great extent elastic until yield strength is reached, followed by a slight plastic deformation before abrupt failure occurs. In a metallic material, the actual slippage strength in the material is much less than the yield strength. However due to the limitation in the movement of dislocations within a metal, the breaking strength is reached before the slippage (gross plastic deformation) occurs. Comparing structural adhesives to brittle materials such as ceramic, the size/scale effect has a considerable effect upon the strength of the test specimens. The influence of size upon test specimens with larger dimensions displays lower strength than do smaller pieces. Equation 2.1 expresses the relationship between scale and strength using effective volume or thickness in the case of adhesives.

$$\sigma_f = \left(\frac{V_{E2}}{V_{E1}}\right)\frac{1}{m} \tag{2.1}$$

where V_{E2}/V_{E1}, is the effective volume ratio, and m the Weibull coefficient of bulk materials. The Weibull coefficient represents the degree of uncertainty for the yield strength value. For most metals, the yield strength will vary within 1% of the

average, whereas for most brittle structures, fracture strength will vary within 10% - 20% of the average. The allowable stress of brittle materials, unlike metals is not a fixed number but varies with the volume that is stressed. The above equation applies when the breakage is caused by a defect in the interior of the test specimen. If the cause of the breakage is at the surface of the specimen, it will then be necessary to write the equations in terms of effective surfaces.

2.7 Surface treatments in adhesive joints

The establishment of intimate molecular contact at the interface is a necessary, though sometimes insufficient requirement for developing strong adhesive joints. This means that the adhesive needs to be spread over the solid substrate, or adherend surface and needs to displace air and any other contaminants that may be present on the surface. Furthermore, the adherend or substrate requires to be a receptive site for the formation of a strong bond where it is free from gross contamination and weak surface layers.

In marine application involving the adhesive bonding of steel adherends, surface penetration plays an important role in both the initial strength of a joint and in its long term durability. In contrast to the case of the aluminium and titanium, where an oxide usually exists, chemical etching procedures are not recommended for steel adherends due to cost, complexity and practicality except for the case of stainless steels [142]. The best results in previous studies have been obtained using shot blasting or mechanical roughening of steel structures [143].

It is necessary to fully characterise how surface preparations affect the critical performance characteristics of structural adhesive joints, especially those describing strength and durability. Prolonged exposure to hot humid environments in the non-stressed condition appears to have little influence on this property. However, a combination of heat, moisture and stress can have a devastating influence if surface pretreatment is ignored. A recent study by Underhill and DuQuesnay investigated single-lap shear joints as a function of surface preparation with and without silane pretreatment under both wet and dry conditions [141]. The fatigue life vs. the applied shear stress was compared for both the silaned and unsilaned joints. It was found that the life of the unsilaned joints was an order of magnitude lower than that of the

silaned joints even in dry conditions for stresses above 15 MPa. This clearly shows how the fatigue life is strongly affected by the surface preparation method.

CHAPTER THREE

EXPERIMENTATION

3.1 Properties of the materials

Advances in adhesive formulations and changing product performance requirements mean that bonded joints are increasingly able to, and required to, sustain large deformations before failing. The key to the reliability of the design is knowledge of the limitation of the adhesive material and the integrity of the joint. In order to understand the nature and the magnitude of the stresses within an adhesive joint, one requires the basic knowledge of the mechanical properties of all the materials used in a joint for a specific engineering application. The adhesive and adherend material forms part of the joint being addressed in this section. In order to fully utilize the potential of these structural materials, it would normally be necessary for designers/engineers to determine the behaviour of each material respectively under specified loading conditions. This could be achieved by carrying out experiments in accordance with suitable standards, in order to determine specific mechanical properties. Using the results produced, accurate values will then provide the essential input for related numerical and analytical work on the joint being studied.

The adhesive adopted in this research is a single part epoxy-based structural adhesive Araldite® AV119, supplied by Huntsman (UK) Ltd. The adhesive is a multipurpose, one component heat curing thixotropic paste adhesive of high strength and toughness. It is suitable for bonding a wide variety of metals, ceramics, glass, rubber, temperature resistant plastics and many other materials. The adhesive is made of up components butanediol diglycidyl ether (5-15%) and bisphenol A-(epichlorhydrin) epoxy resin (40-50%). The physical and chemical properties as given by the manufacturer are listed in Table 5.1.

The adherend used is made of mild (low) carbon steel material, also commonly known as structural steel. Structural steel is one of the most widely used metals and can be found in buildings, bridges, cranes, ships, towers, vehicles and other many

forms of construction. The cold rolled, mild steel material consists of about 0.12 to 0.18 % carbon and was supplied by the manufacturer Kelvin Steels Ltd (UK) in semi-finished form. The designation for the material is 080M15 according to the British Standards and AISI 1016 to the AISI metal standards accordingly [47,48]. The choice of using cold rolled steel in preference to hot rolled steel is such that cold rolled steel provides tighter tolerance and is able to produce a better surface finish. Cold rolled steel is supplied in a wide variety in sizes as it is less susceptible to distortions during machining. Also, the benefit of better machinability makes it an attractive choice of stiffener fabrication.

The standard EN ISO 527-1:1996 [49] specifies the general principles for determining the tensile properties of plastics and plastic composites under defined conditions. This standard was used for the tensile testing of the adhesive material and provided information for the experimentation procedure and the preparation of the adhesive material test specimens. This method was found selectively suitable for use with rigid and semirigid thermosetting moulding materials and has commonly been adopted in commercial and academic research in the strength of adhesive materials. Dean & Duncan [36] use the same method in their research of the performance of adhesive joints.

The standard used for adherend material testing was EN 10002-1:1990, which specifies the method for tensile testing of metallic materials determined at ambient temperatures [50]. The test involves straining the mild steel test specimens with a tensile force, generally to fracture, for the purpose of determining one or more mechanical properties. Along with the earlier standard mentioned, both methods were used to investigate the tensile behaviour of the test specimens and for determining the tensile strength, tensile modulus and other aspects of the tensile stress/strain relationship under defined loading conditions.

In the determination of mechanical properties in the adhesive material, there are generally two approaches in which researchers normally use. The 1st method refers to measuring the properties by preparing bulk specimens of the adhesive. The 2nd method, detailed in Section 3.4 measures these properties by using a specific adhesive joint test. Materials property data are often best obtained from bulk test specimens as

shown here, and such data could give an indication of the cohesive strength of the adhesive. The experimentation of dumbbell-shaped bulk test specimens with a flat beam cross section was undertaken to provide the necessary accurate material data. Tests on bulk adhesive specimens using the standard methods as demonstrated here are less expensive and less complicated to perform. The tests were also likely to yield more accurate material properties as compared to tests carried on specific joints.

3.1.1 Fabrication of material test specimens

A total of five test specimens were fabricated to fulfil the minimum requirements of the test standard. The adhesive material was initially supplied in a one kilogram container that was stored at temperature 4 to 6 °C in a temperature controlled refrigerator. The adhesive material was supplied by the manufacturer in its thixotropic paste state. It was thus necessary to carry out proper surface pretreatments and jig preparation in order to cast the test specimens. Two separate jigs were used in the fabrication of the test specimens. The jig and their components were fabricated and designed for the proper curing of the adhesive material with the minimum defects. Figure 3.1 shows the heat exchanger type bonding jig which was use to fabricate the larger dumbbell shaped test specimen 1B as designated from the British Standards. This jig consists of easily detachable fittings and attachments that would create the dog shape cast directly. Excess adhesive could easily flow out of the cavity with a small recess created by the fittings. The modification facilitated necessary removal of excess adhesive prior to machining. The fittings were attached onto the jig with screws. Prior to adhesive, PTFE was sprayed on the base surface and surrounding parts to prevent adhesive from bonding the securing screws. Pressure was supplied by an upper plate and an attached weight to ensure uniform distribution of the adhesive to the surfaces of the cavity walls.

The fabrication procedure prepared with the jig shown in Figure 3.1 is as follows;

1. The suggested thickness of each test pieces was constrained by the minimum dimensions required by the standard. The thicknesses of the fittings were estimated to be around 3.5 mm which produced a test specimen with minimum thickness of 3 mm. The thickness of each specimen was controlled between 2 to 3 mm since it was suggested that thinner specimens may buckle under

contacting extensometers. Fabrication of thicker specimens was neglected due to the increased possibility of inclusions or other defects. A +0.5 mm thickness allowance was considered for the machining. The surfaces of the mould itself were thoroughly cleaned and degreased with acetone in order to remove all traces of oil, dirt and grease prior to application of the adhesive material. A thin spray of PTFE was used to coat the mould surfaces to assist in the removal of the cured test specimens.

2. A spatula was used to apply the adhesive onto the mould cavity. A load was then placed on top of the cavity to compress the excess adhesive material out of the mould. The excess adhesive material was subsequently removed using the spatula. For cured adhesive specimens, it was especially important that the surfaces and edges be free of obvious scratches, air bubbles, pits and sink marks. This was attainable to a certain degree through proper application and appropriate viscosity of the adhesive along with a required clean and smooth surface of the mould cavity. Lowering the viscosity involved allowing the adhesive to stand at room temperature for an hour prior to application.

3. The mould was cured at a temperature of 160 °C for a minimum of 30 minutes in a hot oven. The recommended curing temperature from the manufacturer is 160 °C for 20 minutes. The temperature was monitored by a thermocouple wire embedded in the adhesive material throughout the cure. The curing conditions were identical to those adopted for the fabrication of the bonded beam specimen.

4. The cured adhesive mould was left to cool in the oven for at least 2 hours before removal.

5. The test specimens were removed and machined milled into the dog shape specimens in accordance to the required dimensions.

The mild steel was supplied in its raw material form in straight lengths of four metres each bar. The materials used in both the tensile test specimens and three point bending beam specimens were obtained from the same batch supplied by the

manufacturer. The manufacture's code for the material was stated as EN 32C with the colour code orange. The material was manufactured in accordance to British Standard BS970 Part 3 [47] that specifies the requirements for various metals including carbon and carbon manganese, alloy, free-cutting and stainless steels that are normally supplied in its bright cold finished condition.

The mild steel specimens were manufactured according to dimensions specified on Figure 3.2. The dimensions of the test specimen were taken from Annex D of the standard BS EN 1002 [50]. The test specimens were fabricated with minimal machining such that the properties and state of the material was not significantly affected by heat transfer during manufacture. The configuration of each test specimens was such that the ends were substantially enlarged for increasing the amount of gripping area. This requirement was due to the limitation of only using large grips associated with the Lloyds tensile testing machine. More effective gripping was desirable as it prevents possible slippages of the specimen. According to the standards, each successful test carried out will require the crack initiation to occur within the gauge length region of each test specimen. In the case that the failure of the test piece initiated at the shoulders or the end of the specimen, the results were excluded. That applied to both the adhesive and adherend test pieces respectively. This phenomenon is attributed to the non-linear uniform stress distribution of the material during experimentation due to a disproportionate cross section area along the test piece.

A waterproof permanent black ink marker was used to indicate the location of measuring instruments on all the test specimens according the standards. These markings were necessary to define the gauge length and the location of where the extensometers should be placed on one face. On the other face, the midpoint of each test specimen was located and clearly marked, for the proper attachment of the linear / rosette strain gauges that were used as primary measuring devices. The test specimens underwent visual observation to check for signs of twist and also to ensure a mutually perpendicular pairs of parallel surfaces. Prior to the attachment of the measuring devices, the dimensions of each test specimens were measured again using venier callipers and a micrometer and recorded.

3.1.2 Tensile testing of material test specimens

The experiment was conducted on the Lloyds tensile testing machine, which was a constant rate of displacement machine. All the experiments conducted on the machine conformed to a displacement rate of 0.5 mm / min. The twin screws drive the cross-head (cross bar) at a constant speed regardless of the resistive load. A close up of the tensile test experiment as seen in Figure 3.3 indicates the test specimen measurement region located between the upper and lower grips. The upper grip directly attached to the cross-head allowed controlled movement during the experiment whilst the lower grip remains stationary.

Besides the availability of the strain gauges and the external extensometer, there exists a built in extensometer in the tensile testing machine. The readings obtained by the built in extensometer were however neglected for the material testing due to the slight deviation from the readings obtained from an external extensometer. The combination of small deflections accumulated from the cross-head, the grips, and the load cell could be a probable reason for this deviation. The deflections generating this substantial error which differed from the other readings, suggest that the measured mechanical properties will not be correct. Tensile testing accordingly to the British Standards eliminates all displacement errors as well as gauge length uncertainty through the use of an external extensometer.

The test procedure was performed as follows,

1. The experiments were conducted in ambient temperature conditions which estimated to be about 18 – 22 °C. Prior to the experiment, each test specimen dimensions was carefully measured and recorded. The cross-sectional area was calculated, recorded and the estimate of the yield load was determined respectively for each test specimen. The preliminary calculations determined the load cell requirements for each test.

2. Prior to each test, the thickness and width of the cross section was measured using an electronic micrometer. The data recorded served as an input into the Lloyds tensile testing software.

3. With the assistance of a technician, the specimen was mounted onto the Lloyds L1000 tensile-testing machine. The test speed was assigned at a loading rate of 0.5 mm / min. A visual inspection was made to ensure that the major axis of the test specimen coincided with the direction of pull through the centreline of the grip assembly. The grips were tightened evenly and firmly to avoid slippage of the test specimen.

4. The associated measuring devices (see Section 3.5) were then configured and attached to the data logger. All devices was calibrated accordingly and checked for possible errors prior to the start of the experiment. The residual stress σ^0 at the start of the test must not exceed 102.5 MPa on the strain gauge. This limitation corresponds to a pre-strain of $\varepsilon^0 \leq 0.05$ %.

5. With the experiment in progress, the data obtained from the measuring devices were displayed simultaneously on the screen of the data logger. All recorded data was saved in a floppy disk that required conversion into tabular form using the supplied conversion software as by Schlumberger® and saved in a Microsoft® Excel format *.DIF.

Material properties of the adhesive and adherend derived from experiments and calculations is presented in Appendix B and presented in Table 3.2. Related graphs and detailed methodology for the determination of following is shown in the appendices;

- Young's modulus, E
- Poisson's ratio, ν

3.2 Details of beam specimens

A series of experiments were developed around representative elements of stiffened steel / steel structure. Stiffened panels in ship structures are frequently subjected to lateral loading and hence the study focuses on the bending strength of various beam profiles. Again the main objectives of this work was;

- To assess the static strength performance and limitations of adhesively bonded beam joints
- To establish a design basis for replacing or complimenting fillet welding of steel / steel connections between skin and stiffeners using bonded connection.

Epoxy adhesive Araldite® AV119 as discussed earlier was used for the bonding of the steel / steel specimens. Carefully formulated small-scale experiments in which the behaviour and design parameters of these load-bearing joints were investigated, and have been presented in this chapter. During this exercise, suitable bonding processes for the fabrication of small model specimens were discussed.

3.2.1 Model idealisation

Figure 3.5 shows an idealised study model which was designed to represent a stiffened beam subjected to lateral loading. Three point bending loading was considered instead of four point bending because it would be difficult to locate a small four point loading jig on the smaller span beam specimens. The model may be used to explain failure mechanism under ultimate design load or stress levels relating to specified service conditions. Furthermore the model enables the study of the influence of the joint area. Five different beam cross sections were considered, namely the T, L, Z, flat (or rectangular) beam and inverted T sections as shown in Figure 3.6. These small idealised model specimens give a good representation of grillage joints used in shipbuilding. The solid beam models were machined out of a solid bar to give a continuous section. The solid sections would represent typical welded beam sections. The bonded models are made of two different parts bonded together. A total of five different spans were adopted for each section, as shown in Figure 3.7. The small models range in span from 50 – 75 mm while the longer specimens range in spans from 150 and 250 mm. The objective was to determine the effectiveness of shorter beams / panels as compared with longer ones, for both the solid and bonded specimens.

In total 116 specimens were manufactured and divided into three main groups. Group one specimens were used to compare the bonded beam sections directly with their welded equivalent under similar loading conditions. All the bonded specimens have an adhesive thickness of 0.5 mm while the welded equivalents were machined into solid beam specimens in reality. The cross sectional dimensions of each section were 20 mm high and 25 mm wide. Group two encompasses the T and L bonded specimens with an adhesive thickness ranging from 0.1 – 0.4 mm. The decrease of adhesive thickness in this case was compensated by the increase of the upper adherend thickness, in order for the section to maintain the overall height and width as stated earlier. Group three comprises of flat section beam specimens also with varying adhesive thickness ranging from 0.1 to 0.4 mm. The overall section thickness was kept constant throughout while the adhesive thickness was varied for each specimen.

Due to the geometric differences of each cross section adopted, the beam sections studied differed in terms of flexural rigidity. An initial study ascertained these differences through analytical work using classical beam theory for the solid sections, and sandwich beam theory for the bonded sections. The section properties obtained were later verified with AMOPS version 1.1 obtained from ESDU 02007. An example may be found in Figure 3.4. The geometric data and dimensions are presented in Table 3.4 accordingly. Later comparisons were made by finite element analysis and experimental work. Details of this can be found in Chapter 6.

3.2.2 Designation of specimens

Details of the beam specimens used in the experiments (and finite element analyses in Chapter 6) are shown in Table 3.4. The designation of each specimen is defined by the code system shown in Table 3.3. The tables illustrate and categorise the different test specimens with their dimensions. For the experimental work, three groups of the test specimens were formulated for testing. The first is shown in Table 3.4(a) to determine the mechanical behaviour of the bonded beams in comparison to their solid equivalent, under similar elastic loading conditions. The second is shown in Table 3.4(b) to determine of the effect of varying the adhesive bondline thickness of the T and L specimens under elastic loading conditions. The third group is shown in Table

3.4(c) to determine the effect of varying the adhesive bondline thickness under elastic and plastic loading conditions.

3.2.3 Surface preparation

In order to obtain optimum adhesion, working directions for the surface preparation procedure was strictly adhered to a standard guide [9] provided by Vantico/Huntsman (UK). For the user of adhesives, trade literature can often provide useful methodology for the application of the adhesive as well as the surface preparation methods. The general guide provides instructions suitable for the removal of grease and loose surface deposits for a variety of adherend surfaces to be joined. A similar method described in the British Standard BS 5350: Part A1 [10] was also employed, where specific details with regards to adherend preparation are elaborated. The main reasons for surface preparation are

1. To remove or prevent the subsequent formation of, any weak boundary layers on the adherend (grease or oils on metals)
2. To maximize the degree of intimate molecular contact that is attained between the adhesive and the adherend during the bonding operation
3. To provide a surface that is microscopically rough (For metals this may involve etching away of crystallites or the deposition of a porous oxide)
4. To protect the surface of the adherend prior to the bonding operation. This is frequently necessary in the case of high-energy substrates such as metals

The adherend surfaces were prepared accordingly to the following procedure;

1. Degreasing, by wiping with halocarbon acetone
2. Abrade by grit blasting with grit size 30/40 mesh following the removal of loose particles
3. Degreasing again with acetone

The aim of the degreasing of surfaces before and after blasting was to avoid the fast contamination of the blasting agent and to increase the efficiency of blasting [54]. The subsequent cleaning serves for the complete removal of blasting agent residues

which may reduce the adhesive strength of the bond. After the application of the degreasing agent, it was necessary to test for a clean bond surface with the affected surfaces. The water-break test procedure was applied in this case due to its suitability for testing metal surfaces. Uniform wetting of the surface by distilled water indicates that a uniform wettability by adhesive was attainable as well.

Satisfactory results on surface preparation on mild steel adherends have been obtained by using grit blasting or mechanical roughening of steel surfaces [56]. Surface roughness will be able to enhance adhesion only if the structure produced will be small enough to enable capillary action and draw the adhesive into the microstructure [56]. Grit blasting was found to give variable durability results in the treatment of steel for ship construction. In one example, after exposure to a sea coast environment, it was shown that grit blasting was able to provide more durable bonds than a variety of chemical treatments [55]. The surfaces were grit blasted using Saftigrit® alumina grits from Guyson Corporation to obtain optimum adhesion. The grit size 30/40 mesh was adopted to produce a level of surface roughness resulting in better adhesion compared to an untreated highly polished surface. The grit blasting procedure was carried out on the Guyson manual blast cabinet equipped with a blast cleaning cabinet and a dust collector unit. The blast pressure of 8kg/cm^2 (recommended pressure: 5.6-10.55 kg/cm^2) was supplied by a blast gun nozzle with the grit material being suction fed. The distance of the adherend's surface to the nozzle gun was maintained at around 50 – 70 mm with the nozzle perpendicular to the blast surface. After each grit blast procedure, the adherend surfaces were blown free using compressed air to ensure removal of the loose particles.

3.2.4 Bonding process

The method of application of the adhesive material to the adherend, following a proper and effective surface preparation, requires important considerations where optimum performance from an adhesive bond is desirable. The bonding process itself can be broken down in several important steps, all of which have to be monitored and observed during the fabrication process.

1. Storage and preparation of the adhesive
2. Application of the adhesive
3. Curing
4. Post-cure procedure

The adhesive material Araldite® AV119 is stored in a refrigerator controlled at the low temperature of 5 °C which is within the recommended temperature 2 - 8 °C stated by the manufacturer. The stated shelf life of the adhesive at this temperature is 2 years, however the adhesive materials that were used were replaced within 6 months of usage and prior to the expiry date. The adhesive preparation process requires careful attention. The adhesive in its molten state was allowed to warm to room temperature for 30 minutes from the cold storage. Although not addressed by the manufacturer, the author finds this process essential as the temperature increase will allow the liquefaction of the adhesive material to take place and promote effective wetting of the adherend surfaces. According to the guide, it was also noted that the thixotropic state of the AV119 adhesive has been specially formulated by the manufacturer for gap-filling purposes. The adhesive paste state was applied using the knife coating procedure. The method employs the use of a spatula to control the deposition of adhesive flowing onto the pretreated and dry adherend surface moving under the blade. The spatula itself had been thoroughly cleaned with acetone. Bonding pressure in the forms of weight loading and clamps was applied to the joint during bond formation.

The joint was cured at the required temperature of 160 °C for 30 minutes in a hot air operated oven. A thermocouple was inserted into the excess fillet of the adhesive to monitor the progression of the temperature. The curing schedule recommended by the manufacturer was 20 minutes at 160 °C but the author allowed the total time of two hours for complete cure within the bond area. It is important to allow time (1½ hours) for the adhesive to attain the cure temperature, bearing in mind that the adherends often act as heat insulators and the heat transfer by convection in the oven is usually slow.

After the curing procedure has finished, the oven is turned off and the specimen is left in the oven to cool for at least two hours gradually. In order to obtain a joint of optimum strength, it is preferable to maintain slow heating and cooling rates for the heat curing procedure. The specimen was then removed from the oven and the fixtures used removed and cleaned. The overall dimension of the joint was then checked after curing, with particular emphasis on the thickness of the bondline and the overall joint dimensions. The adhesive fillet found at the edges of the joint was subsequently chiselled off.

3.3 Controlling the bondline thickness

Most research in adhesive technology has been on studying the effects of varying bondline thickness. Adhesive thickness control by itself is a required skill that can often be a challenging and time consuming experience for researchers. This section is concerned with issues relating to joint assembly prior to curing of the adhesive. Issues such as controlling of bondline thickness, removal of adhesive fillet and bonding and clamping fixtures will be discussed.

To determine the effects of the adhesive thickness in this study, the T, L and the flat beam sections beams were chosen for evaluation. In the fabrication of these specimens, the adhesive bondline was varied between 0.1 – 0.4 mm. It was noted that during fabrication of the joints, difficulties arose trying to control the adhesive thickness of the T & L sections as compared to the flat beam section beams. Not surprisingly, it was the nature of the flat beam section's more simplified geometry and larger exposed surface area made it easier for alignment and clamping purposes. The other likely reason was that due to the higher structural stiffness which made it less susceptible to distortions which arose from the machining process. The increased stiffness derived from its 7.5 mm thickness of the lower adherend as compared to 5 mm for the other models.

Having a smooth, even and level surface of the adherend was important for the uniformity of bondline thickness. It was found that the longer mild steel specimens tended to deform slightly in warping after undergoing various machining processes such as milling and surface grinding. Hardly noticeable to the naked eye, such a defect resulted in a non-uniform adhesive layer thickness throughout the span. As a result, a number of rejects produced during early fabrication were sent for additional rework. A manual bending press shown in Figure 3.8 was adopted to correct the distortion which was found to more significant in the longer beams. A controlled downward force subjected the beam to minimal flexing, which resulted in a more even surface. The adherends were placed on a machine table where height measurements were made using a depth micrometer until the accuracy of 0.05 mm within the specified dimension was obtained.

It was important that the bondline thickness be accurately controlled in order to obtain consistent and reliable joint strength when we compared the various specimens. With this in mind, various methods were considered but most of which could be achieved by mechanical means. However, the selected method should not introduce voids or prohibit the application of the adhesive which normally compromised the joint. It should also be noted that the thicker the bondline the higher the risk of incorporating a high level of voids. Various authors have used the different techniques for controlling the geometry of the joint; however there is no clear distinction which technique is clearly favourable, with each having their own advantages and disadvantages [60,61,62].

Distributed wire spacers are fundamentally a simple method to control the bondline thickness. The mechanism is very much similar to a spacer where the wire's diameter controls the gap between the upper and lower adherend. It requires a simple procedure of embedding the wire into the surrounding adhesive material in the fabrication procedure and using light pressure to hold the upper and lower adherend together. The joint is then clamped with clamping devices on each end of the beam specimen. Distributed wires were used inthe control the adhesive thickness of 0.5 mm of all the various beam sections. The wires were located about 5 mm from both the

edges of the adherend which are known to be regions of low stress concentration. In fact their contribution may be neglected since the wires were embedded outside the span considered in each model. The location of wires could be seen on Figure 3.9 and the darkened region represents the area away from the span considered. The Nichrome 80 engineered wires used were supplied by Comax (UK). Pressure was applied through small clamps near the ends where the surface area is directly above the distributed wires during the cure.

The preferred method to control the bondline thickness was to use wire spacers, however research work in typical adhesive joints carried out at NPL (National Physical Laboratory, UK) showed that this method of bondline control was not always reliable [63]. Although the use of distributed wire spacers seems to be the simplest procedure among the other alternative methods, it does have issues that could possibly affect the strength of the joint. These issues are as important and applicable with any other forms of filler materials, such as tabs, microbeads and shims. Researchers have found that when examining fractured surfaces with a scanning electron microscope (SEM) with a joint that has filler material within the adhesive, there were fine separation layers between the fillers and the adhesive [5]. This indicates that the adhesive did not bond with the filler, creating possible crack nucleation points, potentially weakening the overall bond.

There is also the possibility of the filler material contributing to the overall structural rigidity of the joint. The use of glass beads, which are now commonly used to control the bondline thickness, will require a uniform distribution of the glass beads within the adhesive material. Proper and thorough mixing of the glass beads into the adhesive material which takes place before application is difficult to assess. The amount of glass beads used in the application will also be questioned due to the ability of the glass beads to contribute the structural stiffness of the adhesive layer. Glass beads also tend to be more expensive than wires due to the required minimum order quantity and the made to order procedure, therefore were not considered in this study.

Bonding fixtures tend to be reliable in achieving the correct bond length, accurate alignment of the adherends and a uniform bondline thickness. For this reason, the bonding jig shown in Figure 3.10 was developed to control the adhesive thickness and to ensure that the bonding surfaces of the upper and lower adherends remain parallel. The jig is equipped with two stands on both ends to hold the upper adherend to a desired height. 8 stands were fabricated to control the adhesive thickness from 0.1 to 0.4 millimetres. The base plate thickness is constant and is used to support the lower adherend. Firstly, the adhesive is spread on the lower adherend and the stands are place on either side of the base plate. The adherend is then place on the stands, supported at both ends. Finally a loading bar is placed on top of the adherend to add downward pressure, while being supported by the slots found on each stand. All components of the jig were made of mild steel material similar to the adherends used. Thermal expansion of the components under elevated temperature cure cycles was low and did not affect the alignment of the specimen. The bonding fixture was designed and manufactured to control the adhesive thickness ranging from 0.1 to 0.4 mm and to accommodate the various beam sections in this study. The margin of separation between the adherends was physically controlled using a series of base plates with varying thickness and two supports.

The surfaces of the bonding jig and the related components were thoroughly cleaned with acetone and paper and wiped prior to assembly. The dimensions of the blocks and the supports were inspected with a depth micrometer against a flat surface. Once assembled, the overall height of the joint was measured by taking reference from the top surface of the upper adherend and the base plate. The thickness of the adhesive is the difference of the overall height and the thicknesses of both adherends. The mould release agent of thin polytetrafluorene (PTFE) film was used to guarantee easy release of specimens after the curing process. PTFE was also sprayed on most surfaces of the bonding jig and its components to facilitate removal of small cured adhesive patches left on the fixture during post-cure. The lower adherend was then located on the base plate and the adhesive material was applied. The upper adherend was then placed and aligned with the lower adherend with the aid of marked points made on the supports. The upper adherend was designed and fabricated to have a span overlap of about 10 mm to facilitate the adhesive thickness control. The upper adherend was supported

only by the jig supports at each ends. The bondline thickness was physically controlled by the height of the assigned base plate that supports the lower adherend. Once after the application of the adhesive, the distance between the top surfaces of the upper adherend to the bottom plate surface was measured with the depth micrometer to ensure a uniform height along the specimen's span.

In addition to the supplied heat from the oven, the joint required the application of pressure during bond formation. Applied pressure maintained the integrity of a jointed assembly during adhesive cure and constrained the flow of the hot curing adhesive before finally setting. Weight loading in the form of a mild steel block was used to apply the downward pressure to the top surface of the upper adherends. Slots were produced in the supports to accommodate space for the placement of the mild steel blocks. However is important to note that the weight of the block was completely supported by the upper adherend, which prohibited its movement according to the position of the lower adherend. Placement of the steel blocks was a delicate process in which care was taken to prevent unnecessary movement of the upper adherend. Checks were also made to ensure that there was no mechanical damage due to machining and handling of specimen or jig (i.e. adherend bending).

3.4 Three point bending tests

The three point bend test, usually called the short beam shear test, is one of the most widely used test methods for evaluation of the shearing strength of the composite materials. A study carried out by Roche et al. [111] evaluated the T-peel, wedge opening and single lap shear tests and found that all three methods failed consistently to find defects that were incorporated into the interfacial region of test specimens. Using the three point bend test, they demonstrated that experimental data could provide information that related directly to the interfacial failure of the bonded joint.

The principle of this test consists of applying central loading on a beam in simply supported boundary conditions. In this test, monotonic loading was used and the central deflection and stresses were measured until beam failure or when it reached specified loads. Additional experiments were carried out exclusively on the flat beam section beam to study bending behaviour when subjected to plastic loads and the

initiation point of the joint failure. The experiments were carried out until failure load was reached and a delamination between the adherends was observed. Along with four point bend test, three point bend tests have been regularly adopted in the research of stiffened panels and adhesive joints used in marine structures [18, 65]. The purpose of these research works was directed towards understanding the failure scenario of overall joint instability and the interaction between the adhesive and the upper and lower adherends under compressive loading.

The proposed experiment setup was designed using the standard BS EN 2746:1998 [64]. Another suitable procedure was found in the ISO standard 14679 [66] which was used mainly as a guide. Otherwise, relatively few standard test methods for assessing the performance an adhesively bonded beam joint through three point bending were available for reference. The load-deformation response and strain distribution for each specimen undergoing the three point bend loads were evaluated in the experiments. The three point bending fixture setup is shown in Figure 3.11. The three point test conformed to the requirement of the standard ISO 14679 [66]. With respect to the standard, the three point bending fixture consists of two 15 mm diameter supports that were adjustable horizontally. The support noses could be adjusted to a minimum span of 50 mm and a maximum of 300 mm, which was 15 times the average specimen thickness. To ensure of the support's alignment with the fixture beam, the supports were lightly tapped with a mallet to attain levelness.

Each specimen had a total overlap distance of 30 mm which made the specimen appropriate for extensive deflection without slippages from the supports. A 15 millimetre diameter load application nose was set in the middle of the span of the fixture. Movement of the loading nose was restricted along both the vertical axis through the use of guides/tracks that was connected to the support's stand. The total distance from the top surface of the supports to the base of the fixture is 55 mm. The distance was found suitable to accommodate a 35 mm high displacement transducer located directly below the specimen's bottom surface. After setting up the fixture to the machine, the four screws supporting the three point fixture from the machine base were inspected for proper horizontal alignment with the machine base.

Each specimen was measured in the central section for thickness and width prior to its placement onto the fixture. The specimen was placed on the fixture with the flange facing downwards and the stiffener web on top. The specimen was centrally located in between the supports, and centralised in its width with respect to each support. Reference lines were made on the central point on the upper and lower surfaces of the specimen with a black marker. The lines indicated a reference point for the allocation of the displacement transducer and also to ensure that the loading nose was placed exactly in the middle of the span. This is shown in Figure 3.12. All designated measuring devices (strain gauge, displacement transducer, load cell) were then initialised by the data logger and checked for accuracy and functionality. The experiments were carried out at room temperature conditions of about 21 ±2 °C.

The Lloyd's tensile test machine was able to supply a maximum compressive load of up to 30 kN which was sufficient for the testing of all specimens under elastic loading conditions. Testing was conducted in a displacement control mode with a constant deflection rate of 0.5 mm / min. Three different load levels were considered in the experimentation. The first load was limited to the minimal elastic load of 2 kN and the second load corresponds to 90% of the calculated yield strength of the specimen in bending. Calculation for these 90% loads was carried out by using the stress equation $\sigma_{b,,}$ defined in Appendix B which is found in Pg 180. The yield stress of the mild steel material is substituted into the formulae to determine the yield load (for a given beam section and span), and subsequently factoring it down to 90%. Both elastic loads experiments were carried out on all specimens. The elastic loads were estimated by using the bending beam theory. The third case corresponds to the plastic load, which was assigned to be twice the calculated yield load of the specimen, calculated using the yield strength of the both the adhesive and adherend materials.

The Instron tensile test machine was used to conduct compression tests with plastic loading conditions. The flat beam section specimens were considered for the plastic loads experimentation. Testing was conducted in a displacement control mode with a constant deflection rate of 0.5 mm / min. The machine was equipped with a loadcell

capacity of 200 kN, which was sufficient to supply the necessary plastic loads. The full scale load range was set at 100 kN prior to each test. Load and displacement readings were provided from each test and the test records were plotted on a strip chart recorder. Crosshead displacement readings were measured from an external displacement transducer directly connected to the strip chart recorder.

For each compression test using either machine, the loading nose was positioned near to the specimen's top surface (web for the T&L section or the Inner flange for the inverted T&Z section) with machine's crosshead controls until contact was reached. The loading nose initially induced a small load of about 7-11 N which was also pre-recorded. Such a contact was necessary to prevent a delayed measurement of deflection by the tensile machine. The experimentation for both the solid and bonded specimens was carried out under similar test conditions and three readings were obtained during each test. The 1st reading supplied by the machine consisted of the displacement measured by the displacement of the machine's cross-head from an initial position which plotted a displacement vs. force graph in the computer. The 2nd reading recorded in the data logger machine produced the stress-strain curves as shown in Figure 3.16. The data logger recorded load, displacement and strain measurements in terms of voltage changes. The 2nd reading which was recorded concurrently was used for results comparisons in the form of;

- Flexural stress and deflection of specimens which reached a specified maximum load before or at conventional deflection
- Flexural stress and deflection at failure of specimens which broke before or on reaching conventional deflection

The instrumentation used for the purpose of measurements and data collection was a vital part in the process of experimentation. Prior to the experimentation, consultation was made with the suppliers for the instruments to be used and purchase requirements. The instrumentation used for this research was found to be sufficient for extracting the required data however more elaborate measurement could not be made due to the financial constraints of the project. During the course of the experiment, collection of data was supplied from the four different sources of

instrumentation (load cell, machine displacement, displacement transducer, strain gauges). The load measurement was recorded concurrently in both the assigned computer and the data logger machine during testing. The manufacturers of the Lloyds tensile testing machine have the necessary software which allowed the user to control the machine from a remote source (computer) and also to record real-time data into a XY plot display which was monitored during the progress of the experiment. Results obtained from this source were recorded as an additional reference.

All strain gauges and their accessories used in the course of this research were provided by the Micro-Measurements Division of the Vishay Measurements Group (UK). The main strain gauge used was the universal general-purpose constantan alloy linear strain gauge CEA-06-240UZ-120. These were standard student gauges normally preferred for routine strain-measuring situations, not requiring extremes in performance or environmental capabilities. The strain gauge was used to measure the tensile strain at the bottom surface of the adherend at mid-span. The other strain gauge used was the CEA-13-062UT-120 which was a biaxial "Tee" rosette which was used to measure the poisson ratio in the specimens used for the material properties testing. The recommended procedure for attaching the gauges to the joint was provided by the Vishay Measurements Group (UK) and was strictly adhered to by the author. This ensured proper bonding of the stain gauge and considerable attention to detail to assure a stable and creep-free installation.

Prior to the attachment, the surface must be chemically clean and free of contaminants. Additional surface preparation was carried out according to the recommended surface cleaning procedures as specified for the strain gauge installation. After the proper installation of the strain gauge was carried out, the gauge resistance was measured for each strain gauge. A gauge resistance of 120.0 ohms was required at room temperature (24 °C) with a maximum deviation of 0.6% allowed.

The displacement transducer and related instrumentation was supplied by RDP Electronics (UK). The basic setup consists of a standard LVDT displacement

transducer and an ac powered signal condition unit. The displacement transducer GT0500ZD was used for all experimentation with three point elastic loads. The transducer is designed to provide high precision measurements which proved suitable for the small displacements to be measured in the experiments. The transducer has a working range of ±0.5 mm which allows for the maximum displacement of 1mm with ±0.25 mm for over travel. The selection of this transducer was based on its size requirements for it to be used with the three point bending rig. The gauge's head was positioned at the middle lower surface of the joint using a mounting jig, where the maximum displacement was to be measured.

The transducer was mounted on a mounting bracket which is attached to a vertical stand. The mounting bracket was made from a glass filled nylon (30%) material and its design has been adopted from the manufacturer's MB01 for similar LVDT transducers. The mounting brackets were bolted to the stand with clamping nuts and bolts. The clamping pressure that was used to hold the transducer was transmitted by the tightening of the bolt. It was suggested from the mounting instructions provided that the bracket was sufficient to hold the transducer as with a stroke of 10 mm or less.

The 3531 ORION data acquisition system was used in the experiments to record the data obtained from the measuring devices. The data logger was powered from an ac source and the system accepted a wide range of analogue and digital inputs. The setup and operation was achieved by using the front panel which contained control keys for the main functions. Prior to a setup of the system, the 3 measuring devices (load, displacement and strain) with their output wires are attached to the input connector of the data logger. Upon completion, the system was configured with a channel and task definition procedure. Specific details such as gauge factor and bridge configuration for the strain gauge were defined and programmed in the channel definition procedure. Groups of channels are then allocated to a specific logging task in the task definition procedure. During experimentation, the displacement, force and strain gauge measurement were stored in a floppy disk in the system's built in disk drive. The data recording process was also monitored with a monitoring facility

which provides an instantaneous display of the current readings from the three channels. This facility was especially useful for checking the output coming from the measuring devices and determined if an initialization of current into the devices is required.

Form	: paste
Colour	: beige
Odour	: slight
Thermal decomposition	: > 200 °C
Flash point	: > 100 °C Method:estimated
Vapour pressure	: <0.01 Pa At 20 °C Method:estimated
Density	: 1.175 g/cm^3 at 25 °C
Water solubility	: at 20 °C Note: practically insoluble
Miscibility with water	: immisicible at 20 °C
Vicosity, dynamic	: 900 – 2,300 Pa.s at 25 °C

Table 3.1 The physical and chemical properties of the Araldite AV119 material.

	Adherend (080M15)	Adhesive (AV119)
E (MPa)	205300	3624
ν	0.23	0.36
σ* (MPa)	556	52.05
ε*	> 0.0371	0.043207

4

5 E, Young's modulus; ν, Poisson's ratio; σ*, ultimate strength; ε*, ultimate strain.

Table 3.2 Material properties determined from experiments

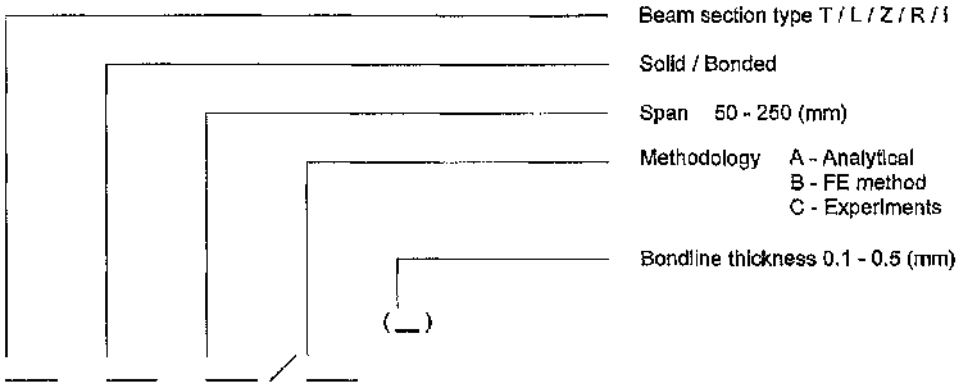

Table 3.3 Designation of specimens.

S/N	TEST SPECIMEN	STIFFENER HEIGHT (mm)	PLATE THICKNESS (mm)	ADHESIVE THICKNESS (mm)	2ND MOMENT OF AREA (mm^4)	STRUCTURAL STIFFNESS (MPa)	LOCATION OF NEUTRAL AXIS FROM BOTTOM SURFACE (mm)
1	TS250 / A	15.0	5.0	NA	6520.833	1336770833	6.500
2	TS200 / A	15.0	5.0	NA	6520.833	1336770833	6.500
3	TS150 / A	15.0	5.0	NA	6520.833	1336770833	6.500
4	TS075 / A	15.0	5.0	NA	6520.833	1336770833	6.500
5	TS050 / A	15.0	5.0	NA	6520.833	1336770833	6.500
6	TB250 / A	14.5	5.0	0.5	6520.833	1334378020	6.500
7	TB200 / A	14.5	5.0	0.5	6520.833	1334378020	6.500
8	TB150 / A	14.5	5.0	0.5	6520.833	1334378020	6.500
9	TB075 / A	14.5	5.0	0.5	6520.833	1334378020	6.500
10	TB050 / A	14.5	5.0	0.5	6520.833	1334378020	6.500
11	LS250 / A	15.0	5.0	NA	6440.972	1320339206	6.389
12	LS200 / A	15.0	5.0	NA	6440.972	1320339206	6.389
13	LS150 / A	15.0	5.0	NA	6440.972	1320339206	6.389
14	LS075 / A	15.0	5.0	NA	6440.972	1320339206	6.389
15	LS050 / A	15.0	5.0	NA	6440.972	1320339206	6.389
16	LB250 / A	14.5	5.0	0.5	6440.972	1319071265	6.389
17	LB200 / A	14.5	5.0	0.5	6440.972	1319071265	6.389
18	LB150 / A	14.5	5.0	0.5	6440.972	1319071265	6.389
19	LB075 / A	14.5	5.0	0.5	6440.972	1319071265	6.389
20	LB050 / A	14.5	5.0	0.5	6440.972	1319071265	6.389
21	ZS250 / A	15.0	5.0	NA	9270.833	1900520833	7.500
22	ZS200 / A	15.0	5.0	NA	9270.833	1900520833	7.500
23	ZS150 / A	15.0	5.0	NA	9270.833	1900520833	7.500
24	ZS075 / A	15.0	5.0	NA	9270.833	1900520833	7.500
25	ZS050 / A	15.0	5.0	NA	9270.833	1900520833	7.500
26	ZB250 / A	15.0	5.0	0.5	9270.833	1895399375	7.500
27	ZB200 / A	15.0	5.0	0.5	9270.833	1895399375	7.500
28	ZB150 / A	15.0	5.0	0.5	9270.833	1895399375	7.500
29	ZB075 / A	15.0	5.0	0.5	9270.833	1895399375	7.500
30	ZB050 / A	15.0	5.0	0.5	9270.833	1895399375	7.500
31	RS250 / A	7.8	7.8	NA	7758.073	1590404948	7.750
32	RS200 / A	7.8	7.8	NA	7758.073	1590404948	7.750
33	RS150 / A	7.8	7.8	NA	7758.073	1590404948	7.750
34	RS075 / A	7.8	7.8	NA	7758.073	1590404948	7.750
35	RS050 / A	7.8	7.8	NA	7758.073	1590404948	7.750
36	RB250 / A	7.5	7.5	0.5	7758.073	1590352474	7.750
37	RB200 / A	7.5	7.5	0.5	7758.073	1590352474	7.750
38	RB150 / A	7.5	7.5	0.5	7758.073	1590352474	7.750
39	RB075 / A	7.5	7.5	0.5	7758.073	1590352474	7.750
40	RB050/ A	7.5	7.5	0.5	7758.073	1590352474	7.750
41	IS250/ A	15.0	5.0	NA	11520.833	2361170833	8.500
42	IS200/ A	15.0	5.0	NA	11520.833	2361170833	8.500
43	IS150/ A	15.0	5.0	NA	11520.833	2361170833	8.500
44	IS075/ A	15.0	5.0	NA	11520.833	2361170833	8.500
45	IS050/ A	15.0	5.0	NA	11520.833	2361170833	8.500
46	IB250/ A	14.5	5.0	0.5	11520.833	2356439479	8.500
47	IB200/ A	14.5	5.0	0.5	11520.833	2356439479	8.500
48	IB150/ A	14.5	5.0	0.5	11520.833	2356439479	8.500
49	IB075/ A	14.5	5.0	0.5	11520.833	2356439479	8.500
50	IB050/ A	14.5	5.0	0.5	11520.833	2356439479	8.500

Table 3.4 (a) Specimens listed in Group 1: Comparison between solid and bonded specimens.

S/N	TEST SPECIMEN	STIFFENER HEIGHT (mm)	PLATE THICKNESS (mm)	ADHESIVE THICKNESS (mm)	2ND MOMENT OF AREA (mm^4)	STRUCTURAL STIFFNESS (MPa)	LOCATION OF NEUTRAL AXIS FROM BOTTOM SURFACE (mm)
51	TB250/ A (0.4)	14.6	5.0	0.4	6520.833	1334711503	6.500
52	TB200/ A (0.4)	14.6	5.0	0.4	6520.833	1334711503	6.500
53	TB150/ A (0.4)	14.6	5.0	0.4	6520.833	1334711503	6.500
54	TB075/ A (0.4)	14.6	5.0	0.4	6520.833	1334711503	6.500
55	TB050/ A (0.4)	14.6	5.0	0.4	6520.833	1334711503	6.500
56	TB250/ A (0.3)	14.7	5.0	0.3	6520.833	1335111481	6.500
57	TB200/ A (0.3)	14.7	5.0	0.3	6520.833	1335111481	6.500
58	TB150/ A (0.3)	14.7	5.0	0.3	6520.833	1335111481	6.500
59	TB075/ A (0.3)	14.7	5.0	0.3	6520.833	1335111481	6.500
60	TB050/ A (0.3)	14.7	5.0	0.3	6520.833	1335111481	6.500
61	TB250/ A (0.2)	14.8	5.0	0.2	6520.833	1335583998	6.500
62	TB200/ A (0.2)	14.8	5.0	0.2	6520.833	1335583998	6.500
63	TB150/ A (0.2)	14.8	5.0	0.2	6520.833	1335583998	6.500
64	TB075/ A (0.2)	14.8	5.0	0.2	6520.833	1335583998	6.500
65	TB050/ A (0.2)	14.8	5.0	0.2	6520.833	1335583998	6.500
66	TB250/ A (0.1)	14.9	5.0	0.1	6520.833	1336135101	6.500
67	TB200/ A (0.1)	14.9	5.0	0.1	6520.833	1336135101	6.500
68	TB150/ A (0.1)	14.9	5.0	0.1	6520.833	1336135101	6.500
69	TB075/ A (0.1)	14.9	5.0	0.1	6520.833	1336135101	6.500
70	TB050/ A (0.1)	14.9	5.0	0.1	6520.833	1336135101	6.500
71	LB250/ A (0.4)	14.6	5.0	0.4	6440.972	1319249100	6.389
72	LB200/ A (0.4)	14.6	5.0	0.4	6440.972	1319249100	6.389
73	LB150/ A (0.4)	14.6	5.0	0.4	6440.972	1319249100	6.389
74	LB075/ A (0.4)	14.6	5.0	0.4	6440.972	1319249100	6.389
75	LB050/ A (0.4)	14.6	5.0	0.4	6440.972	1319249100	6.389
76	LB250/ A (0.3)	14.7	5.0	0.3	6440.972	1319466958	6.389
77	LB200/ A (0.3)	14.7	5.0	0.3	6440.972	1319466958	6.389
78	LB150/ A (0.3)	14.7	5.0	0.3	6440.972	1319466958	6.389
79	LB075/ A (0.3)	14.7	5.0	0.3	6440.972	1319466958	6.389
80	LB050/ A (0.3)	14.7	5.0	0.3	6440.972	1319466958	6.389
81	LB250/ A (0.2)	14.8	5.0	0.2	6440.972	1319728485	6.389
82	LB200/ A (0.2)	14.8	5.0	0.2	6440.972	1319728485	6.389
83	LB150/ A (0.2)	14.8	5.0	0.2	6440.972	1319728485	6.389
84	LB075/ A (0.2)	14.8	5.0	0.2	6440.972	1319728485	6.389
85	LB050/ A (0.2)	14.8	5.0	0.2	6440.972	1319728485	6.389
86	LB250/ A (0.1)	14.9	5.0	0.1	6440.972	1320037924	6.389
87	LB200/ A (0.1)	14.9	5.0	0.1	6440.972	1320037924	6.389
88	LB150/ A (0.1)	14.9	5.0	0.1	6440.972	1320037924	6.389
89	LB075/ A (0.1)	14.9	5.0	0.1	6440.972	1320037924	6.389
90	LB050/ A (0.1)	14.9	5.0	0.1	6440.972	1320037924	6.389

Table 3.4 (b) Specimens listed in Group 2: Effects of varying adhesive thickness under elastic loading conditions.

91	RB250/ A $^{(0.4)}$	7.5	7.5	0.4	7608.883	1559794217	7.700
92	RB200/ A $^{(0.4)}$	7.5	7.5	0.4	7608.883	1559794217	7.700
93	RB150/ A $^{(0.4)}$	7.5	7.5	0.4	7608.883	1559794217	7.700
94	RB075/ A $^{(0.4)}$	7.5	7.5	0.4	7608.883	1559794217	7.700
95	RB050/ A $^{(0.4)}$	7.5	7.5	0.4	7608.883	1559794217	7.700
96	RB250/ A $^{(0.3)}$	7.5	7.5	0.3	7461.619	1529620509	7.650
97	RB200/ A $^{(0.3)}$	7.5	7.5	0.3	7461.619	1529620509	7.650
98	RB150/ A $^{(0.3)}$	7.5	7.5	0.3	7461.619	1529620509	7.650
99	RB075/ A $^{(0.3)}$	7.5	7.5	0.3	7461.619	1529620509	7.650
100	RB050/ A $^{(0.3)}$	7.5	7.5	0.3	7461.619	1529620509	7.650
101	RB250/ A $^{(0.2)}$	7.5	7.5	0.2	7316.267	1499831308	7.600
102	RB200/ A $^{(0.2)}$	7.5	7.5	0.2	7316.267	1499831308	7.600
103	RB150/ A $^{(0.2)}$	7.5	7.5	0.2	7316.267	1499831308	7.600
104	RB075/ A $^{(0.2)}$	7.5	7.5	0.2	7316.267	1499831308	7.600
105	RB050/ A $^{(0.2)}$	7.5	7.5	0.2	7316.267	1499831308	7.600
106	RB250/ A $^{(0.1)}$	7.5	7.5	0.1	7172.815	1470426570	7.550
107	RB200/ A $^{(0.1)}$	7.5	7.5	0.1	7172.815	1470426570	7.550
108	RB150/ A $^{(0.1)}$	7.5	7.5	0.1	7172.815	1470426570	7.550
109	RB075/ A $^{(0.1)}$	7.5	7.5	0.1	7172.815	1470426570	7.550
110	RB050/ A $^{(0.1)}$	7.5	7.5	0.1	7172.815	1470426570	7.550
121	RB150/ A $^{(1)}$	7.5	7.5	1	8533.333	1748913542	8.000

Table 3.4 (c) Specimens listed in Group 3: Effects of varying adhesive thickness under elastic-plastic loading conditions.

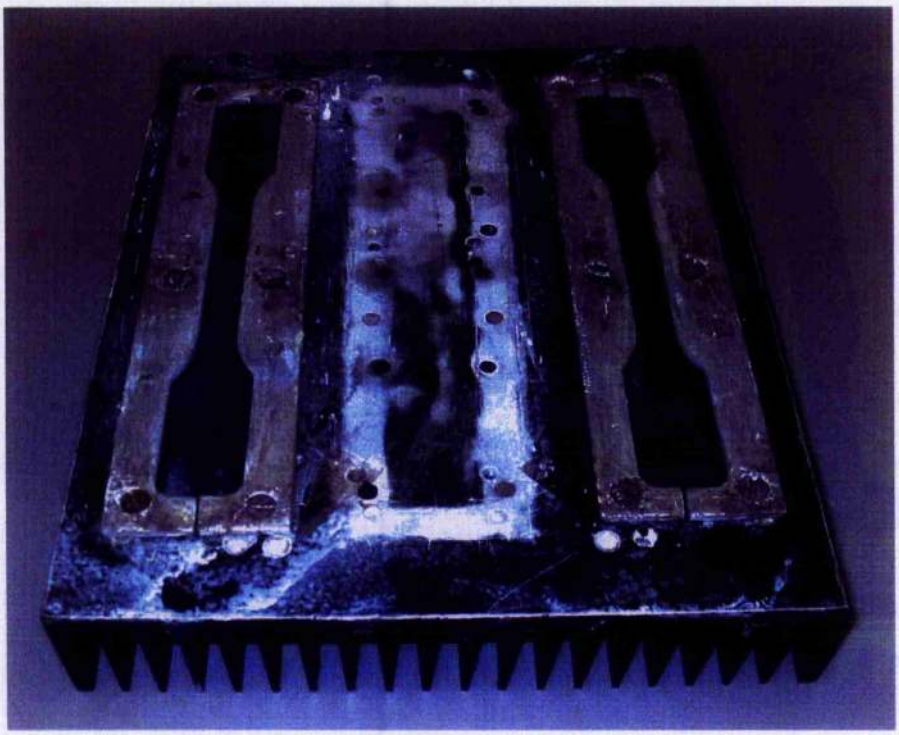

Figure 3.1 Heat exchanger type bonding jig

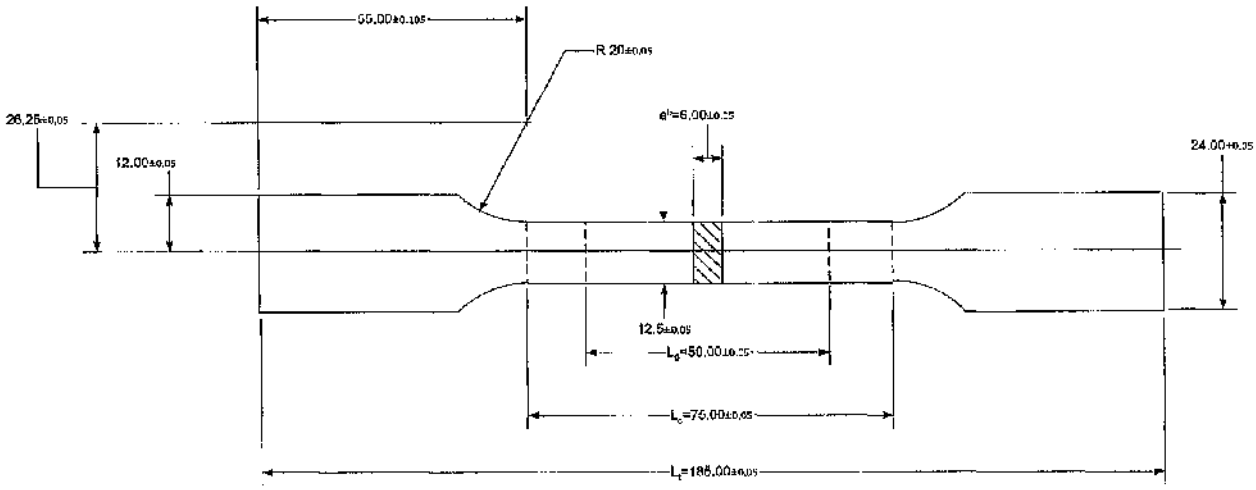

Symbol	Description	Length (mm)
L_o	Gauge length	50
L_c	Parallel length	65
L_t	Total length	180
b	Width of parallel length	12.6
a[b]	Thickness of test piece	3

Figure 3.2 Dimensions for test piece Annex D in EN 10002-1:2001

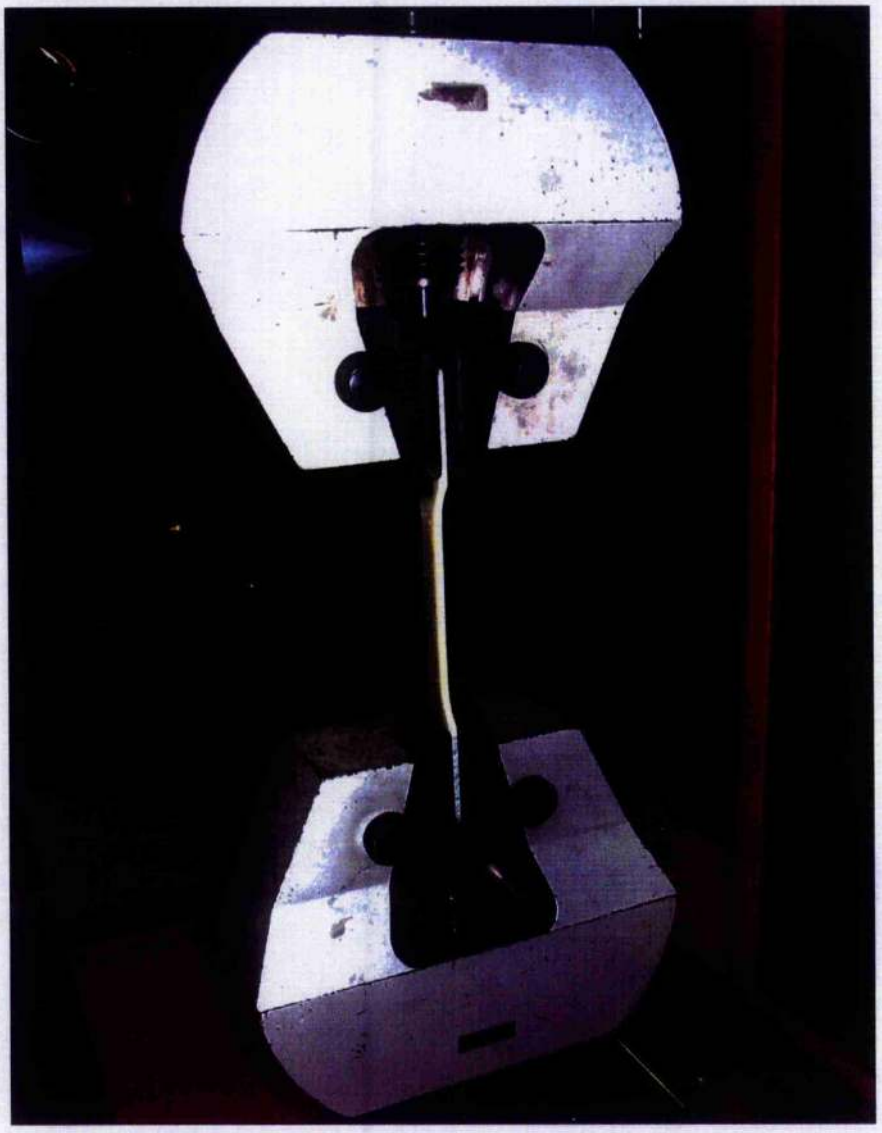

Figure 3.3 Tensile Test of the AV119 adhesive material.

Amops, Version 1.1, 2003

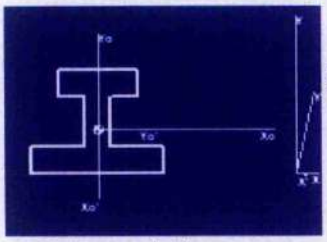

Input File: ipanel.tgf

AN I-SECTION BEAM

Area and first moments about X-Y drawing axes

Area of shape, A	=	250	-
X co-ordinate of centre of area, X_c	=	-37.5	-
Y co-ordinate of centre of area, Y_c	=	8.5	-
First moment of area about X-axis, , M_x	=	2125	-
First moment of area about Y-axis, , M_y	=	-9375	-

Second moments of area about X-Y drawing axes

Second moment of area about X-axis, I_x	=	2.958E+4	-
Second moment of area about Y-axis, I_y	=	3.596E+5	-
Polar second moment of area, I_z	=	3.892E+5	-
Product moment of area, I_{xy}	=	-7.969E+4	-
Radius of gyration about X-axis, k_x	=	10.88	-
Radius of gyration about Y-axis, k_y	=	37.92	-
Polar radius of gyration, k_z	=	39.45	-

Second moments about X'-Y' principal axes on drawing origin

Angle of principal axes, ***alpha***	=	-12.89	degree
Second moment of area about X'-axis, $I_{x'}$	=	1.135E+4	-
Second moment of area about Y'-axis, $I_{y'}$	=	3.778E+5	-
Radius of gyration about X'-axis, $k_{x'}$	=	6.737	-
Radius of gyration about Y'-axis, $k_{y'}$	=	38.88	-

Figure 3.4 Section properties of the I section as obtained from AMOPS version 11.

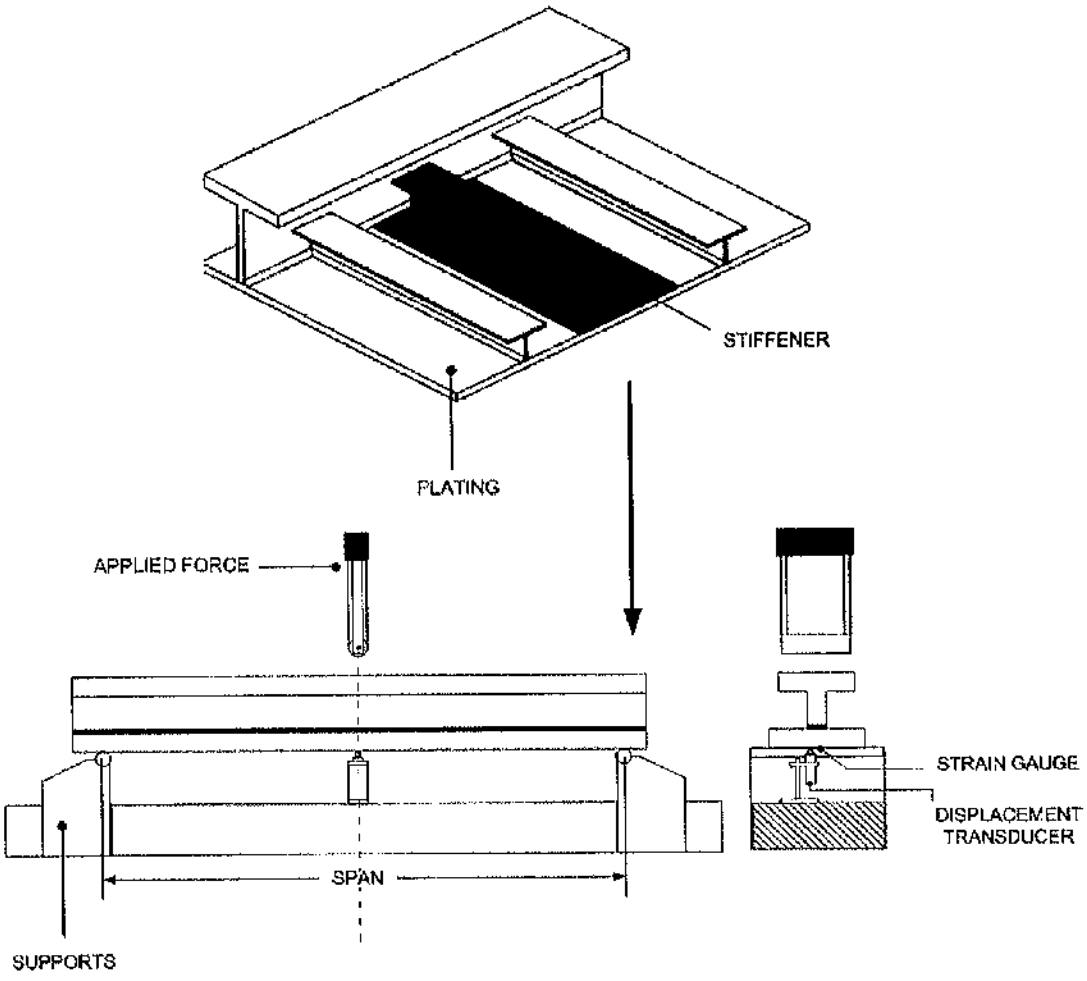

Figure 3.5 Idealised model for stress analysis.

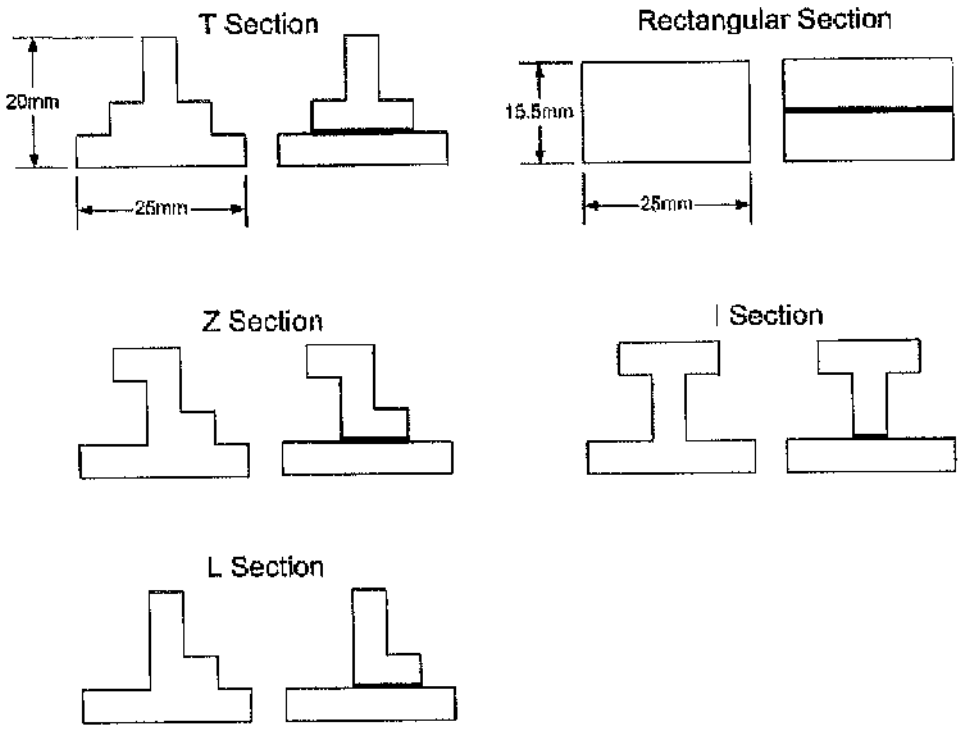

Figure 3.6 Cross section details of the solid and bonded (0.5 Adhesive Thickness) specimens.

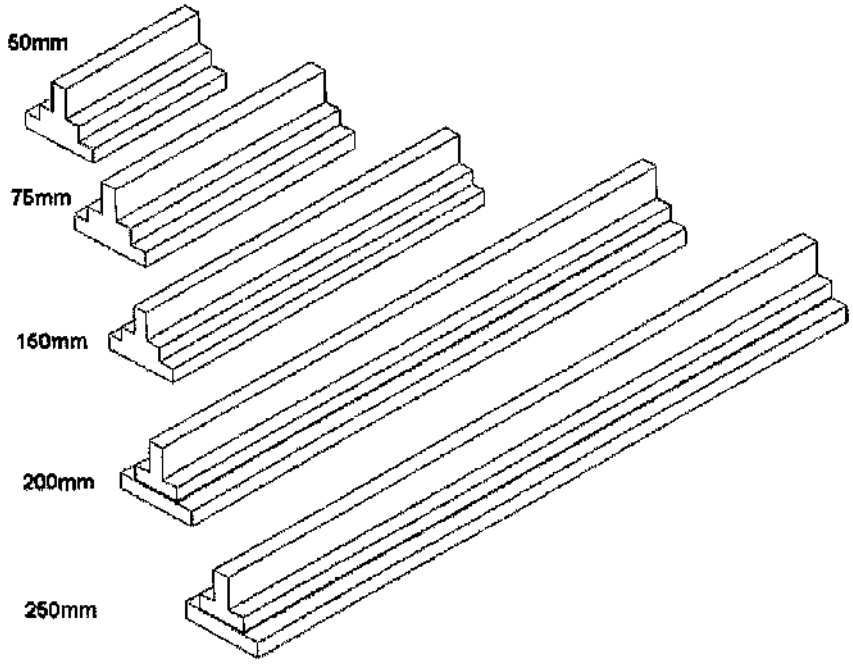

Figure 3.7 Different spans used for the experimental work.

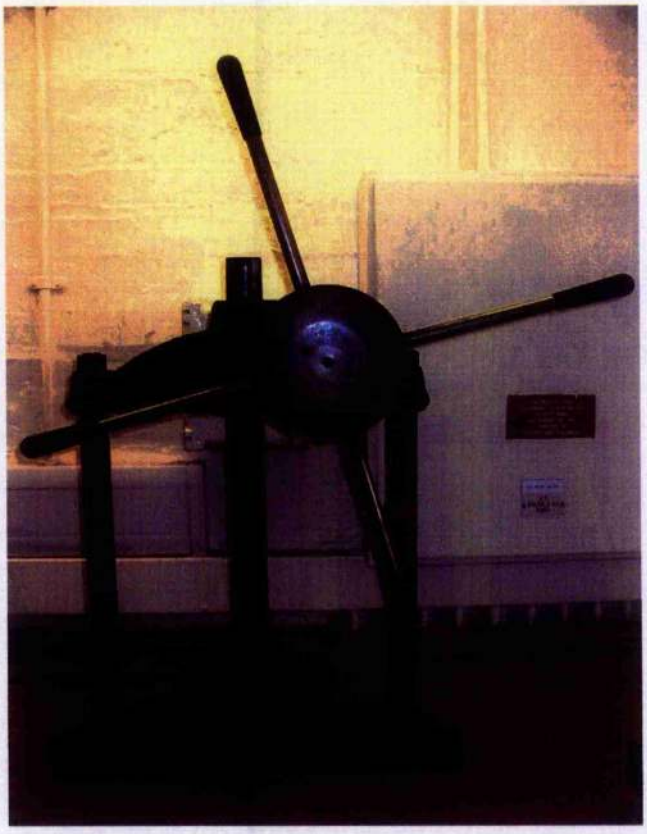

Figure 3.8 The manual bending press which was adopted for the remedy of distorted adherend specimens.

Figure 3.9 Location of distributed wires within the bonded area of the joint.

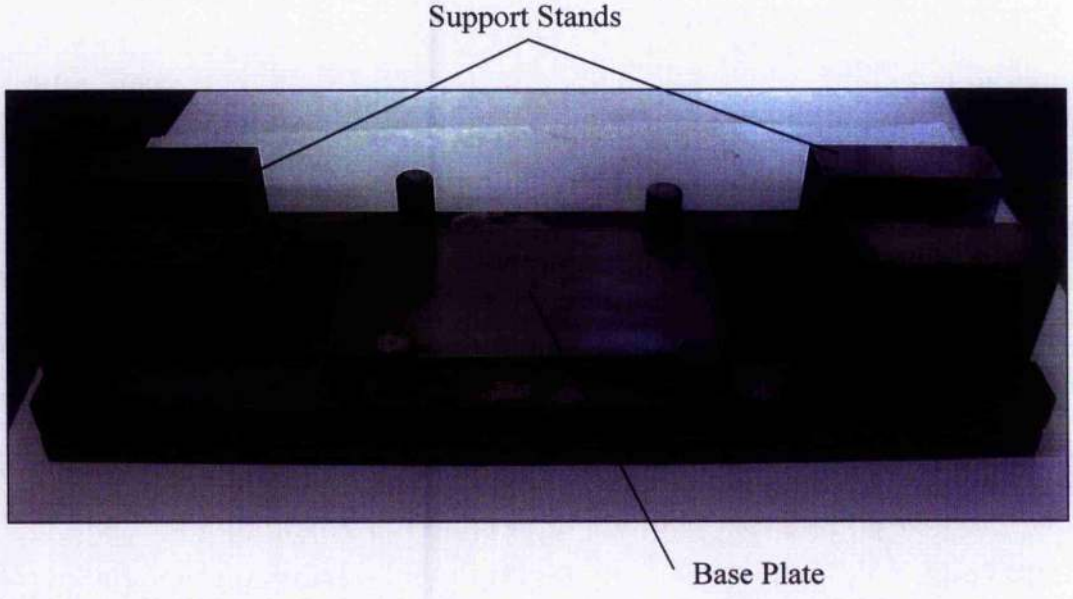

Figure 3.10 Diagram of the bonding jig used in specimen fabrication.

Figure 3.11 Diagram of the three point bend setup.

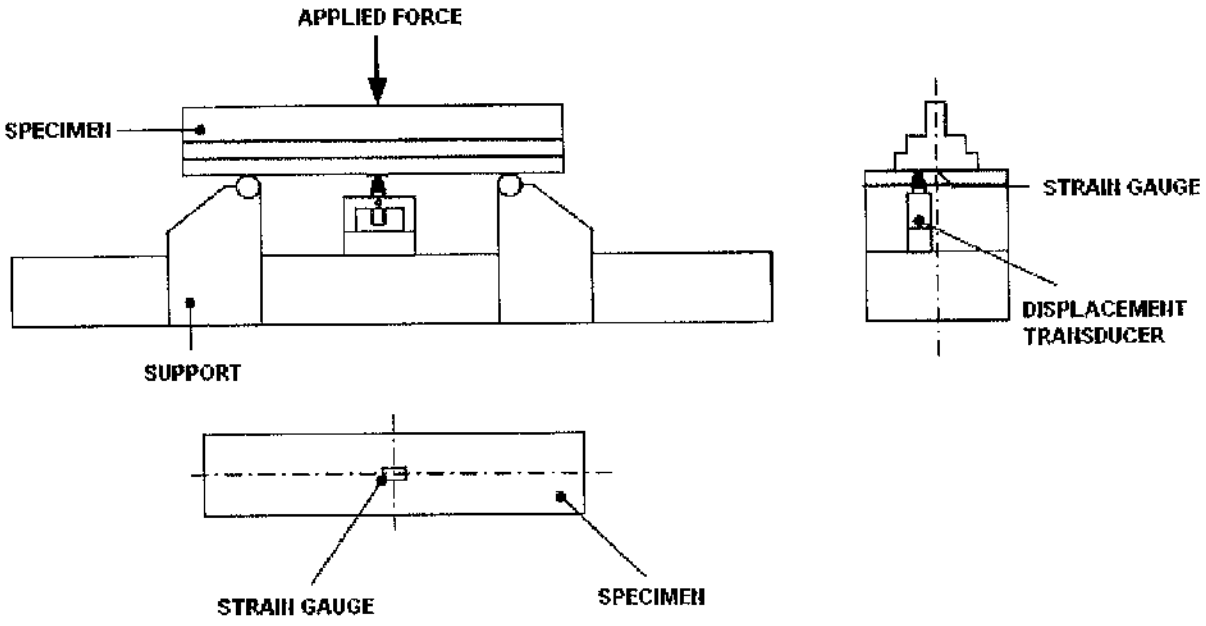

Figure 3.12 Schematic of the location of the strain gauge and the displacement transducer.

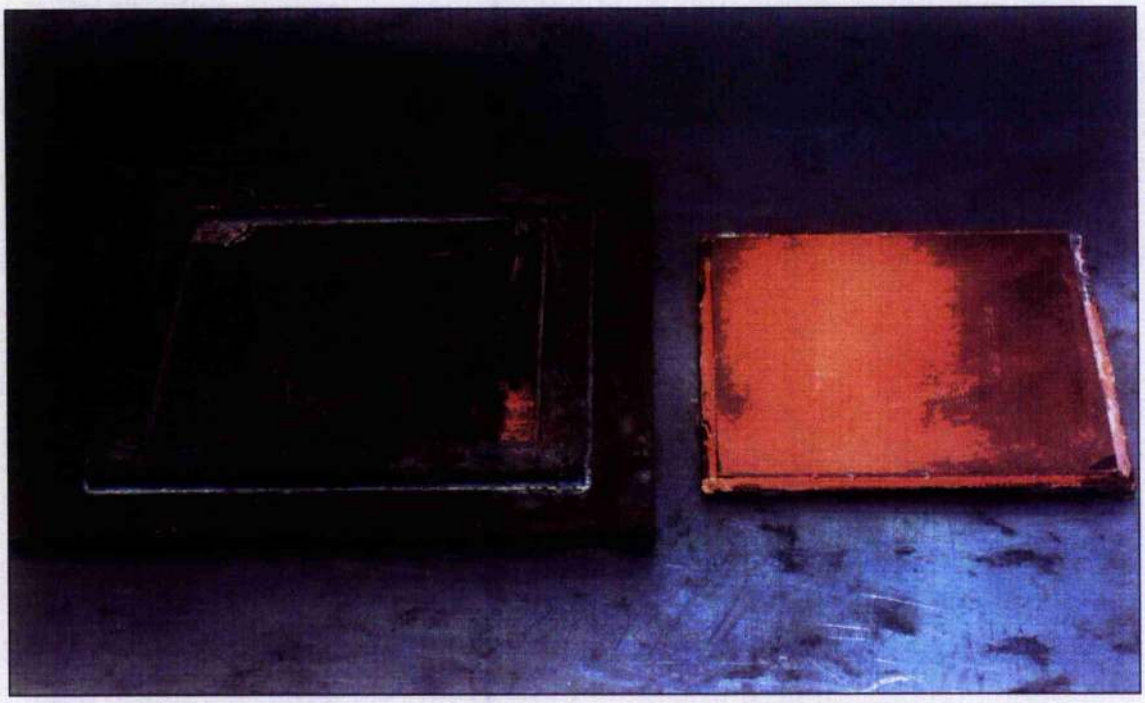

Figure 3.13 Jig used for the fabrication of the adhesive plaque.

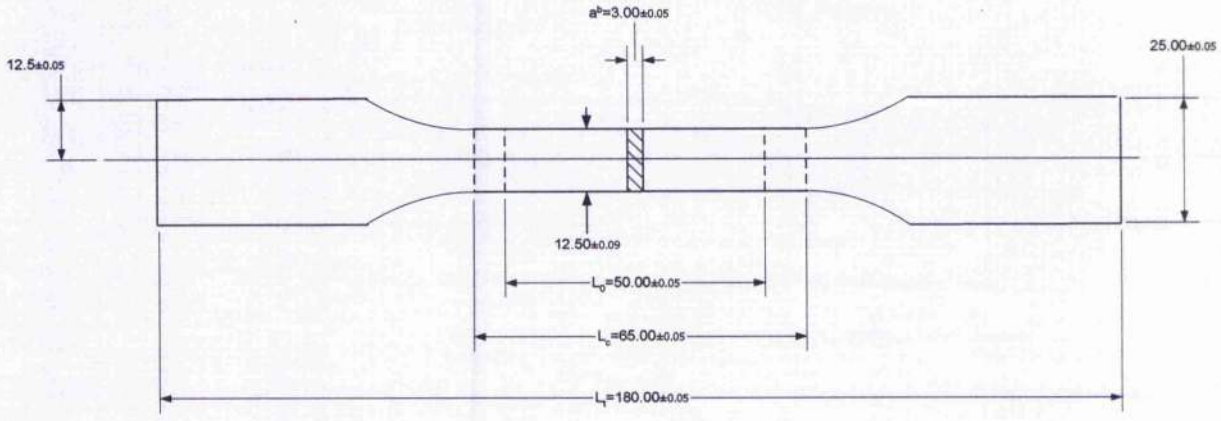

Symbol	Description	Length (mm)
L_o	Gauge length	50
L_c	Parallel length	65
L_t	Total length	180
b	Width of parallel length	12.6
a^b	Thickness of test piece	3

Figure 3.14 Dimensions for test piece 1B in BS EN ISO 527-1:1996

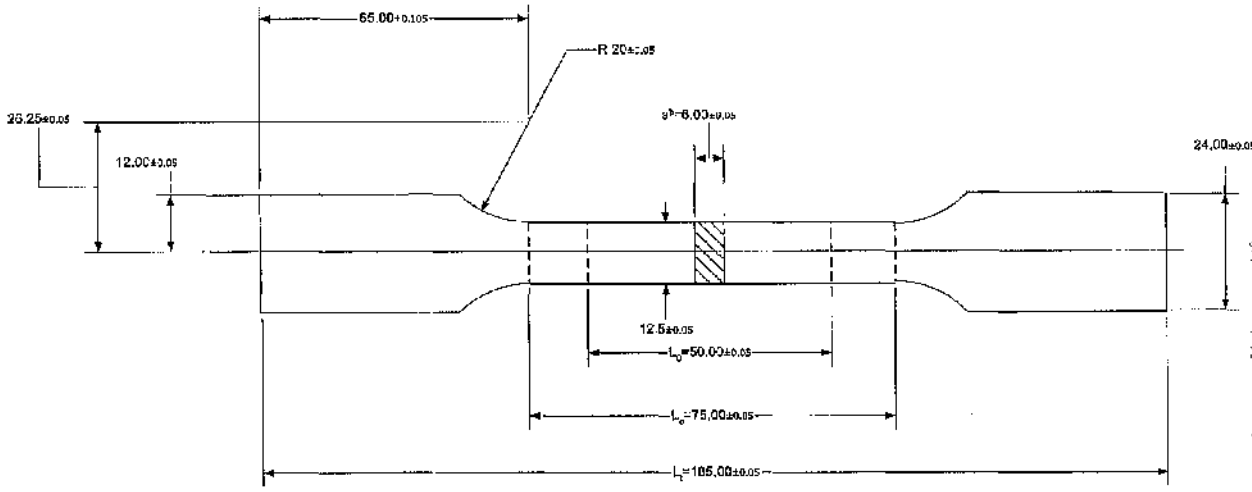

Symbol	Description	Length (mm)
L_o	Gauge length	50
L_c	Parallel length	65
L_t	Total length	180
b	Width of parallel length	12.6
a^b	Thickness of test piece	3

Figure 3.15 Dimensions for test piece Annex D in EN 10002-1:2001

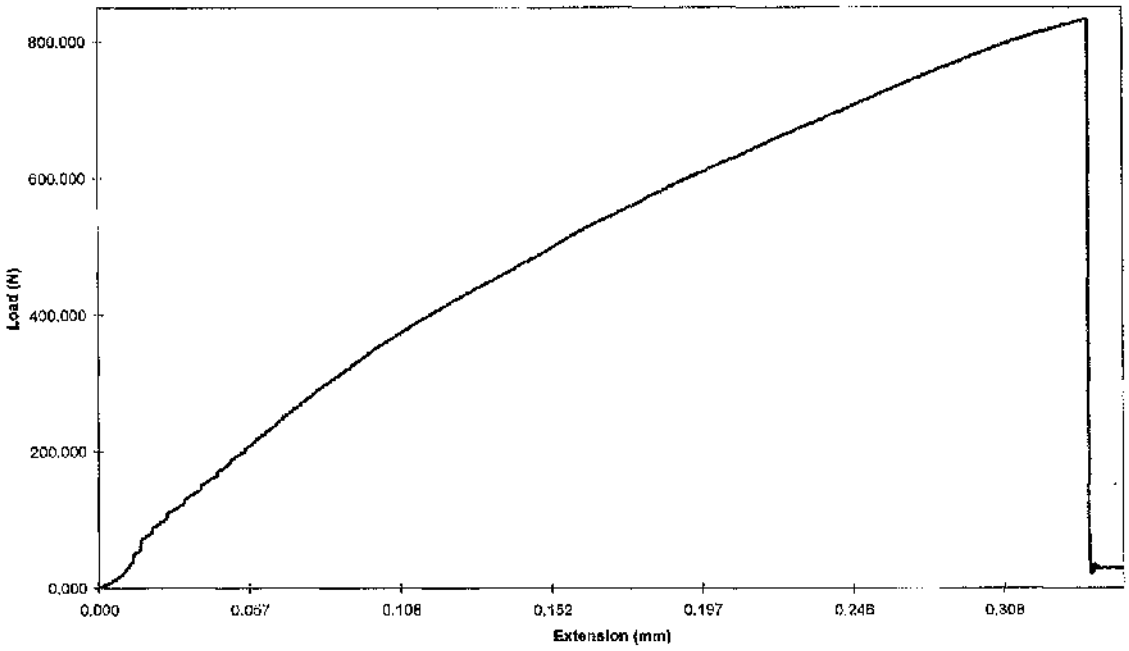

Figure 3.16 Stress vs. strain curve obtained on uniaxial tensile testing of the adhesive material.

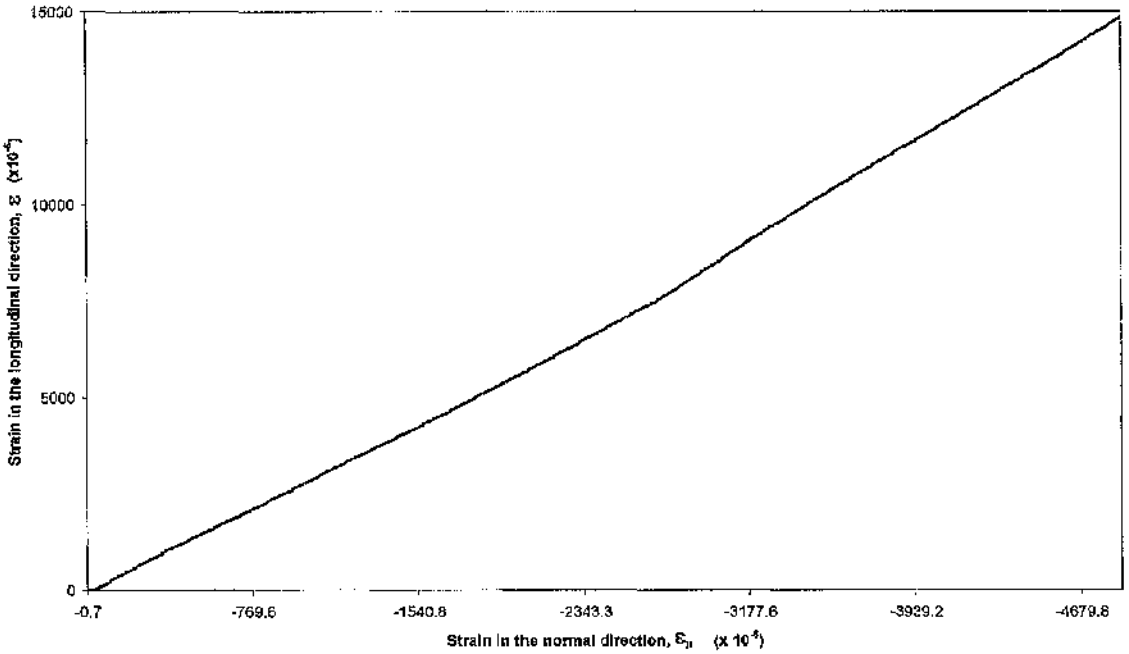

Figure 3.17 The longitudinal versus normal strain curve obtained from the uniaxial tensile testing of the adhesive material.

CHAPTER FOUR

THEORECTICAL WORK

4.1 The solid beam theory

Adhesive bonds are made of one or more adherends and an adhesive. When an adherend is removed from an adhesive or an adhesive bond is subjected to a force, the adherend often acts as though it is a bending beam. The bonded beam sections in the following discussion have been analysed as though the adherends are bending beams. It is therefore appropriate to discuss briefly the basic theory of bending of beams in this chapter. A beam subjected to a three point bending load with simply supported conditions represents a statically determinate structure. The reactions at the supports produced by a given load can be determined from the equation of statics. Much of the discussion shown here was taken from *Strength of Materials* by Timoshenko [80].

One dimensional mathematical models of structural beams are constructed on the basis of beam theories. Because beams are actually three-dimensional solids, all models necessarily involve some forms of approximation to the underlying physics. The simplest and best known models for straight, prismatic beams are the shear-indeformable Euler-Bernoulli theory, also called as the classical beam theory or engineering beam theory, and the shear deformable Timoshenko beam theory. The latter is the theory normally found in fundamental mechanics of materials textbooks and was emphasized in this study [112,113]. The main reason for using Timoshenko's beam theory is that it is simpler to use and can manipulated relatively uncomplicated for the beam configurations being studied here. Advance Timoshenko beam theory has been used to place additional importance in the dynamics and vibration of beam structures [69]. The Euler-Bernoulli theory has also been commonly used in the analysis of various beam structures research [67,68].

A beam that is not subjected to any loads is not deflected. When loads are applied to a beam, its longitudinal axis is deformed into a curve. Imaginary lines drawn perpendicular to the beam length turn in towards the side to which the force is

applied. The imaginary lines drawn parallel to the length of the beam stay parallel to the sides of the beam for small increments down the length of the beam. However, the lines assume the same radius of curvature that the beam assumes under the applied force. At the centre of the beam is a line which does not change in length. This is represented by the neutral axis. The length of the parallel lines changes. Above the neutral axis, the lines shorten in length (compression) while below the neutral axis; the lines become longer (tension).

The resulting strains and stresses in a beam are directly related to the curvature of the deflection curve. Appendix B describes the solid beam theory in greater detail which yields relevant equations for bending stress, shear stress and deflection. In summary, the bending stresses vary linearly with the distance from the neutral axis, as shown in Figure 4.1. The maximum tensile and compressive bending stresses acting at any given cross section occur at points located farthest from the neutral axis. Calculation of shear stresses has been focused on horizontal shear rather than vertical shear, assuming both having the same magnitudes. The existence of horizontal shear stresses in a beam is shown in the bending of two separate beams in Figure 4.2. Since the friction between the beams is small, the beams will bend independently. Each beam will be in compression above its own neutral axis and in tension below its neutral axis, and therefore the bottom surface of the upper beam will slide with respect to the top surface of the lower beam. The shear stress distribution of various beam sections considered in this study is shown in Figure 4.3.

4.2 Sandwich beam theory

The principle of using two cooperating faces with a distance between them was introduced by Delau in about 1820. Since then, the use of sandwich construction has been restricted to less spectacular circumstances. Sandwich constructions aroused great interest only after the Second World War, when the speed of aircraft became so high that laminar-flow sections were considered to be an extremely desirable design feature. The adapted use of the sandwich panel into the aircraft structure was mainly due to the shortage of other materials being available in England during the war.

The simplest type of sandwich construction normally consist of having two thin, stiff, strong sheets of dense material separated by a thick layer of low density material which may be less stiff and less strong. A typical sandwich is normally built up of three elements, consisting of two faces, a core and the joints. The joint is normally made up of the adhesive material that bonds the faces to the core. A comprehensive introduction to the subject of sandwich construction and the development of theoretical analyses up to 1965 is given by Allen [13], and lately updated by Zenkert [70]. Apart from Allen's sandwich theory, there are very few papers that have been published which deal with the bending and buckling of sandwich panels with cores rigid enough to make a significant contribution to the bending stiffness of the panel. Hence Allen's sandwich theory has been effectively used for analysis of T beam configuration in bonded structures [11,33]. In the analytical work that is presented in this chapter, the author has taken view that the adhesively bonded steel joint can be idealised as a sandwich beam under concentrated normal loading. . These faces of the idealised sandwich are thus made up of the adherend mild steel and its core made up purely of the adhesive Araldite® AV119 material.

4.2.1 Definition of a sandwich model

The adhesively bonded stiffened panel/beam used in ship construction is a good representative of a sandwich structure. The structure represents a good example of the optimum use of dissimilar materials. Figure 4.4 shows a schematic of the T section bonded beam. According to the figure, the upper and lower adherends are separated by an adhesive material of thickness c; with the overall width of the beam is b. The distance between the centroid of the upper and lower adherend is represented by d. During calculations, it was assumed that the adherend and adhesive materials were both isotropic.

The upper and lower adherends represent the strong face material in a sandwich while the adhesive represents the weaker core. The upper adherend is the beam element in a panel, normally subjected to lateral loads and moments. In the modelling of stiffened plate panels, the resulting overall stiffness of the structure is contributed mainly by the geometric and material properties of the beam element. The lower adherend which is represented by the plate element is normally made relatively thin in the fabrication of

the panel. Plates represent the important load-carrying parts of the ship hull. The plate element is normally loaded in such way that they have deformations out of their own plane. These deformations can be attributed to the lateral forces or forces along the plate's edge. The core material is represented by the bonding mechanism of the structure. The loads are normally transmitted through the faces by this flexible core material. As a result, the behaviour of the core is more complex than that of the faces.

The core has to fulfil the most complex demands in the sandwich structure. The core by itself has several vital functions. Firstly, the core should be stiff enough in the directions perpendicular to the faces (compression) to ensure that both faces remain the correct distance apart. If the core is significantly stiff enough, it may make a useful contribution to the bending stiffness of the panel as a whole. Such knowledge of the behaviour of the adhesive layer in sandwich beams is important and will help researchers and designers to gain an insight into the underlying mechanisms that significantly affect the performance of sandwich structures. The second function of the core requires it to be stiff enough in shear to ensure that when the panel is bent the faces do not slide over each other. The result of a core that is weak in shear will mean that the faces merely behave as two independent beams or panels and the sandwich effect is lost entirely. In bending or compression, the shear deflection in the core is therefore not ignored and was implemented in the calculations.

The face components must possess sufficient stiffness in the direction normal to the plane of each face. The main function of the faces in a sandwich structure is to carry the overall tensile and compressive stresses in the sandwich. Localised and distributed loading are not unusual in sandwich structures and they often occur as a result of an accidental impact and excessive weight. Bending and in-plane loadings will then be subjected directly onto the faces. The effectiveness of the faces to resist the design load depends on the strength and stiffness of both face plates. The faces also tend to spread the load transmitted to the core over a larger area and thus reduce the maximum core compressive stress.

4.2.2 Global deformation of sandwich beams with thick faces

There exists a general realisation that simple structural theories such as the classical beam or plate theory are not adequate to understand stress and strain distributions in a sandwich structure, particularly under relatively concentrated loads. However a number of advances have been made in the analysis of sandwich structures and the linear elastic theory of sandwich structures under uniform loading has since been well established [13,42]. Petras & Sutcliffe have used the sandwich beam theory developed by Allen [13] in their investigation of sandwich beams subjected to loading under three point bending and found that the experimental data agree satisfactorily with the theoretical predictions [71]. A similar study carried out by Pye & Ledbetter showed how the sandwich theory could be adopted in their analyses of the composite action in T-shaped cross section beams undergoing four point bending loading conditions [11].

However the limits of applicability of linear theories of sandwich structures should be investigated as a function of geometric and material parameters of the sandwich beams used in various applications. Such effects was investigated numerically and experimentally to verify existing mathematical models and to assist in the development of new ones. An example of such work was carried out by Tuhkuri [41]. He proposed a mathematical model that can be successfully used in analysing sandwich beams under concentrated normal loading in the elastic range, focusing on both the global deformation of the entire sandwich structure as well as the local effects of loading on the faces.

In the different versions of the sandwich theory developed separately by Allen & Plantema [13,42], various combinations of the following five assumptions shown below were made:

1. The core has no rigidity in the plane parallel to the faces
2. The shear rigidity of the core in planes perpendicular to the faces is finite; Deflections are small
3. The core is infinitely stiff in planes perpendicular to the faces; i.e. the thickness of the core is not changing

4. The faces are so thin that the bending stiffness of them about their own centroidal axis can be neglected

4.2.3 Beam theory for sandwich panels

In this section we outline the elastic analysis of sandwich beams which was similar to the bonded beams subjected to three point bending. This analysis was used to evaluate the stresses in the core and the skin of the bonded beam. For adaptation of the sandwich theory onto the analysis of the bonded beam sections, the core of the sandwich was replaced by the adhesive layer and the upper and lower faces are replaced by the stiffener and the plate. The stresses in the face and the core may be determined by the use of ordinary bending theory, adapted to the composite nature of the cross section. Because sections remain plane and perpendicular to the longitudinal axis, the strain at the point distant z below the centroidal axis CC is Mz/D as shown on Figure 4.5. This strain may be multiplied by the appropriate modulus of elasticity to give the bending stress at the level z. For instance, the bending/tensile stresses in the face and the core are, respectively,

$$\sigma_{f1} = \frac{Mz}{D} E_f \qquad (0 \le z \le h_1; \quad 0 \le z \le h_2)$$

$$\sigma_{f2} = \frac{Mz}{D} E_f \qquad [(c + h_2) \le z \le h_3] \tag{4.1}$$

$$\sigma_c = \frac{Mz}{D} E_c \qquad (h_2 \le z \le c)$$

The maximum face and core stress are obtained with z equal to ± $h/2$ and ± $c/2$, respectively:

$$(\sigma_f)_{max} = \pm \frac{ME_f}{D} \cdot h_3$$

$$(\sigma_c)_{max} = \pm \frac{ME_c}{D} \cdot (h_2 + c) \tag{4.2}$$

The assumptions of the ordinary theory of bending lead to the common expression for the shear stress τ in a homogeneous beam at depth z, below the centroid of the cross section:

$$\tau = \frac{VQ}{Ib} \tag{4.3}$$

Here V is the shear force at the section under consideration, I is the second moment of area of the entire section about the centroid, b is the width at the level z_1 and Q is the first moment of area of that part of the section which $z > z_1$. For a compound beam such as the sandwich in Figure 4.5, Equation 4.3 must be modified to take account of the moduli of elasticity of the different elements of the cross section:

$$\tau = \frac{V}{Db}\sum(QE) \tag{4.4}$$

In this expression, D is the flexural rigidity of the entire section and $\Sigma(QE)$ represents the sum of the products of Q and E of all parts of the section for which $z > z_1$. For example, The shear stress at level z within the adhesive of the sandwich beam is represented in Figure 4.6.

$$\tau = \frac{V}{Db}\left\{E_f\left(b_2h_2d_2 + b_4h_4d_4\right) + E_c\left(b_3h_3d_3\right)\right\} \tag{4.5}$$

It is noted that Q which represents the first moment of area of a part of the cross sectional area was obtained by multiplying the area bh by the distance d from its own centroid to the neutral axis. The shear stress in the core is therefore,

$$\sum(SE) = E_fS_f + E_cS_c \tag{4.6}$$

$$= E_f\left(b_2h_2d_2 + b_4h_4d_4\right) + E_c\left(b_3h_3d_3\right)$$

4.2.4 Deflection in sandwich beams

Figure 4.7 show the global behaviour of a sandwich structure according to the five assumptions give earlier. The deflections of w_1 and w_2 due to bending moment $M(x)$

and shear force $Q(x)$, respectively, are independent and can be superimposed. The total deflection of w_{TOT} is then

$$w_{TOT}(x) = w_1(x) + w_2(x) \tag{4.7}$$

The transverse displacement w_1 of the beam may be calculated by the theory of bending. For example, Fig 4.7(b) shows the bending deformation of a simply supported beam with a central load of P. The points a, b, c, d and e lie on the centrelines of the faces and the cross sections aa, bb, cc, dd and ee rotate but nevertheless remain perpendicular to the longitudinal axis of the deflected beam. It is obvious that the upper face is compressed as the points a, b, c, d and e move closer together, while the lower face is loaded in tension.

The shear stress in the core at any section is $\tau = V/bd$. This is associated with a shear strain $\gamma = V/Gbd$ which like τ, is assumed constant through the depth of the core; G is the shear modulus of the core material. These shear strains lead to a new kind of deformation illustrated in Figure 4.7(c). On the centrelines of the faces lie the points a, b, c, d and e. They are not moved horizontally but in a vertical direction w_2 due to shear strain. The faces and the longitudinal centreline of the beam tilt, and the relationship between the slope of the beam, dw_2/dx, and the core shear stain γ may be obtained from Figure 4.8. In this figure, which shows a deformation of a short length of the sandwich, the distance de is equal to $d\ (dw_2/dx)$. It is also equal to cf, which in turn is equal to γc. Hence,

$$\frac{dw_2}{dx} = \gamma\frac{c}{d} = \frac{V}{Gbd}\frac{c}{d} = \frac{V}{AG} \tag{4.8}$$

Where

$$A = \frac{bd^2}{c} \tag{4.9}$$

The product AG is often referred to as the shear stiffness of the sandwich. The displacement w_2, associated with shear deformation of the core, may be obtained by integration of Equation 4.8 in any particular problem. For example in the simply supported beam with a central point load P, the shear force V in the left-hand half of

the beam is + *P/2*. Integration of Equation 4.8 with $V = + P/2$ provides the displacement:

$$w_2 = \frac{P}{2AG} \cdot x + \text{constant} \qquad 0 \le x \le \frac{L}{2} \tag{4.10}$$

The constant vanishes because $w_2 = 0$ at $x = 0$. The maximum value of w_2 occurs at the centre of the beam, $x = L/2$, and is equal to.

$$w_2 = \frac{PL}{4AG} \tag{4.11}$$

The total central deflection w_{TOT} is therefore the ordinary bending displacement w_1 with the shear displacement w_2 superimposed:

$$w_{tot} = w_1 + w_2 = \frac{PL^3}{48D} + \frac{PL}{4AG} \tag{4.12}$$

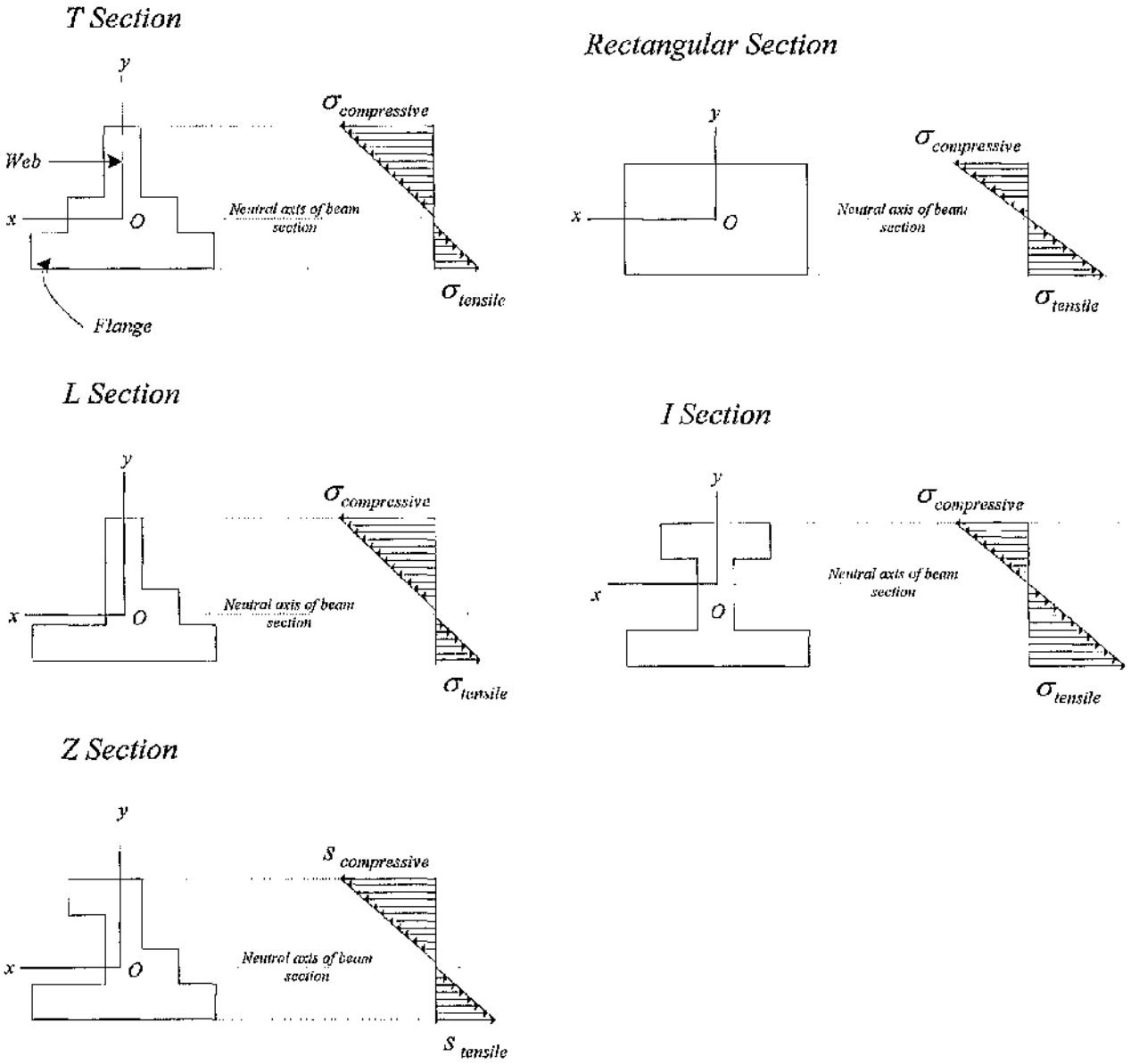

Figure 4.1. Bending stress distribution of the various beam cross sections.

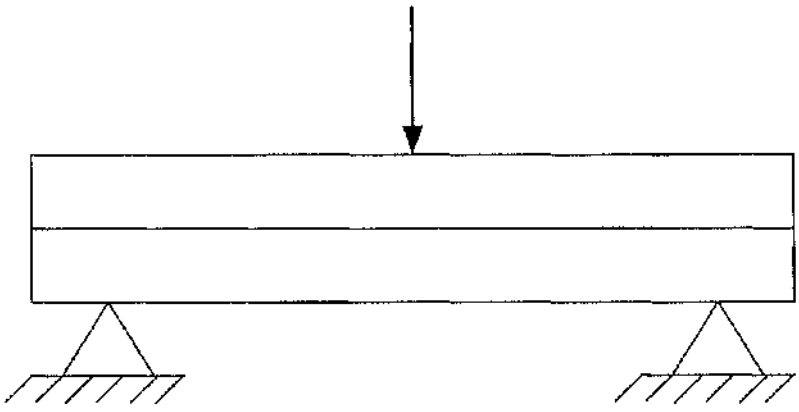

(a)

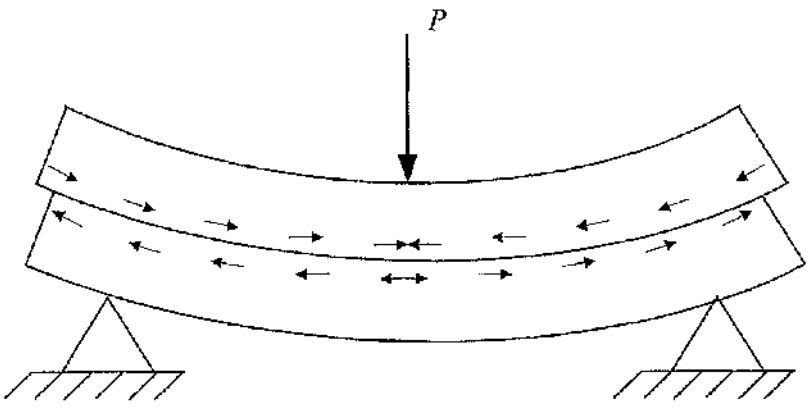

(b)

Figure 4.2. Bending of two separate beams.

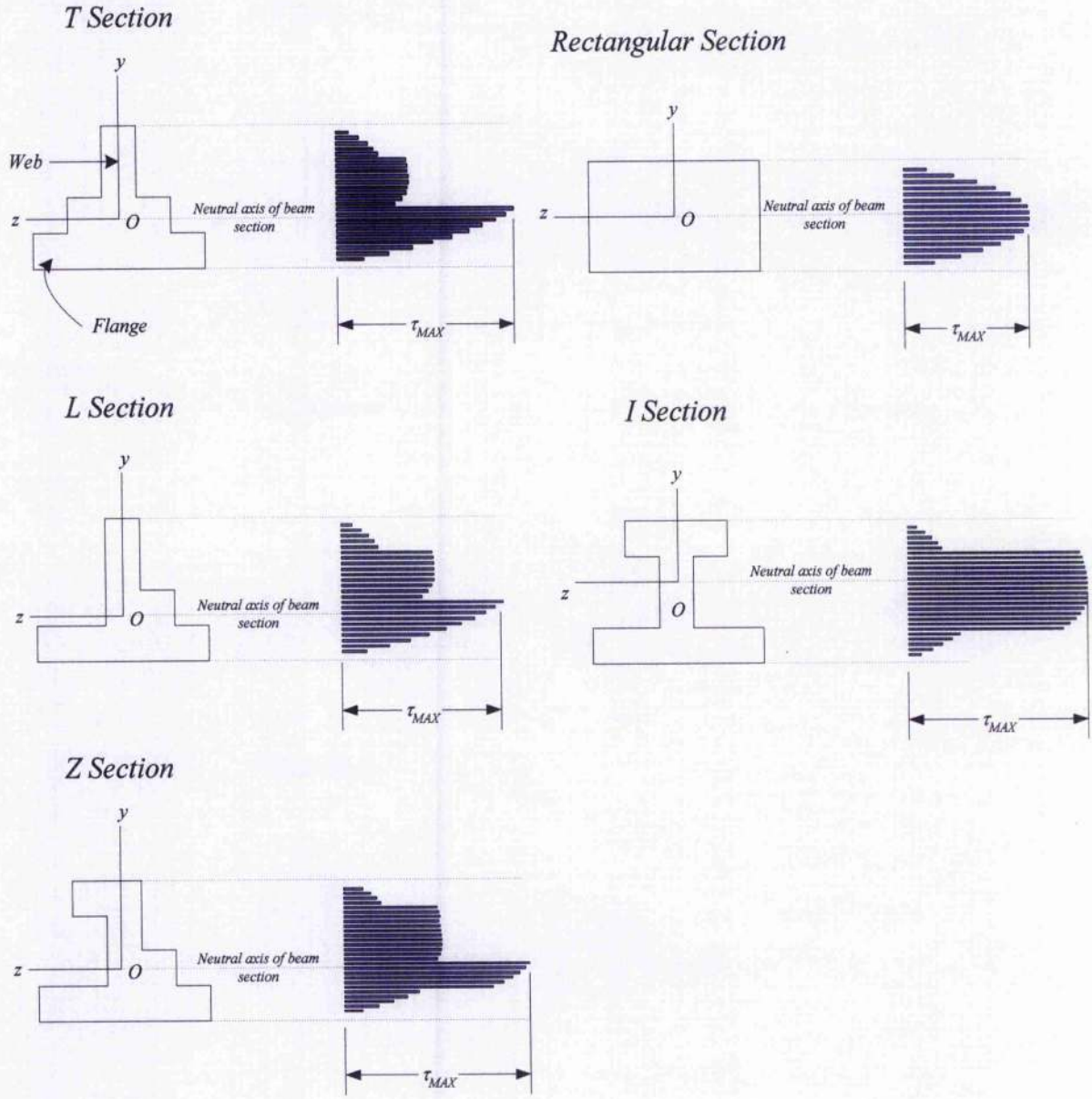

Figure 4.3. Shear stresses in various beam sections.

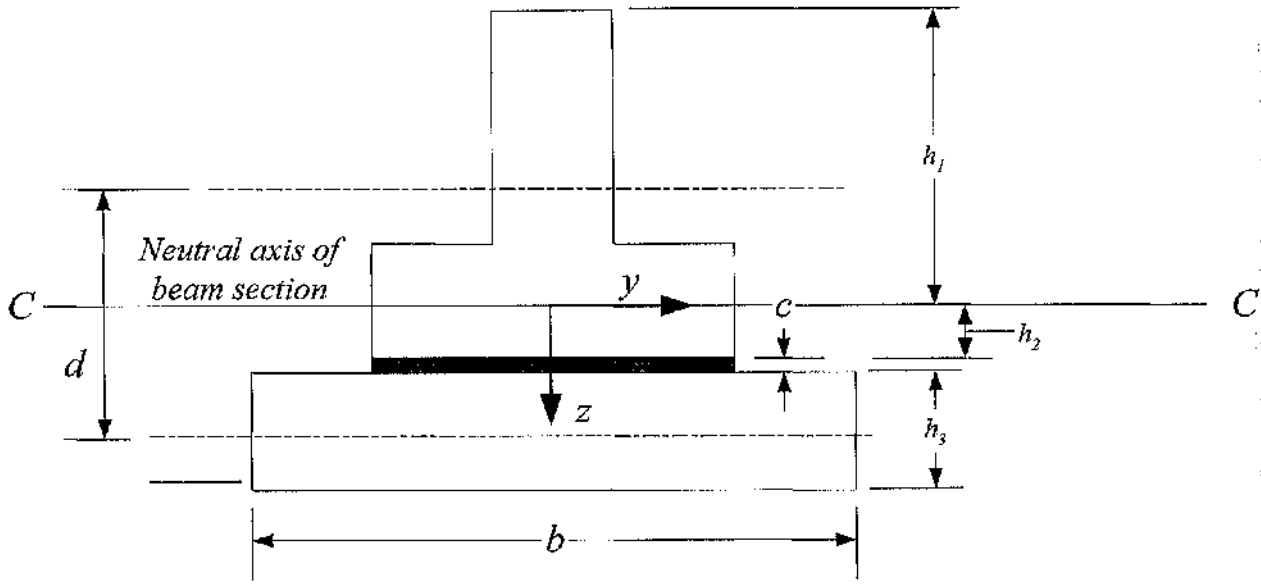

Figure 4.4. Details of a T bonded/sandwich section

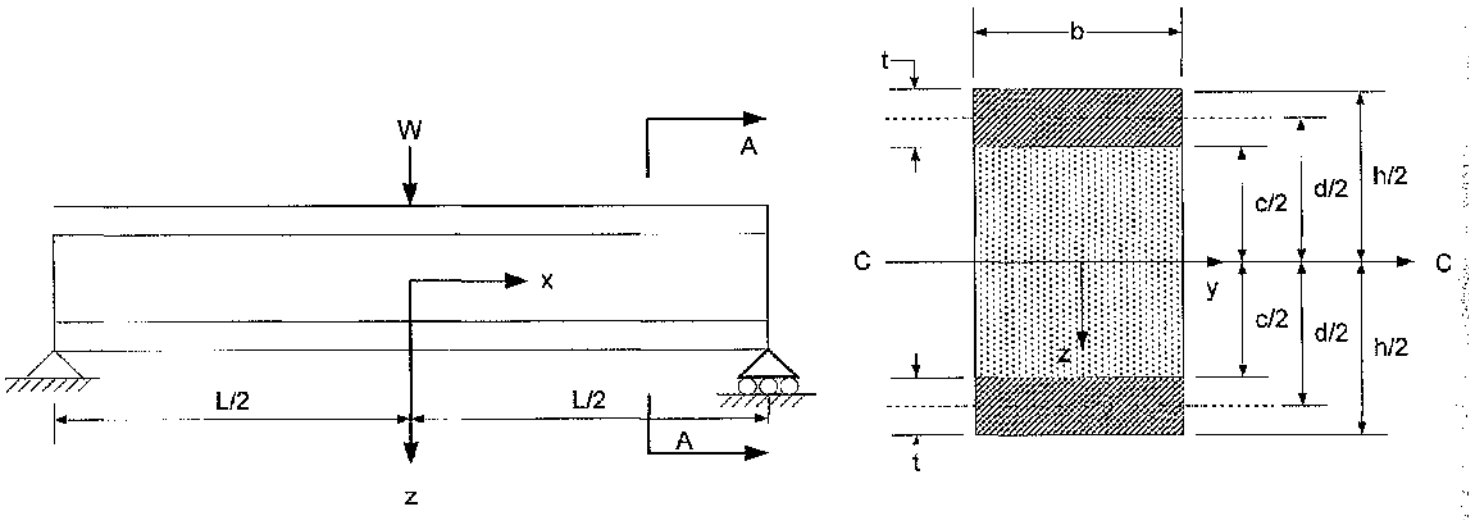

Figure 4.5. Schematic of a typical sandwich beam

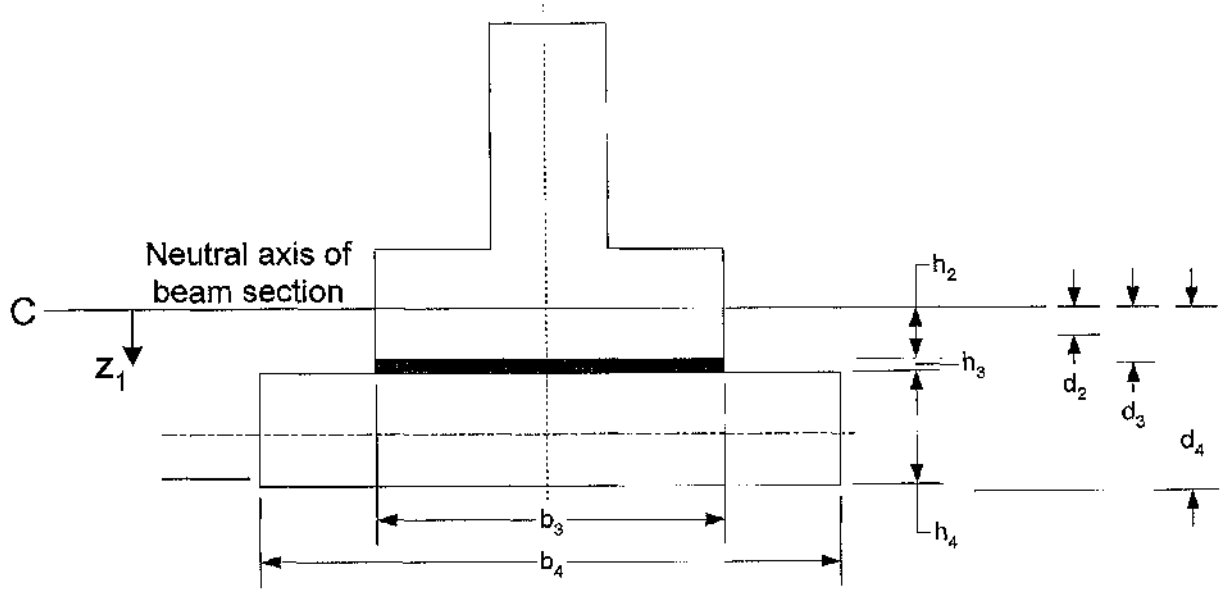

Figure 4.6. Shear stress distribution and 2D schematic of the homogenous T section beam.

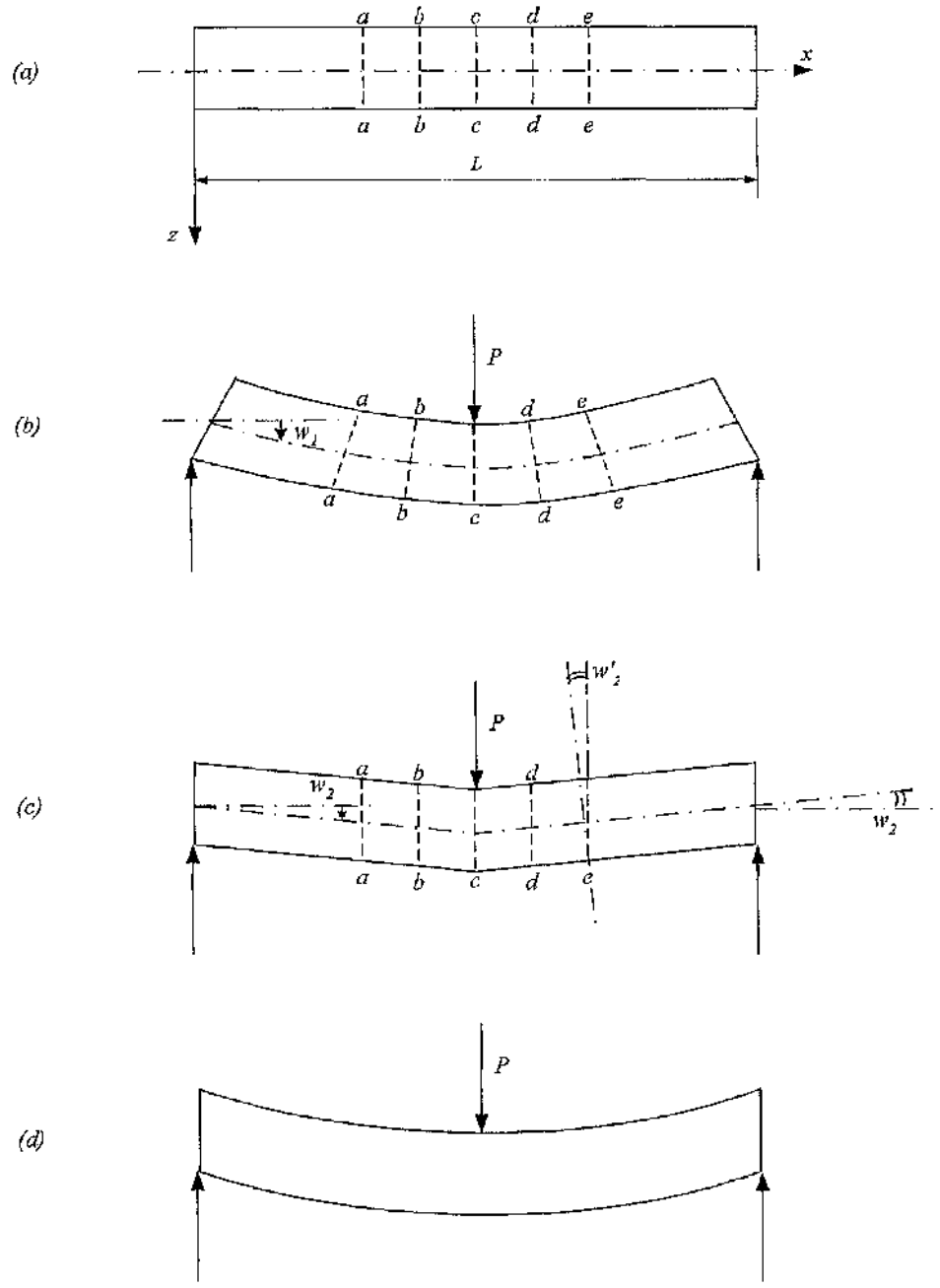

Figure 4.7. Deflections of a sandwich beam under bending moment only (b) and under heavy shear forces only (c) and (d), In (c) the local stiffness of the faces are ignored, and in (d) they are taken into account. Curvature of the beam under the load has an infinite value in (c) while in (d) the value is finite. Diagram adopted from Allen [13]

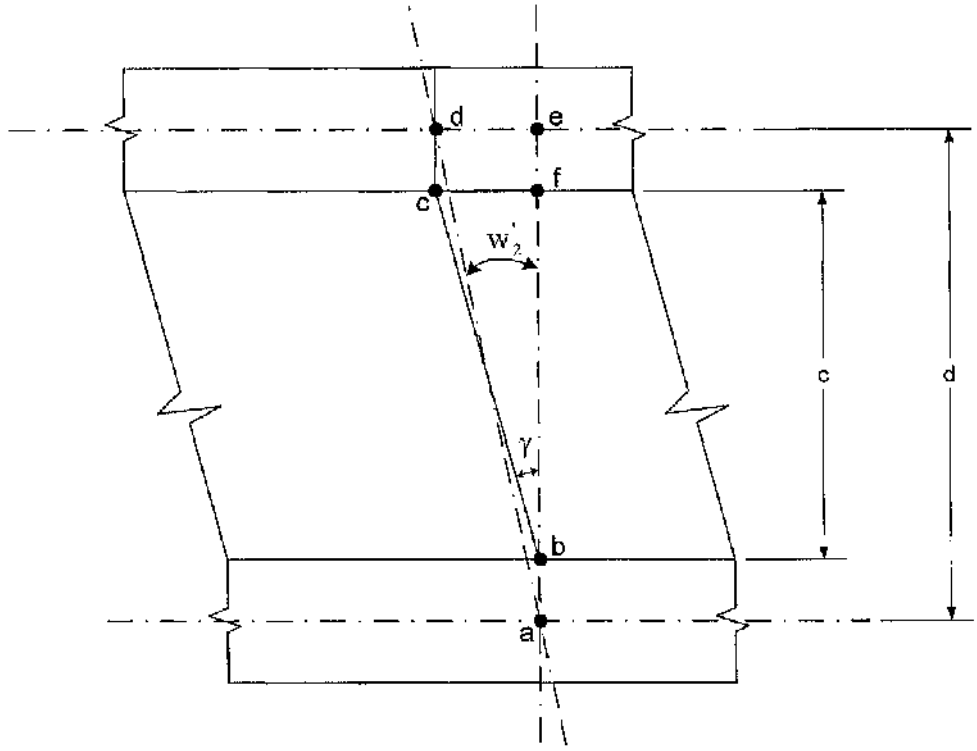

Figure 4.8. Shear deformation of a beam with thick face

CHAPTER FIVE

NUMERICAL WORK

5.1 Introduction

The finite element method is one mathematical methods that is readily available and employed to determine the stress distributions in adhesive joints. The finite element method is a numerical technique to obtain approximate solutions to a wide variety of engineering problems where the variables are related by means of algebraic, differential and integral equations. Rapid engineering analyses can be performed because the structure is represented using the known properties of standard geometric shapes. Modern digital computers have led its extensive use into a wide variety of engineering problems. Finite element work consist of analysis such as solid mechanics, fluid mechanics, heat transfer and acoustics studied in the civil, aerospace, automotive, mechanical and electronic applications.

Finite element analyses were performed to simulate the three-point bending tests for the beam structures studied in this research. Finite element analyses can be used to accommodate such problems with complicated geometries combined with material, geometry and boundary nonlinearities. Substantial research involving the analyses of stiffened panels in ship structures encourages the use of the finite element method, especially in cases involving elastic-plastic loading conditions [37]. In many other similar researches into the behaviour of adhesive joints, finite element analysis performed and compared well with obtained results from experiments or theoretical work [15, 34, 35].

Using finite element analysis, the model is broken down into elements where each element represents a discrete portion of the physical structure. Each element in turn has to be compatible in the force and displacement continuum with adjacent elements. A complete finite element analysis usually consists of three distinct stages: preprocessing, simulation and postprocessing as shown on Figure 5.1. In preprocessing, the physical problem was defined graphically using the software MSC/Patran® to create an input file. This input file was generated directly using a

text editor by a more experienced user although preprocessing with a graphical interface is more conventional. The simulation is the stage where the software ABAQUS/Standard® solves the numerical problem as defined in the input file. During this stage, the displacements, stresses and other fundamental variables associated with the model will be calculated. After each simulation, output files containing displacement and stresses results were then generated for postprocessing. Postprocessing was carried out with the software ABAQUS/Viewer® or ABAQUS/CAE® where the user could evaluate the results. This evaluation is normally does interactively with the software where the output database file is read, and results are displayed in a variety of means, for example colour contour plots, animations, deformed shaped plots and X-Y plots.

Preprocessing in this research was performed using the software MSC/Patran®. MSC/Patran® 2003 is a standard finite element preprocessing tool which allowed the development of the finite element models from the computer-aided design parts. The software is comprised of a robust automatic surface and solid mesh generation and enables the user to control the meshing of the model. The solving process was conducted with the ABAQUS/Standard® solver program. ABAQUS/Standard® provides a dynamically load-balance parallel sparse direct solver that provides significant performance gains for a wide range of finite element model sizes. The direct solver was extremely robust and can be used for all types of analyses with ABAQUS/Standard input files, irrespective of the element types, constraints or other model characteristics being defined in MSC/Patran®. ABAQUS/Standard® was used in the simulation of all the beam models and normally ran as a background process. During the simulation, the software provided the facility to monitor the progress of the ABAQUS analysis job in the form of the status file (*.sta). This allowed the user to check on the progress of the simulation, to identify possible errors in the input deck that may terminate the simulation and take necessary rectifying action.

ABAQUS/Post® and ABAQUS/Viewer® were both used concurrently during the course of the research. ABAQUS/Post® was used initially with ABAQUS/Standard® 5.8 – 6.2 being the solver software for a majority of the linear elastic analyses. Due to a software upgrade within the department to ABAQUS/CAE® 6.4, all analyses were

converted to suit compatibilities with the available ABAQUS/Viewer®. ABAQUS/Viewer® also introduced a vast improvement in terms of efficiency in results generation as compared to its predecessor. Both softwares provided a comprehensive set of visualisation options that help to interpret and communicate the results from the ABAQUS® analyses.

5.2 Preliminary work

In order to obtain a reliable FE solution to a problem, the analyst must have a good grasp of the physical problem and effectively plan an analysis project. Effective planning will require the analyst to anticipate/visualise the structure behaviour and its interactions. The understanding of the behaviour and limitations of finite elements as well as being aware of the options and limitations of the available software is important for analysts. The first step in this procedure was to define the problem, with particular focus on what is known and what is desired. The three point bending procedure in the experimentation was idealised to be that of a static loading finite element analysis of a typical beam. Elastic loading conditions were applied on the linear analyses of the T, L, Z, inverted T and rectangular section beams and material nonlinearity was adopted for the elastic-plastic loading conditions of the rectangular section beams. The material of the beams considered was defined to be isotropic and not temperature dependent. Material data defined in the analysis was obtained from reliable literature references and experimental results conducted by the analyst and covered in Chapter. 4. At this stage, it was also important to identify the specifics of the finite element model, such as load cases, boundary conditions or whether symmetry can be exploited to reduce computational time.

The beam model analysed in this study is a substructure representative of the entire stiffened panel. Submodeling and symmetry was not adopted in the research in the development of an appropriate finite element model. Modelling an FE model of the entire beam structure with similar dimensions will consist of 4000 - 5000 elements. Such a model takes about 15 – 25 minutes in terms of computational time using ABAQUS/Standard® to solve, which corresponds to the majority of all simulations conducted. A complete three dimensional model of the joint also has a few advantages. Analysing the model as a whole also allowed the assessment and

distribution of stresses (shear/peel) found along the span and width of the beam. The other advantage included identifying location of stress concentration in the model otherwise not noted in a two dimensional model.

Theoretical work prior to the FE analyses was used to anticipate the likely behaviour of the structure. The solution serves the purpose of providing insight that improves the FE model to be developed. A theoretical solution is adequate to detect a strange displacement pattern or stress field, or a numerical result in errors by orders of magnitude because of a blunder in data preparation. In fact, it is not uncommon to find research into adhesively bonded structures to have included a theoretical solution for comparison with the FE results [36]. Such a prediction promotes the viewpoint that the FE results are on trial, since there is a normal tendency by the analyst to trust the computed results once the simulation is completed.

There is a tendency to use more elements in an FE model by analysts, as preprocessors and postprocessors improve and computing cost decline. However, such an approach would be considered unwise and attributed to a lack of experience in FE modelling. Most engineering industries now tend to adopt a coarser mesh of the model, in order to conduct a more efficient finite element analysis. Preliminary modelling carried out in this research consisted mainly of simple finite element models created with simplified uniform meshing. An adequate finite element model was then developed from a sequence of simpler FE models, each of which guided the development of the next, such that the final model would consist of sufficient elements of the proper type. These analyses took little computational time and meant that multiple simulations of various mesh refinements could take place simultaneously. It was also easier to identify sources of error after each simulation since fewer variables were being considered and gradually introduced through these trial simulations. The procedure would normally take less time overall than an attempt to construct a very detailed FE model at the outset, only to find that it is inappropriate or inadequate because of some aspects of behaviour not foreseen. An early model constructed as shown in Figure 5.2 shows a T section beam modelled with uniform meshing.

Earlier models developed in this research consist of less than 1000 elements, with the entire beam structure modelled with uniform meshing. During this stage, it was common for the simulation to terminate due to modelling defects. These defects are identified by error messages listed in the output files (*.dat / *.msg) generated by ABAQUS/Standard® and need to be addressed by the analyst before a successful model is created. In the course of the study, most basic errors have been attributed to the boundary and loading conditions on specified nodes. More complicated errors were found in the elastic-plastic analysis of the FE models, which were mainly attributed to element distortion, and the selection of the step analysis. Such errors have resulted in significant difference between certain results sustained from experiments in terms of plastic analysis, which may have required further work into developing a more suitable model for this research.

Each successful model developed served to improve the next by showing clearly where the locations of the stresses were and which stress gradients were large. A Von-Mises stress contour plot of the flat bonded beam is shown in Figure 5.3. This plot is necessary to highlight the regions of high stress such that an optimisation of the FE model can be carried out. As shown, it was clear that the refinement of the elements should be emphasised within the adhesive layer and also in the middle of each beam section. Refinements of the model were carried out in the following modelling session, leading to a sequence of modelling to produce an adequate model where the results compared favourably with the theoretical results.

In order to increase the efficiency and effectiveness while developing a model, considerable time was placed on evaluating examples obtained from the preprocessing and postprocessing software. MSC/Patran® features a list of detailed examples on their website, designed to illustrate the approaches and decisions needed to perform relevant analyses [72]. The tutorials was useful for providing various means of modelling the structure and also the selection of the type of elements to be considered. Most of the tutorials on modelling procedures were undertaken in this research, with PCL (MSC/Patran Command Language) carried out for the defining material nonlinearity behaviour for the non-linear FE analyses. Other modelling examples were obtained from ABAQUS/Standard [73] which tends to be more elaborate. The

input file reference provided in each example allowed for effective comparisons with the input deck created using the MSC/Patran® preprocessor.

5.3 Generating the FE model

Modelling is the simulation of a physical structure or physical process by means of a substitute theoretical or numerical construct. Modelling requires that the physical action of a problem be understood well enough by the analyst to choose suitable kinds of elements, and enough of them, to represent the physical action adequately. The finite element model is compose of several different components to describe the physical problem to be analyzed. These components are;

- Choice of element type and mesh details
- Boundary conditions or supports
- Material properties
- Applied loads

The development of the mesh of the model was efficiently used such a high intensity of smaller elements are found where large stress gradients were assumed present. It is a matter of balancing between using an appropriate number of elements and using the available computer resources required in order to run the simulation. Such a solution was obtained through an informal convergence study where various mesh refinements were compared. Hu and Jiang carried out a convergence study to reduce the number of elements required to sufficiently capture the buckling behaviour of stiffened panels [37]. These panels were expected to experience large plastic deformations and displacements and hence were necessary to develop a suitable FE model to cut down on excessive processing time. As good practice a similar mesh convergence study was carried out on a uniform meshed model against a refined meshed model in this study.

5.3.1 Choice of element type

Continuum elements were used throughout the finite element analysis carried out. These stress/displacement hexahedron elements can be used to model the widest

variety of components and represent the most comprehensive of the element libraries used in ABAQUS®. The continuum element library can be broken down further to

several types of elements, varying in element formulation and levels of integration. General guidelines provided by ABAQUS® explaining specific continuum element's suitability and its proper selection were used as reference while creating trial FE models [74]. Test cases of continuum elements have been conducted in the modelling of structural adhesive joints. Wu & Crocombe used continuum modelling for local deformation of the substrates and to accommodate complete displacement compatibility along the interfaces of the substrates and adhesive of a bonded joint [38].

In the elastic analyses carried out in this research, all of the T, L, Z, inverted T and flat beam sections were modelled with the three dimensional quadratic, reduced-integration hexahedron element 'C3D20'. These second order elements were suitable for elastic analysis because the edges were able to curve easily and do not suffer from the effects of shear locking. According to guidelines provided, a second order fully integrated model provided the best resolution of stress gradients that were likely to occur at various areas of the model at the lowest cost [74]. Wahab & Ashcroft used three dimensional 20-node structural solid elements in the submodeling of adhesively bonded composite beams. Their finite element results show good agreement with the analytical solution and provided confidence in the development of the global FE model [75]. The second order elements also use three integration points in each direction and consist of midside nodes. Elements normally having midside nodes in addition to corner nodes tend to be less sensitive to shape distortion then elements having only corner nodes. [40]. Midside nodes are normally used in the FE analyses to provide additional reference points for result generation, or sometimes for positioning to obtain a better approximate stress singularity in adhesive joints [36].

The incompressible nature of plastic deformation in metals places limitations on the type of elements that can be used for elastic-plastic simulations. Fully integrated, second order, solid elements such as the 'C3D20' elements are very susceptible to volumetric locking when modelling incompressible material behaviour and therefore were not used in the elastic-plastic simulations of the flat beam sections. The solid,

general-purpose continuum element type chosen for the elastic-plastic analyses was the linear element, 'C3D8' which is simply a brick element with eight nodes in each

corner. Each element uses linear interpolation in each direction and consists of a total of eight nodes with a single node located at each corner. These corner nodes act as a connector between two or more elements. First order elements are suitable for simulations involving a large mesh distortion which is an effective representation of a beam model undergoing plastic deformation.

5.3.2 Mesh details

The inverted T beam model shown in Figure. 5.4 was developed using MSC/Patran®. The model shown is represented by the three separate sections; the upper adherend, the adhesive layer and the lower adherend. Results obtained from theoretical work were used to define the specimen's mechanical behaviour and determine the type of stresses that were present in certain areas under the three point loading conditions. Such a practice was found suitable to determine where the expected stresses were qualitatively and how the finite element model could be refined in certain areas. From the theoretical results, it was noted that;

- Maximum tensile bending stresses were found along at the centre of the bottom surface where the beam undergoes tension under the neutral axis.
- Maximum compressive bending stress was found on the along the middle of the top surface where the beam undergoes compression above the neutral axis.
- Yielding has taken place when elements of the beam cross section at the centre of the span show stresses that reached the material (steel) yield stress. Yield begins from the outermost surface of the adherends and transmit gradually to the rest of the beam section.
- Horizontal shear stresses were acting between the horizontal layers of the beams with the maximum shear stress found along the neutral axis of the beam.
- Shear stress is assumed negligible at the top and bottom faces of the beam as a result of pure bending.
- Maximum displacement is found in the middle of the span and on the bottom surface of the model.

- Highly localised stresses should appear in the regions where the point of loading was placed and where the supports were situated. The model was fully constrained from rigid body rotations at the supports to induce pure bending while undergoing loads.

To model a beam structure undergoing load conditions effectively, emphasis was placed on identify specific areas of interest that symbolised its overall mechanical behaviour. This emphasis was made through the placement of the mesh seeds. The initial step into mesh development was to properly seed the mesh. This was critical in the modelling process as the model contained three separate solids which would need to be mesh separately. The seeding process dictates how the mesh layout will be developed and the intensity of elements in specific parts of the joint. Uniform positioning of the seeds in along the height of the structure was crucial for the resulting nodes to be equivalenced such that the three solids were connected computationally. For equivalencing to work correctly, the nodes along the adherend/adhesive interface on all sides need to be coincident. Therefore, the distribution of elements in the x & y axes must be constant in all three separate solids as shown in the Figure. 5.5.

Non-uniform horizontal (*x-direction*) arrangement of the mesh seeds was used to intensify the amount of elements along the span of the finite element beam model. The meshing in these areas necessitated more detail especially when the tensile bending stresses and overall displacements were the object of study. Two-way bias meshing was defined for the mesh seed arrangement along the span (*x-direction*) of the specimen. The *L2/L1* bias ratio was chosen to be an arbitrary value between 0.4 - 0.65. This range was also used for the basis of facilitating the placement of nodes on the boundary conditions for the varying spans (50 – 250 mm) of the beam sections. However, this did not affect the results of the analysis substantially as the overall measurements for stress and displacement were made near the centre of the beam where there was a high intensity of elements for evaluation.

The distribution of elements along the y and z axis was made constant across the model as shown in Figure. 5.5. The upper and lower adherends were each modelled with 3 - 5 layers of elements within its overall height and width. Uniform meshing of

elements were defined throughout the thickness of the beam. As most of the stress analyses were made along the span of the FE beam model, uniform meshing was also adopted across the width of the beam. An average of 5000 elements was modelled for each beam specimen analysed. The number of elements used in each simulation was limited by the computational ability of the computer hardware resources. Models with 6000 elements or more tend to have issues attributing to insufficient memory or limited hard disk space availability which terminated the analyses.

5.3.3 Modelling the adhesive layer

Using the three dimensional finite element analysis methods, the effect of thickness of the adhesives on the stress distribution in the beam joints was studied to address the role of the adhesive layer. Modelling of the adhesive layer required attention to detail. The thickness of the adhesive layer was varied from a 0.1 mm to 0.5 mm for the T, L and flat beam section models. Overall, about 1200 elements and 9600 nodes were consisted in the mesh of the adhesive layer. The mesh for the adhesive layer is shown in detail in Figure. 5.6.

The adhesive layer included two layers of meshes. The mesh refinement within the thickness of the adhesive material provided the opportunity to determine the shear stresses within the adhesive material. The approach has been adopted by many researchers who similarly created multiple layers of the adhesive material [15, 40, 76]. It was found useful to understand how the magnitude for stresses and deflection changed through the thickness of the bondline. Information on shear stress within the adhesive or at the interfaces was not readily available through experimentation due to the difficulties and the reliability of the results being questioned. Experimentally, it would be difficult to place a strain gauge within the adhesive layer in order measure the shear strains and was not implemented in this research.

5.4 Loads and boundary conditions

The support conditions were dictated by the FE software as well by physical considerations. The mesh of the FE model was arranged such that there was a node at each location where the restraint should be placed. The restraint, which was simply a zero displacement in the vertical axis (*y-axis*), must appear at a node rather than between nodes. The other two translational d.o.f (degrees of freedom) which lies

along the x and z axes.f were not suppressed in order to allow for the beam to deflect laterally. The rotational d.o was not restrained in the x, y, and z axis, to simulate the experimental setup accurately. A series of evenly spaced nodes were used for the location of the restraints as shown in Figure. 5.7. Each node across the width of the beam section was uniformly spaced apart at approximately two millimetres. The boundary conditions were represented by a total of about 20 nodes, with 10 nodes on each end of the beam. The boundary conditions were located 15 mm from both ends of the beam horizontally, similar to the experimental setup. The distance between both supports varied between 50 - 250 mm accordingly to the required span.

In finite element analysis, a load may be applied as a moment at a point or a surface pressure. Similar to the restraints used, a concentrated load was applied at specified nodes and the mesh biasing was used for nodes to be positioned where the concentrated load must be applied. With the possible exception of beam elements, most standard softwares were not structured to accept non-nodal concentrated loads as input data [40]. Such a scenario was found true when initial FE simulations modelled with having the loads applied on points instead of specified nodes could not be solved properly with ABAQUS/Standard®. Distributed loading was adopted as the load condition for each finite element model. In a three-point bending setup, the distributed loading was represented by a line load. This line load is a representation of combined forces or moments distributed along a line, where this line is centrally located in the middle of the beam model's span on the beam joint's upper surface. The load applied was fixed in the downwards (negative *y-axis*) and was constant throughout the simulation. The magnitude of the load was divided equally into the amount of nodes found on the line load. There was found to be about 6 - 8 nodes across the width of the upper surface, and varied in accordance to the beam's geometric shape. The vertical load was then applied on each of these equally spaced nodes, contributing to a distributed loading condition across the width of the beam.

5.5 Elastic-Plastic FE analyses

Elastic-plastic finite element analysis was carried out on the flat beam models. A total of 35 solid and bonded models varying in beam spans and adhesive thickness were studied. Material nonlinearity was introduced for both the adhesive and adherend materials in the analysis. There are three concepts which must be defined prior to

conducting an elastic-plastic finite element analysis. The first concept is the yield criterion which relates to the onset of yielding to the state of stress. For metals the von Mises criterion is most commonly used. The second concept is the flow rule. It relates to stress increments, strain increments and the state of stress in the plastic range. The third concept is the hardening rule. It describes how the yield surface grows and moves as plastic strains accumulate. Many metals have approximately linear elastic behaviour at low strain magnitudes and the stiffness of the material, known as the Young's or elastic modulus is constant. At higher stress and strain magnitudes, metals begin to have nonlinear, inelastic behaviour which is commonly known as plasticity.

The elastic-plastic analysis serves to determine the stress levels and distribution in the bonded beam especially within the bondline. It was essential to also determine where possible cracks/delamination took place within the adhesive as this could not be determined easily in the experiments without sophisticated equipment. All of the elastic-plastic response models provided in ABAQUS® (except the deformation theory model in ABAQUS/Standard®, which is primarily provided for fracture mechanics applications) have the same general form. In the simplest plasticity model ("perfect plasticity") the yield surface acts as a limit surface and there are no hardening parameters at all: no part of the model evolves during the deformation. Perfect plasticity means that the yield stress does not change with plastic strain. It can be defined in tabular form for a range of temperatures or field variables; a single yield stress value per temperature and or field variable specifies the onset of yield. Perfect Plasticity was defined for both the adhesive and mild steel materials used in the bonded beam joint.

The perfect plastic behaviour of a material is described by its yield point and its post-yield hardening. The shift from elastic to plastic behaviour occurs at a certain point, known as the elastic limit or yield point, on a material's stress-strain curve. In most metals the initial yield stress is 0.05 to 0.1% of the material's elastic modulus. The nominal stress-strain curves in Figure. 5.8 were used to define the joint materials perfect plastic behaviour into the appropriate input format for ABAQUS®. The properties of the adhesive Araldite AV119® is shown in the Figure. 5.9. The figure shows the testing of the adhesive in bulk form in compression, tension and in lap

shear joints. The yield stress in compression was found to be about 120 – 125 MPa according to the results obtained in a study [78]. The mesh seed arrangement used in elastic-plastic analysis is quite similar to the arrangement used in linear elastic analysis. 'C3D8' type solid elements were used in the development of the finite element mesh. In the simulations carried out, it was found that the shorter span beams (50 - 75 mm) were very susceptible to element distortion. Nonlinear solutions are sensitive to element distortion, and the discontinuity of these elements forces the solver to unnecessarily iterate a higher strain, plastic solution when none should have been required. If an explicit nonlinear transient solution is required, distorted elements tend to skew the time stepping algorithm unnecessarily as well. The mesh at contact region was then refined to capture the contact stresses that will be developed. As the contact area gets smaller, the need for more refinement increases. Un-refinement of the mesh was carried out in regions where the stress is low, and did not affect the overall model's structural stiffness

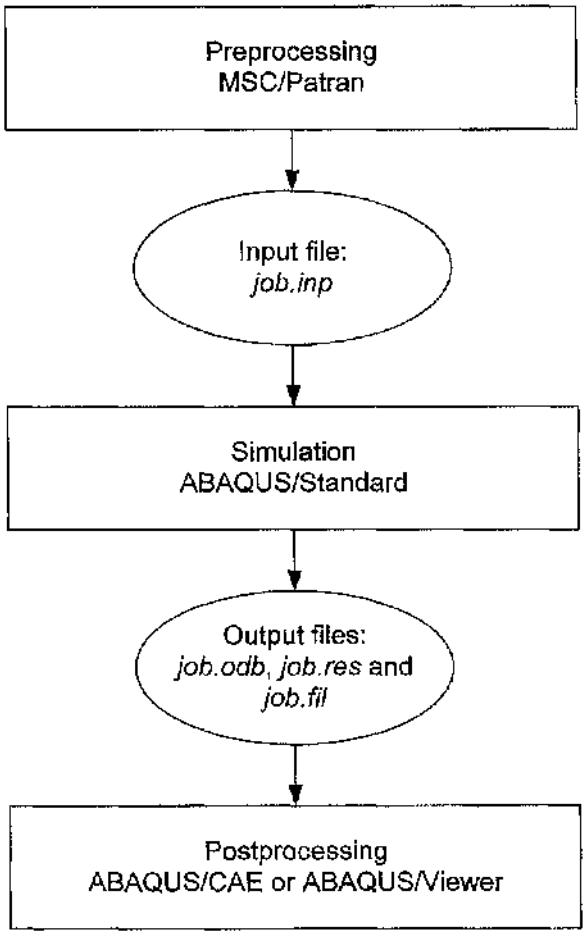

Figure 5.1 Stages in a finite element analysis where the three stages are linked together by files.

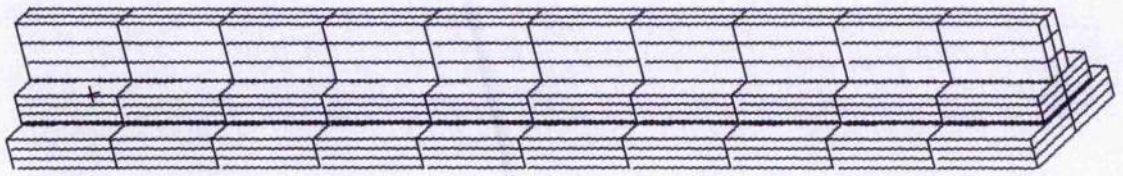

Figure 5.2 FE model of a T beam section with a uniform mesh.

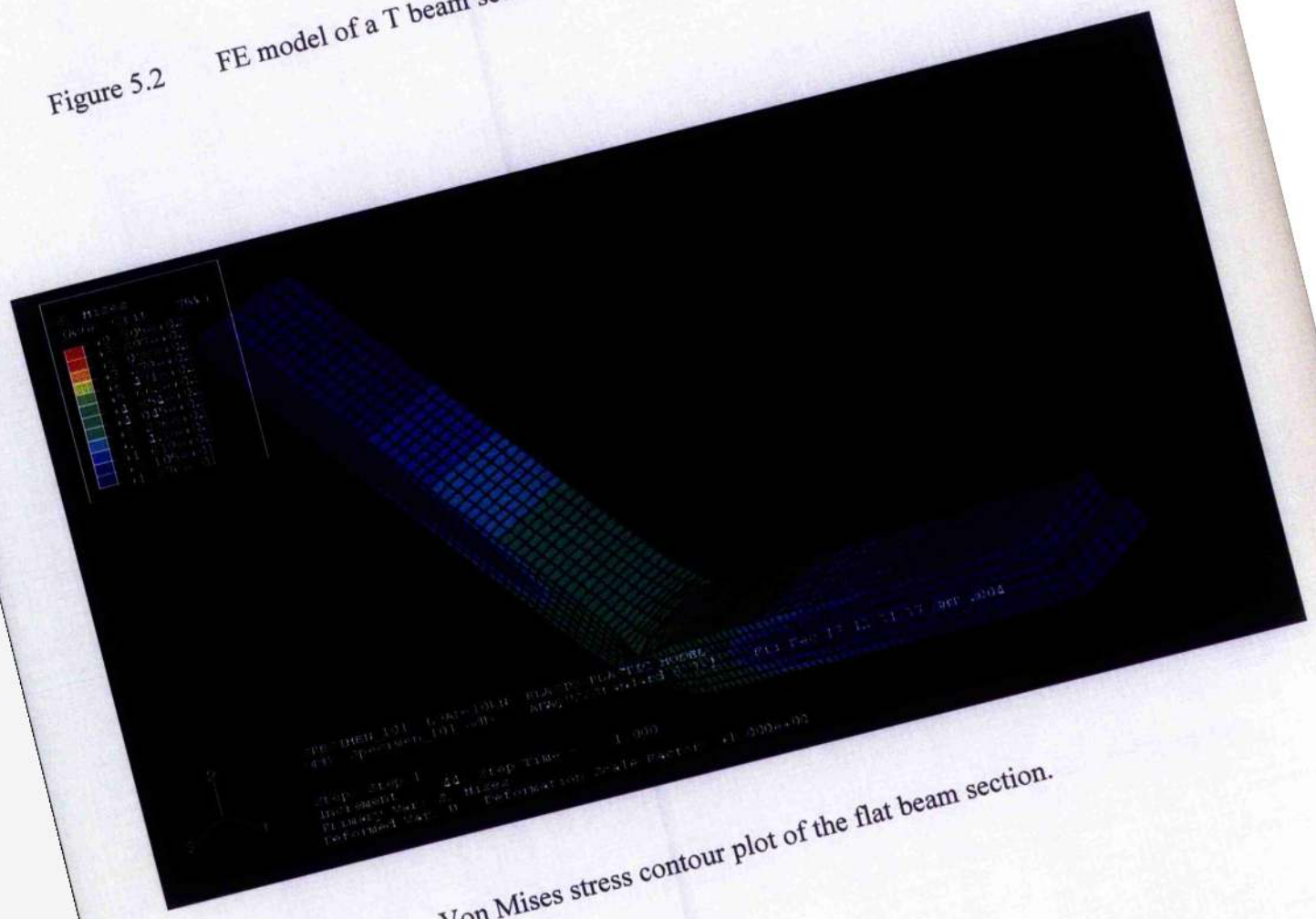

Figure 5.3 Von Mises stress contour plot of the flat beam section.

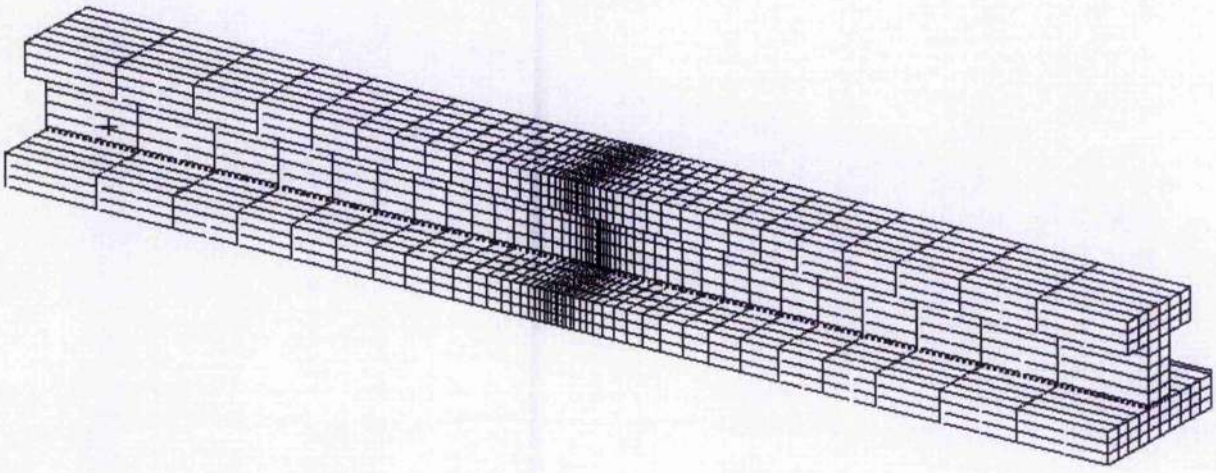

Figure 5.4 FE model of an inverted T beam section

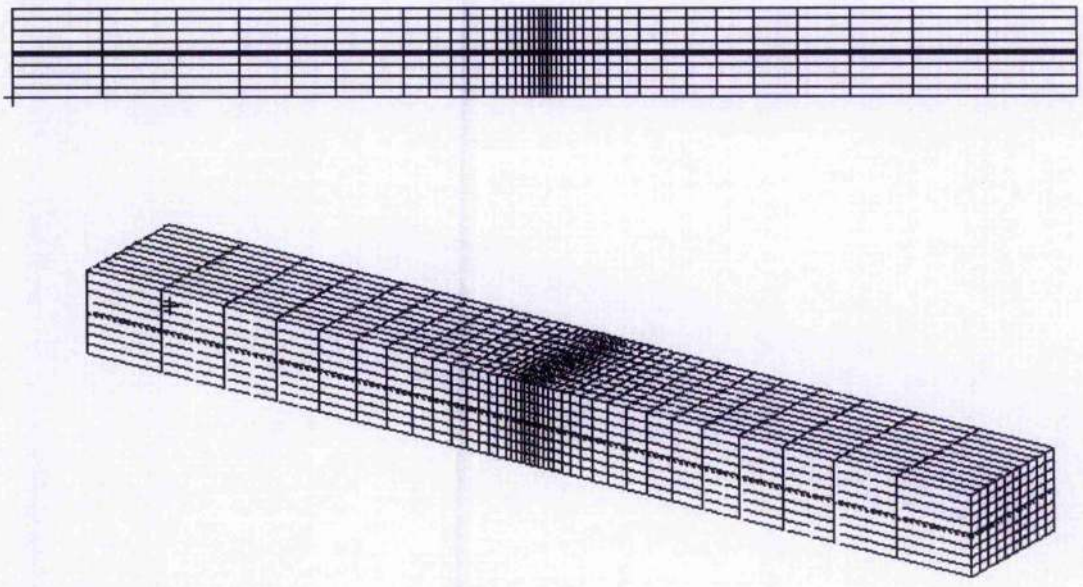

Figure 5.5 FE meshing of the flat beam section (3D view)

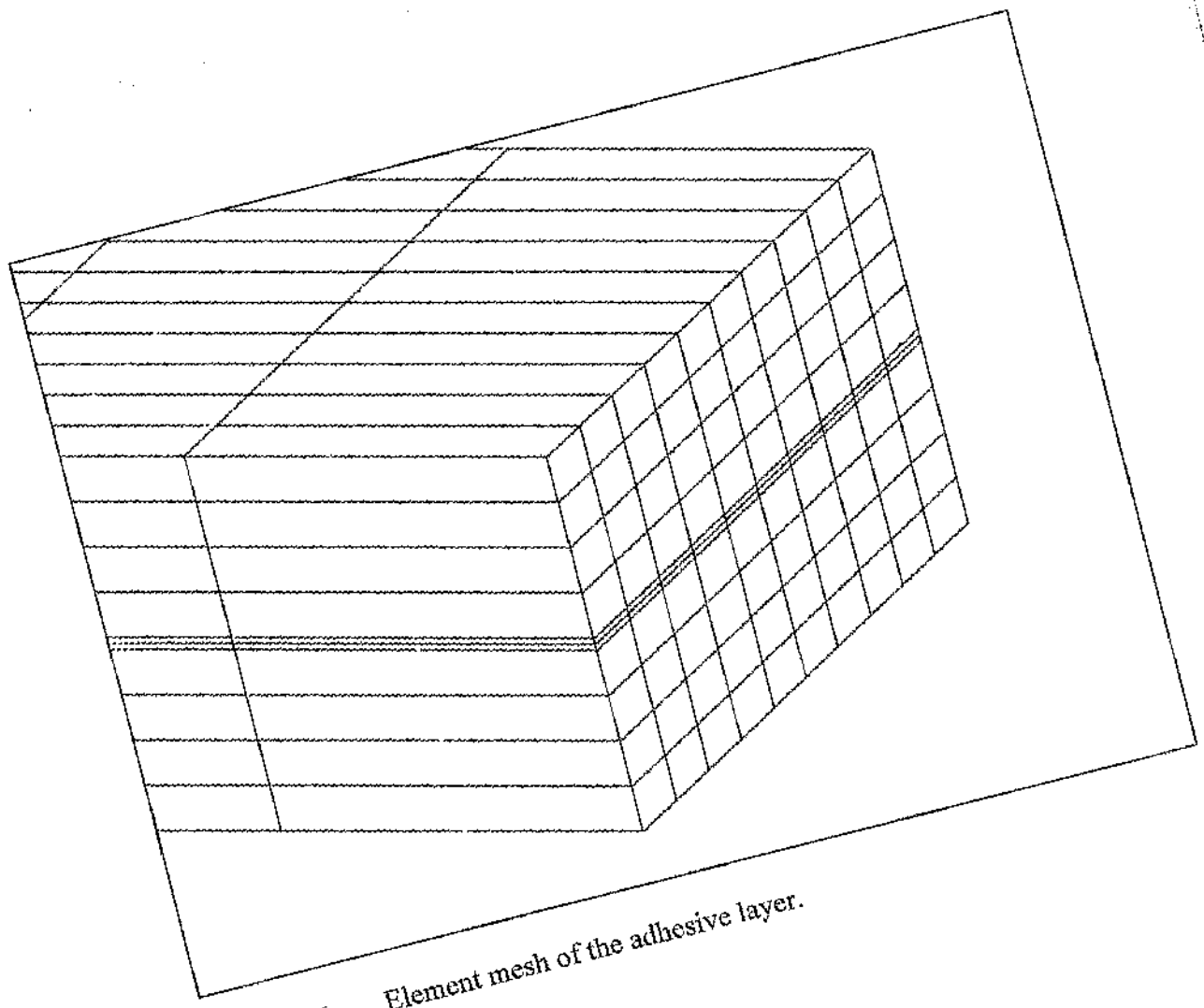

Figure 5.6 Element mesh of the adhesive layer.

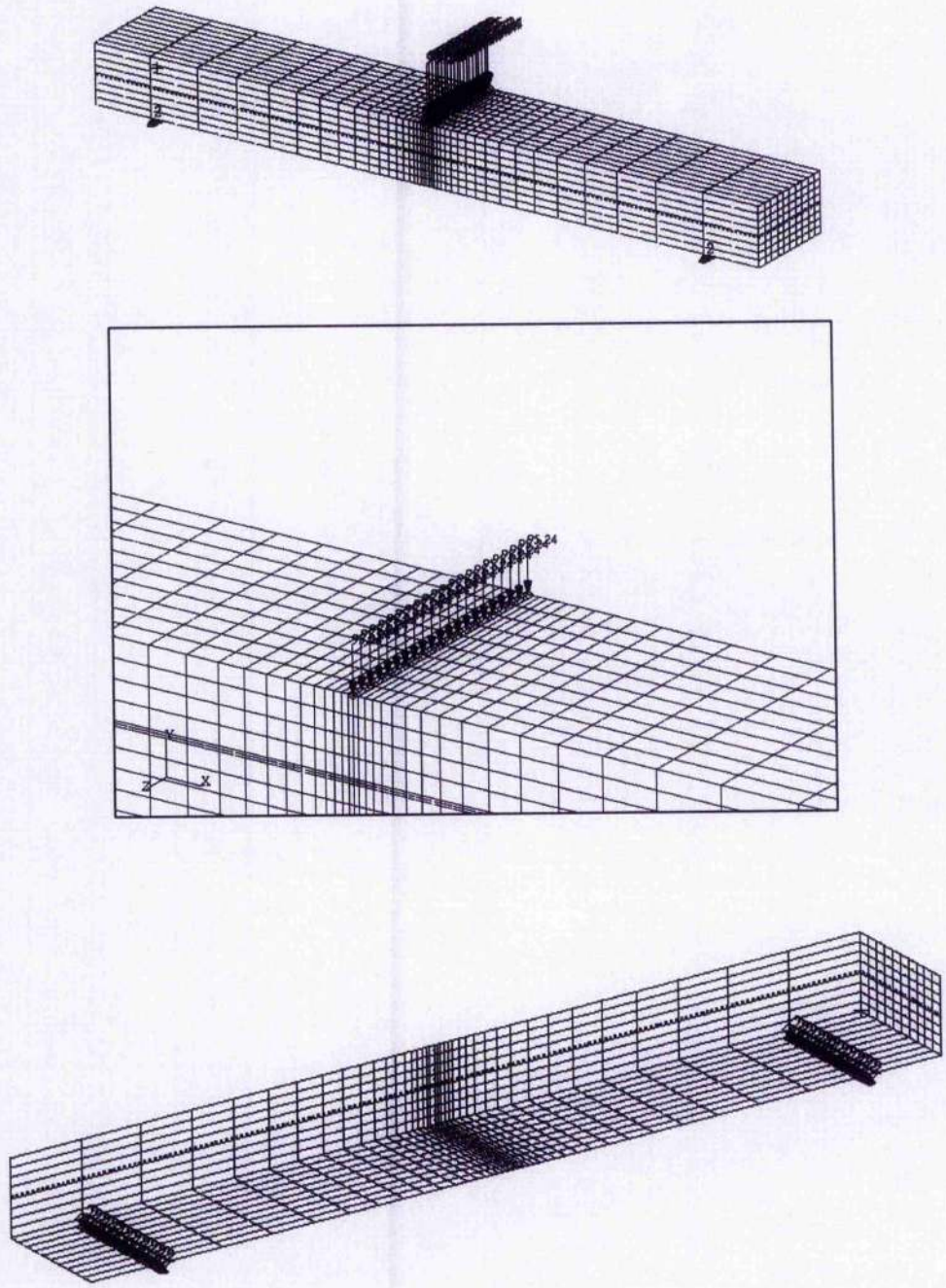

Figure 5.7 View of the boundary conditions in the FE model

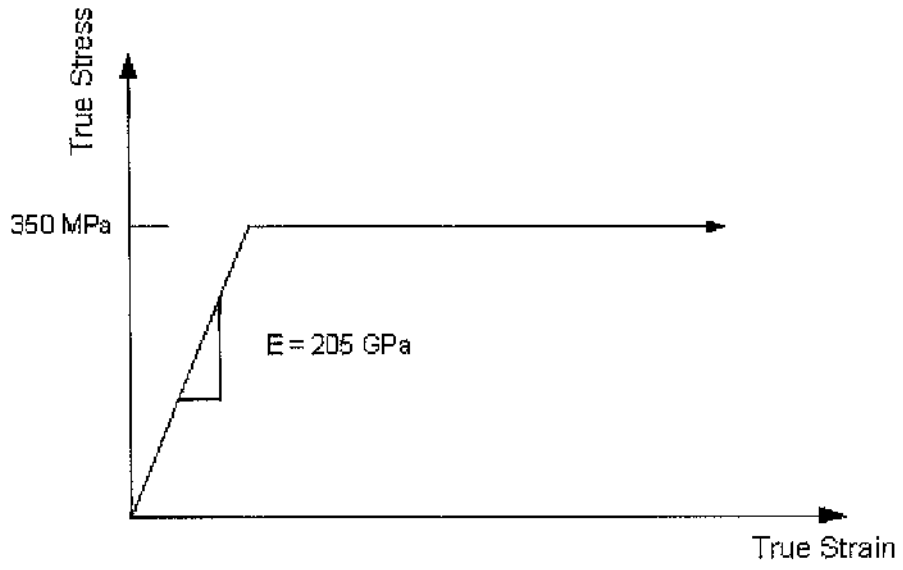

Stress - strain behaviour for the 080M15 mild steel material

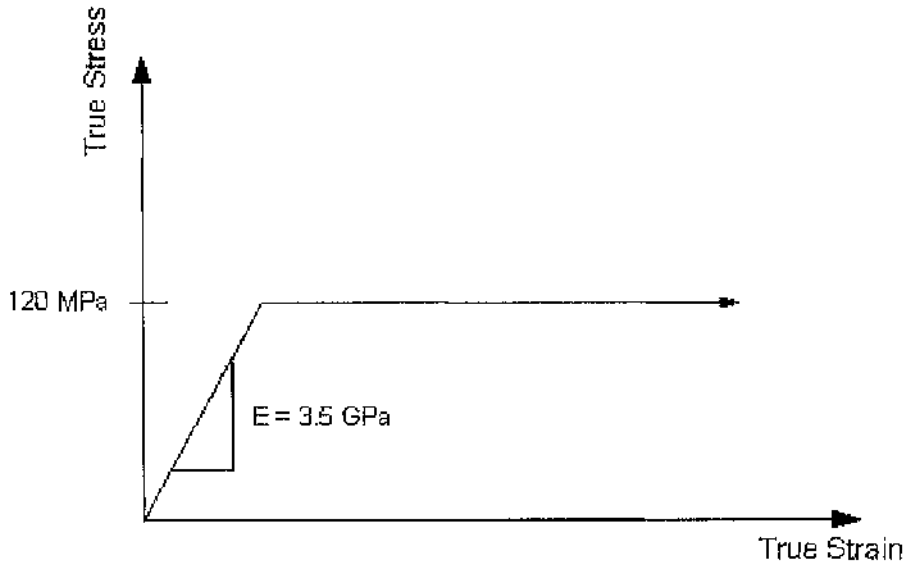

Stress - strain behaviour for the Araldite AV119 adhesive material

Figure 5.8 Stress-strain behaviour for the materials used in the joint.

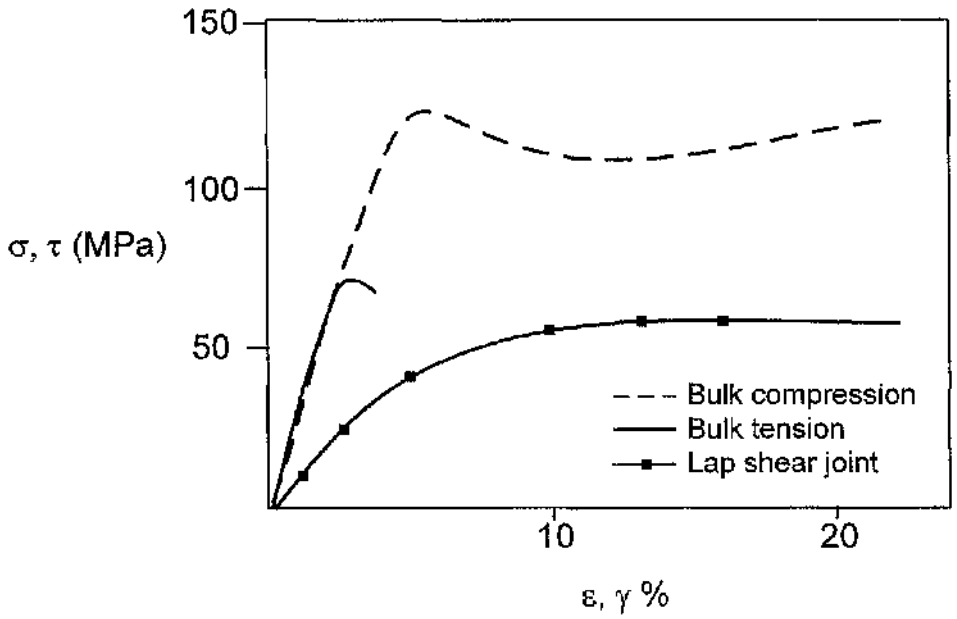

Figure 5.9 Properties of the structural epoxy adhesive Araldite AV119® [78]

CHAPTER SIX

RESULTS

6.1 Introduction

The results from the experimental, analytical and numerical techniques are summarised in Table 6.1 - Table 6.7. In addition, many graphical figures are based on data from these tables to highlight the study findings. As mentioned earlier (in Chapter. 3.2.2) model designations (e.g. TS050/X as used in Table 6.1) are used to case the model's description. Throughout the text the letters A, B or C replace the letter "X" to distinguish the analytical, numerical or experimental results respectively (e.g. Model TS050/**B** corresponds to numerical results). Unless otherwise mentioned in the superscript (e.g. Model TB050/$B^{(X)}$), all adhesive thickness of bonded models discussed are taken as 0.5 mm.

Most of the findings refer to the numerical results which are usually more consistent than the experimental and analytical result. The analytical results based on using classical beam theory and sandwich beam theory for solid and bonded sections respectively, did not exhibit a difference between the solid and bonded models in terms of bending stress. However the general observation from the tables is that there are similar trends in most cases with apparent non-linearity associated with various level of loading conditions, i.e. 2 kN, reaching 90% yield loading and plastic loading conditions. Experimental results did not include shear stress derivation due to experimental difficulties.

Figure 6.1 describes the basic structural behaviour of solid and bonded beams showing typical distributions for the stresses and deflection along the span of the beam under simply supported boundary conditions. The following results largely deal with the maximum bending and shear stresses and central deflection of such beams, with modification in various parameters. Using the results obtained, a comparison between the bonded models behaviour with their solid equivalent was made. With the exception of the flat beam sections the neutral axes for the remaining beam sections is situated in the upper adherend, within 6 – 7 mm from the lower surface and varies

according to the beam cross sections. The shear stress was measured along the lower interface region of the bondline in the centre of the beam cross section.

6.2 Comparison between solid and bonded beams under similar loads

6.2.1 Deflection

Figure 6.6 (and Table 6.1) show the experimental and finite element results obtained for the inverted T section beams under a 2 kN load. The experimental results exhibit slightly higher measurements compared to the finite element analysis. Overall, it was observed that both methodologies give similar trends for all the spans. The bonded models exhibit higher deflection than their solid equivalent and the difference in behaviour increases for longer spans models comparison. In terms of percentage, the difference in deflection between the bonded and solid model appears to be quite the contrary. The longer beam span bonded model IB250/C has a deflection which is 17% higher than the solid model IS250/C. Comparing the shorter models, bonded model IB050/C gives 64% higher deflection than model IS050/C. The corresponding finite element results showed a similar trend. This suggests that the bonded beams at the shorter spans are structurally less efficient than their solid (welded) counterparts, under similar loading conditions. A probable explanation for this behaviour is the contribution from the adhesive shear strain to the overall deflection of the joint. This contribution is normally highlighted in the deflection calculations involving sandwich beams [13].

Figure 6.7 (and Table 6.2) show the results from experimental and finite element analysis for the inverted T section beams, under a load at 90% of the yield stress. The experiments and finite element results have a similar trend, confirming that the bonded beam exhibits higher deflection than solid equivalent under all spans considered. In terms of magnitude, the shorter beam exhibits less deflection compared to the longer beams. However in terms of percentage, it was noted the difference in deflection was more profound at the shorter spans. Model IB050/C exhibits 65% more deflection than model IS050/C under a 4.5 kN load. The corresponding results obtained from the finite element analysis indicate that the bonded beam exhibitsdd 37% higher deflection. Comparing models at the 250 mm span under a 2 kN load in the same figure, model IB050/C exhibits 18% higher

deflection than its solid equivalent. In the corresponding finite element results, the bonded model exhibits 11% higher deflection than the solid model.

6.2.2 Bending stress

Figure 6.4(and Table 6.1) compares the experimental and linear elastic finite element results for the flat section beam, under 2 kN. It shows that the bonded beams exhibit higher bending stress than their solid equivalent for all the spans. For example model RB050/C exhibits 14% higher bending stress than the solid equivalent model RS050/C. From the finite element curves, a similar trend was noted where the model RB050/B exhibits 17% higher bending stress than model RS050/B. Looking towards the long beam span of 250 mm, the experimental curves show that model RB250/C exhibits only 6% higher bending stress as compared to model RS250/C. The finite element results indicate a similar behaviour, with model RB250/B gives 4% more bending stress than model RS250/B.

Figure 6.5(and Table 6.1) compares the experimental and finite element results obtained for the flat section beam, under a precalculated 90% yield load. In this case, it is clearly visible that the bonded beam exhibits a higher bending stress than its solid equivalent. Considering both methodologies, the experimental results tend to produce higher magnitudes of stress as compared with the finite element analyses, which was consistent throughout the study. Focusing on the model with the 50 mm span, we note that model RB050/C exhibits 39 MPa (18.5%) higher stresses for model RS050/C. Similarly, the corresponding finite element results for model RB050/B gives 29.8 MPa (15%) higher stress than its solid equivalent. The longer span models indicate that model RB250/C giving only 4.3% higher stress than its solid equivalent. The corresponding finite element results show that the model RB250/B exhibits 3.5% higher stress than the solid equivalent.

6.2.3 Shear stress

Figure 6.2 (and Table 6.1) shows the results determined from the finite element analysis of the solid and bonded models of the L section with various spans. The graph is a comparison of the peak shear stresses exhibited by the solid and bonded models along the span of each beam, at the lower interface region as indicated in

Figure 6.2a. In this case, the bonded models have an adhesive thickness of 0.5 mm and subjected to a 2 kN three point load.

Whilst under a 2 kN applied load, it was observed that the solid beam undergoes more shear stress than the bonded beam across the five different spans considered. A probable reason could be found in the ability of the solid model to effectively transmit the shear flow due to its nature of being a continuous/homogenous section of high stiffness material. The neutral axis is located within 1-2 mm of the lower adherend-adhesive interface of the bonded model. However for both solid and bonded models, theoretical calculations suggest that the shear centre was contained in the upper adherend for all beam sections with the exception of the flat beam models. However this location varies from the beams that were studied and is shown in Figure 4.3. For the horizontal location of the shear centre, apart from the other beams considered, the load is not exactly centred on the elastic axis of the beam section for the Z beams. Hence it was observed that the Z beam experienced slight twisting in the FE analysis

The difference in shear stress between the bonded and solid models was at a maximum for the short spans. According to Figure 6.2, model LS050/B exhibits 46% higher stress than for model LB050/B at the lower bondline interface. On the other hand, long span model LS250/B produces just 11% higher stress over model LB250/B.

Table 6.2 shows the results for the models subjected to a 90% calculated yield stress/load. The table shows similar trends to Table 6.1 with some evidence of non linearity, especially for the short span models. A possible explanation for the non linear behaviour of beams may be the result of the beams undergoing sideways deflection instead of lateral deflection which is ideal. There are many possible factors for this phenomenon including material non-linearity. A noticeable reason may be due to the geometric shape of the beam section. For example, the geometric shape of the L beam section does not allow for a proper transfer of load through the middle of the cross section. Due to the unsymmetrical nature of the L section which was bonded to the lower adherend, there is a possibility that a percentage of the load transferred transversely as well as vertically.

Figure 6.3 shows the relationship between shear stress and span and confirms non-linear behaviours within the elastic load limit. According to Figure 6.3, the shear stress determined at shorter span beams was higher in comparison to the longer span beams. This is due to the combination of increased bending stiffness and high compressive stresses in the shorter beams. Similar to the results presented earlier, the solid beam exhibits higher shear stress than the bonded beam at the five different spans considered. The shear stress exhibited by model TS050/B is 40% higher than model TB050/B at 50 mm span. With respect to the earlier graph, the marginal difference in terms of shear stress tends to decrease in magnitude at the longer span beams. As indicated for the 250 mm span, model TS250/B exhibits only 9% more shear than its bonded equivalent model TB250/B under 2.5 kN load.

6.3 Effect of adhesive thickness in bonded T & L section beams

The following results represent the experimental and numerical work carried out on 40 models, in order to evaluate the effect of varying the adhesive thickness. The T and L section beams were considered for this with adhesive thicknesses of 0.1, 0.2, 0.3 and 0.4mm (as shown in the designation system). Figure 6.8 compares the geometry of bonded T section models with 0.1 mm and 0.4 mm adhesive thicknesses. Comparatively, both models comprise of similar overall cross sectional dimensions, with an overall height of 20 mm. However, a close inspection of both models shows that the thickness of their upper adherend is varying very slightly to compensate for the variation in the adhesive thickness, keeping the same overall height for all sections. For each comparison described in this section, four models of the same span were subjected to similar loading conditions. Again, comparing experimental and analytical methodologies, it was observed that the experimental results tended to give higher values.

6.3.1 Deflection

Figure 6.9 (and Table 6.3) represents the results obtained for the T section for 200 mm span beams under 2 kN. The figure shows a linear reduction in the deflection with decreasing adhesive thickness. Experimental results show that model TB200/C$^{(0.4)}$ exhibits a deflection of 0.286 mm while model TB200/C$^{(0.1)}$ exhibits a lesser deflection of 0.260 mm, which is 10% less deflection. The corresponding finite

element analysis shows a similar trend, with the model TB200/B$^{(0.4)}$ resulted in 3% more deflection compared to the model TB200/B$^{(0.1)}$.

Figure 6.10 (and Table 6.3) represents the results obtained from the experimental and finite element analysis of the L section beams with a 75 mm beam span, under a 2 kN load. Experimental results in this case show that model LB075/C$^{(0.4)}$ exhibits 31.8% more deflection than model LB075/C$^{(0.1)}$. Similarly, the finite element model LB075/B$^{(0.4)}$, gives 15.7% more deflection than model LB075/B$^{(0.1)}$.

6.3.2 Bending stress

Figure 6.11 (and Table 6.4) compares four 50 mm L beam models subjected to a similar load of 7 kN (90% yield). In this case, it is apparent that the experimental results give lower bending stress as compared with the results from the finite element analysis. This corresponds to the comparisons made on the T section beams. This is possibly due to the work hardening of the materials in the joint which was not accounted for in the finite element analysis. This non-linear behaviour occurs when the materials of the joint is strained beyond the yield point, apparent at the centre of the beam. Increased stress is required to produce additional plastic deformation as the materials apparently becomes stronger and stiffer to deform. According to Figure 6.11, the experimental results show that the model LB050/C$^{(0.4)}$ exhibits a bending stress of 106 MPa while model LB050/C$^{(0.1)}$ exhibit a bending stress of 102.5 MPa, equates to 4%. The corresponding finite element analysis shows a similar trend, with the model LB050/B$^{(0.4)}$ with a 0.4 mm adhesive thickness exhibiting 3.5% more bending stress as compared to the model LB050/B$^{(0.1)}$.

Figure 6.12 (and Table 6.4) represents the results obtained from experimental and finite element analysis of the T sections with a 150 mm span, under 4 kN load (90% yield). In this case, the experimental and finite element results as shown tend to be comparable, and this is observed in the comparison of the 150, 200 and 250 mm spans of the T & L beam models. The experimental results indicate that model TB150/C$^{(0.4)}$, with an adhesive thickness of 0.4 mm exhibits only 2.05 MPa higher bending stress than model TB150/C$^{(0.1)}$. The corresponding finite element results for model TB150/B$^{(0.4)}$ produces 1.3 MPa more bending stress than model TB150/B$^{(0.1)}$.

Comparing both Figure 6.11 and Figure 6.12, results suggest that the long bonded beams are less sensitive to change in the adhesive thickness.

6.3.3 Shear stress

Figure 6.13 (and Table 6.4) compares four finite element models for the 150 mm T section beams under 4 kN. The curve remains nearly constant throughout the four different thicknesses. Models TB150/B$^{(0.4)}$ and TB150/B$^{(0.1)}$ exhibit shear stresses of 9.96 MPa and 10.2 MPa respectively. The differences between both models are very small, and this was observed for the five different spans considered for the T models.

Figure 6.14 (and Table 6.4) shows finite element results obtained for the 150 mm L section beams under 4 kN. In this case, the difference is more noticeable in comparing the models LB150/B$^{(0.4}$ and LB150/B$^{(0.1)}$. The shear stresses are 16.7 MPa and 19 MPa respectively, which equates to a 14% difference. Comparing the models under the different span groups, all indicate that the shear stress tend to be higher at the thinner adhesive bondlines.

6.4 Effects of adhesive thickness on flat section beams

The following results represent the experimental and numerical work carried out on 32 models, in order to evaluate the effect of varying the adhesive thickness. The flat beam section was considered in this study due to its stability in plastic loading and ease of fabrication and bonding process. As a reminder, the objectives are:

- To quantify the mechanical behaviour of the bonded beams due to the effect of the adhesive thickness, up to 1mm
- To make a comparison of four models with adhesive thickness ranging from 0.1 mm to 0.4 mm.

The bending stiffness of the bonded model tends to be higher as a result of the increased adhesive thickness. Therefore it is important at this point to highlight the difference between the T & L sections and the flat (rectangular) beam section studied here, and to treat both cases separately. Figure 6.15 (and Table 6.5) compares the overall cross section of the 0.4 mm model with the 0.1 mm model. The increase in cross sectional area of the 0.4 mm model may result in a greater second moment of area and hence structural stiffness. However it is uncertain that the model with the

smaller thickness will behave insubstantially under similar loading conditions. This section aims to determine the effect of the varying adhesive thickness whilst keeping the adherend dimensions constant.

6.4.1 Deflection

Figure 6.17 (and Table 6.5) shows the results obtained from the experiments and finite element analysis for the flat section beams at 200 mm span. The comparison shown here consists of 4 different models with the adhesive thickness of 0.1, 0.2, 0.3 and 0.4 mm. Maximum deflection was similarly measured at the underside of the lower adherend. According to Figure 6.17, both methodologies are showing linear trends and the results are comparable. Focusing our attention on experimental results, model RB200/$C^{(0.4)}$ exhibits a deflection of 0.695 mm while model RB200/$C^{(0.1)}$ exhibits a deflection of 0.706 mm. The slight difference of 0.011 mm corresponds to the difference of 4 MPa in terms of bending stress experienced by both models. Finite element results are more consistent in showing an increase of deflection with respect to the reduction in adhesive thickness. Model RB200/$B^{(0.4)}$ exhibits a deflection of 0.683 mm whilst the thinner model RB200/$B^{(0.1)}$ exhibits a deflection of 0.7 mm. The small difference was similar to the experimental results. As mentioned earlier, any significant distinction between the 4 models desired must take into account the use of higher loads in experimentation.

6.4.2 Bending stress

For the comparison as described in this section, six models with adhesive thickness 0.1, 0.2, 0.3, 0.4, 0.5 and 1 mm were compared under similar elastic loading conditions. Figure 6.16 represents the results obtained for the 150 mm flat beam sections subjected to an elastic load of 8 kN. Comparing both methodologies, it was observed that the experimental results tend to exhibit higher bending stresses as compared to the finite element results. Similar to previous measurement procedures, the bending strain was measured along the reference line shown in Figure 6.8.

Accordingly to Figure 6.16, experimental results show that the model RB150/$C^{(1)}$ (with 1mm adhesive thickness) exhibits bending stress of 309.6 MPa while model RB150/$C^{(0.1)}$ exhibits stress 321.9 MPa. This corresponds to a 4% increase of bending stress experience by the model RB150/$C^{(0.1)}$. Between the two models considered, the

other models tend to exhibit bending stress between 320 – 328 MPa. It is worth noting here that it was difficult to make any significant distinction between the models subjected to elastic loads. Focusing attention on the analytical work carried out on the models, the difference in behaviour is more obvious. According to beam theory calculations, model RB150/$A^{(0.1)}$ exhibits bending stress of 324.1 MPa while model RB150/$A^{(1)}$ exhibits stress of 272.5 MPa. Using the theoretical calculations, the model with 0.1 mm adhesive thickness exhibits 18.9% more stress than the 1 mm model.

The experimental results obtained tend to be much higher than the results obtained from finite element analysis. The flat section beams display pure lateral bending more easily due to the even and homogenous transfer of load attributed to the increase loading area. Comparing both methodologies, the finite element results however tend to show more consistency. Between the models containing 0.2 mm to 0.5 mm thickness, the results show a small difference of 0.7 – 1.2 MPa separating each model, with bending stress increasing with reducing the adhesive thickness. Focusing our attention on the model with 1 mm adhesive thickness, model RB150/$B^{(1)}$ exhibited a bending stress of 283.6 MPa. At the other extreme, model RB150/$B^{(0.1)}$ exhibited a bending stress of 293.9 MPa. The difference of 10.3 MPa corresponds to 4% increase exhibited by model RB150/$B^{(0.1)}$. This was found comparable to the experimental results.

6.4.3 Shear stress

`Figure 6.18 (and Table 6.5) shows the results obtained from finite element analysis which aims to determine the effect of varying the adhesive thickness on the shear stress of the adhesive. Again, the shear stress values were taken at the lower interface of the bondline for the finite element model. `Figure 6.18 compares four 50 mm flat section models subjected to an elastic load of 15 kN. The finite element analysis on all models analysed shows an increase in the shear stresses with reducing adhesive thickness. According to the results, model RB050/$B^{(0.1)}$ produces about 34% higher stress than model RB050/$B^{(0.4)}$. This signifies that models with a thinner adhesive bondline will experience higher shear stress as compared to the model with a thicker bondline under similar loading conditions. With this in mind, designers may take advantage of subjecting the joint to higher shear loads whilst maintaining the beam's

cross sectional area. This observation is true with testing of other joints such as lap shear joints, etc.

6.5 Elastic-plastic behaviour of flat section bonded beams

The following results represent the experimental and numerical work carried on 32 models, subjected to three-point bending under plastic loads. In this section, the following methodologies were used;

- to differentiate between flat bonded beam models and models with varying thickness
- to distinguish between the solid and bonded models and models in terms of deflection, bending and shear stress.

Figure 6.19 (and Table 6.6) represents a typical load-displacement curve test record of a flat bonded model subjected to plastic failure. The test record represents a baseline curve for models with high bond strength. The initial portion of the curve represents the elastic behaviour of the model. At around 20 kN load value, the slope changes and the load take up becomes more gradual. The stress point on the load-deformation curve exhibits a "knee" also known as the yield stress of the joint. In this region of the bonded model, the load values represent a slight metal deformation mixed with the energy required to overcome the adhesion of the adhesive-adherend interface. The joint is said to have been plastically deformed which is also a sign that the adhesive material is absorbing energy. The energy required to overcome these interfacial forces was represented by a definite break in the test record at a displacement of 11.24 mm. The load value at this point was taken as the yield strength of the bonded interface. It was at this point that the experimentation ceased.

6.5.1 Effect of adhesive thickness on deflection

The following results represent the experimental work in order to evaluate the effect of varying the adhesive thickness. The results of the flat beam models with 75 mm and 55 mm beam span were chosen for comparison in this section. It is worth noting, that the results for bending strain were not presented here due to the failure of the strain gauges during testing on most models prior to reaching the plastic load.

Figure 6.20 (and Table 6.7) represents the results obtained from experimental work with the flat beam models with 55 mm span. The four models compared were subjected to an estimated plastic load of 59.2 – 65 kN in the experiments. Figure 6.20 shows a significant deflection increase with increasing adhesive thickness within the plastic limit of the adherends. Comparing this with the elastic results as shown in Table 6.5, a similar trend is noted. However comparing the models under elastic loads, the difference of only 9.5% in terms of deflection between models RB050/$C^{(0.4)}$ and RB050/$C^{(0.1)}$. When we compare the same models under plastic loads, model RB055/$C^{(0.4)}$ exhibit a deflection of 1.66 mm at failure, while the model RB055/$C^{(0.1)}$ exhibits a deflection of 1.24 mm. The difference of 0.42 mm in deflection corresponds to an increase of 34% more deflection achieved with the thicker 0.4 mm model. It is worth noting that the effects of the varying thickness in terms of deflection became more pronounced as the models were subjected to plastic loads.

Figure 6.21 (and Table 6.7) represents the other set of results obtained from the 75 mm span models. The models were subjected to a lower plastic load of the range 43 – 50 kN, where 4 models with varying adhesive thickness of 0.1 – 0.4 mm were tested. Again, we noticed that as the adhesive thickness increases, the model undergoes further deflection prior to failure. Accordingly to Figure 6.22, the 0.4 mm model RB075/$C^{(0.4)}$ exhibits a deflection of 2.4 mm, while the thinner model RB075/$C^{(0.1)}$ exhibits a deflection of 1.26 mm at failure. This corresponds to a difference of 90% more deflection in which the thicker model RB075/$C^{(0.4)}$ was able to operate.

6.5.2 Effect of adhesive thickness on failure load.

The following results were obtained from experiments on the flat beam models, with the aim of determining the effect of adhesive thickness on the failure load. The four different models under consideration here have a span of 55 mm. According to Figure 6.22, the *y-axis* represents the failure load of each model determined from the test records of the experimental testing. The *x-axis* on the graph represents the four different adhesive thicknesses considered, 0.4, 0.3, 0.2 and 0.1 mm. Experimental results show that model RB055/$C^{(0.4)}$ reaches failure load at 65 kN while model RB055/$C^{(0.1)}$ reaches failure at 59.2 kN. The difference corresponds to the ability of the thicker model to undergo a 10% higher load than the thinner model before failure.

The trend of the curve is such that as a higher failure load is achieved with a thicker adhesive bondline.

Figure 6.23 (and Table 6.7) shows the results for the 75 mm span models where failure load tends to be lower than the earlier comparison due to the increased span. The results are more consistent here, where the failure load decrease almost linearly along the decreasing adhesive thickness. Experimental results show that model RB075/C$^{(0.4)}$ exhibits a failure load of 49.10 kN, while the thinner 0.1 mm model RB075/C$^{(0.1)}$ exhibits a failure load of 43 kN. The difference between both model corresponds to 14%. The curve tends to show a decrease of failure load of 1-3 kN as the thickness is reduced by 0.1 mm. The results here concur with the results shown previously. This is discussed further in Section 7.8.

6.6 Elastic-plastic behaviour of solid and bonded flat beam models

Figure 6.24 shows a schematic curve for the force-deflection curve obtained for the flat section beam models RS150/C and RB150/C. The elastic region shown is represented by a three-point load between 0–15 kN. In this region, both curves obtained from both models shows a linear response up to a load of 15 kN. A reduction in the bonded beam flexural stiffness was found to exist up to this point, resulting in increased bending stress and deflection. However, this may be avoided as the difference in the deflection or stiffness is less apparent for long beams (200 – 250 mm). After 15 kN, the curve slope changes and the load take up becomes more gradual for both the solid and bonded models. In this region, the load values represent a slight metal deformation mixed with the energy required to overcome the adhesion of the adherend adhesive interfaces in the bonded model.

Figure 6.25 shows a schematic curve for the force-deflection curve for models at TS150/C and TB150/C under plastic loading conditions. The elastic region which is represented in the three-point load range of 0 – 12 kN, with both the solid and bonded beams show a similar response. At about 12.5 kN, the slope changes for both models where the bonded model slope increases steeply. At about 4 mm deflection, the solid beam undertakes a load of 14.8 kN while the bonded beam undertakes a load of 16 kN. The applied load continues to increase gradually for both until the bonded beam fails at a deflection of 8.89 mm. The load on the solid beam continues to increase and

was expected to supersede the maximum load reached by the bonded model. In summary, the bonded beam fails earlier than its solid counterpart and future analysis should focus on the determination of the effective working load for similar joints.

Specimen Designation	Length between supports (mm)	Applied Force (N)	Analytical Results			Numerical Results			Experimental Results	
			σ_{bx} (MPa)	$\tau_{Adhesive}$ (MPa)	δ (mm)	σ_{bx} (MPa)	$\tau_{Adhesive}$ (MPa)	δ (mm)	σ_{bx} (MPa)	δ (mm)
TS050/X	50	2000	24.920	5.112	0.004	28.170	5.391	0.005	24.600	0.016
TS075/X	75	2000	37.380	5.112	0.013	41.220	5.644	0.017	38.950	0.033
TS150/X	150	2000	74.760	5.112	0.105	77.820	5.075	0.110	73.800	0.130
TS200/X	200	2000	99.681	5.112	0.249	102.300	5.663	0.255	100.450	0.267
TS250/X	250	2000	124.601	5.112	0.487	127.900	5.678	0.499	127.100	0.523
TB050/X	50	2000	24.985	5.199	0.006	29.680	3.244	0.009	38.950	0.039
TB075/X	75	2000	37.447	5.199	0.016	42.550	4.178	0.021	41.000	0.036
TB150/X	150	2000	74.894	5.199	0.112	79.440	4.917	0.120	79.950	0.146
TB200/X	200	2000	99.859	5.199	0.258	104.100	5.062	0.269	102.500	0.303
TB250/X	250	2000	124.824	5.199	0.498	129.900	5.111	0.517	129.950	0.567
LS050/X	50	2000	24.798	7.547	0.004	30.490	8.764	0.006	28.700	0.035
LS075/X	75	2000	37.197	7.547	0.013	43.810	9.345	0.018	41.000	0.034
LS150/X	150	2000	74.395	7.547	0.107	80.370	9.002	0.115	51.250	0.131
LS200/X	200	2000	99.193	7.547	0.252	104.400	9.587	0.262	102.500	0.298
LS250/X	250	2000	123.991	7.547	0.493	129.900	9.598	0.509	127.100	0.534
LB050/X	50	2000	24.823	7.618	0.007	33.330	4.753	0.008	28.700	0.032
LB075/X	75	2000	37.324	7.618	0.018	46.020	6.519	0.023	36.900	0.047
LB150/X	150	2000	74.466	7.618	0.116	82.850	8.109	0.125	73.800	0.146
LB200/X	200	2000	99.291	7.618	0.266	107.100	8.406	0.282	104.550	0.327
LB250/X	250	2000	124.114	7.618	0.510	132.900	8.526	0.537	133.250	0.589
ZS050/X	50	2000	20.225	6.742	0.003	30.080	9.468	0.006	24.600	0.036
ZS075/X	75	2000	30.337	6.742	0.009	40.080	10.220	0.015	43.050	0.058
ZS150/X	150	2000	60.674	6.742	0.074	70.960	11.240	0.087	65.600	0.104
ZS200/X	200	2000	80.899	6.742	0.175	91.720	11.430	0.196	86.100	0.240
ZS250/X	250	2000	101.12	6.742	0.343	112.400	6.060	0.372	114.900	0.376
ZB050/X	50	2000	20.279	6.760	0.006	33.310	5.096	0.009	28.700	0.070
ZB075/X	75	2000	30.419	6.760	0.014	42.570	6.743	0.020	43.050	0.092
ZB150/X	150	2000	60.838	6.760	0.084	74.060	8.672	0.103	75.850	0.120
ZB200/X	200	2000	81.117	6.760	0.189	94.680	9.029	0.217	102.500	0.248
ZB250/X	250	2000	101.397	6.760	0.360	115.600	9.160	0.399	123.000	0.460
RS050/X	50	2000	24.974	3.871	0.008	29.930	3.485	0.004	24.600	0.023
RS075/X	75	2000	37.461	3.871	0.011	36.050	3.431	0.012	32.800	0.031
RS150/X	150	2000	74.922	3.871	0.088	73.370	3.507	0.090	69.700	0.111
RS200/X	200	2000	99.896	3.871	0.210	98.400	4.094	0.212	96.350	0.241
RS250/X	250	2000	124.870	3.871	0.409	123.400	4.123	0.413	123.000	0.444
RB050/X	50	2000	24.975	3.867	0.005	28.770	2.600	0.006	28.700	0.040
RB075/X	75	2000	37.462	3.867	0.014	41.230	3.132	0.016	47.150	0.039
RB150/X	150	2000	74.924	3.867	0.095	78.680	3.672	0.099	79.950	0.144
RB200/X	200	2000	99.899	3.867	0.218	103.700	3.741	0.224	106.600	0.258
RB250/X	250	2000	124.874	3.867	0.420	128.800	3.753	0.429	131.200	0.515
IS050/X	50	2000	18.445	13.020	0.002	25.700	10.660	0.005	22.650	0.012
IS075/X	75	2000	27.667	13.020	0.007	35.040	10.090	0.012	32.000	0.018
IS150/X	150	2000	55.335	13.020	0.030	62.010	11.230	0.069	61.500	0.085
IS200/X	200	2000	73.779	13.020	0.141	80.460	11.290	0.155	77.900	0.179
IS250/X	250	2000	92.224	13.020	0.276	98.900	11.230	0.293	96.350	0.302
IB050/X	50	2000	18.487	13.049	0.005	28.010	6.349	0.008	26.650	0.033
IB075/X	75	2000	27.730	13.049	0.012	36.170	8.544	0.019	36.900	0.040
IB150/X	150	2000	55.460	13.049	0.069	63.840	11.660	0.088	59.450	0.132
IB200/X	200	2000	73.946	13.049	0.154	82.430	12.400	0.182	65.600	0.217
IB250/X	250	2000	92.433	13.049	0.292	101.000	12.730	0.328	88.400	0.366

Table 6.1 Results of various beam sections under 2 kN load.
(X designation, A = Theoretical, B = Numerical and C = Experimental)

Specimen Designation	Length between supports (mm)	Applied Force (N)	Analytical Results			Numerical Results			Experimental Results	
			σ_{max} (MPa)	$\tau_{Adhesive}$ (MPa)	δ (mm)	σ_{max} (MPa)	$\tau_{Adhesive}$ (MPa)	δ (mm)	σ_{max} (MPa)	δ (mm)
TS050/X	50	10000	124.601	25.559	0.019	140.900	26.960	0.027	137.350	0.050
TS075/X	75	8000	149.521	20.447	0.053	164.800	22.570	0.066	157.950	0.083
TS150/X	150	4000	149.521	10.224	0.210	155.600	11.350	0.221	155.830	0.246
TS200/X	200	3000	149.521	7.668	0.374	153.400	8.495	0.383	153.750	0.400
TS250/X	250	2400	149.521	6.134	0.584	153.400	6.790	0.596	157.950	0.610
TB050/X	50	10000	124.824	25.605	0.030	148.400	16.220	0.038	135.300	0.064
TB075/X	75	8000	149.789	20.447	0.065	170.000	16.760	0.082	164.000	0.104
TB150/X	150	4000	149.789	10.224	0.223	158.900	9.854	0.240	161.950	0.273
TB200/X	200	3000	149.789	7.668	0.387	166.200	7.593	0.404	157.850	0.459
TB250/X	250	2400	149.789	6.134	0.597	155.900	6.134	0.620	157.850	0.621
LS050/X	50	7000	86.794	26.416	0.014	106.700	90.680	0.020	98.400	0.066
LS075/X	75	6000	111.592	22.642	0.040	131.400	28.030	0.054	118.900	0.086
LS150/X	150	4000	148.790	15.058	0.213	160.700	19.210	0.229	159.900	0.296
LS200/X	200	3000	148.790	11.321	0.378	156.700	14.350	0.393	155.800	0.421
LS250/X	250	2400	148.790	9.057	0.592	155.900	11.520	0.611	159.900	0.649
LB050/X	50	7000	86.880	26.663	0.025	116.600	16.630	0.030	104.440	0.063
LB075/X	75	6000	111.703	22.854	0.054	138.000	19.560	0.070	125.350	0.095
LB150/X	150	4000	148.937	15.059	0.232	165.700	16.220	0.256	161.950	0.309
LB200/X	200	3000	148.937	11.321	0.398	160.600	12.610	0.428	159.900	0.460
LB250/X	250	2400	148.937	9.057	0.612	159.400	10.230	0.644	169.900	0.685
ZS050/X	50	8000	80.899	26.966	0.011	120.300	37.810	0.024	102.500	0.079
ZS075/X	75	7000	106.180	23.596	0.032	140.200	35.760	0.052	127.100	0.103
ZS150/X	150	6000	162.022	20.225	0.222	212.900	33.750	0.262	202.950	0.250
ZS200/X	200	4500	162.022	15.169	0.395	206.400	25.710	0.440	200.900	0.501
ZS250/X	250	3500	176.966	11.798	0.599	196.800	10.530	0.650	207.050	0.568
ZB050/X	50	8000	61.117	27.039	0.024	133.300	20.360	0.036	114.800	0.095
ZB075/X	75	7000	106.467	23.659	0.049	149.000	23.600	0.071	131.200	0.129
ZB150/X	150	6000	162.514	20.225	0.251	222.200	26.020	0.309	211.500	0.309
ZB200/X	200	4500	162.514	15.169	0.425	213.000	20.032	0.487	211.900	0.538
ZB250/X	250	3500	177.444	11.830	0.629	202.200	16.030	0.699	202.500	0.740
RS050/X	50	15000	187.305	29.032	0.025	161.7	25.64	0.030	172.2	0.070
RS075/X	75	12000	224.766	23.226	0.066	200.7	20.57	0.074	217.3	0.122
RS150/X	150	8000	299.688	15.484	0.354	274.1	13.60	0.382	293.2	0.404
RS200/X	200	6000	299.688	11.613	0.629	275.4	10.10	0.636	297.3	0.671
RS250/X	250	5000	312.175	9.667	1.023	287.4	8.45	1.026	315.7	0.842
RB050/X	50	15000	187.311	29.002	0.041	191.5	19.30	0.045	211.2	0.117
RB075/X	75	12000	224.773	23.202	0.086	226.2	19.19	0.096	248.1	0.133
RB150/X	150	8000	299.698	15.468	0.379	291.5	14.82	0.398	325.9	0.466
RB200/X	200	6000	299.698	11.601	0.654	288.3	11.24	0.674	317.8	0.734
RB250/X	250	5000	312.185	9.668	1.050	298.1	9.39	1.067	330.1	1.184
IS050/X	50	4500	41.501	29.295	0.005	59.420	21.670	0.012	55.350	0.020
IS075/X	75	4000	55.335	26.040	0.015	89.650	20.620	0.024	83.550	0.030
IS150/X	150	3500	96.835	22.785	0.104	109.700	18.590	0.122	106.600	0.128
IS200/X	200	3000	110.669	19.530	0.212	121.800	15.960	0.234	125.050	0.250
IS250/X	250	2000	92.224	13.020	0.276	99.520	10.640	0.293	100.450	0.297
IB050/X	50	4500	41.595	29.361	0.012	65.360	14.080	0.019	63.550	0.058
IB075/X	75	4000	55.460	26.098	0.025	73.210	16.920	0.037	71.750	0.064
IB150/X	150	3500	97.055	22.836	0.121	113.600	20.340	0.154	110.700	0.149
IB200/X	200	3000	110.919	19.574	0.231	125.400	18.600	0.274	123.000	0.313
IB250/X	250	2000	92.433	13.049	0.292	102.000	12.720	0.328	104.500	0.383

Table 6.2 Results of various beam sections under a 90% yield stress.

Specimen Designation	Adhesive Thickness (mm)	Length between supports (mm)	Applied Force (N)	Analytical Results			Numerical Results			Experimental Results	
				σ_{bm} (MPa)	$\tau_{Adhesive}$ (MPa)	δ (mm)	σ_{bm} (MPa)	$\tau_{Adhesive}$ (MPa)	δ (mm)	σ_{bm} (MPa)	δ (mm)
TB050 / X$^{(0.4)}$	0.4	50	2000	24.959	5.115	0.004	29.760	3.742	0.008	30.750	0.031
TB050 / X$^{(0.3)}$	0.3	50	2000	24.951	5.114	0.004	29.570	4.035	0.007	30.750	0.030
TB050 / X$^{(0.2)}$	0.2	50	2000	24.492	5.112	0.004	29.380	4.412	0.007	34.850	0.043
TB050 / X$^{(0.1)}$	0.1	50	2000	24.932	5.110	0.004	29.150	4.898	0.006	28.700	0.032
TB075 / X$^{(0.4)}$	0.4	75	2000	37.438	5.115	0.013	40.690	5.699	0.016	43.050	0.036
TB075 / X$^{(0.3)}$	0.3	75	2000	37.427	5.114	0.013	38.170	3.959	0.016	45.100	0.046
TB075 / X$^{(0.2)}$	0.2	75	2000	37.413	5.112	0.013	41.530	4.760	0.016	45.100	0.041
TB075 / X$^{(0.1)}$	0.1	75	2000	37.398	5.110	0.013	41.330	5.016	0.017	43.050	0.046
TB150 / X$^{(0.4)}$	0.4	150	2000	74.876	5.115	0.105	79.420	4.980	0.119	79.950	0.127
TB150/ X$^{(0.3)}$	0.3	150	2000	74.853	5.114	0.105	79.220	5.009	0.117	79.950	0.140
TB150 / X$^{(0.2)}$	0.2	150	2000	74.827	5.112	0.105	79.010	5.028	0.115	77.900	0.128
TB150 / X$^{(0.1)}$	0.1	150	2000	74.796	5.110	0.105	78.740	5.098	0.113	77.900	0.137
TB200 / X$^{(0.4)}$	0.4	200	2000	99.834	5.115	0.250	104.400	5.077	0.268	104.500	0.286
TB200/ X$^{(0.3)}$	0.3	200	2000	99.804	5.114	0.250	104.200	5.073	0.265	104.450	0.300
TB200 / X$^{(0.2)}$	0.2	200	2000	99.769	5.112	0.250	103.900	5.054	0.263	102.500	0.266
TB200 / X$^{(0.1)}$	0.1	200	2000	99.728	5.110	0.249	103.600	5.099	0.260	102.500	0.260
TB250 / X$^{(0.4)}$	0.4	250	2000	124.793	5.115	0.487	129.600	5.108	0.511	127.100	0.523
TB250/ X$^{(0.3)}$	0.3	250	2000	124.755	5.114	0.487	129.300	5.090	0.508	127.100	0.517
TB250 / X$^{(0.2)}$	0.2	250	2000	124.711	5.112	0.487	129.000	5.061	0.504	127.100	0.510
TB250 / X$^{(0.1)}$	0.1	250	2000	124.660	5.110	0.487	128.700	5.099	0.501	127.100	0.539
LB050 / X$^{(0.4)}$	0.4	50	2000	24.819	7.554	0.007	33.880	5.640	0.009	34.850	0.043
LB050 / X$^{(0.3)}$	0.3	50	2000	24.815	7.553	0.007	33.530	6.186	0.008	32.800	0.040
LB050 / X$^{(0.2)}$	0.2	50	2000	24.810	7.551	0.007	33.170	6.939	0.008	30.750	0.038
LB050 / X$^{(0.1)}$	0.1	50	2000	24.805	7.549	0.007	32.720	8.031	0.007	30.750	0.033
LB075 / X$^{(0.4)}$	0.4	75	2000	37.229	7.554	0.018	45.360	6.909	0.022	45.100	0.058
LB075 / X$^{(0.3)}$	0.3	75	2000	37.223	7.553	0.018	45.160	7.387	0.021	45.100	0.052
LB075 / X$^{(0.2)}$	0.2	75	2000	37.216	7.551	0.018	44.920	8.012	0.020	41.000	0.046
LB075 / X$^{(0.1)}$	0.1	75	2000	37.207	7.549	0.018	44.560	8.849	0.019	41.000	0.044
LB150 / X$^{(0.4)}$	0.4	150	2000	74.458	7.554	0.116	82.880	8.361	0.120	82.000	0.168
LB150/ X$^{(0.3)}$	0.3	150	2000	74.446	7.553	0.116	82.410	8.639	0.124	82.000	0.165
LB150 / X$^{(0.2)}$	0.2	150	2000	74.431	7.551	0.116	82.110	9.006	0.121	79.950	0.160
LB150 / X$^{(0.1)}$	0.1	150	2000	74.414	7.549	0.116	81.700	9.501	0.118	77.900	0.141
LB200 / X$^{(0.4)}$	0.4	200	2000	99.278	7.554	0.266	107.500	8.588	0.280	110.700	0.321
LB200/ X$^{(0.3)}$	0.3	200	2000	99.261	7.553	0.266	107.200	8.810	0.277	106.800	0.307
LB200 / X$^{(0.2)}$	0.2	200	2000	99.242	7.551	0.266	106.900	9.109	0.273	106.800	0.313
LB200 / X$^{(0.1)}$	0.1	200	2000	99.219	7.549	0.265	106.500	9.524	0.268	104.550	0.284
LB250 / X$^{(0.4)}$	0.4	250	2000	124.097	7.554	0.510	132.500	8.607	0.529	133.250	0.542
LB250/ X$^{(0.3)}$	0.3	250	2000	124.077	7.553	0.510	132.200	8.864	0.524	133.250	0.537
LB250 / X$^{(0.2)}$	0.2	250	2000	124.052	7.551	0.510	131.800	9.139	0.519	133.250	0.510
LB250 / X$^{(0.1)}$	0.1	250	2000	124.023	7.549	0.509	131.400	9.535	0.514	131.200	0.523

Table 6.3 Results for T & L sections at various adhesive thickness under 2 kN.

Specimen Designation	Adhesive Thickness (mm)	Length between supports (mm)	Applied Force (N)	Analytical Results			Numerical Results			Experimental Results 1	
				σ_{max} (MPa)	$\tau_{Adhesive}$ (MPa)	δ (mm)	σ_{max} (MPa)	$\tau_{Adhesive}$ (MPa)	δ (mm)	σ_{max} (MPa)	δ (mm)
TB050 / X (0.4)	0.4	50	12000	149.751	30.692	0.024	178.500	22.450	0.045	168.100	0.071
TB050 / X (0.3)	0.3	50	12000	149.707	30.683	0.024	177.400	24.210	0.043	166.500	0.078
TB050 / X (0.2)	0.2	50	12000	149.654	30.672	0.024	176.300	26.470	0.041	157.850	0.091
TB050 / X (0.1)	0.1	50	12000	149.592	30.659	0.024	174.900	29.390	0.038	157.850	0.091
TB075 / X (0.4)	0.4	75	8000	149.751	20.461	0.053	167.200	17.430	0.077	153.750	0.105
TB075 / X (0.3)	0.3	75	8000	149.707	20.455	0.053	152.700	15.840	0.066	153.750	0.111
TB075 / X (0.2)	0.2	75	8000	149.654	20.448	0.053	166.100	19.040	0.071	153.750	0.100
TB075 / X (0.1)	0.1	75	8000	149.592	20.439	0.053	165.300	20.060	0.068	153.750	0.116
TB150 / X (0.4)	0.4	150	4000	149.751	10.231	0.211	158.800	9.960	0.238	157.850	0.245
TB150/ X (0.3)	0.3	150	4000	149.707	10.228	0.211	158.400	10.020	0.234	157.850	0.267
TB150 / X (0.2)	0.2	150	4000	149.654	10.224	0.211	158.000	10.350	0.230	155.800	0.243
TB150 / X (0.1)	0.1	150	4000	149.592	10.220	0.211	157.500	10.200	0.226	155.800	0.263
TB200 / X (0.4)	0.4	200	3000	149.751	7.673	0.375	156.600	7.616	0.402	155.800	0.424
TB200/ X (0.3)	0.3	200	3000	149.707	7.671	0.374	156.300	7.609	0.398	155.800	0.438
TB200 / X (0.2)	0.2	200	3000	149.654	7.669	0.374	155.900	7.581	0.394	155.800	0.398
TB200 / X (0.1)	0.1	200	3000	149.592	7.665	0.374	155.400	7.548	0.390	153.750	0.391
TB250 / X (0.4)	0.4	250	2400	149.751	6.138	0.585	155.500	6.129	0.614	155.800	0.615
TB250/ X (0.3)	0.3	250	2400	149.707	6.137	0.585	155.200	6.108	0.609	153.750	0.572
TB250 / X (0.2)	0.2	250	2400	149.654	6.134	0.585	154.800	6.073	0.605	153.750	0.539
TB250 / X (0.1)	0.1	250	2400	149.592	6.132	0.585	154.400	6.119	0.601	155.800	0.611
LB050 / X (0.4)	0.4	50	7000	86.868	26.439	0.025	118.600	19.740	0.031	106.600	0.086
LB050 / X (0.3)	0.3	50	7000	86.854	26.435	0.025	117.400	21.650	0.030	106.600	0.084
LB050 / X (0.2)	0.2	50	7000	86.837	26.429	0.025	116.100	24.290	0.028	104.550	0.082
LB050 / X (0.1)	0.1	50	7000	86.816	26.423	0.025	114.500	28.110	0.026	102.500	0.064
LB075 / X (0.4)	0.4	75	6000	111.688	22.662	0.054	136.200	20.730	0.066	133.250	0.134
LB075 / X (0.3)	0.3	75	6000	111.669	22.658	0.055	135.500	22.160	0.063	131.200	0.119
LB075 / X (0.2)	0.2	75	6000	111.647	22.654	0.055	134.700	24.040	0.060	129.150	0.107
LB075 / X (0.1)	0.1	75	6000	111.621	22.648	0.055	133.700	26.550	0.055	127.100	0.096
LB150 / X (0.4)	0.4	150	4000	148.917	15.108	0.232	165.400	16.720	0.254	164.000	0.318
LB150/ X (0.3)	0.3	150	4000	148.892	15.105	0.233	164.800	17.280	0.248	159.900	0.304
LB150 / X (0.2)	0.2	150	4000	148.863	15.102	0.233	164.200	18.010	0.243	159.900	0.296
LB150 / X (0.1)	0.1	150	4000	148.828	15.099	0.233	163.400	19.000	0.237	157.850	0.284
LB200 / X (0.4)	0.4	200	3000	148.917	11.331	0.398	161.300	12.880	0.421	161.950	0.466
LB200/ X (0.3)	0.3	200	3000	148.892	11.329	0.398	160.800	13.220	0.415	155.800	0.448
LB200 / X (0.2)	0.2	200	3000	148.863	11.327	0.398	160.400	13.660	0.407	157.850	0.470
LB200 / X (0.1)	0.1	200	3000	148.828	11.324	0.398	159.700	14.293	0.402	155.800	0.421
LB250 / X (0.4)	0.4	250	2400	148.917	9.065	0.611	159.000	10.400	0.635	159.900	0.645
LB250/ X (0.3)	0.3	250	2400	148.892	9.063	0.612	158.600	10.640	0.629	157.850	0.619
LB250 / X (0.2)	0.2	250	2400	148.863	9.061	0.611	158.200	10.970	0.623	155.800	0.593
LB250 / X (0.1)	0.1	250	2400	148.828	9.059	0.611	157.800	11.440	0.616	155.800	0.626

Table 6.4 Results for T & L sections at various adhesive thickness under 90% yield stress.

Specimen Designation	Length between supports (mm)	Adhesive Thickness (mm)	Applied Force (kN)	Analytical Results			Numerical Results			Experimental Results		
				σ_{ten} (MPa)	$\tau_{Adhesive}$ (MPa)	δ (mm)	σ_{ten} (MPa)	$\tau_{Adhesive}$ (MPa)	δ (mm)	σ_{ten} (MPa)	ε	δ (mm)
RS250 / X	250	0.5	5	312.2	9.677	1.023	287.4	8.4	1.026	315.7	1540	0.812
RS200 / X	200	0.5	6	299.7	11.613	0.629	275.4	10.1	0.636	297.3	1450	0.371
RS150 / X	150	0.5	8	299.7	15.484	0.354	274.1	13.6	0.362	293.2	1430	0.404
RS075 / X	75	0.5	12	224.8	23.226	0.066	200.7	20.6	0.074	217.3	1060	0.122
RS050 / X	50	0.5	15	187.3	29.032	0.025	161.7	25.6	0.030	172.2	840	0.070
RB50 / X	250	0.5	5	312.2	9.667	1.050	298.1	9.4	1.067	330.1	1610	1.134
RB200 / X	200	0.5	6	299.7	11.601	0.654	288.3	11.2	0.674	317.8	1550	0.734
RB150 / X	150	0.5	8	299.7	15.468	0.379	291.5	14.8	0.398	325.9	1590	0.467
RB075 / X	75	0.5	12	224.7	23.202	0.086	226.2	19.2	0.096	248.1	1210	0.133
RB050 / X	50	0.5	15	187.3	29.003	0.041	191.5	19.3	0.045	211.2	1030	0.117
$RB250 / X^{(0.4)}$	250	0.4	5	318.3	9.734	1.070	300.2	9.4	1.084	330.1	1610	1.102
$RB250 / X^{(0.3)}$	250	0.3	5	324.6	9.802	1.091	302.3	9.4	1.097	323.9	1580	1.095
$RB250 / X^{(0.2)}$	250	0.2	5	331.0	9.867	1.112	304.3	9.3	1.110	330.1	1610	1.145
$RB250 / X^{(0.1)}$	250	0.1	5	337.6	9.934	1.134	305.8	9.2	1.123	334.2	1630	1.159
$RB200 / X^{(0.4)}$	200	0.4	6	305.6	11.680	0.667	291.2	11.3	0.683	311.6	1520	0.695
$RB200 / X^{(0.3)}$	200	0.3	6	311.6	11.760	0.679	292.8	11.3	0.689	317.5	1540	0.708
$RB200 / X^{(0.2)}$	200	0.2	6	317.8	11.840	0.692	294.3	11.3	0.694	319.8	1560	0.705
$RB200 / X^{(0.1)}$	200	0.1	6	324.1	11.921	0.706	295.2	11.1	0.700	317.8	1550	0.706
$RB150 / X^{(1)}$	150	1	8	272.5	14.945	0.347	283.6	14.1	0.394	309.6	1510	0.480
$RB150 / X^{(0.5)}$	150	0.5	8	299.7	15.468	0.379	291.0	14.8	0.399	321.9	1570	0.459
$RB150 / X^{(0.4)}$	150	0.4	8	305.6	15.574	0.385	292.2	14.9	0.400	328.0	1600	0.495
$RB150 / X^{(0.3)}$	150	0.3	8	311.6	15.680	0.393	293.2	15.0	0.400	321.9	1570	0.459
$RB150 / X^{(0.2)}$	150	0.2	8	317.8	15.786	0.401	293.9	14.9	0.400	326.0	1590	0.467
$RB150 / X^{(0.1)}$	150	0.1	8	324.1	15.890	0.408	293.9	14.7	0.400	321.9	1570	0.485
$RB075 / X^{(0.4)}$	75	0.4	12	229.2	23.361	0.087	225.1	19.9	0.093	235.7	1150	0.102
$RB075 / X^{(0.3)}$	75	0.3	12	233.7	23.520	0.088	224.1	20.6	0.091	235.7	1150	0.110
$RB075 / X^{(0.2)}$	75	0.2	12	238.3	23.680	0.090	222.4	21.3	0.088	237.8	1160	0.133
$RB075 / X^{(0.1)}$	75	0.1	12	243.1	23.841	0.091	219.6	21.7	0.085	231.7	1130	0.101
$RB055 / X^{(0.4)}$	50	0.4	15	191.0	29.201	0.041	186.6	19.1	0.047	203.0	990	0.053
$RB055 / X^{(0.3)}$	50	0.3	15	194.7	29.400	0.042	189.3	22.1	0.042	198.9	970	0.056
$RB055 / X^{(0.2)}$	50	0.2	15	198.6	29.600	0.042	186.8	23.8	0.040	198.9	970	0.062
$RB055 / X^{(0.1)}$	50	0.1	15	202.6	29.801	0.043	182.2	25.6	0.037	194.8	950	0.057

Table 6.5 Result for flat beam sections with various adhesive thickness under 90 % yield stress.

Specimen Designation	Length between supports (mm)	Adhesive Thickness (mm)	Numerical Results				Experimental Results		
			Reached Load (kN)	σ_{ten} (MPa)	$\tau_{Adhesive}$ (MPa)	δ (mm)	Reached Load (kN)	ε	$\delta_{Machine}$ (mm)
RS250 / X	250	0.5	10.0	380.34	38.94	41.134	10.0	3920	2.58
RS200 / X	200	0.5	15.0	327.71	210.13	79.476	15.0	5440	2.78
RS150 / X	150	0.5	30.0	402.55	177.55	59.648	19.7	5140	2.00
RS075 / X	75	0.5	33.0	407.71	59.06	2.245	49.6	8900	2.13
RS050 / X	50	0.5	22.0	228.71	36.66	0.042	49.5	2630	1.79
RB50 / X	250	0.5	10.0	379.66	44.13	50.675	10.0	3950	2.75
RB200 / X	200	0.5	15.0	399.93	31.93	80.210	15.0	8000	3.00
RB150 / X	150	0.5	30.0	410.21	55.49	64.028	19.8	6080	2.00
RB075 / X	75	0.5	32.0	415.47	79.43	9.773	49.6	11220	2.89
RB050 / X	50	0.5	32.0	400.78	49.30	0.183	49.6	4260	1.85

Table 6.6 Results obtained from flat section solid and bonded beams subjected to plastic loads

Specimen Designation	Length between supports (mm)	Adhesive Thickness (mm)	Numerical Results				Experimental Results		
			Reached Load (kN)	σ_{ten} (MPa)	$\tau_{Adhesive}$ (MPa)	δ (mm)	Reached Load (kN)	ε	$\delta_{Machine}$ (mm)
$RB250 / X^{(0.4)}$	250	0.4	10.0	378.60	39.04	57.632	10.0	4400	2.87
$RB250 / X^{(0.3)}$	250	0.3	10.0	377.90	39.46	60.542	10.0	3610	2.77
$RB250 / X^{(0.2)}$	250	0.2	10.0	377.46	39.90	64.767	10.0	4680	2.95
$RB250 / X^{(0.1)}$	250	0.1	10.0	376.74	45.76	67.579	10.0	4980	3.44
$RB200 / X^{(0.4)}$	200	0.4	15.0	400.27	37.66	81.016	15.0	5870	2.67
$RB200 / X^{(0.3)}$	200	0.3	15.0	399.22	39.90	81.077	15.0	6060	2.71
$RB200 / X^{(0.2)}$	200	0.2	15.0	397.94	42.79	80.986	15.0	6260	2.69
$RB200 / X^{(0.1)}$	200	0.1	15.0	396.34	46.13	80.663	15.0	6880	2.90
$RB150 / X^{(1)}$	150	1	22.5	423.37	62.87	72.426	28.9	5670	15.56
$RB150 / X^{(0.5)}$	150	0.5	22.5	422.56	63.78	72.879	27.8	29480	13.34
$RB150 / X^{(0.4)}$	150	0.4	22.5	421.44	63.66	72.884	24.1	18910	3.00
$RB150 / X^{(0.3)}$	150	0.3	22.5	420.12	62.98	72.824	27.5	3970	13.10
$RB150 / X^{(0.2)}$	150	0.2	22.5	418.41	62.98	72.707	28.7	2190	7.84
$RB150 / X^{(0.1)}$	150	0.1	22.8	414.94	63.52	72.145	25.5	5550	5.40
$RB075 / X^{(0.4)}$	75	0.4	30.0	407.29	73.13	4.882	49.1	1950	2.40
$RB075 / X^{(0.3)}$	75	0.3	30.0	409.76	76.18	6.698	46.8	28400	2.00
$RB075 / X^{(0.2)}$	75	0.2	31.5	321.12	65.89	10.195	45.0	22430	1.58
$RB075 / X^{(0.1)}$	75	0.1	31.0	413.63	88.51	10.141	43.0	19150	1.26
$RB055 / X^{(0.4)}$	55	0.4	22.0	304.54	31.77	0.066	65.0	23640	1.66
$RB055 / X^{(0.3)}$	55	0.3	37.5	423.44	81.12	1.718	63.9	35210	1.66
$RB055 / X^{(0.2)}$	55	0.2	37.5	425.39	80.99	1.707	61.7	23920	1.54
$RB055 / X^{(0.1)}$	55	0.1	37.5	426.02	77.68	1.955	59.2	16270	1.24

Table 6.7 Results obtained from flat section bonded beams with various adhesive thickness subjected to plastic loads.

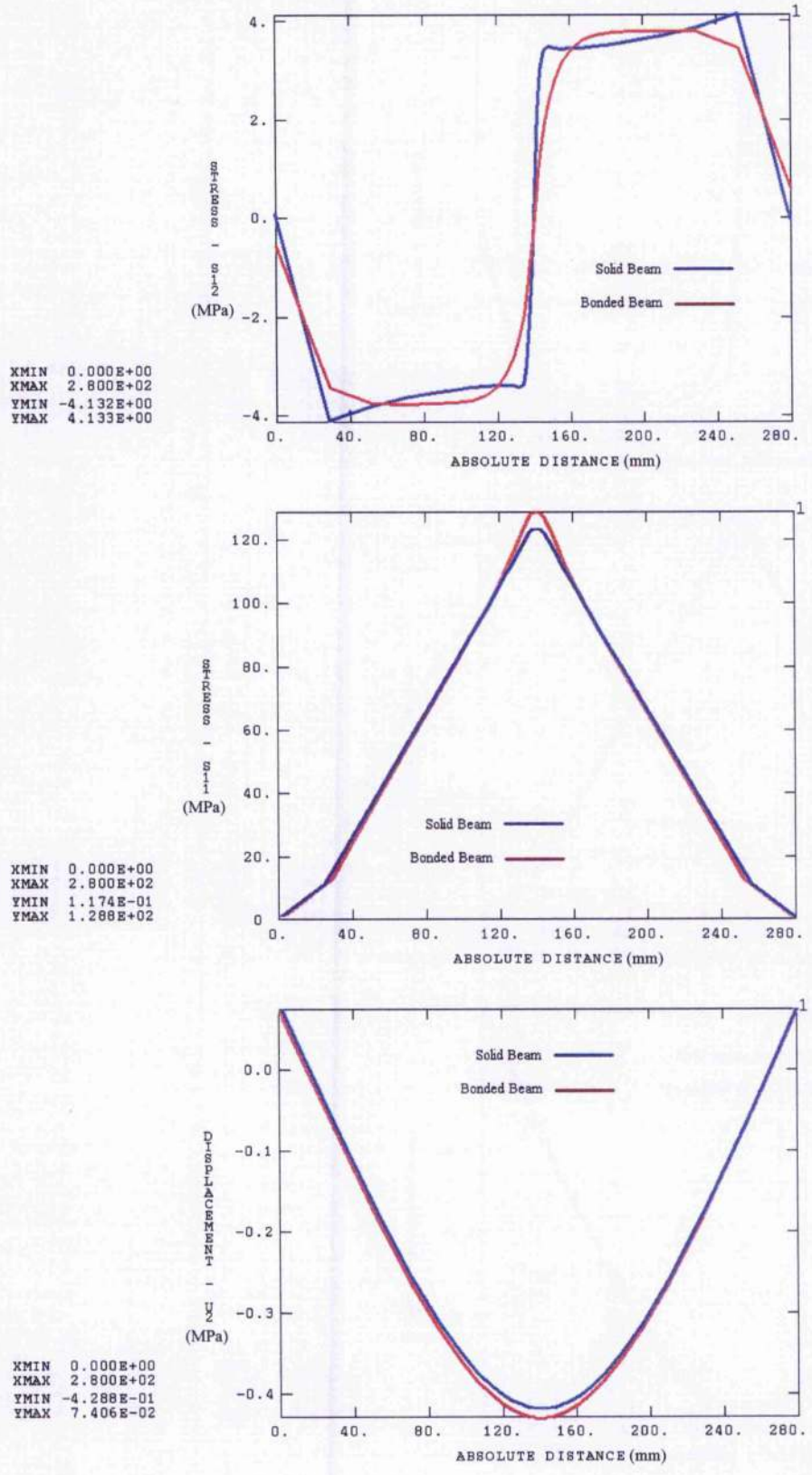

Figure 6.1 a) Shear stress, b) bending stress and c) deflection results computed via FEA along the span of the flat beam.

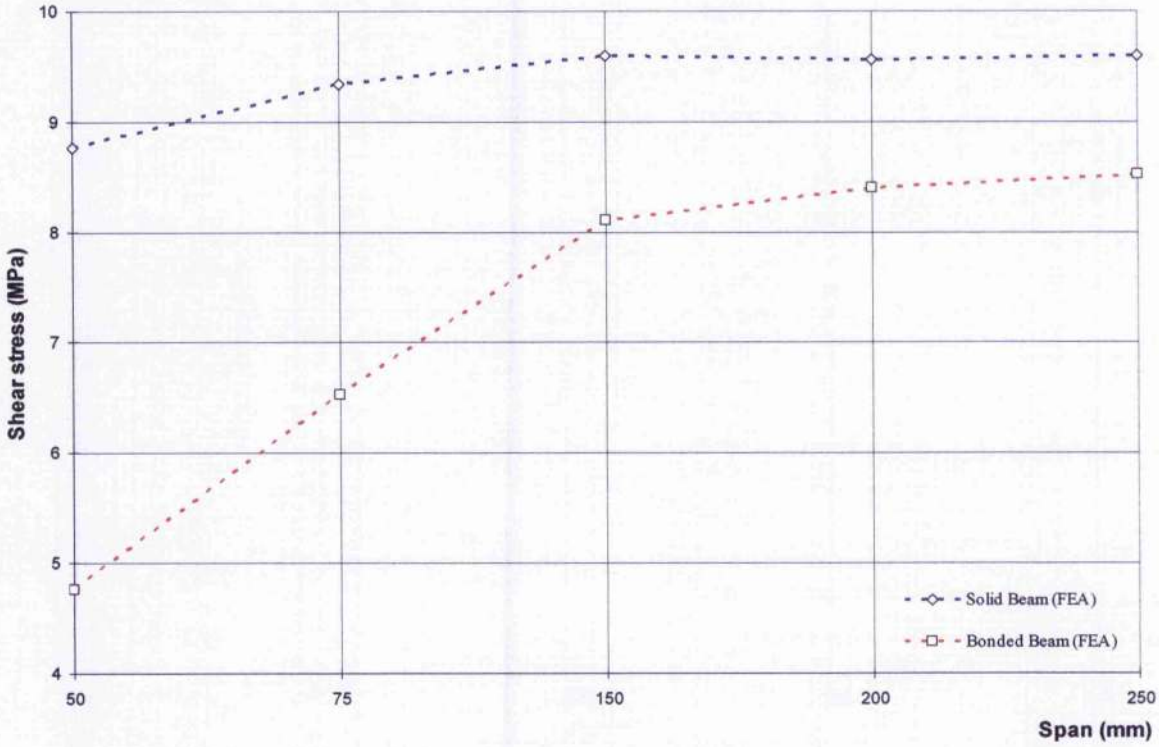

Figure 6.2 Shear stress results computed via FEA along of the span of the L beam section under a 2kN load.

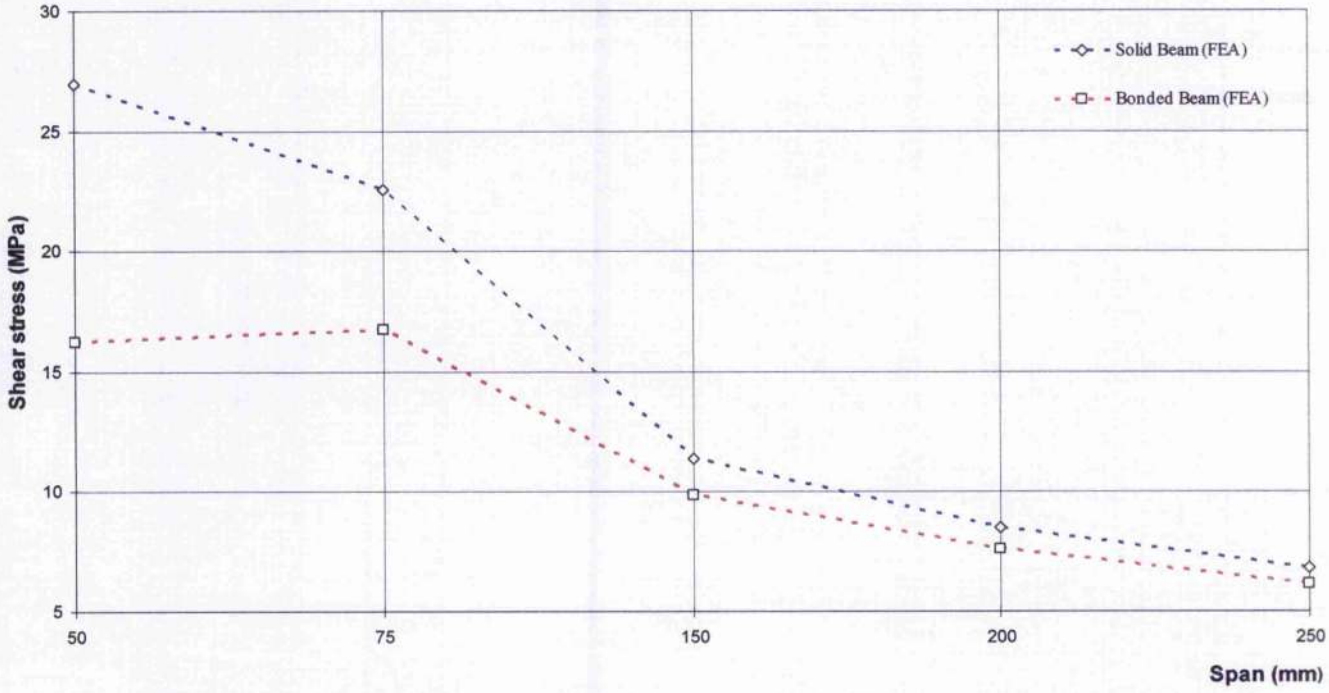

Figure 6.3 Shear stress results computed via FEA along of the span of the T beam section undergoing 90% of the yield load.

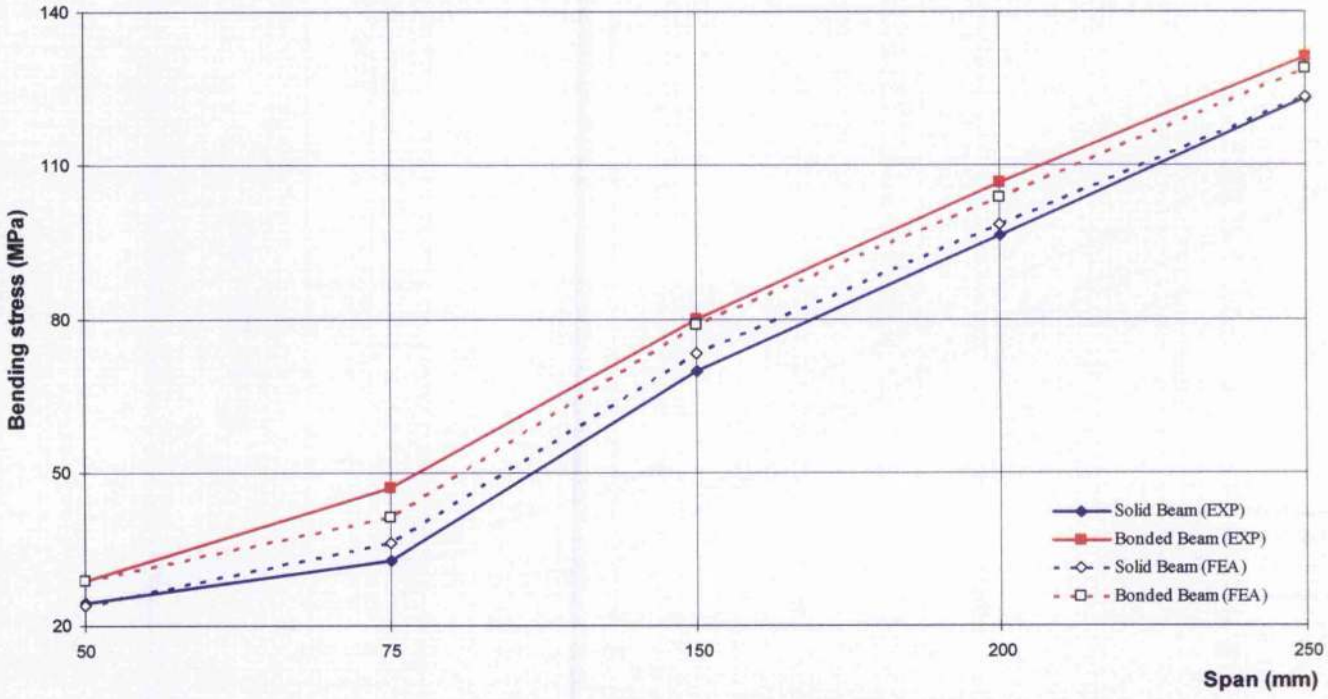

Figure 6.4 Bending stress computed via experiments and FEA along of the span the flat beam section undergoing a 2kN load.

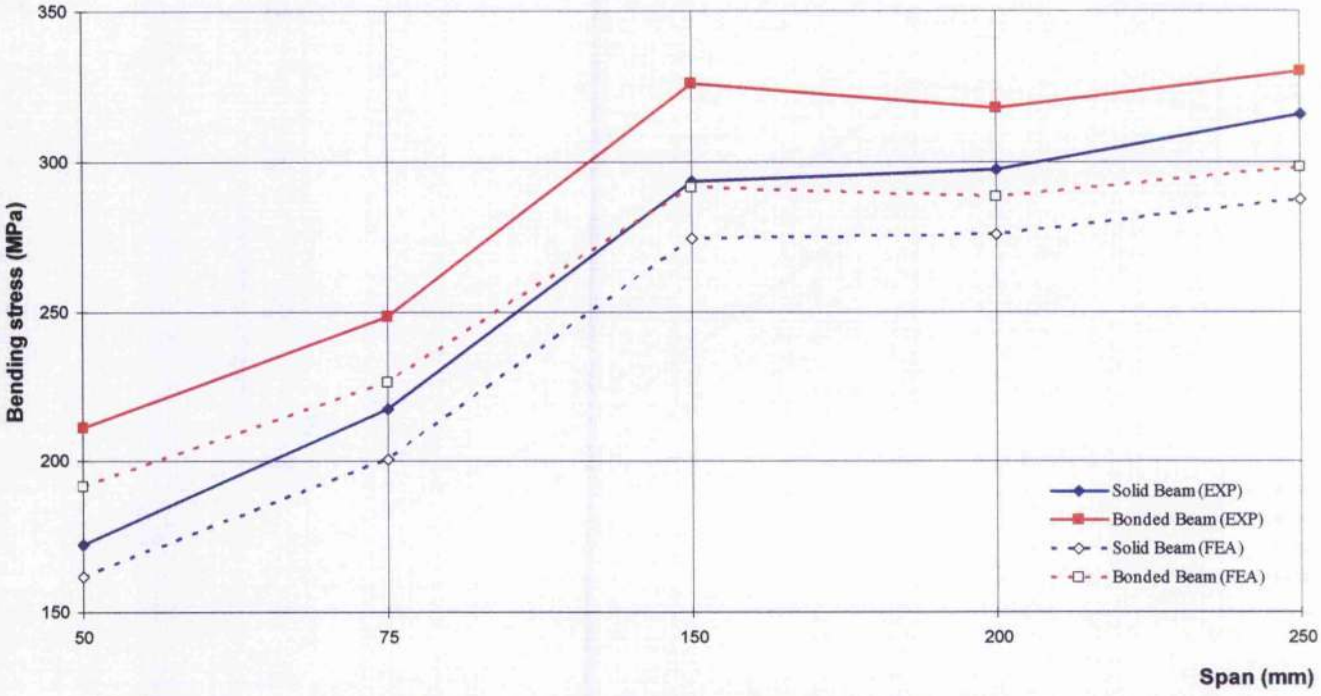

Figure 6.5 Bending stress computed via experiments and FEA along of the span of the flat beam section undergoing a 90% yield load.

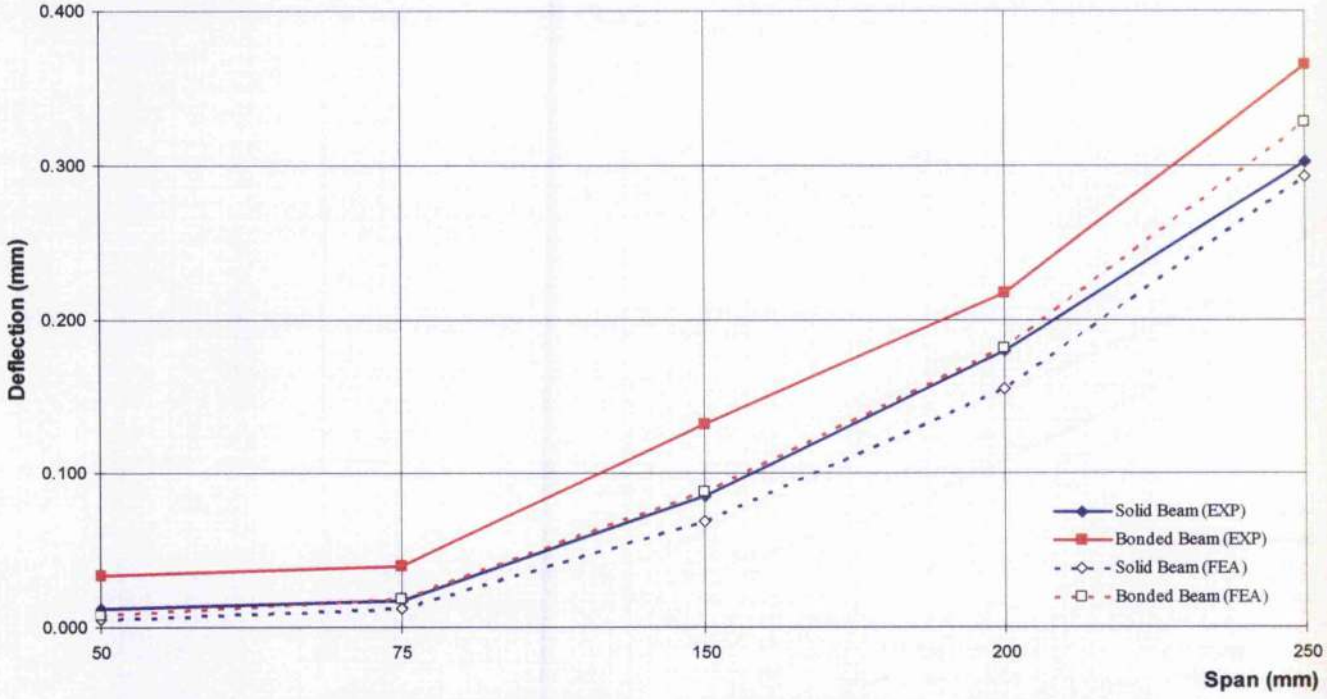

Figure 6.6 Maximum deflection computed via experiments and FEA along of the span of the inverted T section beam undergoing a 2kN three point load.

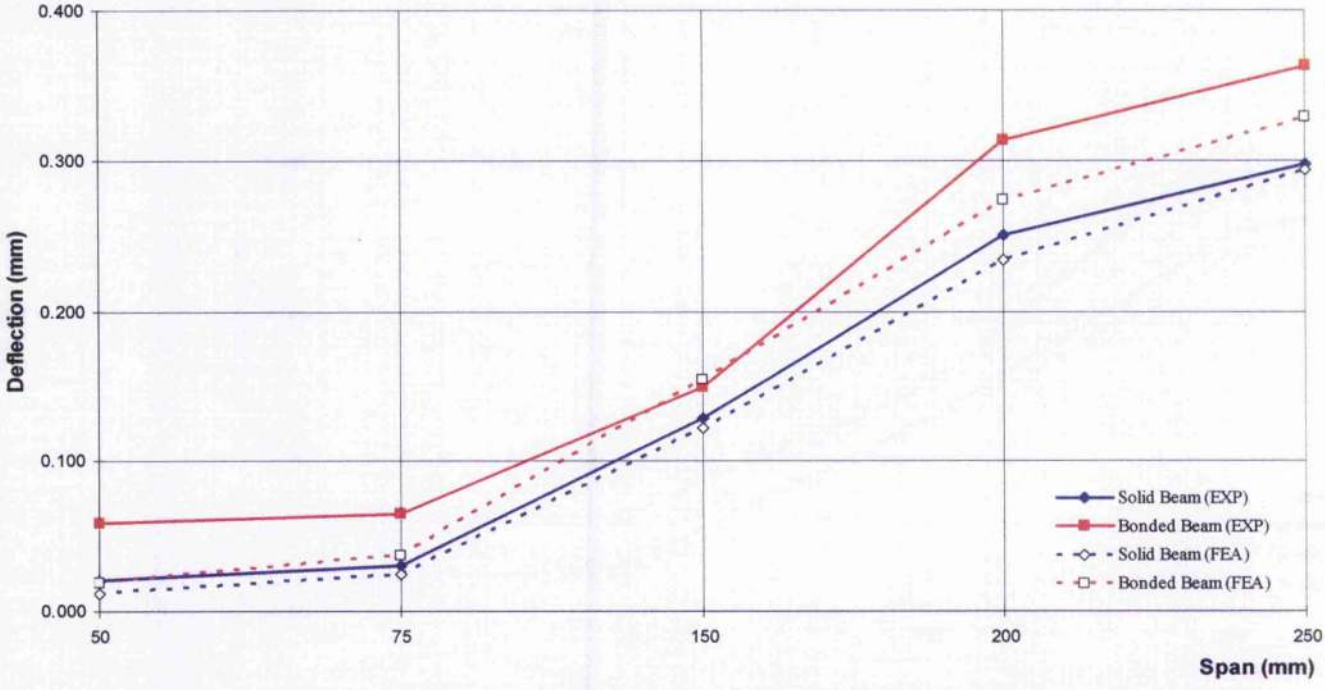

Figure 6.7 Maximum deflection computed via experiments and FEA along of the span of the inverted T section beam undergoing a 90% calculated yield load.

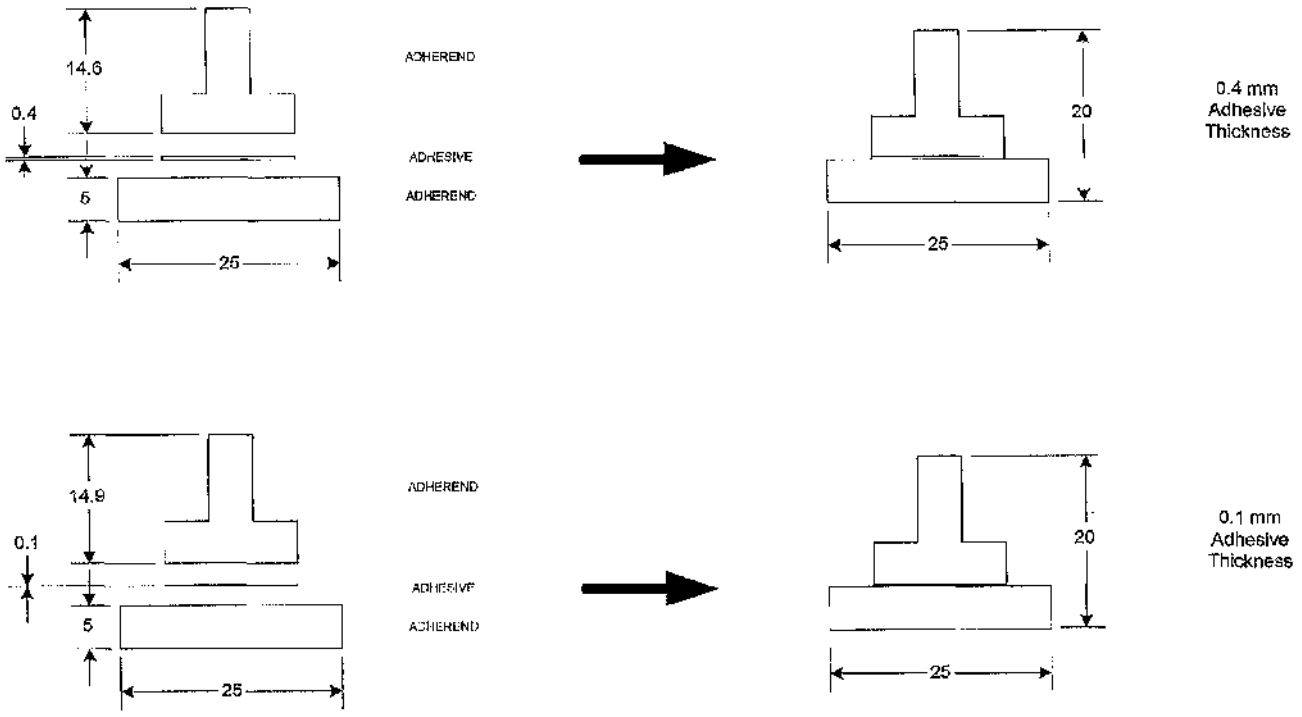

Figure 6.8 Comparison between T models with 0.4 and 0.1 mm adhesive thickness

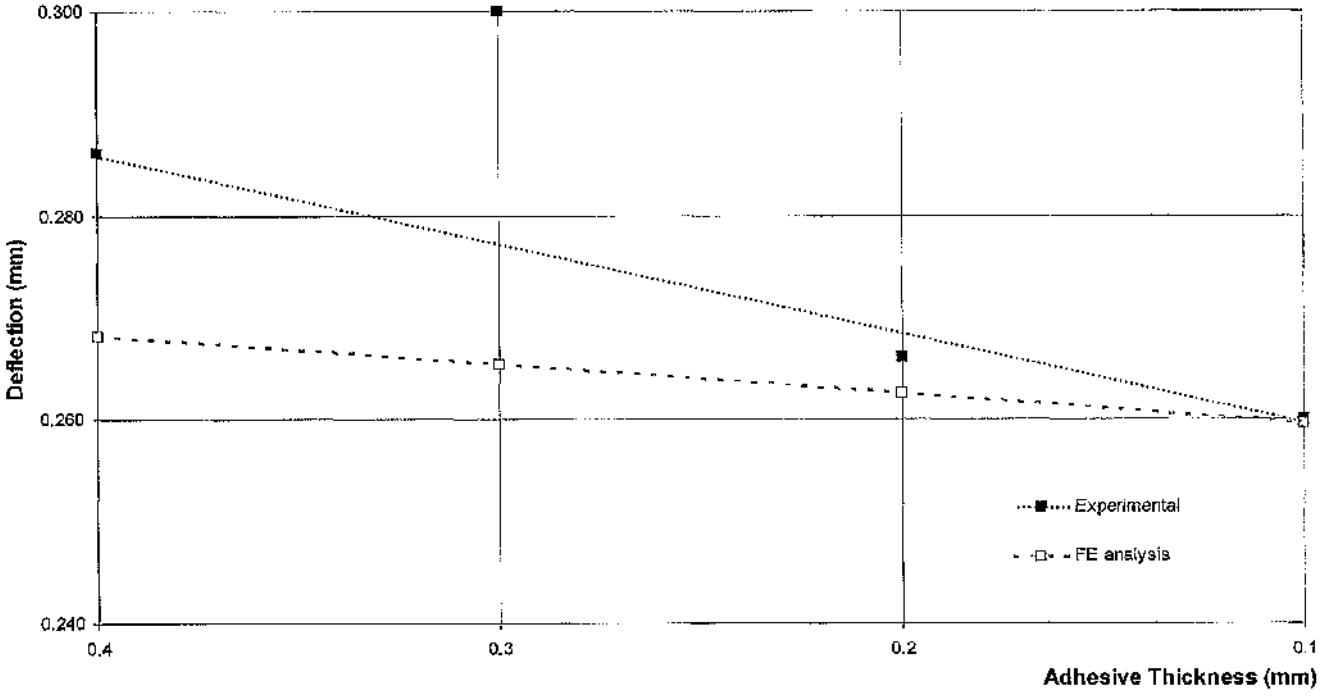

Figure 6.9 Effect of adhesive thickness on deflection of T beam section (200 mm) undergoing a 2 kN load.

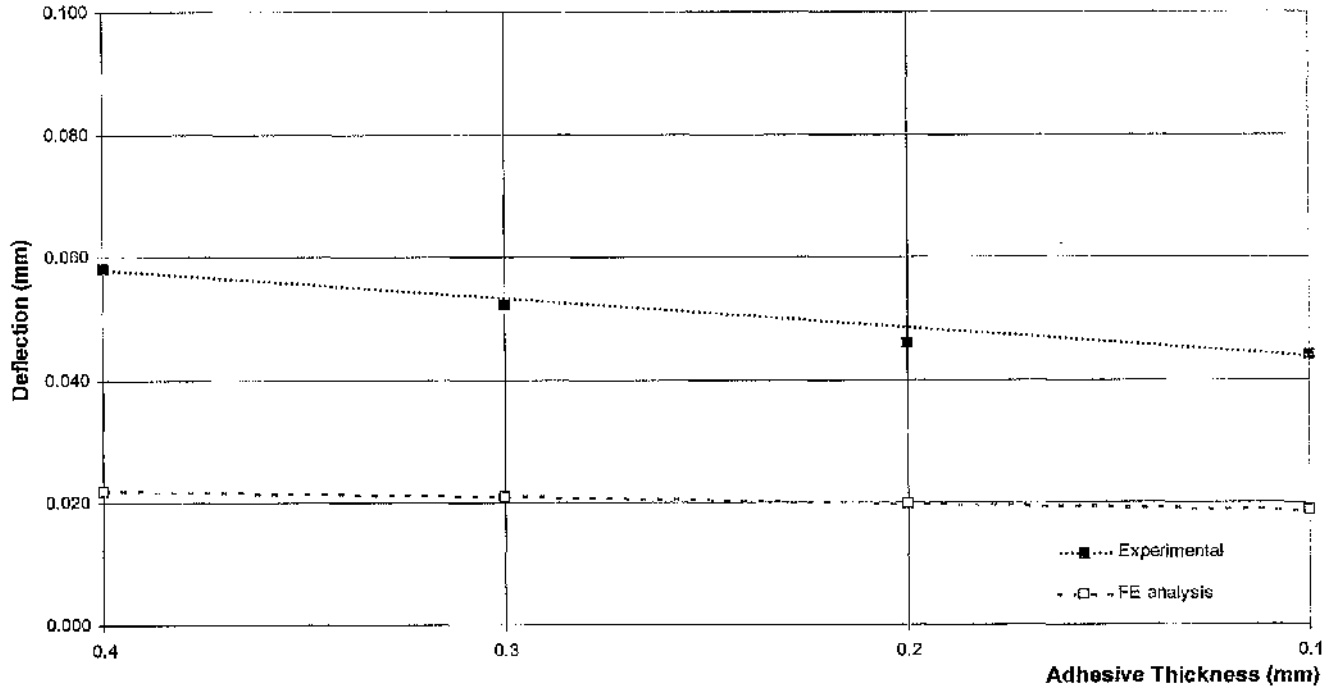

Figure 6.10 Effect of adhesive thickness on deflection of L beam section (75 mm) undergoing a 2 kN load.

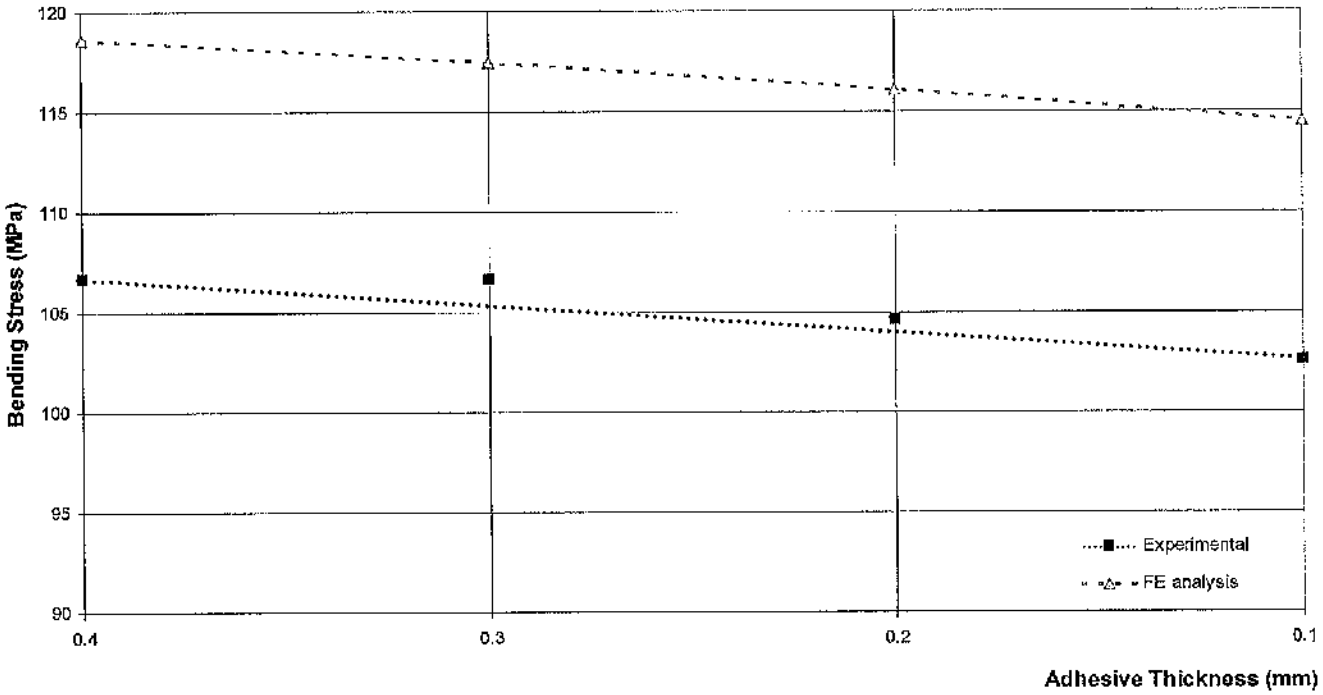

Figure 6.11 Effect of adhesive thickness on bending stress of the L beam section (50 mm) undergoing a 90% yield stress.

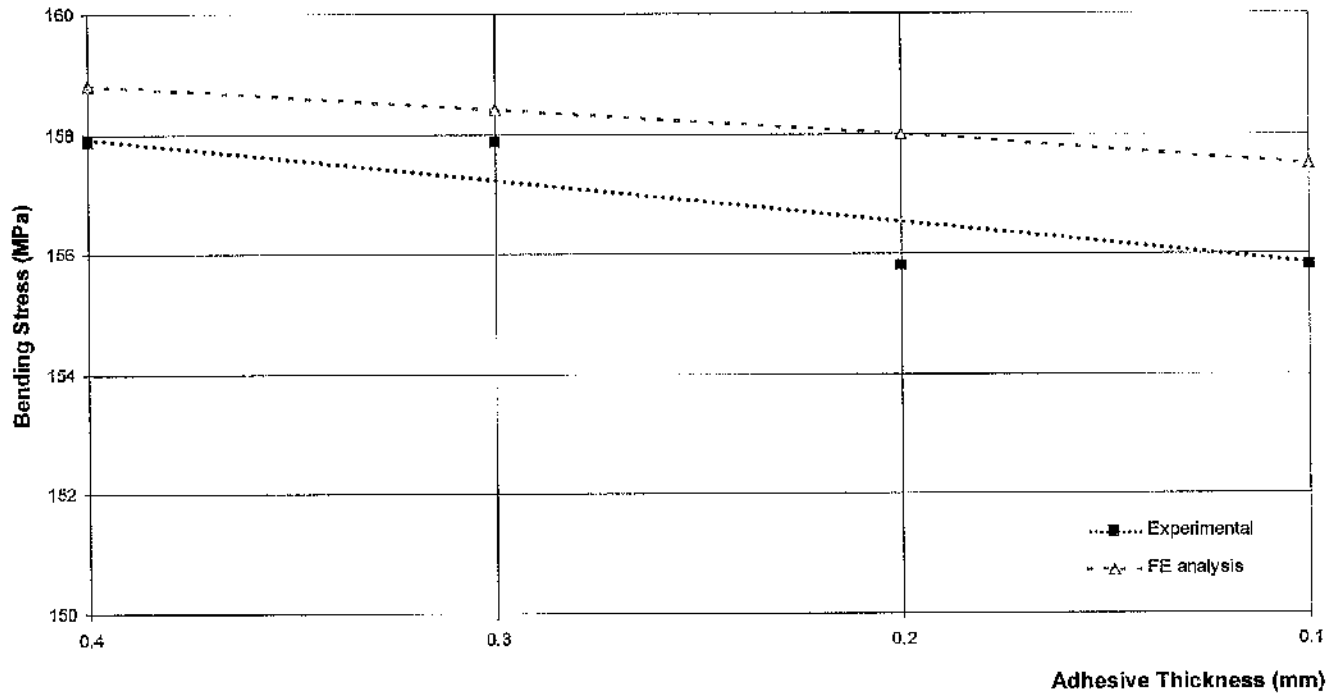

Figure 6.12 Effect of adhesive thickness on bending stress of the T beam section (150 mm span) undergoing a 90% yield stress.

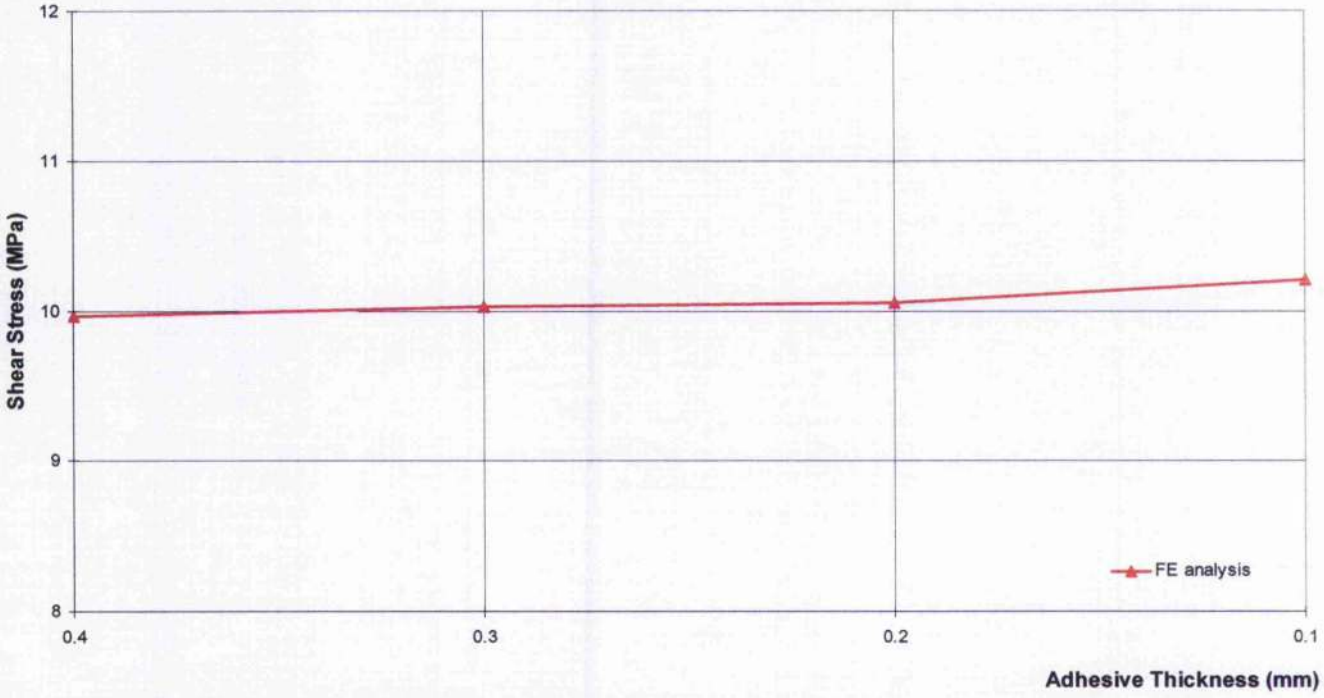

Figure 6.13 Effect of adhesive thickness on shear stress of the T beam section (150 mm) undergoing a 90% yield stress.

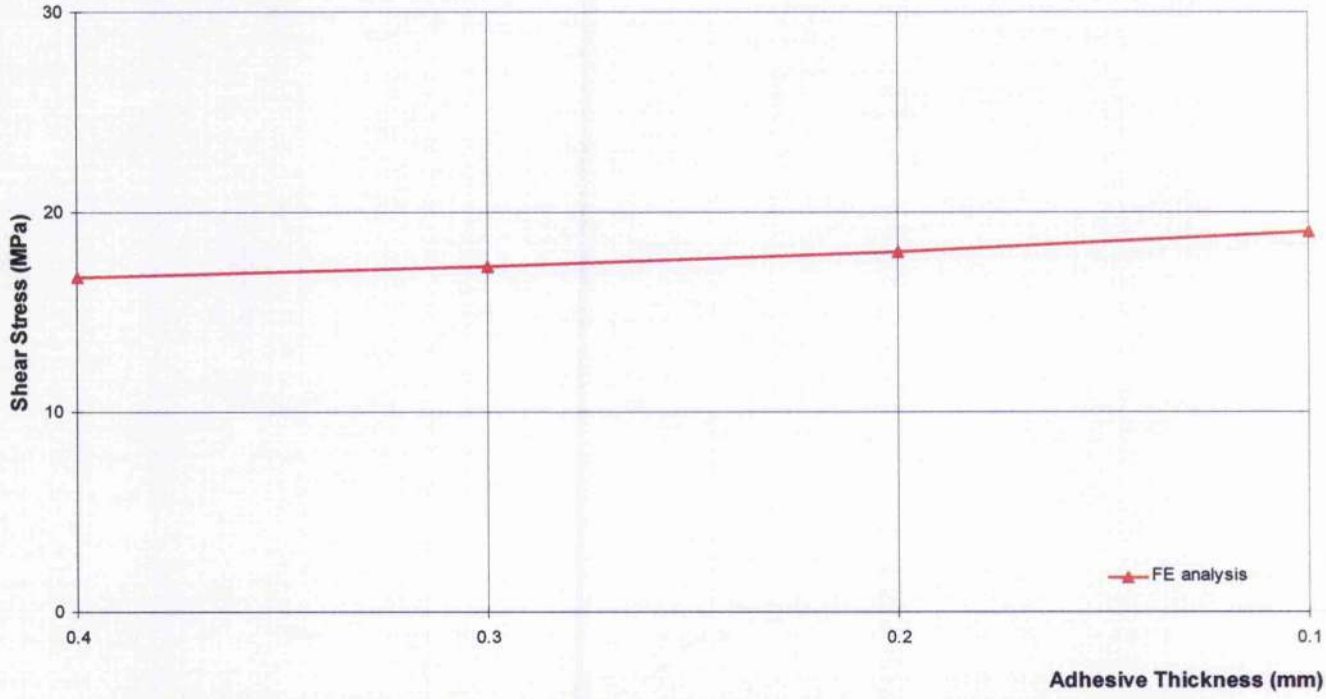

Figure 6.14 Effect of adhesive thickness on shear stress of the L beam section (150 mm) undergoing a 90% yield stress.

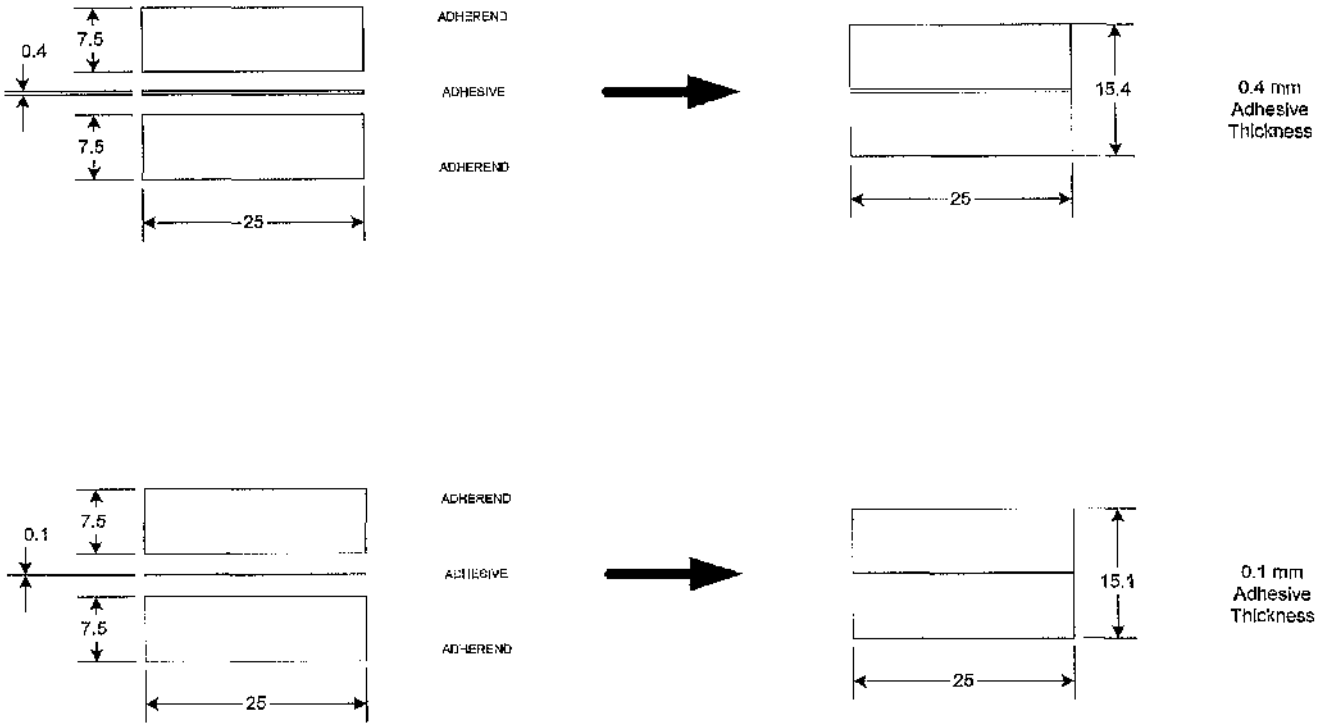

Figure 6.15 Comparison between T models with 0.4 and 0.1 mm adhesive thickness

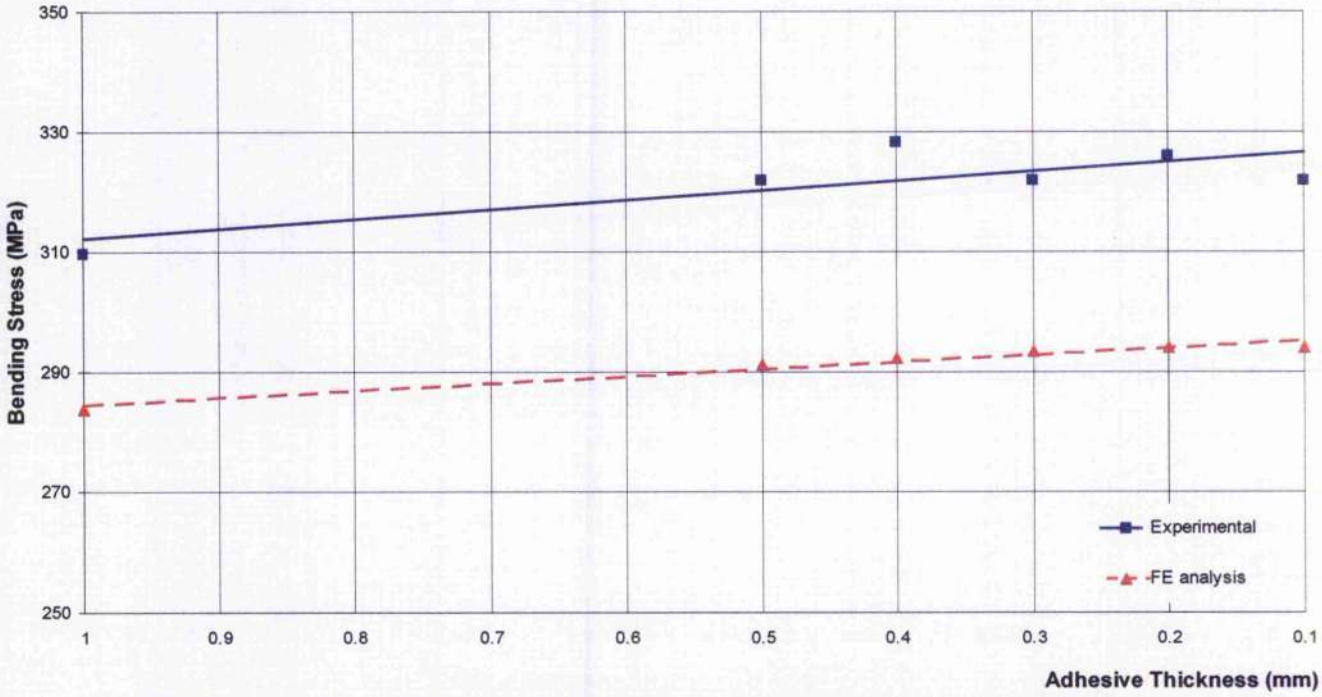

Figure 6.16 Effect of adhesive thickness on bending stress of the flat beam section (150 mm) undergoing a 90% yield stress.

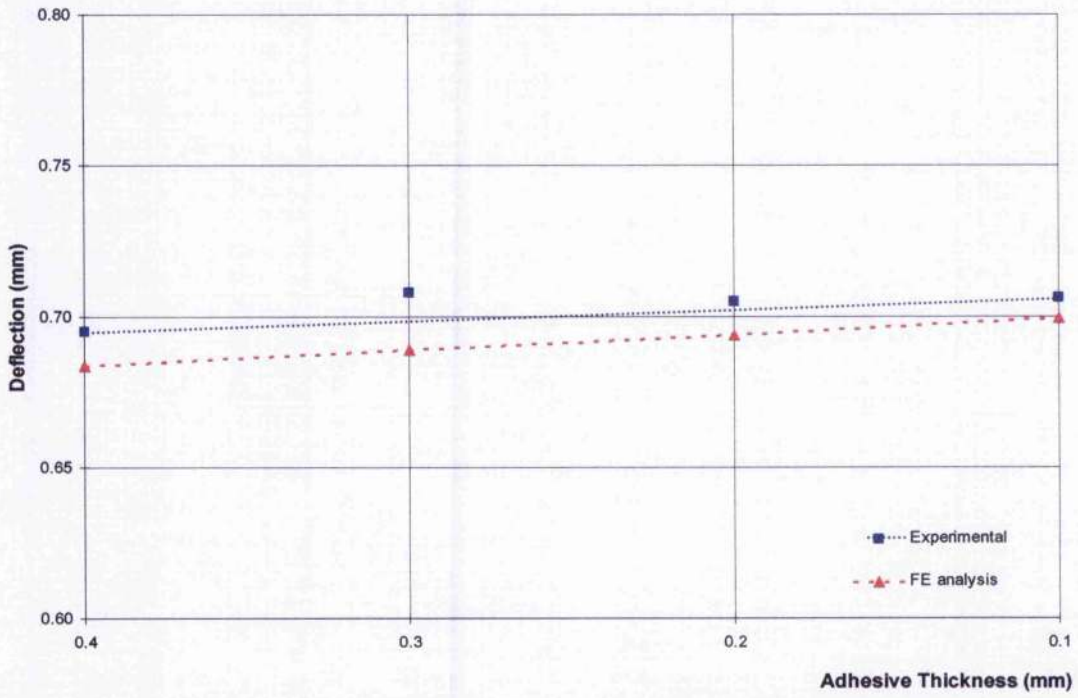

Figure 6.17 Effect of adhesive thickness on deflection of the flat beam section (200 mm) undergoing a 90% yield stress.

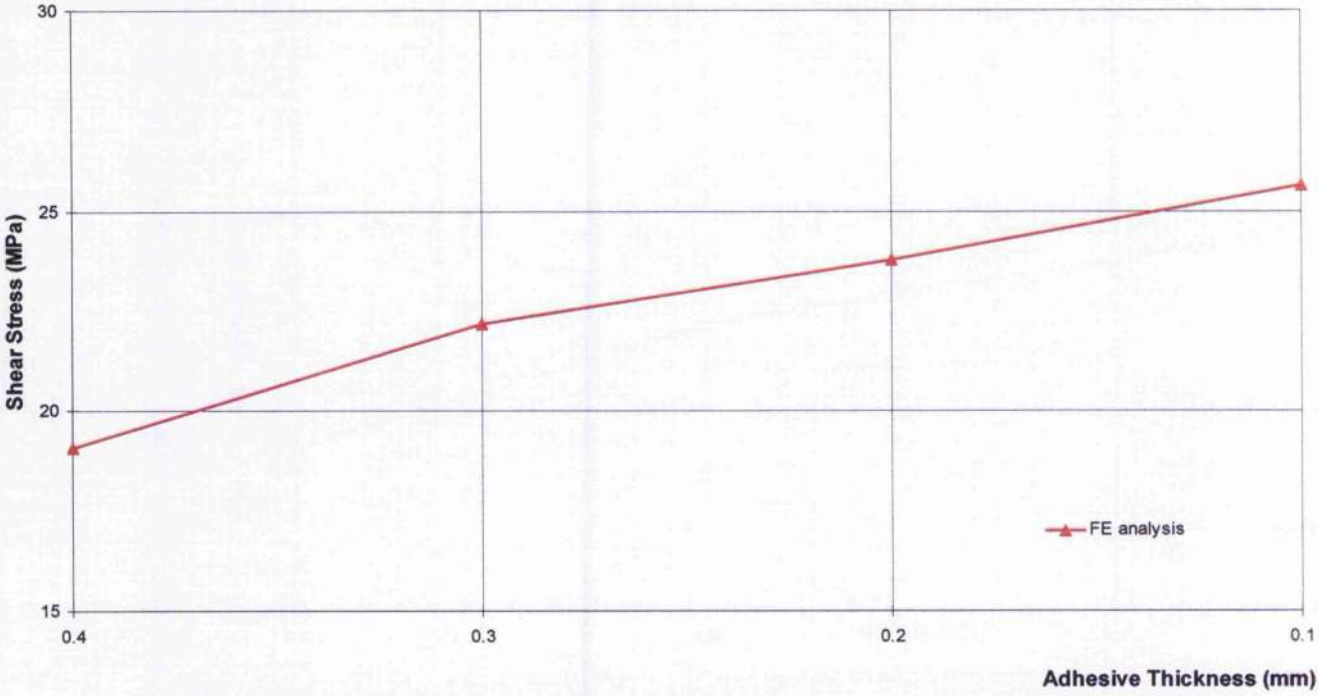

Figure 6.18 Effect of adhesive thickness on shear stress of the flat beam section (55 mm) undergoing a 90% yield stress.

Figure 6.19 Load-displacement curve for 150mm span flat bonded beam model with 1 mm adhesive thickness.

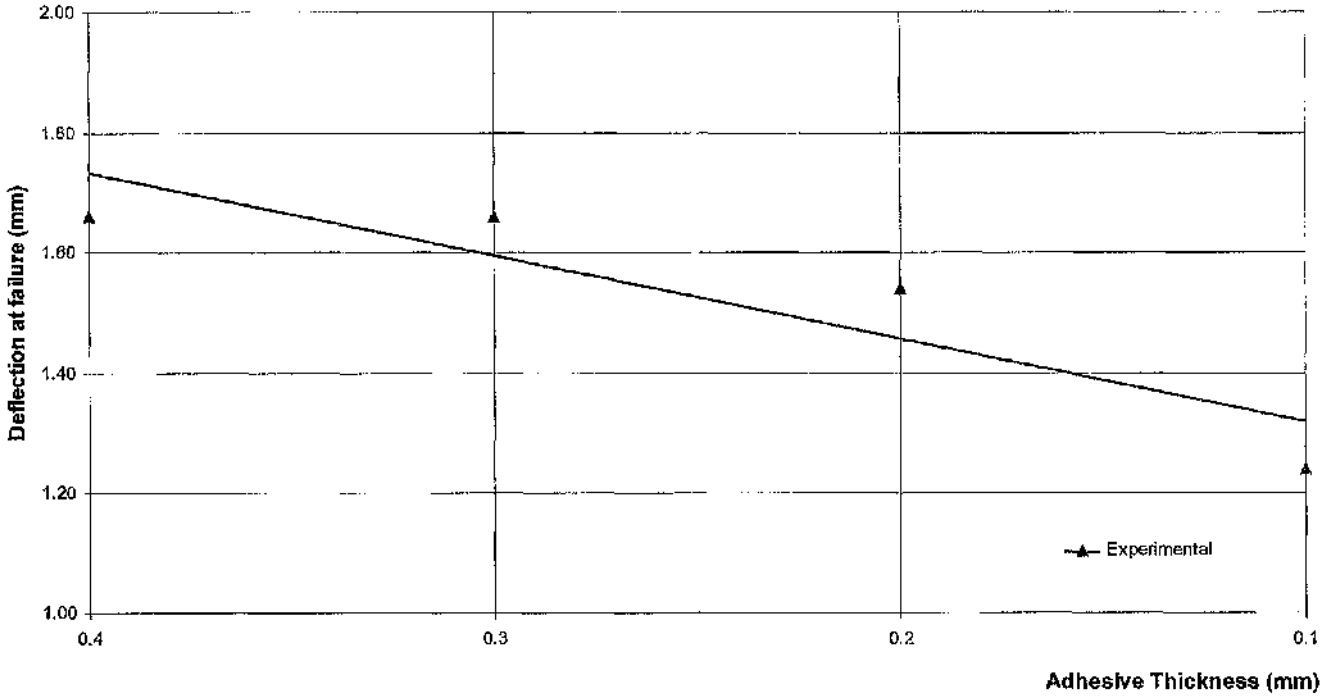

Figure 6.20 Maximum deflection at failure computed via experiments of the flat beam section (55 mm) undergoing a 59.2 - 63 kN failure load.

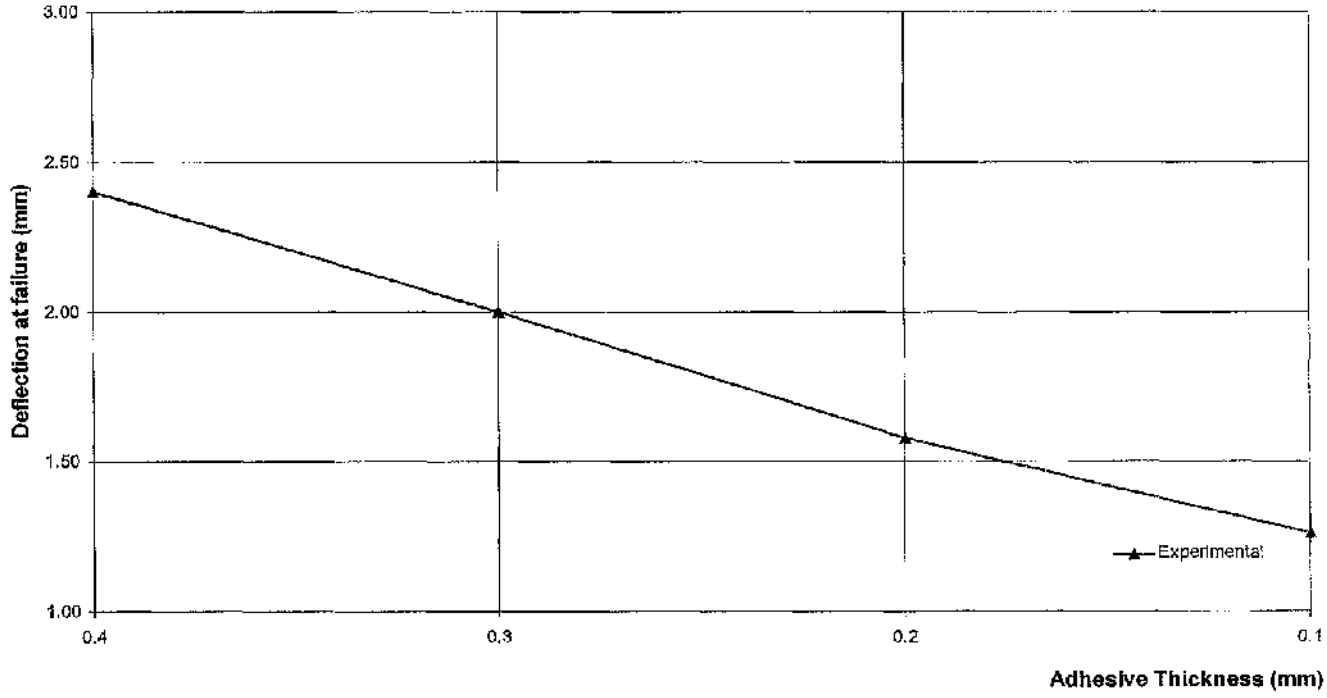

Figure 6.21 Maximum deflection at failure computed via experiments of the flat beam section (75 mm) undergoing a 43 - 50 kN failure load.

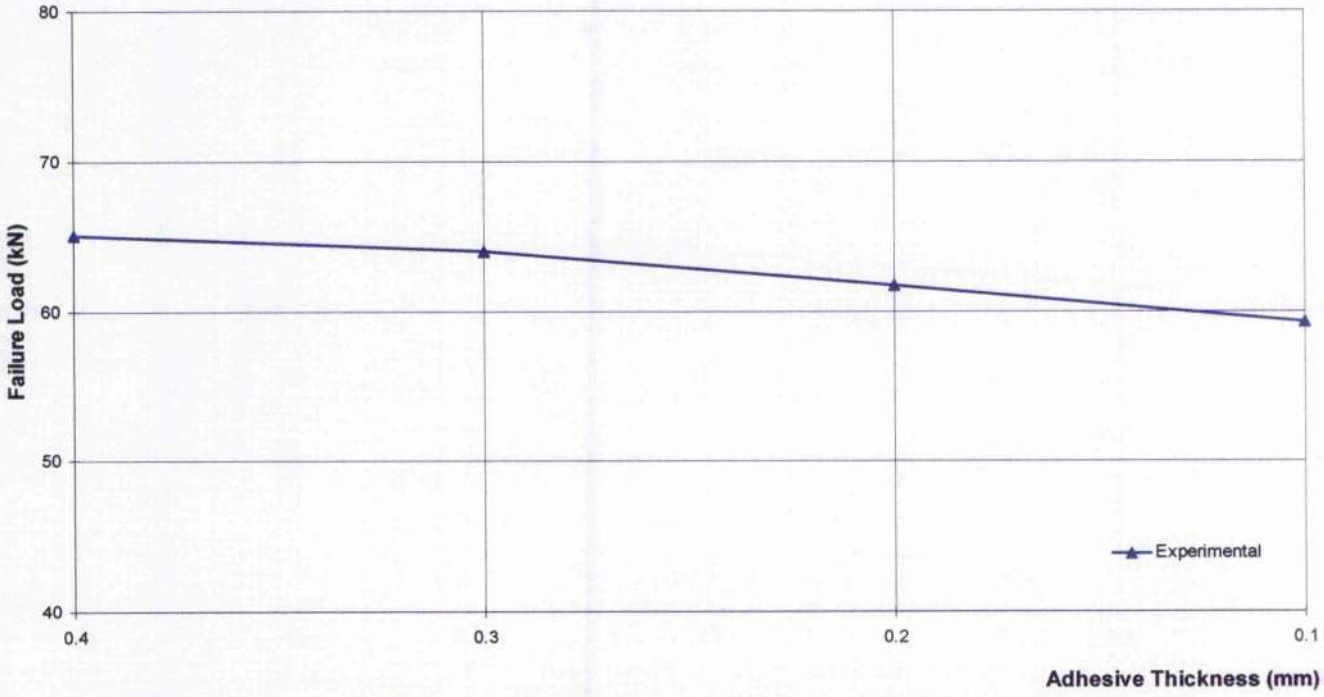

Figure 6.22 Failure load computed via experiments of the flat beam section (55 mm) undergoing plastic loads.

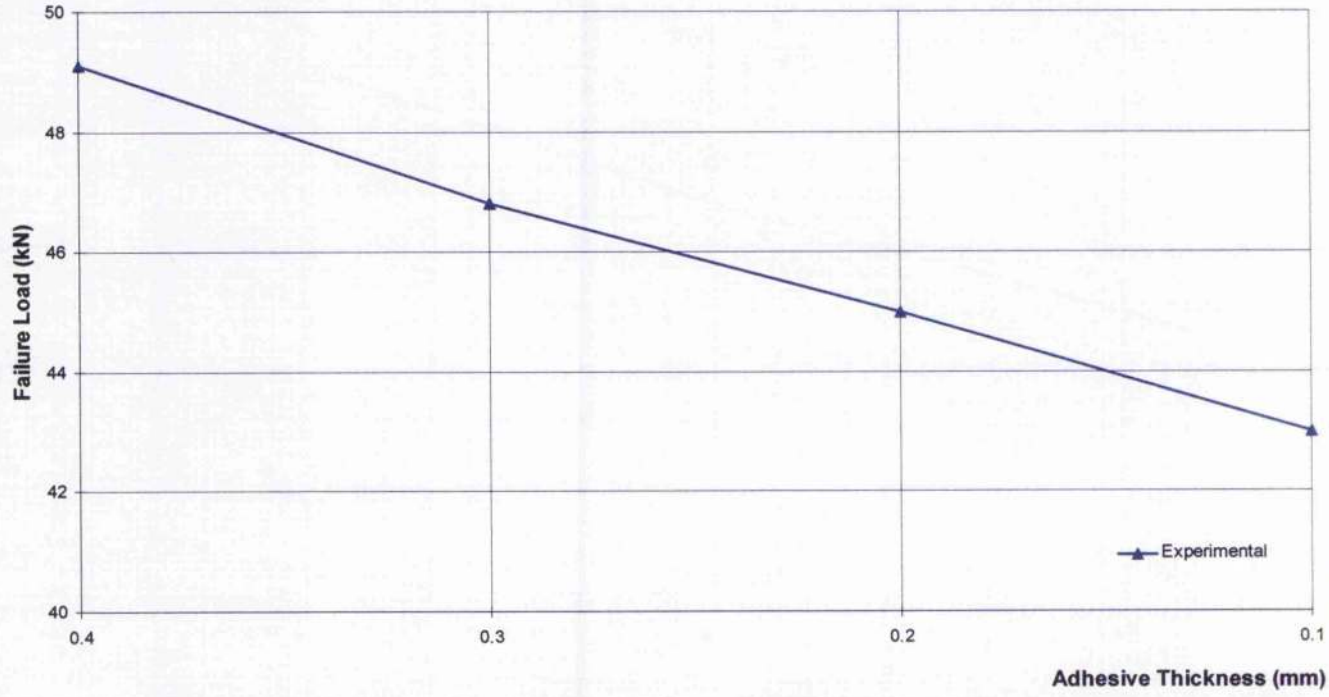

Figure 6.23 Failure load computed via experiments of the flat beam section (75 mm) undergoing plastic loads.

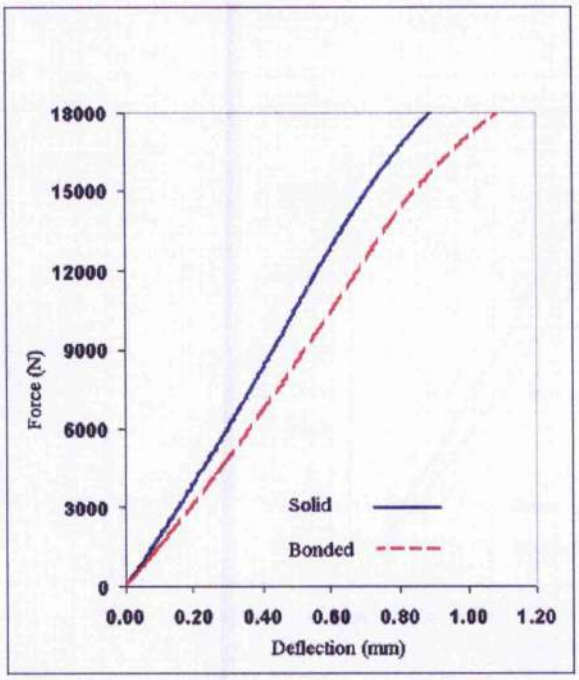

Figure 6.24 Force-deflection curve of the 150 mm flat beam models under a 20 kN elastic-plastic load.

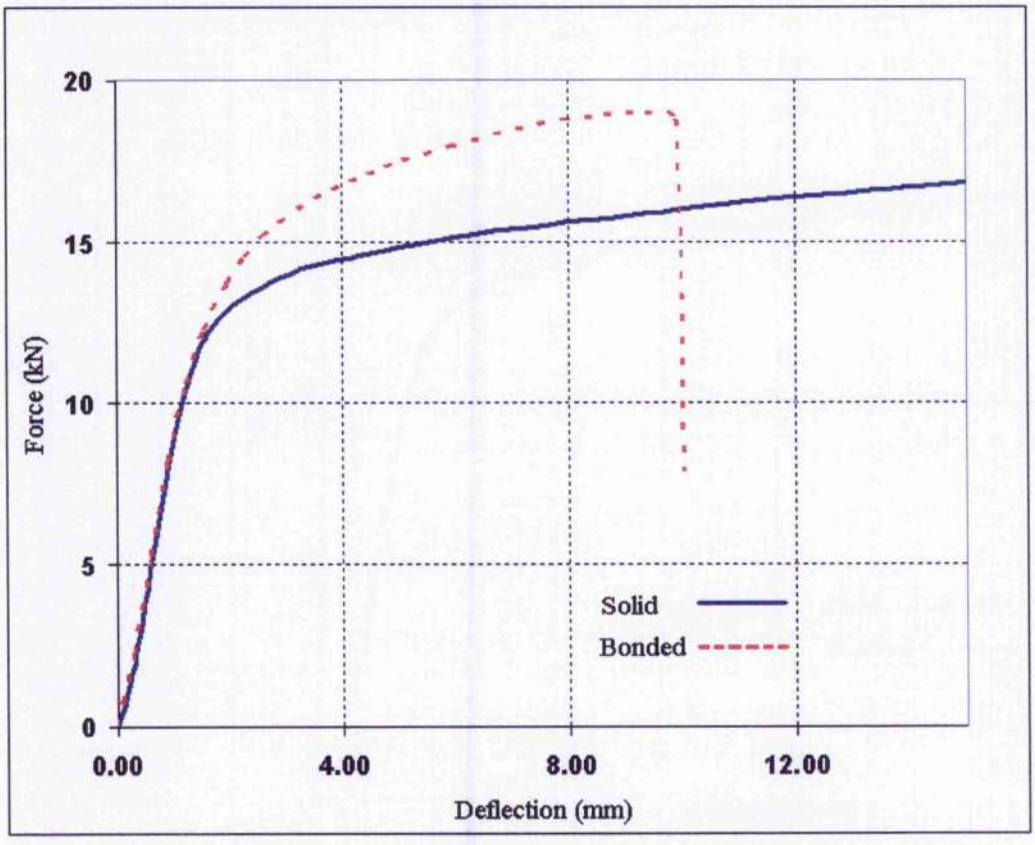

Figure 6.25 Force-deflection curve of the 150 mm T beam models under a 15-20 kN elastic plastic load.

Chapter Seven

DISCUSSION

7.1 Introduction

The initial part of this research aims to quantify the difference between mechanical behaviour of solid and adhesive bonded beams under similar loading conditions. For simplification purposes, the assumption used was that each solid beam would be a realistic representative of a full penetration welded beam. Bonded panels appear to be slightly heavier and do not perform as well as their welded equivalent. However the associated production and corrosion advantages mean there is a potential in a bonded beam design to save overall weight and cost. The difference between the bonded and welded beams would be smaller when we consider a weldable metal of relatively low Young's modulus such as aluminium as the adherend material. Since the difference between the elastic modulus of both aluminium and the structural adhesive is smaller compared with steel and adhesives, the failure of the bonded joint could be initiated by the both adherends and joining mechanism. In certain cases, the adhesive material could resist the failure loads of the aluminium material. Studies involving the buckling stress analysis of bonded aluminium structures demonstrates the possibility that no adhesive failure occurring during elastic buckling [133].

The degree of deviation of the bonded joint and its solid equivalent in terms of overall stresses and deflections under similar loading conditions was investigated. The study aims to produce a design guide for the calculations of stresses and deflections of bonded beams. Such design calculations already exist for welded beams but have yet to be implemented for bonded beams. The effects of using various spans and beam section configuration were also investigated. Such design configurations contribute to overall behaviour of the stiffened panel under a lateral load.

The bond length, the adhesive thickness and the adherend thickness are important design factors as they will influence the stress distribution in a joint. A paper by Li et al. studied the effect of adhesive thickness in bonded tee-joints as shown in Figure 7.1 with the finite element method [15]. The adhesive thickness used ranged from 0.05 to 0.5 mm. Subjecting the beam to an elastic tensile load in the y direction, the author

has found that increasing the thickness of the adhesive led to a reduction of the peak stress along the adhesive bonded layer. This was found to have a similar effect when the same joint undergoes cleavage loads P_x & M, except that this led to an increase in the stress at the joint's free ends. The follow up paper by the same authors determined that the linear stiffness of the same joint is lower when thickness of the adhesive is increased [32], where linear stiffness was calculated from the gradient of the force-deflection curve. The authors concluded that the smallest possible adhesive thickness should be recommended for joints subjected to tensile and cleavage loads.

The effect of adhesive thickness variation in this study was determined through experimental and numerical means. As mentioned earlier, this variation of the adhesive thickness was achieved in two different approaches. The first approach consist of modifying the upper adherend thickness in order to compensate the varying adhesive thickness, which maintains the overall height of the section at 20 mm. This approach was adopted in the experimentation of the T and L section beams. The second approach was solely increasing the adhesive thickness, which resulted in an increase of the height of the entire joint. The approach was adopted in the fabrication of the flat section beams. The objective of both approaches was to determine the effect of varying the adhesive thickness of all the models considered under similar elastic loading conditions. According to most studies carried out on single lap joints, the thinner the bondline the stronger the bond is. However the results from the study show otherwise, especially in the plastic deformation of the bonded specimens.

The structural behaviour of each model considered depends on the amount of material and the geometry of the cross section. Consideration of the bending stress distribution along the depth of the cross section of each beam is required for economical design, that most of the material of the beam should be placed as far as possible from the neutral axis. There is a limit which may be somewhat approached in practice by the use of an I section with most of the material in the flanges. Due to the necessity of putting part of the material in the web of the beam, the limiting condition is normally never realised. Studies have shown that a wide flange section like an I section is much more economical than a flat section of the same depth. In addition, due to its wide flanges and geometry orientation, the I beam section will always be more stable with respect to L beam sections in terms of sidewise buckling tripping or twisting

action. An I section is shown also to have a better resistance / allowable to side cleavage loading as compared to other beam sections.

The motivation behind the use of various beam sections was to compare the structural behaviour of each bonded joint profile and determine their correction factors. Correction factors already exist for structures to portray a more accurate determination of the strength criteria of the joint, for example implementing a plastic correction factor on elastic buckling of structures [134]. These factors can provide a more accurate understanding of the bonded beam behaviour, advantages and their limitation. The T, L, Z, flat and inverted T section beams were considered in this study, with the models having a benchmark adhesive thickness of 0.5 mm. The objective of the study was to identify also which beam sections are more suited for bonded joints. Distinguishing the effective profiles instead of using generic beam sections adopted in welded joints was also analysed.

The study of the structural behaviour of the beam joints subjected to elastic-plastic loading conditions forms the essential part of this research. Few research projects previously carried out have considered of all the beam sections used in this study and implementing an elastic-plastic analysis would give a fuller picture. This phase enabled the assessment of the structural stiffness of the bonded beam joint as it undergoes extensive plastic deformation. Two important issues were considered in this study, namely the influence of the varying adhesive thickness and the behaviour of the bonded beam as compared to its solid equivalent.

Earlier results obtained from experimentation and finite element analysis of all the beam section considered suggest that the bonded beam does not deviate significantly from its solid equivalent in terms of bending stresses and deflection. The comparison was made with bonded specimens/models of a benchmark adhesive thickness of 0.5 mm subjected to an elastic load. A reason could be found in the overall dimensions of the solid and bonded specimens/models being similar, and therefore only slight differences in behaviour were observed under elastic loading. The comparison of the T & L beam sections with adhesive thickness variation (0.1 – 0.4 mm) also yield small differences between each specimen/model. This variation represents values often used in the fabrication of bonded joints used in aerospace and similar

engineering structures [138]. However, the lack of deviation could be found in the small difference in adhesive thickness considered. The nature of the test evaluates the joint's structural stiffness in compression. The difference in mechanical behaviour of both solid and bonded models was emphasised when a better dimensional control was maintained followed with plastic deformation testing of the specimens. By testing the bonded joints to failure, we could determine the failure load of the bonded model as well as comparing the maximum amount of deflection under plastic loads. .

7.2 Theoretical evaluation methods

The mathematical models for the structural beams studied were based mainly on the beam theories for solid and sandwich sections discussed by Timoshenko and Allen [13,80]. Both theories represent a simplified approach for the calculation of structural stiffness. The sandwich structure stiffness analysis was based on the thin core with thick faces approach. The core in the sandwich calculations represented the properties of the adhesive. Calculations for maximum tensile bending stresses, shear stresses and lateral deflections were made. The stress distribution within the adhesive shows areas of stress concentration and possible failure initiation that exists not easily determined through experimentation. The aim of the theory places emphasis of the core and takes into account of the effects of the shear stiffness present in the bonded beams. The global deformation of the bonded beam integrated both the shear displacement and the normal displacement obtained from the associated bending moments.

In the finite element modelling, emphasis was placed on the locations of the applied loads and the simply supported boundary conditions. A convergence analysis carried out on the T solid section finite element models found that minor adjustments of these reference nodes led to a change in stress behaviour. Good agreement was found in the elastic analysis carried out involving both methodologies of beam theories and finite element analysis. When we compare the bending stress values obtained from the T section beams, results deviate between 2-18 % in comparison of both methodologies as shown in Table 6.1. In terms of deflection values, results from both methodologies differ between 4-26 % in comparison according to the different spans considered. This comparison was important in validating stress analysis, as in any bonded joint analysis, because it is very difficult to obtain experimental strain measurement in the adhesive bondline due to accessibility. The finite element analysis provided values of

shear stress and its distribution present within the interfaces of the adhesive layer. Determination of shear stress using typical experimental methods is both difficult and questionable in terms of reliability. An alternative method to experiments may be found in using thermoelastic stress analysis (TSA). Thermoelastic stress analysis was used in a study to obtain full field stress data from sandwich construction tee joints loaded in compression [122].

Determination of the stresses and deflection of the models under plastic loading condition proved difficult. The results obtained through the finite elements analysis differed from experiments, therefore experimental results would be evaluated and used in the determination of the interface coefficients. A possible explanation could be found in the distortion of the element mesh under plastic loading conditions, which continued to occur after several refinements of the model was introduced.

Figure 7.4 shows a comparison of results obtained from all three methodologies considered. In terms of linear elastic analysis, all three methodologies seemed to be comparable. For model IB250/$X^{(0.5)}$ accordingly to Table 6.1, it was noted that the experimental results exhibit 24 % more deflection than theoretical results and 10 % for the corresponding results from finite element analyses. The comparison shown here was based on an elastic load of 2–4.5 kN loads tested on models with varied beam spans for the models. The accuracy of deflection measurements was slightly influenced by the exact positioning of the transducer centralised at the bottom surface of the lower adherend. In these circumstances the correlation between the three methodologies is appropriate. This trend was found true for the rest of the models discussed in the Chapter 6, which show comparable results among the three methodologies.

7.3 Experimental evaluation methods

In the development of adhesive applications, experiments remain the most important and reliable techniques available for evaluating adhesives, adhesive joints and the performance of bonded structures. The small-scale models used in this research represent structural components within stiffened panel structures. Each model represents the stiffener-plating combination normally found in steel marine structures. Five different beam sections were studied closely and the dimensions were intended

to resemble that of a real joint in smaller proportions. The three-point loading considers the design assumption for ship structures where panels are treated as beams under concentrated loading.

Both central deflection and plate bending stress were measured. It was desirable to measure the strain within the adhesive but lack of suitable instrumentation prevented this. Seventy percent of all tests were performed within elastic limits of the steel and the adhesive. The maximum limit load (90% of the calculated yield strength) for the joint was determined through various methodologies. The joint failure strength was determined by experimentation where the joint underwent gross plastic deformation. Such information will prove useful for designers even for lightly loaded design considerations in case unexpected loading conditions arise.

In the initial phase of this project, the overall dimensions of the solid and bonded model were not controlled precisely, resulting in the bonded beam having an increase in the overall height due to the inclusion of the bondline thickness. As a result, the experiments demonstrate that some bonded beams exhibit lower bending stresses and deflection as compared with the solid equivalent. However, theoretical investigation does not demonstrate considerable differences in the structural rigidity of both sections. This was due to the effect of the bondline being accounted for in the sandwich beam theory. A more justifiable comparison was obtained by configuring equivalent overall sectional dimensions for both bonded and solid beams. This amendment is shown in detail in Figure 6.10 where the relative height of the upper adherend was reduced to compensate for the thickness of the adhesive material

The deviation from ideal solid beam behaviour for the bonded beam was emphasised, and whilst presenting our study the response from fellow researchers has been apprehensive [140]. Researchers in adhesion have suggested that the author should in fact carry out test on actual welded beams in order to determine a more suitable comparison with the bonded beams. Having said that, small specimens were specially fabricated using fusion welding but the decision to carry out experiments was abandoned due to the limited welding techniques available. Upon receiving the specimens, the author found that it was difficult to quantify the amount of welding material that was included in the welded joint, and hence difficult to accurately

compare its behaviour with the bonded beams under similar loading conditions. Hence, the choice of using solid beams was mainly to simplify the fabrication process and to control the dimensions effectively, which are more difficult to achieve by welding small specimens.

7.4 Comparison between solid and bonded beam joints

Table 6.1, 6.2, 6.3, 6.4, 6.5 and 6.6 showed the theoretical, numerical and experimental results of the elastic behaviour for various beam sections. Overall results show that bonded beams behave differently from their welded equivalents. Generally, bonded specimens with shorter spans produce higher bending stress and deflection than the equivalent solid/welded ones. Solid specimens tend to have comparative higher structural stiffness, which was validated by theoretical calculations, finite element analyses and experiments. On the other hand, the shear stress found in the joint's interface is relatively lower for the bonded beams. The author feels that the shear load is undertaken through both interfaces in the bonded structure; hence the shear stress measured at once interface represents part of the entire shear load. The solid beam however, will experience higher shear stress near the corresponding measured location. While the experimental results in Tables 6.1-6.7 show higher values than the numerical ones, the trend of the results seems to be the same as seen in the stress & deflections graphical comparisons. In addition, analytical results based on the earlier beam equations are also in agreement with these results.

Under equal bending load, shorter span beams exhibit lower bending stresses and deflection when compared to longer ones. However when we extend the comparison to the solid equivalent, the longer span bonded beams excel especially under a 90% yield load. From the results shown in Chapter 6, it may be concluded that shorter span bonded beams exhibit significantly higher deflection and bending stress than the solid equivalent. Being stiffer, shorter beams were subjected to higher shear loads (8-10 kN), where the longer beams undergo a smaller 90 % yield load (2-5 kN). This means bonded shorter beams were more likely to collapse under shear stress in comparison with longer bonded beams. Having a smaller bonded surface area to resist shear resulted in a higher deviation from its solid equivalent in terms of bending stress and deflection for shorter span beams.

7.5 Determination of correction factors

The concept of the correction factor which is used for laminated composites is very useful for determining the deviation between solid and bonded sections. The correction factors are represented by the ratio, between the stress and deflection values (numerical) for bonded sections and those of their solid equivalents. Thus the following general equation for the correction factors of deflection, bending stress and shear stress may be used.

$$f_\delta = \frac{\delta_b}{\delta_s}, \quad f_\sigma = \frac{\sigma_b}{\sigma_s}, \quad f_\tau = \frac{\tau_b}{\tau_s} \tag{7.1}$$

Plotting the correction factors versus $\frac{I_c}{I}$ gives a set of useful design curves for the various sections as shown in Figure 7.5 – Figure 7.9. From these curves equations of the polynomial lines for deflection, bending stress and shear stress for the Z, T and L section can be generated and used by designers as shown in Table 7.1. The polynomial equations for the T section beam is shown below.

Deflection	$f_\delta = A_1 x^2 - A_2 x + A_3$	(7.2)
Bending	$f_b = B_1 x^2 - B_2 x + B_3$	(7.3)
Shear	$f_\tau = C_1 x^2 - C_2 x + C_3$	(7.4)

From the curves shown in Figure 7.5 – Figure 7.9, it was observed that correction factors for bending and shear are slightly above unity, depending on beam spans and section types. The correction factors for deflection however are significantly higher as compared to bending and shear stresses. Since the results obtained for deflection through finite element analysis are comparable with those obtained from theoretical calculations, equations shown in Chapter 4 may be used to generate equations for the correction factors as a function of beam geometry and materials, including adhesive thickness. For example the deflection equation is;

$$f_s = 1 + \frac{E_s * A_s * h * c}{12 * L^2 * G_a * d * b} \tag{7.5}$$

For the bonded T models, the correction factors for bending stress and deflection is above unity. The deviation from unity is more prominent for beams with shorter spans. This trend applies to all beam sections considered. The correction factor for shear is below unity but it also depending on contact area between stiffener and plate. Using ordinary shear formula would result in the overestimation of the shear stress in bonded joints. The results shown can be utilised in conjunction with the simple bending beam theory to account for more accurate stresses and deflection in bonded beams.

Generally, it appears that the design of bonded beam is more sensitive for deflections than bending stress within the elastic limit of the adherends. Beyond this, plastic deformation can result in excessive deformation of the adhesive and adherend causing catastrophic failure. This may be seen in Figure 7.10 for the bonded T specimen that underwent extensive plastic deformation, which resulted in the delamination of the upper and lower adherend. Thus high deflections in a bonded panel may imply increase material requirements in the bonded beam design to sustain the required loads. Such a requirement may result in bonded structures being slightly heavier than their welded equivalents. However, increased deflection of a bonded panel could be compensated by its advantages in joining panels instead of welding techniques. Firstly, the absence of welding residual stresses in the plating will mean that bonded panels would have less structural defects. Secondly, the technique gives the freedom to join thinner plates with closer stiffeners without the technical and economical problems associated with controlling thermal distortions during welding of such geometries. Bonded stiffeners would also increase the effective breadth of panels due to the possibility of wide flange attachment and absence of distortions.

7.6 Comparison of various beam sections

To compare various beam sections, the correction factors are plotted collectively in the Figure 7.11 – Figure 7.13. The graphs were plotted from finite element results. As mentioned before, the shorter beams behave significantly different from longer ones,

especially for shear stress and deflection. For all sections, the correction factors for bending stress were slightly higher than 1 (unity). The unity line as indicated by the dotted black line represents the ideal behaviour for the bonded beams. Under elastic loading conditions, the correction factors obtained for all four beam sections range from 1 -1.1. The choice of stiffener shape has a direct impact on the level of stresses and it was found that the most suitable section was the T section. The bonded T section was found to be the most efficient connection with respect to longitudinal bending as shown in Figure 7.11. Although the Z and L section beams seem suitable for bonding with respect to longitudinal bending, lateral bending/loading conditions may cause critical cleavage stresses due to lack of symmetry (in comparison with the T section). From exaggerated deformation of finite element models, a direct three point load subjects the Z and L section bonded beams to deflect laterally as well as horizontally. This results in higher shear stresses in the interface region along the horizontal axis.

Figure 7.12 shows the corrections factor for deflection for the four beam sections considered. Similar to the earlier graph, the bonded T section was found to behave comparatively to its solid counterpart. In terms of beam spans, correction factors for shorter span beams are significantly higher in terms of both deflection and bending stress. It is also noted that from comparison of the three graphs, the T and L sections tend to display similar values of correction factors for bending stress, deflection and shear stress. This may be because both beam sections have very similar structural flexural rigidity.

Figure 7.13 shows the correction factor for shear stress for the various beam sections. The adhesive shear stresses found in the inverted T section were the highest among all models due to the small bond area. The Z section bonded beam at 250 mm span seemed to have higher shear stress than other models. According to post-processing results of the displaced finite element model, the model had displaced laterally as well as sideways, therefore extensive shear was experienced in the interfaces of the joint and is a possible reason for the high correction factor at 250 mm span. With the exception of the inverted T section, all bonded sections produced shear stresses lower than their solid section equivalent.

7.7 Elasticity and Plasticity in bonded beams

To explain the behaviour of beams under plastic loads, the author restricted the investigation to the flat beam sections. Such beams may not be widely accepted in real structures but provide a simplified model for analysis. In the three-point bending of bonded beams, there are shear forces generated at the bond causing shear stresses that are not that much different from lap shear joints. Similarly, typical adhesive elements along the beam will be subjected to compressive and shear stresses which can be added algebraically to give von-Mises Stress. Adhesive failure in the bonded beams is more likely to initiate from the centre as a result of combined shear and compressive stress, as found in the finite element analysis. Two specimens were taken apart at the bondline to determine the source of failure of the joint as shown in Figure 7.2 & 7.3 From the figures shown it was difficult to tell where initiation of failure started. During experimentation, the failure of the joint is noted by the sound of the fracture and a sudden drop in the force-deflection curve plotted by the computer-controlled monitoring software. It would have been useful to use a high-speed video camera to capture the initiation of the fracture, but one suspects it could have initiated in the middle of the joint rather than the edges.

However, the plastic deformation of the adhesive and the stress distribution of the bonded beam could be explained by consideration of perfectly plastic material under pure bending [125], and this is shown in Figure 7.16. When the yield load (adhesive) is reached in the flat beam bonded section, the upper and lower interface of the bondline have just reached the yield point stress. As the bending load is increased, the region near the interfaces begin to yield and plastic deformation penetrates further into the adhesive material. At beam failure load, the regions of plasticity approach the neutral axis of the middle section of the flat beam section. When the plastic deformation reaches the neutral axis, the resistance to bending at this point of the cross section ceases, and the joint will fail. Complete failure is reached when a crushing rupture is initiated within the adhesive material. This may have initiated from the bondline interfaces or defects in the adhesive material. The two adherends subsequently rotate with respect to each other about the neutral axis as about a hinge. This behaviour refers to a plastic hinge. Theoretical work covering deformation of beams beyond their elastic limit has been studied extensively [123,124], but not with

reference to bonded beams. There is hence a possibility of extending the models in this study to correction factors in plastic beam equations for future work.

The perfect plastic material theory was adopted in the elastic-plastic analysis carried out in the finite element study. The behaviour of the material models used in the analysis closely follows the different stages of the stress distribution as defined by a perfectly plastic material. This elastic to plastic transition of a solid flat beam section is shown in Figure 7.14. This behaviour was found to similar when reviewing results of the finite element model as the applied load increased progressively in a series of load increments. Comparing the elastic and plastic behaviour of the adhesive material as shown in Figure 7.15, we noticed certain important differences. Under an elastic load, the stress distribution in the adhesive material tends to be constant along the beam span. Under a plastic load, the plastic stress peaks nearer the centre of the beam where the adhesive failure might initiate. On further plastic loading, the peak principle stress reached above 120 MPa to tie in with the adhesive compressive strength. The author feels that the initiation of the crack has to lie within the centre of the beam span rather then the edges.

7.8 Effects of varying adhesive thickness in joints

Figure 7.16 shows experimental curves for the 0.1 and 1 mm models under three-point loading. This shows the influence of adhesive thickness beyond the elastic limit for the 150 mm span. Both joints were taken to the maximum possible load to trigger an adhesive failure in the joint as shown in Figure 7.17. The influence of the adhesive thickness on the results obtained from both finite element and experimental work shows that a thicker adhesive line could produce a stronger joint, especially within the plastic limit of the steel adherend. From experimentation and finite element analysis, the model $RB150/X^{(1)}$ is producing smaller stresses than the thinner model $RB150/X^{(0.1)}$. Under plastic loads, increasing the adhesive thickness increases the maximum deflection of the beam significantly. Increasing the thickness from 0.1 to 1mm resulted in increasing the central deflection by 188%. A thicker adhesive accommodates higher shear stresses within the bondline and resulting in less shear strain and stress at the interfaces between the adhesive and adherends. It might be said here that for bonded beams the thicker the adhesive the stronger the joint is in bending. However, a stiffened panel in other cases may be required to resist various

types of loads, and in such cases a thicker bondline may be detrimental to a bonded joint subjected to pure shear in certain loadcases. For certain types of bonded joints, namely shear, cleavage, and butt the opposite trend is normally expected when the adhesive thickness is increased [34,116].

When a lap shear joint is subject to pure shear, the effect of porosity and voids within the adhesive reduces the joint's strength due to slippages occurring at the movement of dislocations along the axes of the applied tensile loads. These slippages provide large local stress gradients surrounding the dislocation and easy localised fracture (micro-fracture). These microcracking areas in the bondline under load transfer are the best candidates for fracture initiation and catastrophic failure of the component. The behaviour of a bonded joint in compression could be explained with concepts similar to brittle materials. For a brittle material under compression, the effective/operative force in compression is actually the value of the Poisson ration ν multiplied by a comparative tension force. The range of the Poisson's ratio ν of such materials is between 0.2 – 0.5. This clearly explains that the apparent strength of the brittle material is thus greater in compression than when it is in tension.

Similar to ceramics, porosity in structural adhesives is normally unavoidable during the fabrication of the joint. This is shown in the specimens taken apart at the bondline in Figures 7.2 and 7.3. As described earlier in Chapter. 2, the effect of porosity contributes to a deterioration of the integrity of the material structure and the overall bonded joint. The increase of dislocations present is found proportional to the thickness of the bondline in a joint. Research relating to lap shear joints tend to show that a thinner bondline makes a stiffer joint. The overall structural response of the joint is directly attributed to the amount of dislocations present in a thinner bondline. However, a thinner adhesive bondline in this case produces lower local moments on the edge of the joint.

Under a concentrated three-point load, the load is transferred to the middle of the adhesive bondline. The local stress gradients surrounding the dislocations is different to a similar joint subjected to pure shear. Compressive stress is directly subjected to bondline and localised fracture may occur within each individual dislocation. However the fracture collapses the dislocation upon itself, instead of initiating a

fracture that propagates to another dislocation, as in a lap shear joint in tension. This could be a possible explanation for the higher compressive stiffness associated to the increasing adhesive thickness of the test specimens studied here.

T - Section	Deflection:	$y = 0.0029x^2 - 0.2661x + 1.6451$
	Bending:	$y = 0.0033x^2 - 0.0288x + 1.0777$
	Shear:	$y = -0.0257x^2 - 0.2294x + 0.3955$
L - Section	Deflection:	$y = 0.0259x^2 - 0.2583x + 1.6942$
	Bending:	$y = 0.0067x^2 - 0.0565x + 1.1407$
	Shear:	$y = -0.0289x^2 - 0.2609x + 0.3058$
Z - Section	Deflection:	$y = 0.0182x^2 - 0.2143x + 1.6821$
	Bending:	$y = 0.0063x^2 - 0.0573x + 1.1568$
	Shear:	$y = -0.0283x^2 + 0.2247x + 0.3379$
Flat Beam - Section	Deflection:	$y = 0.038x^2 - 0.3441x + 1.8134$
	Bending:	$y = 0.0102x^2 - 0.0984x + 1.2752$
	Shear:	$y = -0.0354x^2 + 0.3024x + 0.4825$
Inverted T - Section	Deflection:	$y = 0.0161x^2 - 0.2266x + 1.8358$
	Bending:	$y = 0.0073x^2 - 0.0606x + 1.1487$
	Shear:	$y = -0.0346x^2 + 0.351x + 0.3123$

Table 7.1 Polynomial equations for various beam sections developed with results from finite element analysis.

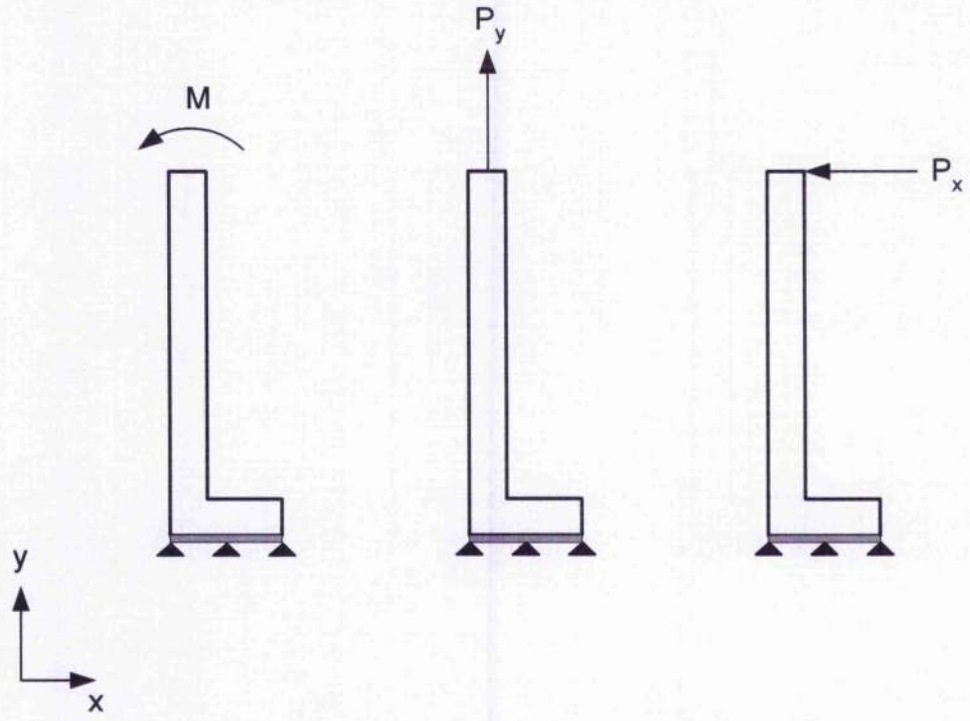

Figure 7.1 Loading of the joints in the x, y directions and loading in the moment M [15,23]

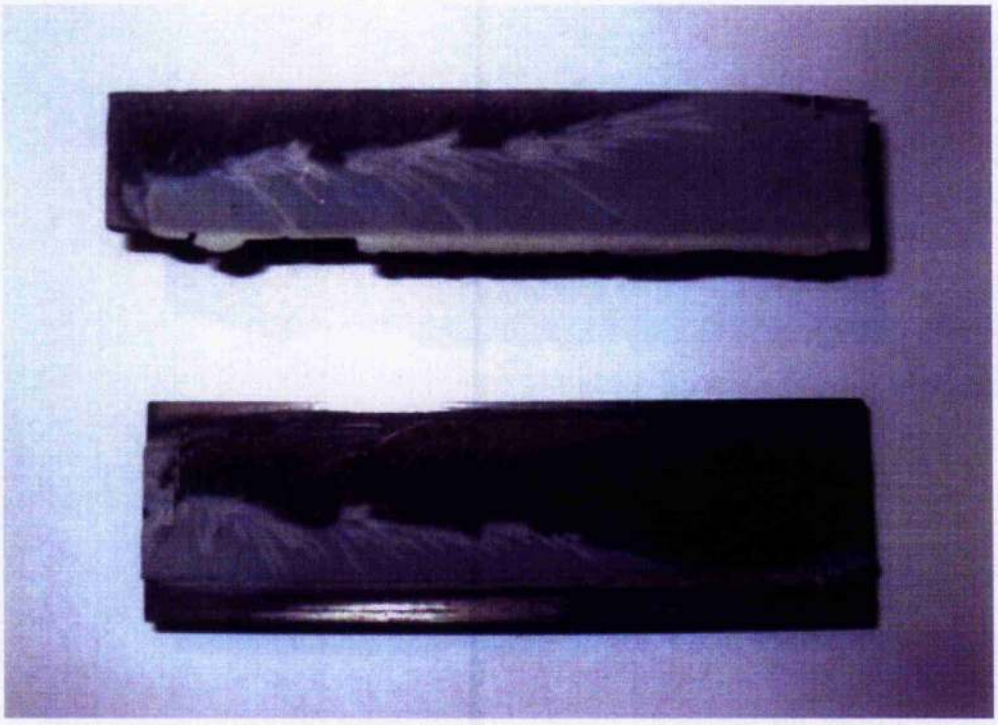

Figure 7.2 Fractured surfaces of standard steel/steel 75mm T bonded beam specimens.

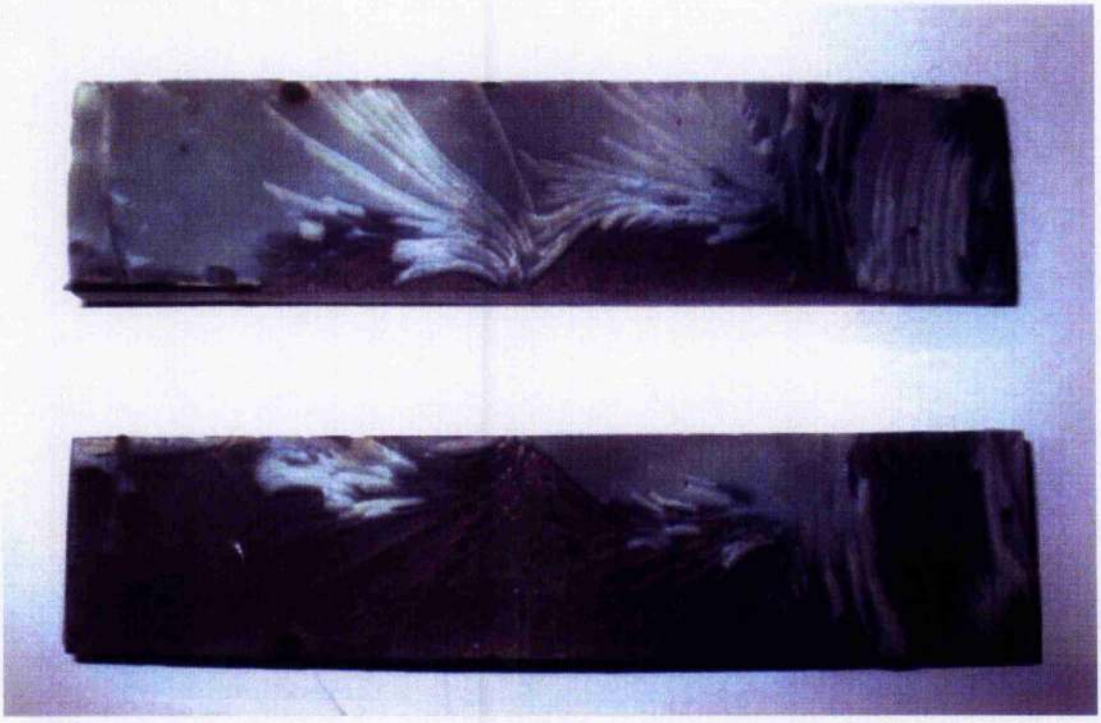

Figure 7.3 Fractured surfaces of standard steel/steel 150mm flat beam specimens.

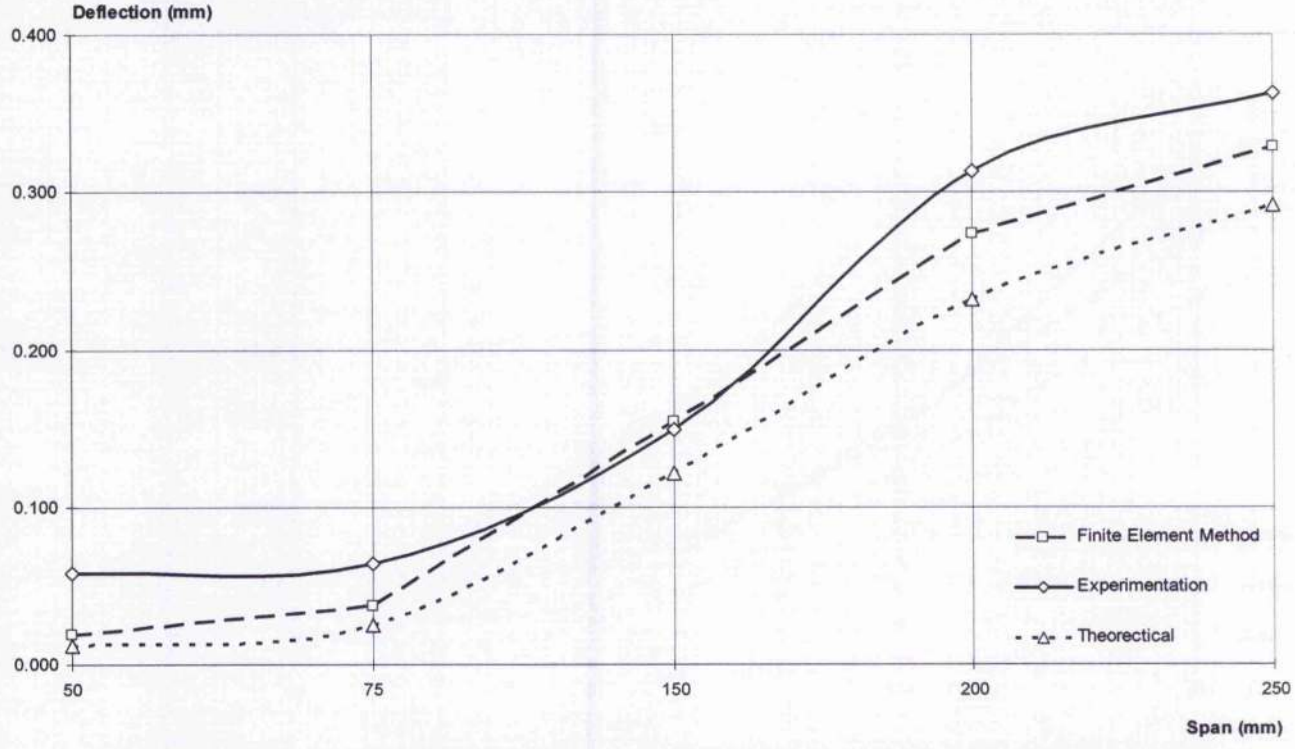

Figure 7.4 Comparing the deflection obtained for the inverted T bonded beam for all three methodologies considered.

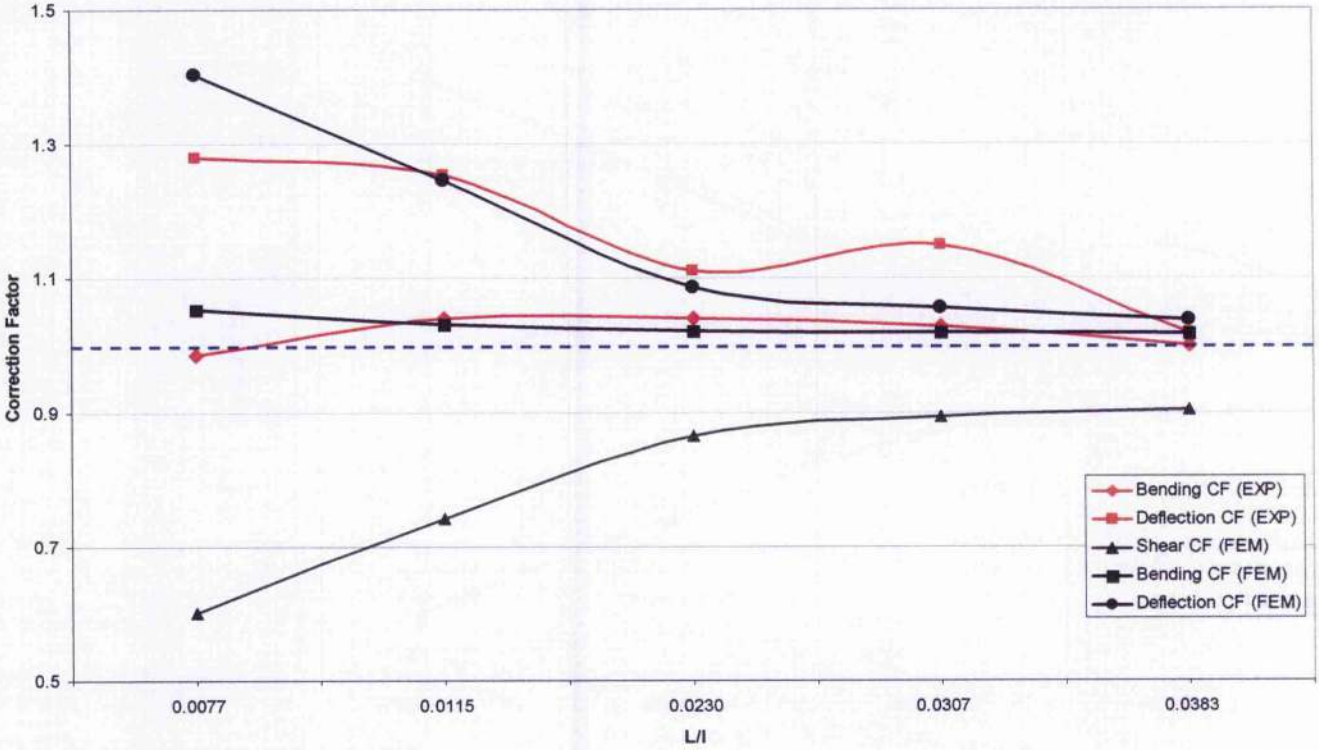

Figure 7.5 Graph for interface coefficients in terms of deflection, bending and shear stress for the T beam section under elastic loading conditions.

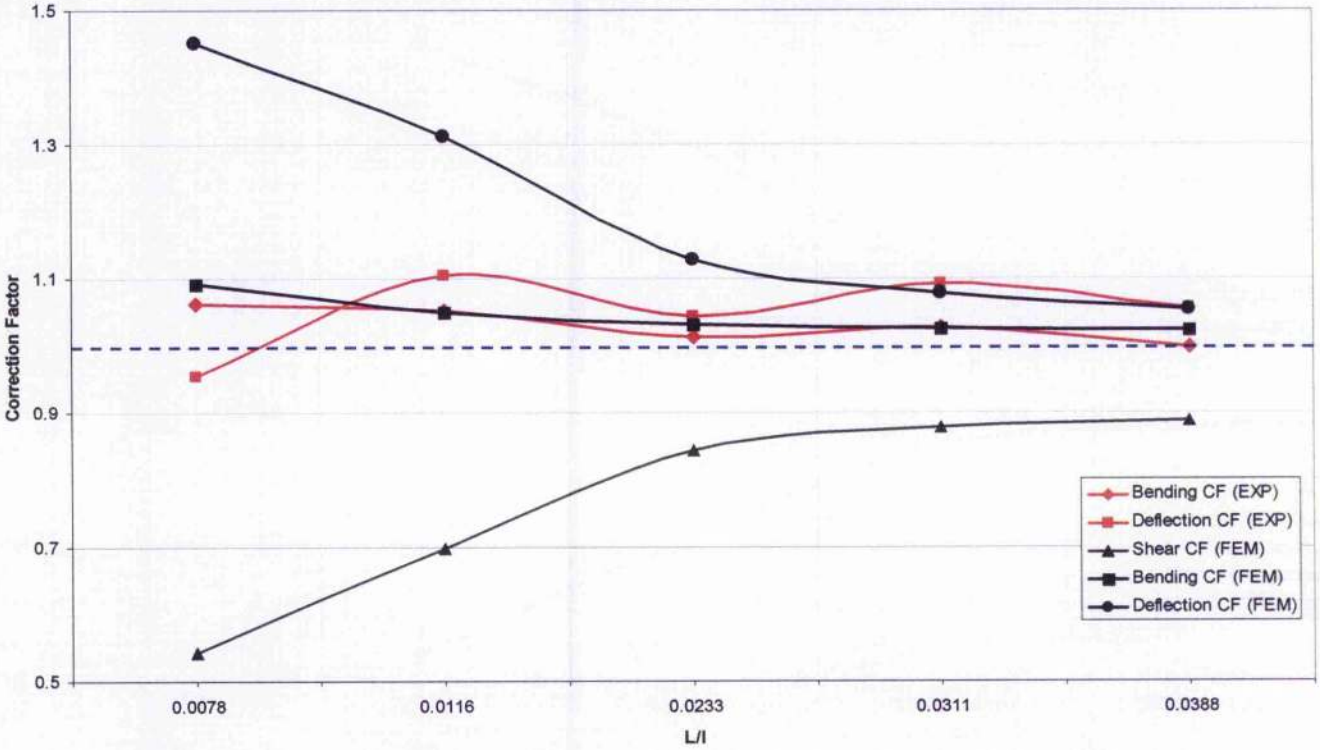

Figure 7.6 Graph for interface coefficients in terms of deflection, bending and shear stress for the L beam section under elastic loading conditions.

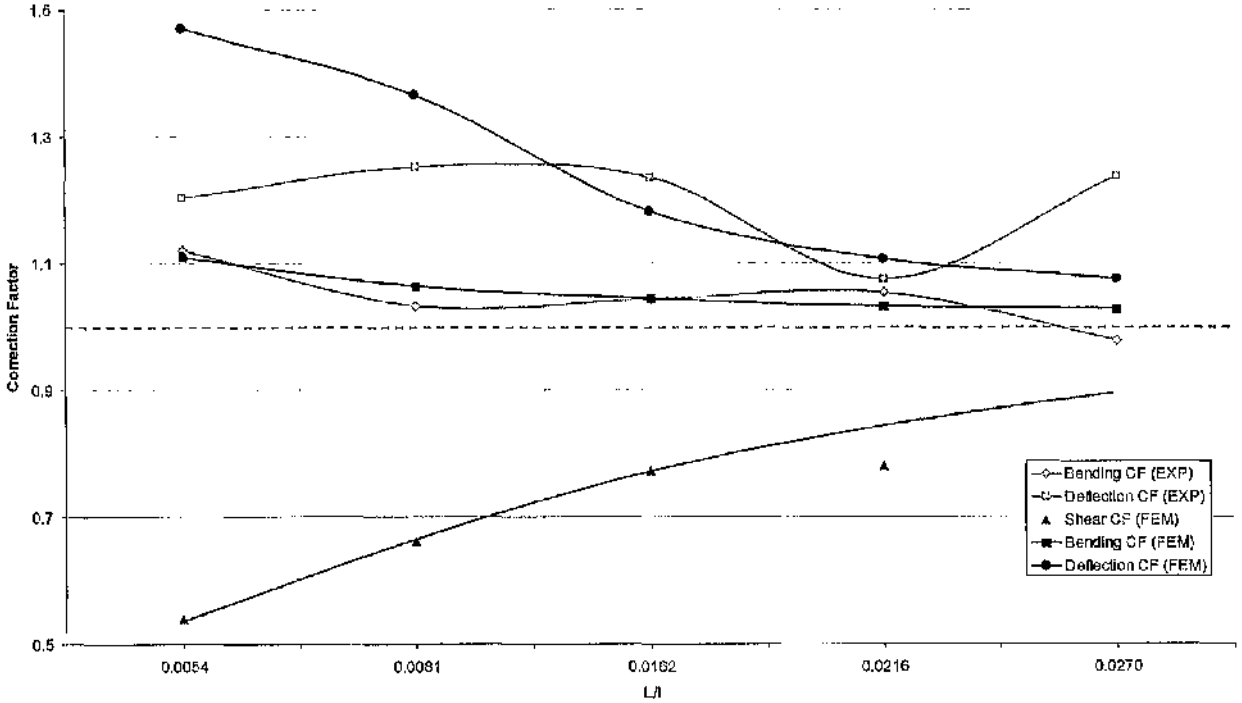

Figure 7.7 Graph for interface coefficients in terms of deflection, bending and shear stress for the Z beam section under elastic loading conditions.

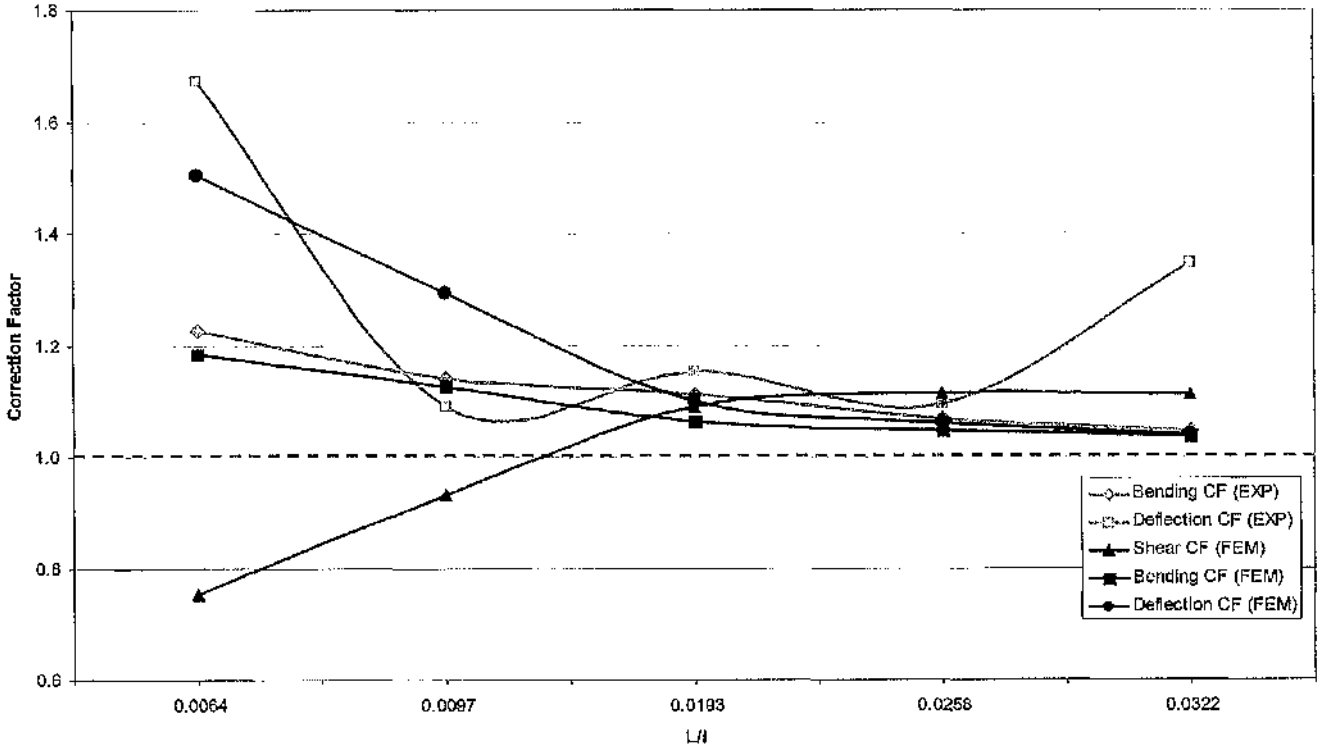

Figure 7.8 Graph for interface coefficients in terms of deflection, bending and shear stress for the flat beam section under elastic loading conditions.

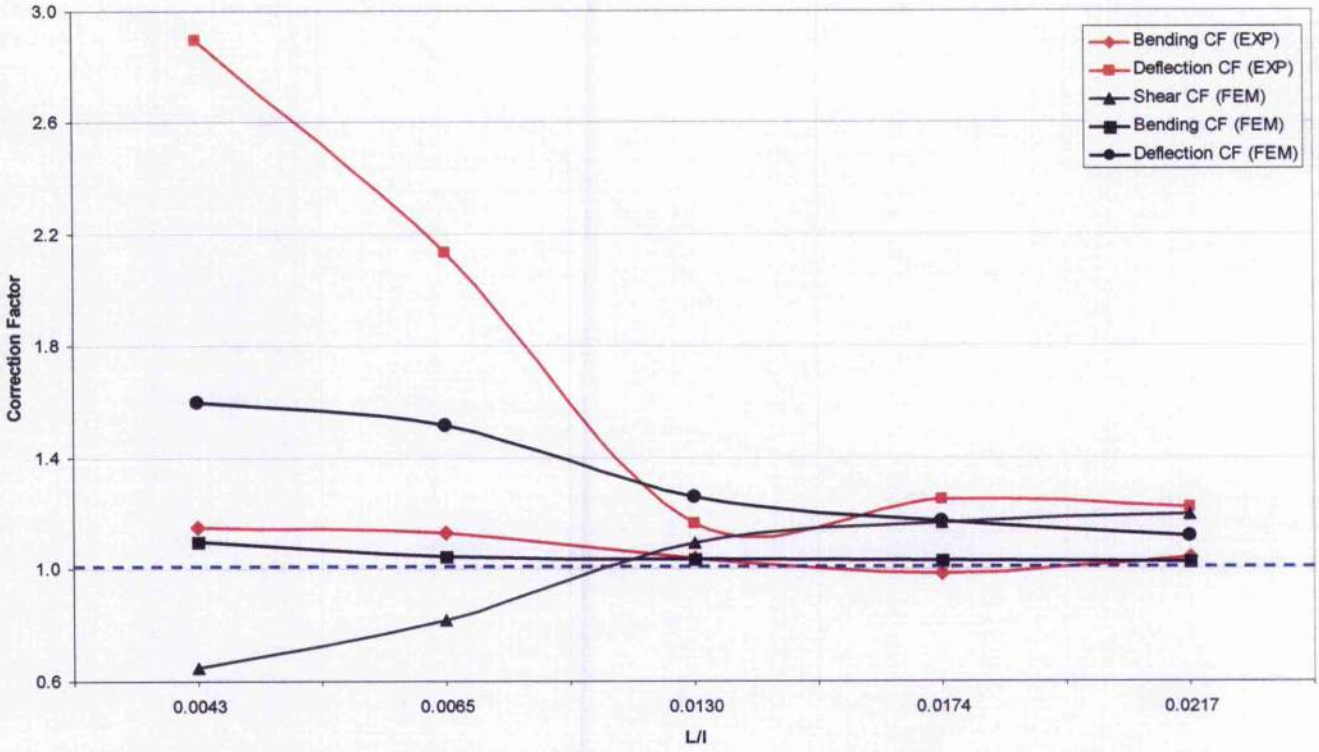

Figure 7.9 Graph for interface coefficients in terms of deflection, bending and shear stress for the inverted T beam section under elastic loading conditions.

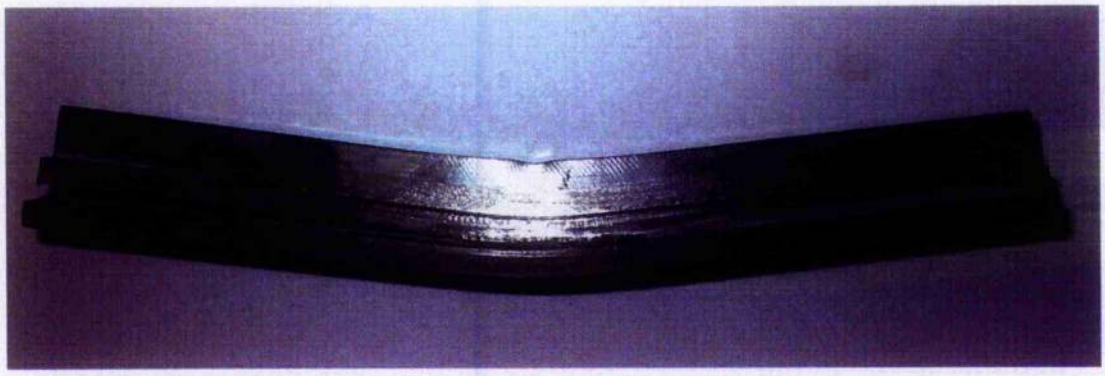

Figure 7.10 Deformed T beam specimen (150 mm)

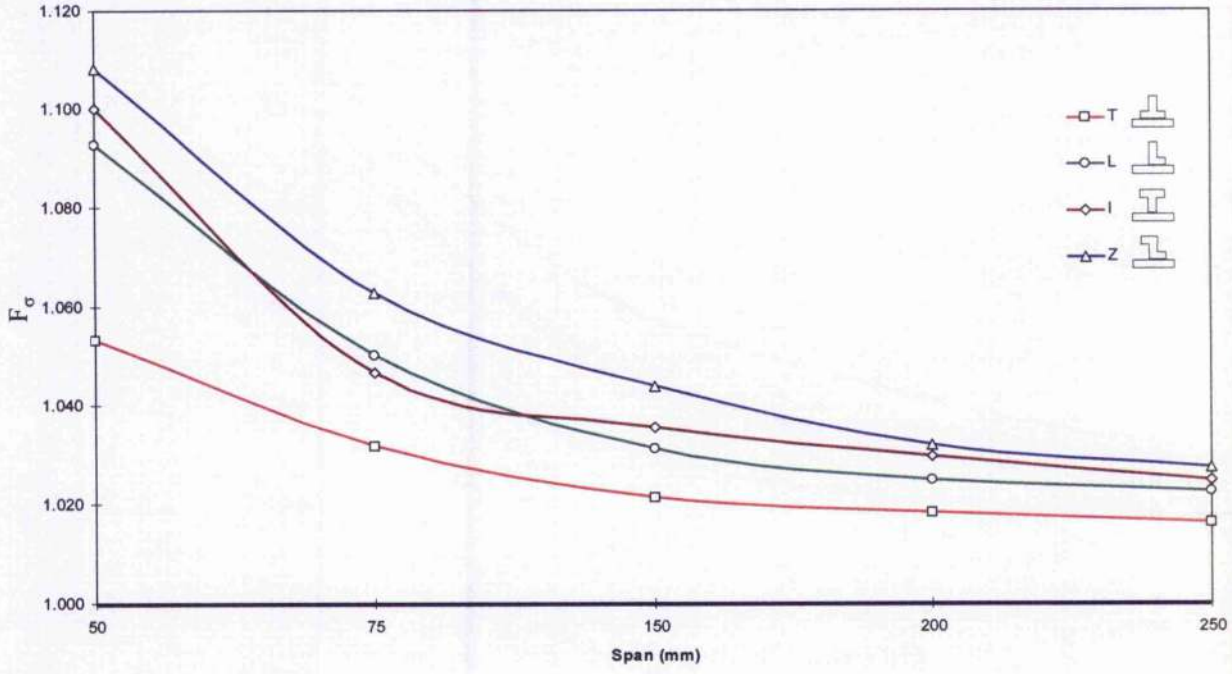

Figure 7.11 Comparison of correction factors for tensile bending stress obtained for the T, L, Z and inverted T profiles.

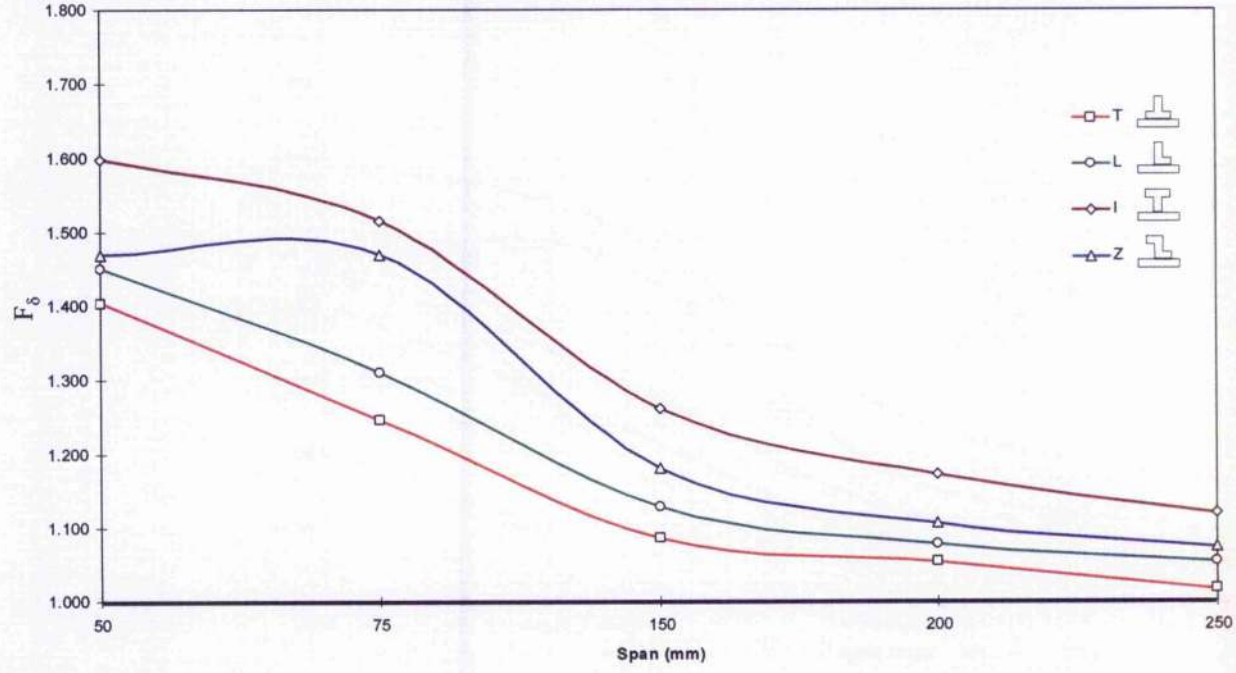

Figure 7.12 Comparison of correction factors for deflection obtained for the T, L, Z and inverted T profiles.

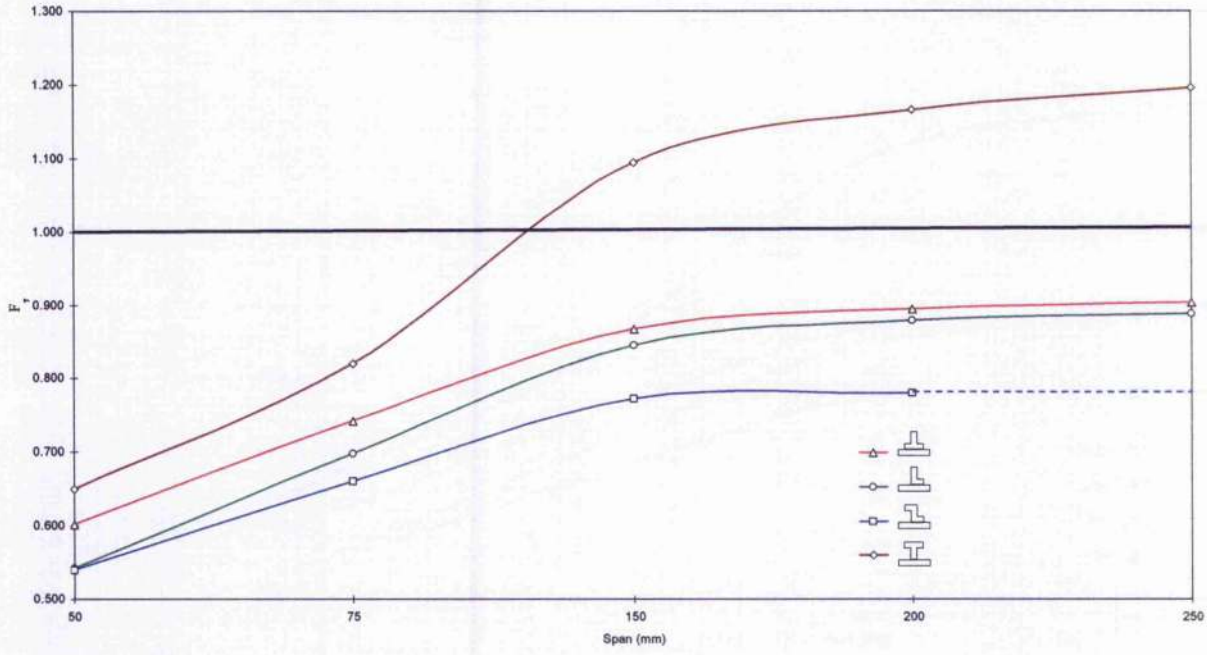

Figure 7.13 Comparison of correction factors obtained for shear stress for the T, L, Z and inverted T profiles.

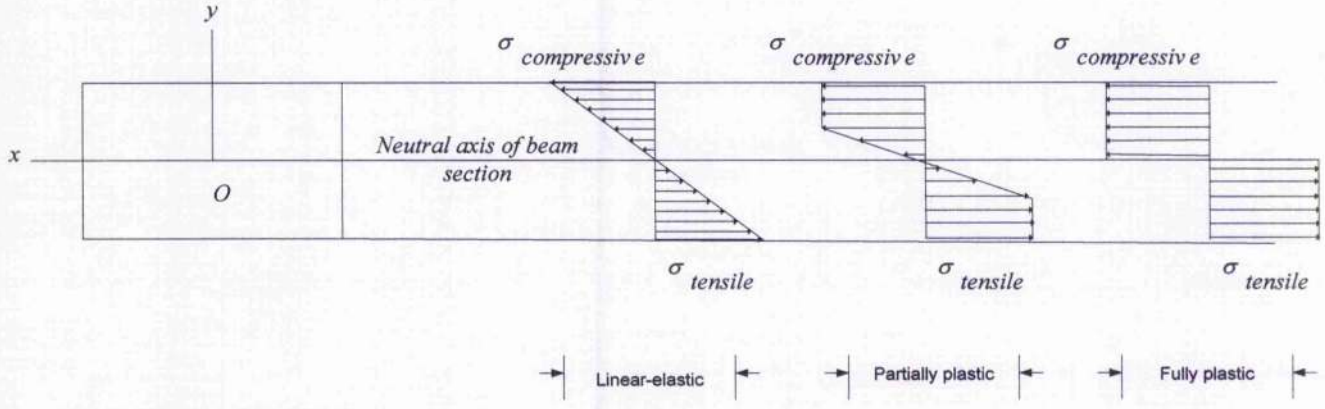

Figure 7.14 Bending stress distribution of the T section under an elastic-plastic load transition.

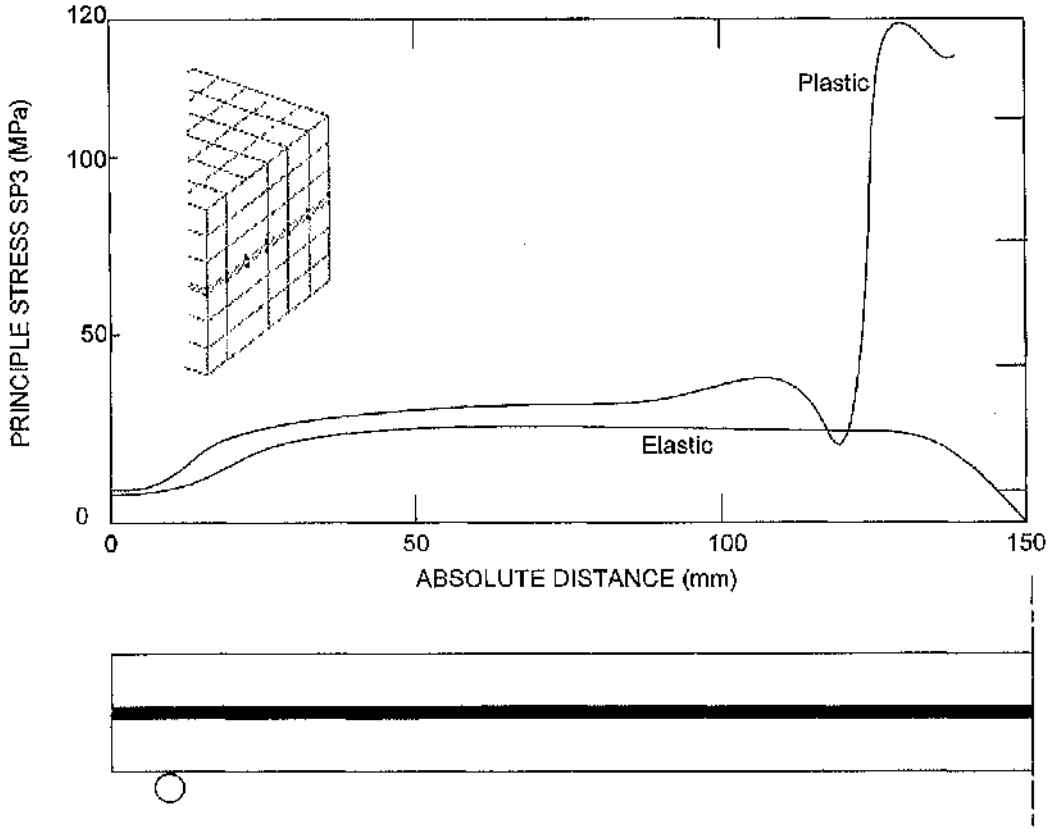

Figure 7.15 Generalised adhesive stress distribution along bondline (250 mm span).

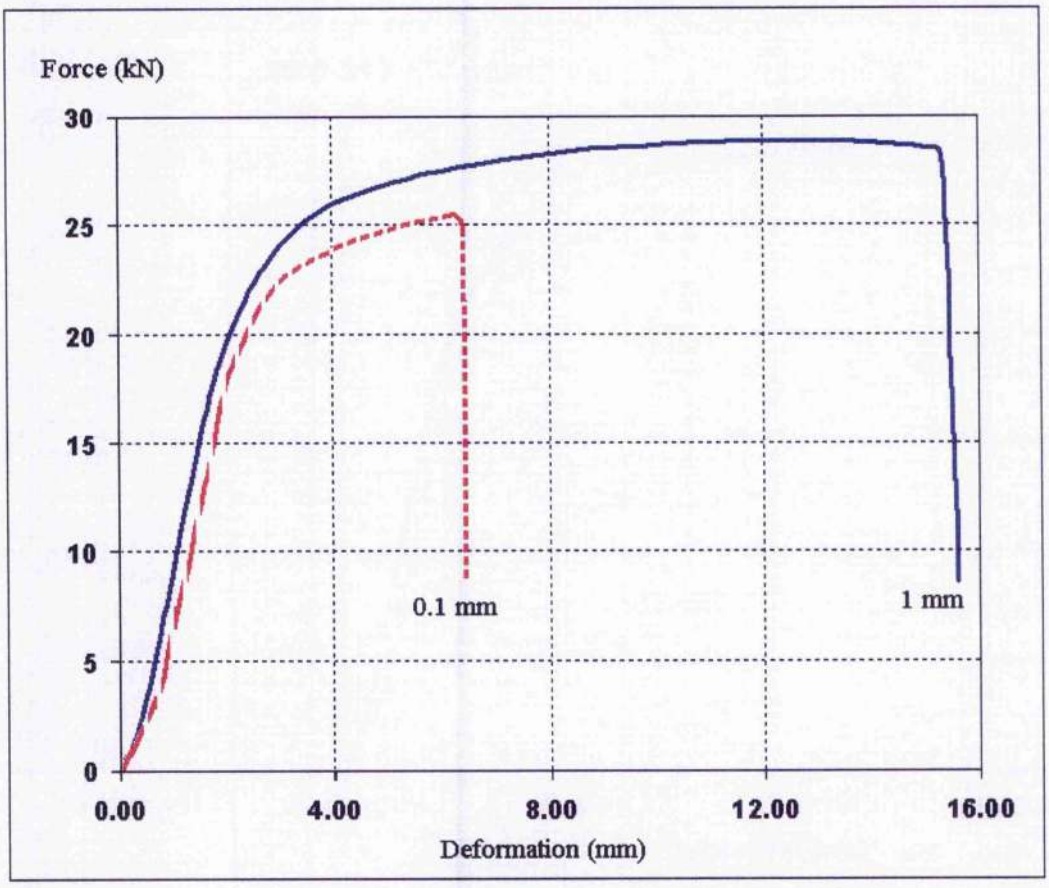

Figure 7.16 Force-deflection curve of the 150 mm flat beam section with specimens of two adhesive thickness

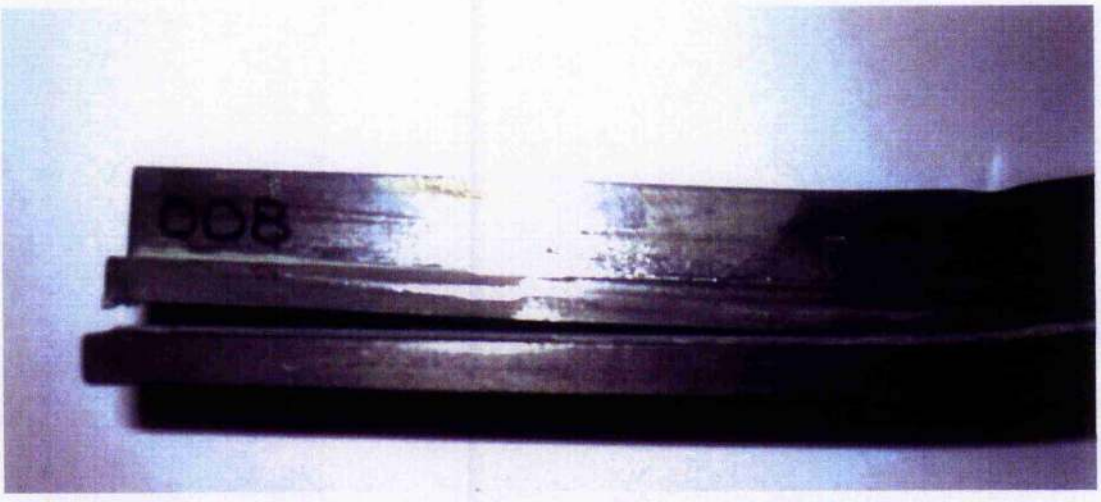

Figure 7.17 Critical failure within the adhesive for the bonded T section (Span = 150 mm)

CHAPTER EIGHT

CONCLUSION AND RECOMMENDATIONS FOR FUTURE WORK

8.1 Conclusions

The conclusions drawn from the present study are summarised below:

1. The machining of the solid beam section to represent the welded stiffened beam is somewhat conservative but is the closest representative to welded beams.
2. The bonded beams behave differently from their welded equivalent. Bonded beam models exhibit higher bending stress and deflection, with the highest deviation found when comparing shorter span beams. Shorter beam models tend to experience higher interfacial shear stress than the longer beam models and are more likely to collapse under shear stress in comparison
3. The bonded beams/panels appear to be slightly heavier than the welded equivalent, with this being more significant for the shorter beams. However, this factor may be compensated by production and corrosion advantages of using adhesives.
4. The choice of stiffener shape has a direct impact on the level of stresses and its distribution in the joint. In terms of deflection and bending stress, the most suitable stiffener shapes are the T and L beam section configuration. In terms of shear stress, the Z beam section represents the most suitable stiffener shape. Overall, the T beam section was found to be the most suitable stiffener shape to resist lateral loads taking into consideration of maximum stress levels of both shear and bending found in the joint.
5. The concept of correction factor, which is used as a means for manipulating stress data in laminated composites, is very useful for determining the deviation between solid and bonded beam sections.
6. The generation of polynomial equations for the correction factors have direct applicability to determination of deflection, bending and shear stresses. Extrapolation of these equations could be made to real panel structures.

7. Adhesive failure in the bonded beams is more likely to initiate from the centre of the beam and arises from combined shear and compressive stresses.
8. Under elastic loads, increasing the adhesive thickness increases bending stiffness and reduces adhesive stresses.
9. Under plastic loads, increasing the adhesive thickness increases the deflection of the beam significantly. Increasing the thickness from 0.1 to 1mm resulted in increasing the central deflection by 188%. Bonded models with thicker bondlines tend to accommodate higher shear stresses under plastic loading, resulting in a stiffer and more durable joint in bending.

8.2 Recommendation for Future Work

Further work is recommended in the following areas to improve our understanding of the behaviour of adhesively bonded beam joints under bending.

1. The use of small-scale models will require identification of suitable techniques such as similitude theories thus allowing the behaviour extrapolation to the real scale.
2. The mechanical testing and finite element modelling of large bonded panel representing a specific stiffener shape
3. Determination of the bonded beam joint under various types of loading, which will include static and fatigue loading conditions.
4. Behaviour of bonded beam joints in wet environments
5. Better production methods of models to control the adhesive thickness and to reduce defects.
6. The study of alternative steel section designs, which are specially used for bonding structures in engineering.
7. The development of mathematical models to predict the failure load of adhesively bonded beam joints.
8. Detailed 3-D modelling and sub-modelling of bonded beam joint under plastic loading.

REFERENCES

1. Darwish, S.M. (2003). Characteristics of weld-bonded commercial aluminum sheets, International Journal of Adhesion and Adhesives 23, pp169-276.

2. Pires, I., Quintino, L., Durodola, J.F., Beevers, A., (2003) Performance of bi-adhesive bonded aluminium lap joints, International Journal of Adhesion and Adhesives 23, pp 215-223.

3. Adams R.D., Comyn J., Wake W.C., (1997) Structural Adhesive Joints in Engineering, Vols. 2nd Edition, Chapman & Hall. pp 18-20.

4. Kaye R.H., Heller M., (2002). Through-thickness shape optimisation of bonded repairs and lap-joints. International Journal of Adhesion and Adhesives 22, pp 7-21.

5. Rispler, A.R., Tong, L., Steven, P., Wisnom, M.R., (2000). Shape optimisation of adhesive fillets. International Journal of Adhesion and Adhesives 20, pp 221-231.

6. Hildebrand, M. (1994). Non-linear analysis and optimization of adhesively bonded single lap joints between fibre-reinforced plastics and metals, International Journal of Adhesion and Adhesives 14, pp 261-267.

7. Groth, H.L., Nordlund, P., (1991). Shape optimization of bonded joints. International Journal of Adhesion and Adhesives 11, pp 204-212.

8. You, M., Zheng, Y., Zheng, X.L., Liu, W.J., (2003) Effect of metal as part of fillet on the tensile shear strength of adhesively bonded single lap joints, International Journal of Adhesion and Adhesives 23 pp 365-369

9. van Tooren, M.J.L., Gleich, D.M., Beukers, A., (2004). Experimental verification of a stress singularity model to predict the effect of bondline thickness on joint strength. Journal of Adhesion Science and Technology. 18, pp 395-412.

10. Shields, J., (1976) Adhesion Handbook, Butterworth & Co Ltd. ISBN: 0408002107.

11. Pye, A., Ledbetter, S., (1998), The selection of an adhesive for the construction of a glass-adhesive T-beam, International Journal of Adhesion and Adhesives 18, pp 159-65

12. Knox, E.M., Cowling, M.J., Winkle,.I.E. (1998). Adhesively bonded steel corrugated core sandwich construction for marine applications. Marine Structures 11, pp 185-204

13. Allen, H. (1969), Analysis and Design of Structural Sandwich Panels Oxford: Pergamon Press.

14. Chang, P.H., Fung, C.P., Teng, T.L., Yang, W.C., (2001). Analysis of residual stresses and distortions in T-joint fillet welds. International Journal of Pressure Vessels and Piping 78, pp 523-538.

15. Li, W., Blunt, L., Stout, K.J., (1999). Stiffness analysis of adhesive bonded Tee joints. International Journal of Adhesion and Adhesives 19, pp 315-20.

16. Pasternak, H., Schwarzlos, A., Schimmack, N., (2004), The application of adhesives to connect steel members, Journal of Constructional Steel Research 60, pp 649-58.

17. Darwish, S.M., Samhan, A.A., (2004). Design rationale of weld-bonded joints. International Journal of Adhesion and Adhesives 24, pp 367-377.

18. Mossac, C..E., Shenoi. R.,A., Philips, H.J., (1999). Damage mechanics of top-hat stiffeners used in FRP ship construction. Marine Structures 12, pp 1-19.

19. van Straalena, I.J.J., Wardenierb, J., Vogelesangc, L.B., Soetensa, F. (1998) Structural adhesive bonded joints in engineering - drafting design rules, International Journal of Adhesion and Adhesives 18, pp 41-49

20. Paik, J.K., Thayamballi, A.K., Kim, D.Y., (1999). An analytical method for the ultimate compressive strength and effective plating of stiffened panels. Journal of Constructional Steel Research 49, pp 43-68.

21. Lehta, H.W., Mansour, A.E., (1997) Reliability-based Method for Optimal Structural Design of Stiffened Panels. Marine Structures 10, pp 323-352.

22. Fujikubo, M., Yao, T., (1999) Elastic local buckling strength of stiffened plate considering plate/stiffener interaction and welding residual stress. Marine Structures 12, pp 543-564.

23. Li, W., Blunt, L., Stout, K.J. (1997). Analysis and design of adhesive-bonded Tee joints, International Journal of Adhesion and Adhesives 17, pp 303-311.

24. Santos, I.O., Zhang, W., Goncalves, V.M., Bay, N., Martins, P.A.F., (2004) Weld bonding of stainless steel. International Journal of Machine Tools and Manufacture 44, pp 1431-1439.

25. Kaya, A., Tekelioglu, M.S., Findik, F., (2004). Effects of various parameters on dynamic characteristics in adhesively bonded joints, Materials Letters 58, pp 3451-3456.

26. Darwish, S.M., (2003) Weldbonding strengthens and balances the stresses in spot-welded dissimilar thickness joints, Journal of Materials Processing Technology 134, pp 352-362

27. Pereira, A.B., Morais, A.B. (2003) Strength of adhesively bonded stainless steel joints. International Journal of Adhesion and Adhesives Volume 23, pp 315-322.

28. Chang, B., Shi, Y., Dong, S., (1999), Comparative studies on stresses in weld-bonded, spot-welded and adhesive-bonded joints, Journal of Materials Processing Technology 87, pp 230-236.

29. Hu, S.Z., Zimmerman, T.J.E., Pegg, N., (1997) Ultimate collapse tests of stiffened-plate ship structural units, Marine Structures 10, pp 587-610.

30. Shanmugam, N.E., Arockiasamy, M., (1996), Local Buckling of Stiffened Plates in Offshore Structures. Journal of Constructional Steel Research 38, pp 41-59.

31. Samhan, A.A., Darwish, S.M., (2003), Finite element modeling of weld-bonded joints, Journal of Materials Processing Technology 142, pp 587-598.

32. Dong, P., Zhang, J., (1999) Residual stresses in strength-mismatched welds and implications on fracture behaviour, Engineering Fracture Mechanics 64, pp 485-505.

33. Pye, A., Ledbetter, S., (1999) Realising composite glass-adhesive beams in practice. Glass in buildings, pp 185-190.

34. Lucas, F.M., Adams, R.D., (2002) The strength of adhesively bonded T-joints. International Journal of Adhesion and Adhesives 22, pp 311-315.

35. Knox, E.M, Cowling, M.J., Hashim, S.A. (2000) Creep analysis of adhesively bonded connections in GRE pipes including the effect of defects. Composites Part A: Applied Science and Manufacturing 31, pp 583-590.

36. Ducan, B., Dean, G., (2002) Measurements and models for design with modern adhesive, International Journal of Adhesion and Adhesives 23, pp 141-149.

37. Hu, S.Z., Jiang, L., (1998) A finite element simulation of the test procedure of stiffened panels. Marine Structures 11, pp 75-99.

38. Wu, G., Crocombe, A.D., (1996) Simplified finite element modelling of structural adhesive joints, Computers and Structures 61, pp 385-391.

39. Feih, S., Shercliff, H.R., (2005) Adhesive and composite failure prediction of single-L joint structures under tensile loading, International Journal of Adhesion and Adhesives 25, pp 47-59.

40. Robert, D.Cook., (2004) Finite element modeling for stress analysis John Wiley & Sons. ISBN: 0471107743

41. Tuhkuri, J., (1996) Sandwich structures under ice loading. Marine Structures 9, pp 259-80.

42. Plantema, F.J., (1966). Sandwich Construction John Wiley & Sons, Inc.

43. Pokharel, N., Mahendran, M., (2004). Finite element analysis and design of sandwich panels subject to local buckling effects, Thin walled structures 42, pp 589-611.

44. Lanzi, L., (2004) A numerical and experimental investigation on composite stiffened panels into post-buckling, Thin walled structures 42, pp 1645-1664.

45. Shanmugam, N.E., Lian, V.T., Thevendran, V., (2004) Finite element modelling of plate girders with web openings, Thin walled structures 40, pp 443-464.

46. Gonclaves, J.P.M., de Moura, M.F.S.F,, de Castro, P.M.S.T., (2002) A three-dimensional finite element model for stress analysis of adhesive joints. International Journal of Adhesion and Adhesives 22, pp 357-365

47. BRITISH STANDARDS. (1996) BS 970 - 1:1996, Wrought Steel for mechanical and allied engineering purposes, Part 3. Bright bars for general engineering purposes

48. ASTM (American Standards for Testing and Measurement). (2004) Standard Specification for Steel, Sheet, Carbon, and High-Strength, Low-Alloy, Hot-Rolled and Cold-Rolled, General Requirements for. Rep. A568

49. BRITISH STANDARDS. (1996). BS EN ISO 527-1:1996, Plastics-Determination of tensile properties Part 1

50. BRITISH STANDARDS. (1990) BS EN 10002-1:1990, Tensile testing of metallic materials, Part 1: Method of test at ambient temperature.

51. BRITISH STANDARDS. (1996) BS EN ISO 527-2, Plastics-Determination of tensile properties- Part 2 Test conditions for moulding and extrusion plastics.

52. Dean, G., Crocker, L., Read, B., Wright, L., (2004) Prediction of deformation and failure of rubber-toughened adhesive joints, International Journal of Adhesion and Adhesives 24, pp 295-306.

53. Andruet, R.H., Dillard, D.A., Holzer, S.M., (2001) Two- and three-dimensional geometrical nonlinear finite elements for analysis of adhesive joints. International Journal of Adhesion and Adhesives 21, pp 17-34.

54. Elbing, F., Anagreh, N., Dorn, L., Uhlmann, E., (2005) Dry ice blasting as a pretreatment of aluminium surfaces to improve the adhesive strength of aluminium bonding joints. International Journal of Adhesion and Adhesives 23, pp 69-79

55. Minford, J.D., (1978) Adhesives Age. Adhesive Age 21, pp 17-23.

56. Pocius, A.V., (1997) Adhesion and adhesives technology: an introduction Hanser/Gardner Publications.

57. Critchlow, G.W., Brewis, D.M., (1996) Review of surface pretreatments for aluminium alloys. International Journal of Adhesion and Adhesives 16, pp 255-275.

58. Critchlow, G.W., Brewis, D.M., (1995). Review of surface pretreatments for titanium alloys. International Journal of Adhesion and Adhesives 15, pp 161-72.

59. Kinloch, A.J., (1987) Surface Pretreatments, Adhesion and Adhesives, pp. 101-170. Chapman & Hall.

60. Bardis, J., Kedward, K., (2001) Effects of Surface Preparation on Long-Term Durability of Composite Adheisve Bonds. Rep. DOT/FAA/AR-01/8, Washington, DC 2051, Office of Aviation Research

61. Zhao, W., Ramani, K., Mueller, B.E., (2000). Processing and fracture behavior of a polyethylene-based thermoplastic adhesive and a glaa-fiber filled epoxy adhesive. International Journal of Adhesion and Adhesives 20, pp 409-413.

62. Loh, W.K., Crocombe, A.D., Wahab, M.M.A., Ashcroft, L.A., (2005). Modelling anomalous moisture uptake, swelling and thermal characteristics of a rugger toughened epoxy adheisve. International Journal of Adhesion and Adhesives 25, pp 1-12.

63. National Physical Laboratory (UK) (2005) Design and Test of bonded and bolted joints. Appendix 1

64. BRITISH STANDARDS, (1998). BS EN 2746:1998 Glass fibre reinforced plastics - Flexural Test - Three point bend method, Rep. BS EN 2746:1998

65. Phillips, H.J., Shenoi, R.A., (1998). Damage tolerance of laminated tee joints in FRP structures. Composites Part A: Applied Science and Manufacturing 29, pp 465-478.

66. ISO. 2005. ISO 14679 (1997), Measurement of adhesion characteristics by a three-point bending method.

67. Kim, Y.Y., Kim, T.S., (2000), Topology optimization of beam cross section. International Journal of Solids and Structures 37, pp 477-93.

68. Dai, J., Hahn, H.T., 2003, Flexural behavior of sandwich beams fabricated by vacuum-assisted resin transfer molding. Composite Structures 61, pp 247-53.

69. Matsunaga, H., (1996) Buckling instabilities of thick elastic beams subjected to axial stresses. Computers and Structures 59, pp 859-868.

70. Zenkert, D., (1997) An introduction to sandwich construction EMAS 1995 ISBN:0947817778.

71. Petras, A., Sutcliffe, MPF., (1999), Failure mode maps for honeycomb sandwich panels. Composite Structures 44, pp 237-52.

72. MSC Inc, MSC/Patran Software Training. (2005).

73. Hibbitt, K&SI., (2005). ABAQUS/Standard User's Manual Version 6.3

74. Hibbitt, K&SI., (2005) Getting started with ABAQUS/Standard Version 6.3

75. Wahab, M.M.A., Ashcroft, L.A., (2002) Failure Prediction using FEA and analytical solutions for adhesively bonded composite beams, European Adhesion Conference. 10-10-2002, pp 137-140.

76. Chang, B.H., Shi, Y.W., Dong, J., (2005) A study on the role of adhesives in weld-bonded joints. Welding Research Supplement , pp 275-279.

77. Brown, L., (2001) New fabrication technologies for US navy 21st century surface combatants.

78. Hashim, S.A., (1999) Adhesive bonding of thick steel adherends for marine structures. Marine Structures 12, pp 405-423.

79. Bowditch, M.R., Harper, T.I., Lane, J.M., (2004). Feasibility study to compare steel and adhesive/ composite-based emergency repair methods for damaged hulls. Rep. DERA Research report 293.

80. Timoshenko, S., (1955), Stresses in laterally loaded symmetrical beams. In Strength of materials, New York: D. Van Nostrand, pp. 92-130.

81. Hashim, S.A., Winkle,.I.E., Knox, E.M., Cowling,.M.J., (1993) Advantage of adhesive bonding in offshore marine structural applications. EMAS 1993, Chapter 19, Intergrity of offshore structures

82. Knox, E.M., (1996) Marine applications for structural adhesives. Ph.D thesis. University of Glasgow

83. Joint Institut de Soudure France, TWI UK, (1996), Laser welding in thick section steel fabrication. Rep. GP/ALS/1107-REV1

84. TWI UK, (2001). UK Patent No. E1846179

85. Shenoi, R.A., Hawkins, G. L., (1995) An investigation into the performance characteristics of top-hat stiffener to shell plating joints. Composite Structures 30, pp 109-121

86. Judd, G., Dodkins, A., Thornycroft, Vosper., Maddison, A., (1996) Adhesively bonded aluminium superstructures, International Conference on Lightweight Materials in Naval Architecture, Southampton. 28-2-1996, pp 1-21.

87. Hashim, S.A., Knox, E.M., (1999) Structural performance of thick adherend steel-composite adhesive joints, Proceedings of the Institution of Mechanical Engineers 213, pp 47-57.

88. Hashim, S.A., Winkle,.I.E., Cowling,M.J., (1989) A structural role for adhesives in shipbuilding. The Royal Institution of Naval Architects, Spring Meetings of The Royal Institution of Naval Architects, Paper no 9, 1-11.

89. Herrington, P.D., Latorre, R.G., (1998) Development of an aluminium hull panel for high-speed craft. Marine Structures 11, pp 47-71.

90. Grondin, G.Y., Chen, Q., Elwi, A.E., Cheng, J.J., (1998) Stiffened steel plates under compression and bending. Journal of Constructional Steel Research 45, pp 125-148.

91. Sheikh, I.A., Elwi, A.E., Grondin, G.Y., (2003) Stiffened steel plates under combined compression and bending. Journal of Constructional Steel Research 59, pp 911-930.

92. Sheikh, I.A., Elwi, A.E., Grondin, G.Y., (2002) Stiffened steel plates under uniaxial compression. Journal of Constructional Steel Research 58, pp 1061-1080.

93. Hashim, S.A., (1992) Assessment of adhesive bonding for structural design with thick adherends. Ph.D thesis. University of Glasgow.

94. Rigo, P., (2001) A module-oriented tool for optimum design of stiffened structures—Part I. Marine Structures 14, pp 611-629.

95. Kong, C.W., Lee , I.C., Kim, C.G., Hong, C.S., (1998) Postbuckling and failure of stiffened composite panels under axial compression. Composite Structures 42, pp 13-21.

96. Hughes, O.F., Ghosh, B., Cheng, Y., (2004). Improved prediction of simultaneous local and overall buckling of stiffened panels. Thin walled structures 42, pp 827-856.

97. Alinia, M. M., (2005). A study into optimization of stiffeners in plates subjected to shear loading. Thin walled structures 43, pp 845-860.

98. Kang, J.H., Kim, C.G., (2005) Minimum-weight design of compressively loaded composite plates and stiffened panels for postbuckling strength by Genetic Algorithm. Composite Structures 69, pp 239-246.

99. Bedair, O.K., (1997) The elastic behaviour of multi-stiffened plates under uniform compression. Thin walled structures 27, pp 311-335.

100. Wang, X., Rammerstorfer, F.G., (1996) Determination of effective breadth and effective width of stiffened plates by finite strip analyses. Thin walled structures 26, pp 261-286.

101. Baker, E., (1953) Introduction to steel shipbuilding McGraw-Hill College, ISBN: 0070033595.

102. Lee, M.M.K., Pine, T., Jones, T.B., (2001) An experimental and finite element study on the torsional behavior of T-joints in automotive structures, Proceedings of the Institution of Mechanical Engineers, Part D: Journal of Automobile Engineering 215, pp 231-240.

103. Tsai, M.Y., Morton, J., (1994). An experimental investigation of nonlinear deformations in single-lap joints. Mechanics of Materials 20, pp 183-194.

104. Bogdanovich, A.E., Kizhakkethara, I., (1999) Three-dimensional finite element analysis of double-lap composite adhesive bonded joint using submodeling approach. Composites Part B:engineering 30, pp 537-551.

105. Liu, J., Sawa, T., (2003) Strength and finite element analyses of single-lap joints with adhesively-bonded columns. Journal of Adhesion Science and Technology 17, pp 1773-1784.

106. Liu, J., Liu, J., Sawa, T., (2004) Strength and failure of bulky adhesive joints with adhesively-bonded columns. Journal of Adhesion Science and Technology 18, pp 1613-1623.

107. Edlund, U., Klarbring, A., (1990), A geometrically nonlinear model of the adhesive joint problem and its numerical treatment. Computer methods in applied mechanics and engineering 96, pp 329-350.

108. AISI 1016 Steel, cold drawn. 205. www.MatWeb.com

109. Ozel, A., Aydin, M.D., Temiz, S., (2005) The effects of overlap length and adherend thickness on the strength of adhesively bonded joints subjected to bending moment. Journal of Adhesion Science and Technology 18, pp 313-325.

110. Broughton, W.R., Hinopoulos, G., (1999). Evaluation of the Single-Lap Joint Using Finite Element Analysis. Report 15, Project PAJ3 – Combined Cyclic Loadind and hostile environments, 1996-1999.

111. Roche, A.A., Romand, M.J., Sidoff, F., (1984) Practical Adhesion Measurement in Adhering systems, A Phase Boundary Sensitive Test. Adhesive Joints: Formation, Characteristics and Testing, pp 19-30.

112. Gere, J.M., (2004) Mechanics of materials, Vols. 1. California: Brooks/Cole-Thomson Learning. ISBN: 8123908946.

113. Shigley, J.E., Mischke, C.R., (2005) Mechanical engineering design Singapore: McGraw-Hill Book Company.

114. Somiya, S., (1989). Advanced Technical Ceramics San Diego, California: Academic Press, Inc. pp 223-227.

115. Mortimer, A., (1998) Application for structural adhesives within James Hawden and Company Ltd. Unpublished Report.

116. Shahid, M., Hashim, S.A., (2000) Cleavage Strength of Steel/Composite Joints. Journal of Adhesion 73, pp 365-384.

117. Beevers, A., Kho, A.C.P., (1983) The performance of adhesive-bonded thin-gauge sheet metal structures with particular reference to box-section beams. International Journal of Adhesion and Adhesives 3, pp 25-39.

118. Beevers, A., Kho, A.C.P., (1984) The performance of adhesive-bonded thin-gauge sheet metal structures with particular reference to box-section beams. Adhesive joints: Formation, Characteristics, and Testing, Kansas City, Missouri, USA, 12-17 Sept. 1982, pp 627-637.

119. Hart-Smith, L.J., (1995) An engineer's viewpoint on design and analysis of aircraft structural joints. Journal of Aerospace Engineering 209, pp 226-238.

120. Volkersen, O., (1938) Dio Niekraftverteilung in Zugbeanspruchten Nietverbindungen Mit Konstaten Laschenquerschnitten. Luftfahrforschung 15, pp 41-47.

121. Goland, M., Reissner, E., (1944) The stresses in cemented joints. Journal of Applied Mechanics 11, pp 17-27

122. Dulieu-Barton, J.M., Earl, J.S,, Shenoi, R. A. (2001) Determination of the stress distribution in foam cored sandwich construction composite tee joints. Journal of Strain Analysis 36, pp 545-560.

123. Bhatt, P., Nelson, H.M., (1999) Structures: A Revision of Structures by P. Bhatt and H.M. Nelson, Longman Publishing Group. ISBN: 0582312221

124. Utku, S., Norris, C.H., Wilbur, J.B., (1990). Elementary Structural Analysis Mcgraw-Hill College.

125. Timoshenko, S., (1956) Deformations beyond the elastic limit. In Strength of Materials, Part 2, Advance Theory and Problems, D. Van Nostrand Company, pp. 346-386.

126. Armstrong, K.B., (1974). Aircraft floor panel developments at British Airways (1967-1973). Composites 5, pp 165-173.

127. Lupton, D.C., (1983) Selection of an adhesive for bonding FRP automotive panels. International Journal of Adhesion and Adhesives 3, pp 155-159

128. Earl, J.S., Dulieu-Barton, J.M., Shenoi, R.A., (2002) Determination of hygrotermal ageing effects in sandwhich construction joints using thermoelastic stress analysis. Composite Science and Technology 63, pp 211-233.

129. Heslehurst, R.B., (1999) Observations in the structural response of adhesive bondline defects. International Journal of Adhesion and Adhesives 19, pp 133-154

130. Dexter, R.J., Pilarski, P.J. (2002) Crack propagation in welded stiffened panels. Journal of Constructional Steel Research 58, pp 1081-1102

131. Serrano, E., Gustafsson, P.J., (1998) Influence of bondline brittleness and defects on the strength of timber finger-joints. International Journal of Adhesion and Adhesives 19, pp 9-17.

132. Silva, L.F.M., Adams, R.D., Gibbs, M., (2004) Manufacture of adhesive joints and bulk specimens with high-temperature adhesives. International Journal of Adhesion and Adhesives 24, pp 69-83

133. Lu, J., Newaz, G.M., Gibson, R.F., (2005). Buckling strength analysis of adhesively bonded aluminium hat sections. International Journal of Solids and Structures 42, pp 4947-4957.

134. Moan, T., (2003) Marine Structures for the future, National University of Singapore, National University of Singapore. Keppel Offshore & Marine, pp 1-31.

135. Shankar, K., Wu, W., (2001) Effect of welding and weld repair on crack propagation behaviour in aluminium alloy 5083 plates. Materials & Design 23, pp 201-208.

136. Taib, A.A., Boukhili, R., Achiou, S., Gordon, S., Boukehili, H., (2006) Bonded joints with composite adherends. Part I. Effect of specimen configuration, adhesive thickness, spew fillet and adherend stiffness on fracture. International Journal of Adhesion and Adhesives 26, pp 226-236

137. Samhan, A.A., Darwish, S.M., (2004). Factors influencing thermo-mechanical stresses developed in bonded tools. International Journal of Adhesion and Adhesives 25, pp 379-388.

138. Durand, S., (2006) Assystem European Composite Materials Workshop.

139. Allman, D.J., (1977) A Theory For Elastic Stresses in Adhesive Bonded Lap Joints. The Quarterly Journal of Mechanics and Applied Mathematics 30, pp 415-436.

140. Loke, D, Hashim, S.A. (2004) Comparison of bonded beams sections in bending – 27th, Annual Meeting of the Adhesion Society, Wilmington, NC, Feb (2004).

141. Underhill, P.R., DuQuesnay, D. L. (2006) The dependence of the fatigue life of adhesive joints on surface preparation. International Journal of Adhesion and Adhesives 26, pp 62-66.

142. Brockmann, W (1983) Durability of Structural Adhesives, Elsevier Applied Science Publishers, ISBN 08533421488, Chap 7, pp306

143. Brockmann, W (1983) Durability of Structural Adhesives, Elsevier Applied Science Publishers, ISBN 08533421488, Chap 7, Figure 3&4

APPENDIX A

Fabrication and bonding process

The success of an adhesively bonded structure depends to a large extent on a few parameters that were present in the fabrication process as emphasised in Chap. 3. The parameters discussed here include the choice of adhesive, surface preparation, application of the adhesive, proper clamping and the curing process. The adhesive material selected in the fabrication of the joints was a well established structural epoxy adhesive. Consultations were made with Huntsman (UK) Ltd for recommendation of their most suitable structural adhesive for this study. This adhesive was also studied extensively in research conducted at the Glasgow Marine Technology Centre [82, 94].

Surface preparation of the affected surfaces is a key to the durability of the joint. However, it may affect short term strength of a bond. The primary guideline was to use a standard surface preparation to commensurate with the proposed use of the adhesive bond. The surface preparation carried out in this study consists of a combination of simple grit-blast and degreasing technique. Since a standard surface preparation was adopted for all specimens, it is important to note that the surface preparation did not influence the different behaviour of the specimens under loading.

The adhesive Araldite® AV119 has a good gap filling capabilities for the quality of the bond which for up to 1 mm adhesive thickness. The T and flat bonded models were wedged open for inspection in order to evaluate the quality of the bond. According to Fig. 7.2 and 7.3, the bond area of the beam seems voids-free. However, the presences of voids in the adhesive layer were unavoidable in the fabrication of adhesive bonded joints in this research. Figure 7.3 shows a visible bond defect resulting from incomplete gap filling resulting from inadequate clamping of the flat beam specimen. Such defects could be removed by using a vacuum oven curing procedure where the voids are extracted by adjusting the pressure in the oven. However, joints fabricated under such conditions will require a gap fill of 2-3 mm and the joint may need to be sealed in order to prevent the loss of adhesive due to the

suction effect. However, the author feels that the presence of such defects did not affect the beam's behaviour. The presence of defects was discussed in detail in Section 7.6. In reality such a procedure will normally be difficult to implement in the fabrication of a large joint like a stiffened panel. For a first time user of the adhesive for a major structural application, one would consider complementing the adhesive joints with other joining methods to consider a fail safe design. In addition to the psychological barriers, the problems of impact and fire risk may dictate such a decision. A feasibility study [115] carried out by a steel fabricator/manufacturing company examined the possibility of using the manual arc welding process in conjunction with the bonded joint (both ends of a 1 m long beam were fillet welding at an L stiffener to an 8mm plate attachment without significant damage to the bonded joint. The heat affected adhesive areas were only charred locally due to the intensity of the heat from welding and did not spread further because of the poor thermal conductivity of the adhesive and large heat capacity of the bonded steel beam.

Proper clamping was essential to ensure adequate contact pressure along the adhesive joint. The test specimens were subjected to clamp pressure through the use of small G-clamps and dead weights. For thickness control of the adhesive, a bonding jig was fabricated to control the relative positioning of the upper and lower adherends and also to avoid disturbances during the curing process. In terms of the varying adhesive thickness in certain models, the L and T section beam were found difficult to work with due to lack of adequate contact area found on the upper adherend. Rework in terms of debonding was necessary in order to preserve the fabricated specimens and to obtain a thickness within tolerance. The specimens with the flat beam section however, proved easier to control due to their bond area and adequate contact area for clamping, hence less handling time was needed.

Clamping of real joints in shipbuilding to fabricate a panel would require more sophisticated equipment such as a hydraulic press or the use of magnetic clamps for steel adherends. It is important to note that when we use such equipment, the amount of clamping pressure must be controlled in order to fabricate the joint. The issue of using excessive and minimal force by itself will determine the strength of the bond. Sufficient pressure is necessary for squeezing excessive adhesive to reach the desired thickness. Curing of the joints was carried out in a hot air oven at 160° C for a

minimum period of 30 minutes. It is obvious that the adhesive within the specimens will not reach curing temperature as rapidly as the temperature in the oven or the steel specimens. It was essential, therefore, to monitor the temperature at the glue line itself with a thermocouple when timing the curing cycle. For such joints to be cured in the industry, using heating elements similar to the kind used in post-weld treatment could be used into the fabrication process. Such curing methodologies are versatile as compared to others and are not limited by the size and configuration of the joint. Another curing method such as induction heating could be considered for its strength to reach the cure temperature within the adhesive layer quickly. Adhesives have been formulated which lend themselves to this curing method and provide fixturing strength in a short period of time.

APPENDIX B

THEORETICAL WORK – BEAM THEORIES

Thus, the following bending stress, shear stress and deflection are used for the bonded beam sections;

$$\sigma_b = \frac{M * z * E_s}{D}$$

$$\tau_{\max} = \frac{0.5 * F * E_s * h * A_s}{D * b}$$

$$\delta_b = \frac{F * L^3}{48 * D} + \frac{\tau_{nax} * c * L}{G_a * d * 2}$$

The resulting strains and stresses in a beam are directly related to the curvature of the deflection curve. To illustrate the concept of curvature, consider a beam subjected to a load P acting in the middle of the span as shown in Figure B.1. For purposes of analysis, two points n and q are identified on the deflection curve. At each of these points we draw a line normal to the tangent to the deflection curve. Both normals intersect at point O', which is the centre of curvature of the deflection curve. The distance nO' from the curve to the centre of curvature is called the radius of curvature ρ and the curvature κ which is defined as the reciprocal of the radius of curvature. Thus

$$\kappa = \frac{1}{\rho} \qquad \text{(B.1)}$$

The curvature is a measure of how sharply a beam is bent. The curvature and the radius of curvature are functions of the distance x measured along the x axis. It follows that the position O' of the centre of curvature also depends upon the distance x. The curvature at a particular point on the axis of the beam depends upon the properties of the beam itself which is made up of the cross sectional shape and the type of material used. Therefore, if the beam is prismatic and the material is homogenous, the curvature will vary only with the bending moment. Consequently, a

beam in pure bending will have constant curvature and the beam in nonuniform bending will have varying curvature.

The longitudinal strains in a beam can be found by analysing the curvature of the beam and the associated deformations. Consider a portion *AB* of a beam in pure bending subjected to positive bending moments *M* as shown in Figure B.1. The cross sections of the beam, such as sections *mn* and *pq* in the figure, remain plane and normal to the longitudinal axis. The initial distance *dx* between the two planes is unchanged at the neutral surface hence $\rho\, d\theta = dx$. However, all other longitudinal lines between the two planes either lengthen or shorten, thereby creating normal strains ε_x. To evaluate the normal strains, consider a typical longitudinal line *ef* located within the beam between planes *mn* and *pq* where line *ef* is identified by its distance *y* from the neutral surface. Thus, the length *L* of line *ef* after bending takes place is

$$L = (\rho - y)\,d\theta = dx - \frac{y}{\rho}dx \tag{B.2}$$

in which we have substituted $d\theta = dx/\rho$. Since the original length of line ef is *dx*, it follows that its elongation is $L - dx$ or $-ydx/\rho$. The corresponding longitudinal strain is equal to the elongation divided by the initial length dx; therefore the strain curvature relation is defined as

$$\varepsilon_x = -\frac{y}{\rho} = -\kappa y \tag{B.3}$$

Bending stresses in beams

In deriving the relations for the normal bending stresses and deflections in beams, we normally make the following idealisations:

1. We assume that the beam has an axial plane of symmetry and the load act in this plane. Then, from considerations of symmetry, we conclude that bending must also occur in this same plane. In most practical cases this condition of symmetry is fulfilled since the usual cross-sectional shapes of beams, such as L-section, Z-section, rectangular, I-section, or T-section are symmetrical.

2. The beam is subjected to pure bending; this means that the shear force is zero, and that no torsion or axial loads are present
3. The material of the adherend is isotropic and homogeneous.
4. Plane sections originally normal to the longitudinal axis of the beam remain plane and normal to the deformed longitudinal axis upon bending.
5. The proportions of the beam are such that it would fail by bending rather than by crushing, wrinkling, or sidewise buckling.

The most common stress-strain relationship encountered in engineering is the equation for a linearly elastic material. For such materials we substitute Hooke's law for uniaxial stress ($\sigma = E\varepsilon$) into Eq. B.3 (above) and obtain

$$\sigma_x = E\varepsilon_x = -\frac{Ey}{\rho} = -E\kappa y \tag{B.4}$$

One of the objectives in designing a beam is to use the material as efficiently as possible within the constraints imposed by function appearance, manufacturing cost and so on. From the standpoint of strength alone, efficiency in bending depends primarily upon the shape of the cross section. In particular, the most efficient beam is one in which the material is located as far as practical from the neutral axis. The farther a given amount of material is from the neutral axis, the larger the section modulus becomes. This results in a larger the bending moment being resisted for a given allowable stress. To obtain the neutral axis from the first equation of statics, consider an element of area dA in the cross section of the Z section beam shown in Figure. B.2. The element is located at distance y from the neutral axis. The force acting on the element is equal to $\sigma_x\, dA$ and is compressive when y is positive. The first equation of statics states,

$$\int_A \sigma_x \, dA = -\int_A E\kappa y \, dA = 0 \tag{B.5}$$

eliminating the nonzero constants, curvature κ and modulus of elasticity E,

$$\int_A y \, dA = 0 \tag{B.6}$$

The first equation of statics state that the first moment of area of the cross section, evaluated with respect to the z axis, is zero. In other words, the z axis must pass through the centroid of the cross section. The neutral axis passes through the centroid of the cross-sectional area when the material follows Hooke's law and there is no axial force acting on the cross section. The assumption makes it relatively simple to determine the position of the neutral axis.

Using the location of the neutral axis with the moment-curvature relationship, we can determine the stress in terms of bending moment in the flexure formula equation. The flexure formula shows that the stresses are directly proportional to the bending moment M and inversely proportional to the moment of inertia I of the cross section.

$$\sigma_x = -\frac{My}{I} \tag{B.7}$$

The stresses vary linearly with the distance y from the neutral axis, as observed from Figure. B.3. If the bending moment in the beam is positive, the bending stresses will be positive (tension) over the part of the cross section where y is negative, that is, over the lower part of the beam. The stresses in the upper part of the beam will be negative (compression). The maximum tensile and compressive bending stresses acting at any give cross section occur at points located farthest from the neutral axis. Consideration of the stress distribution along the depth of the cross section leads to the conclusion that for economical design most of the material of the beam should be put as far as possible from the neutral axis. The distance from the neutral axis to the extreme elements in the positive and negative y directions are represented by c_1 and c_2. This is illustrated from Figure. B.4 which shows the relationship between the bending moments and associated normal stresses. The maximum normal stresses σ_1 and σ_2 from the flexure formula are

$$\sigma_1 = -\frac{Mc_1}{I} = -\frac{M}{S_1} \qquad \sigma_2 = -\frac{Mc_2}{I} = -\frac{M}{S_2} \tag{B.8}$$

in which

$$S_1 = \frac{I}{c_1} \qquad S_2 = \frac{I}{c_2} \tag{B.9}$$

where the quantities S_1 and S_2 are known as the section moduli of the cross sectional area.

The section modulus is normally calculated when designing a beam to resist bending stresses. If the beam has a doubly symmetric cross section and the allowable stresses are the same for both tension and compression, we can calculate the required modulus by dividing the maximum bending moment by the allowable bending stress for the material.

$$S = \frac{M_{max}}{\sigma_{allow}} \tag{B.10}$$

The allowable stress is based upon the properties of the material and the desired factor of safety. To ensure that this stress is not exceeded, we must choose a beam that provides a section modulus at least as large as that obtained from the above equation. To minimise weight and save material, we usually select a beam that has the least cross-sectional area while still providing the required section moduli.

The analysis presented in this section was for the pure bending of prismatic beams composed of homogenous, linearly elastic materials. Should a beam be subjected to nonuniform bending, the shear forces will normally produce warping or out-of-plane distortion of the cross sections. Thus, a cross section that was plane before bending is no longer plane after bending. Warping due to shear deformations greatly complicates the behaviour of the beam. However, detailed investigations show that the normal stresses calculated from the flexure formulae are not significantly altered by the presence of shear stresses and the associated warping [112]. Thus we may justifiably use the theory of pure bending for calculating normal stresses in beams subjected to nonuniform bending as well.

The flexural formula gives results that are accurate only in regions of the beams where the stress distribution is not disrupted by changes in the shape of the beam or by discontinuities in loading. For instance, the flexure formula is not applicable near the supports of the beam or close to a concentrated load. Such irregularities produced localized stresses, or stress concentrations, that are much greater than the stresses obtained from the flexure formula.

Effect of shear stresses

When a beam is in pure bending, the only stress resultants are the bending moments and the only stresses are the normal stresses acting on the cross sections. However, most beams are subjected to loads that produce both bending moments and shear forces (nonuniform bending). In such cases, normal and shear stresses are developed in the beam. The normal stresses are calculated from the flexure formula provided the beam is constructed of a linearly elastic material. The shear stresses will be discussed in detail in the following section.

The rectangular cross section beam shown in Figure. B.5 is subjected to a positive shear force V. It is assumed that the shear stresses τ acting on the cross section are parallel to the shear force, which is parallel to the vertical sides of the cross section. It is also reasonable to assume that the shear stresses are uniformly distributed across the width of the beam, although they may vary over the height. Using these two assumptions, it was possible to determine the shear stress at any point on the cross section.

This section focuses on evaluating the horizontal shear stresses rather than the vertical stresses in a beam. Horizontal shear stresses are easier to determine and also have the same magnitudes as the vertical shear stresses. The existence of horizontal shear stresses in a beam is shown in the bending of two separate beams in Figure. B 6(a). The two identical rectangular beams are placed together on simple supports and loaded by a force P. Since the friction between the beams are small, the beams will bend independently. Each beam will be in compression above its own neutral axis and in tension below its neutral axis, and therefore the bottom surface of the upper beam will slide with respect to the top surface of the lower beam. Bonding the two beams along the contact surface will result in a single solid beam. When loaded, the horizontal shear stresses will develop along the glue surface in order to prevent the sliding found in B.6(b). Because of the presence of these shear stresses, the single beam is much stiffer and stronger than the two separate beams.

Consider the rectangular section beam undergoing nonuniform bending shown in Figure. B.7. Taking two adjacent cross sections with distance dx apart, and consider the element mm_1n_1n. Isolating a subelement mm_1p_1p by passing a horizontal plane pp_1

through element mm_1n_1n, where the subelement is shown separately in Figure. 4.7c. Since the subelement is in equilibrium, we can sum the forces in the x direction and obtain;

$$F_3 = F_2 - F_1$$

$$F_3 = \int \frac{(M + dM)y}{I} dA - \int \frac{My}{I} dA = \frac{dM}{I} \int y dA \tag{B.11}$$

If the shear stresses τ are uniformly distributed across the width b of the beam, the force F_3 is also equal to the following:

$$F_3 = \tau b\, dx \tag{B.12}$$

where $b\ dx$ is the area of the bottom face of the subelement. Combining Eq. 4.12 and 4.13 and solving for the shear stress τ, we get

$$\tau = \frac{V}{Ib} \int y dA \tag{B.13}$$

where

$$Q = \int y dA \tag{B.14}$$

The integral in Eq. B.14 is evaluated over the shaded part of the cross section shown in Figure. B.7(d) is the first moment Q of the shaded area with respect to the neutral axis. With this notation, the equation for the shear stress become,

$$\tau = \int \frac{VQ}{Ib} \tag{B.15}$$

This above equation, known as the shear formula, can be used to determine the shear stress τ at any point in the cross section of a rectangular beam. Note that for a specific cross section, the shear force V, moment of inertia I, and width b are constants. However, the first moment Q varies with the distance y_1 from the neutral axis.

The elementary shear theory presented in this section is suitable for determining the vertical or horizontal shear stresses in the web of a wide flange beams. Figure. B.8

shows the shear stress distribution of the various beam sections considered in this study. However, when investigating vertical shear stresses in the flanges, we can no longer assume that the shear stresses are constant across the width of the section, which is across the width *b* of the flanges. The distribution of the shear stresses at the junction of the web and the flange is quite difficult and cannot be investigated with elementary methods.

THEORETICAL WORK – MATERIAL PROPERTIES

The mechanical properties that are essential and obtained from the series of experiments were as follows;

- Elastic modulus, E
- Poisson Ratio, ν
- Secant modulus, E_s
- Tangent modulus, E_t

Along with the measurement of stresses and displacement, tensile force was measured from the tensile testing machine and recorded simultaneously into the data logger. The force was measured in terms of voltage supplied by the machine, represented the total tensile force subjected across the flat beam cross section of the test specimens. The axial strain measurements were obtained through the use of biaxial rosette strain gauges. The modulus of elasticity in tension stated as the ratio of the stress difference σ_2 minus σ_1 to the corresponding measured strain difference values ε_2 minus ε_1 is shown in Figure. 3.6. The calculation of the modulus of elasticity is shown below,

$$E_t = \frac{\sigma_2 - \sigma_1}{\varepsilon_2 - \varepsilon_1}$$

where

E_t is Young's modulus of elasticity, expressed in megapascals

σ_1 is the stress, in megapascals, measured at the strain value ε_2=0,0005;

σ_2 is the stress, in megapascals, measured at the strain value ε_2=0,0025;

As tabulated in Chapter 3 Table 3.2, the average elastic modulus obtained from the experimentation on the eight test pieces for the AV119 adhesive material was 3.624 GPa. According to the manufacturer Ciba Speciality Chemicals (UK), the modulus of elasticity was given as 3.5 GPa for the AV119 material. Similarly, material properties used in FE analyses carried out by different authors indicated that the modulus was likely be within the range of 3 - 3.5 GPa [109,110]. The elastic modulus varies in accordance to the specified curing temperatures and schedules. The average elastic modulus obtained for the 10 adherend mild steel test pieces from experiments was 205 GPa. This was similar to the elastic modulus for 080M15 mild steel material as stated by MatWeb [108].

The Poisson's ratio was taken from measuring the tensile strain ε_n in one of the two axes normal to the direction of pull, to the corresponding strain ε in the direction of pull within the initial linear portion of the longitudinal versus normal strain curve as shown in Figure. 3.7. Measurements for the Poisson's ratio were made while the materials were within the elastic region. The principle strains were measured using a biaxial rosette pattern strain gauge developed by Vishay Measurements (UK). The pattern has two measuring grids perpendicular to one another as shown in Figure. 3.8. Two independent measurements could be made in perpendicular directions about a single point, which is the centre of the dumbbell shaped test specimen in this case. Calculation of the Poisson's ratio is defined as follows;

$$\mu_n = -\frac{\varepsilon_n}{\varepsilon}$$

where

μ_n is the Poisson's ratio, expressed as a dimensionless ratio with n = b (width) indicating the normal direction chosen.

ε is the strain in the longitudinal direction.

ε_n is the strain in the normal direction, with n = b (width).

As shown on Figure. 3.15, the mean poisson ratio obtained from the experiments for the adhesive material is 0.36. According to the manufacturer, the mean poisson ratio suggested under the specified curing conditions should be 0.37. With this in mind, it should also be noted that similar testing was carried by various author indicate that the

Poisson ratio fall in the range of 0.34 – 0.38 [109,110], depending on their corresponding curing conditions. The average Poisson ratio obtained for the adherend material from experimental results was 0.23. However, the results were much lower than values specified by the material database MatWeb, which indicated that the Poisson's ratio should be 0.29.

The derivation of the tangent and secant moduli can be estimated from the true inelastic stress-strain curves obtained from both the adhesive and adherend materials. The theoretical work shown was obtained from the ESDU 89052, which also includes a program which is useful in the prediction of the structural element's behaviour over its full inelastic range up to failure.

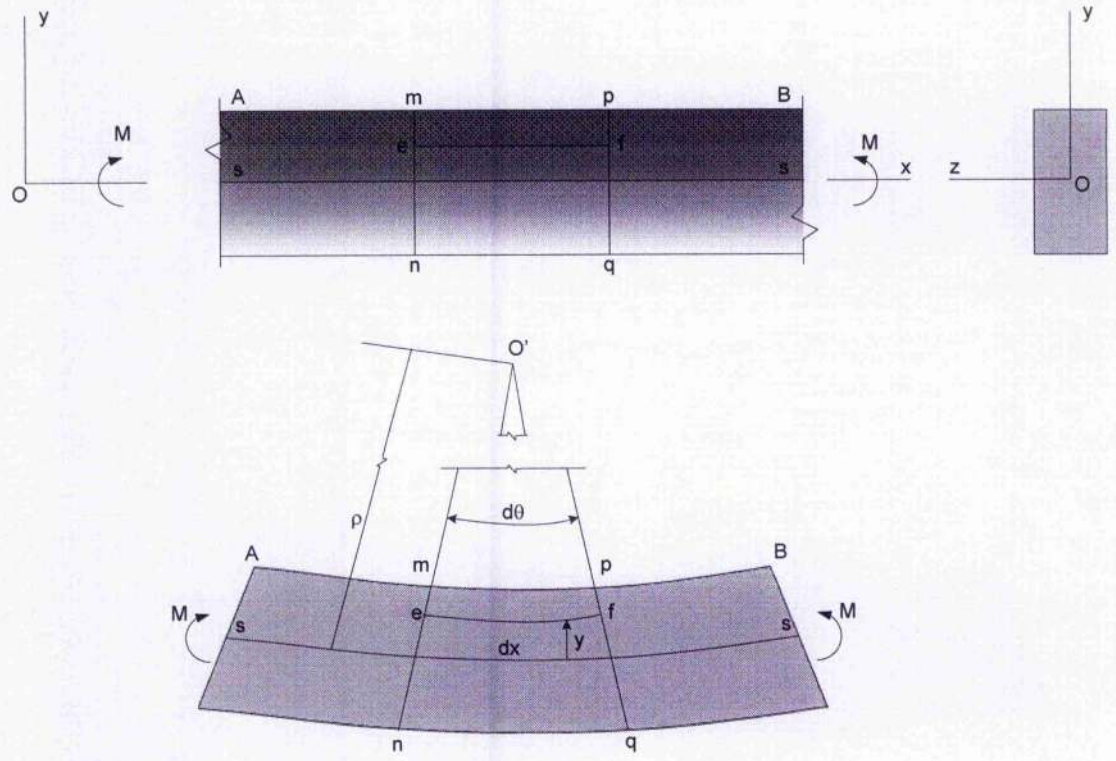

Figure B.1. Curvature of a bent beam

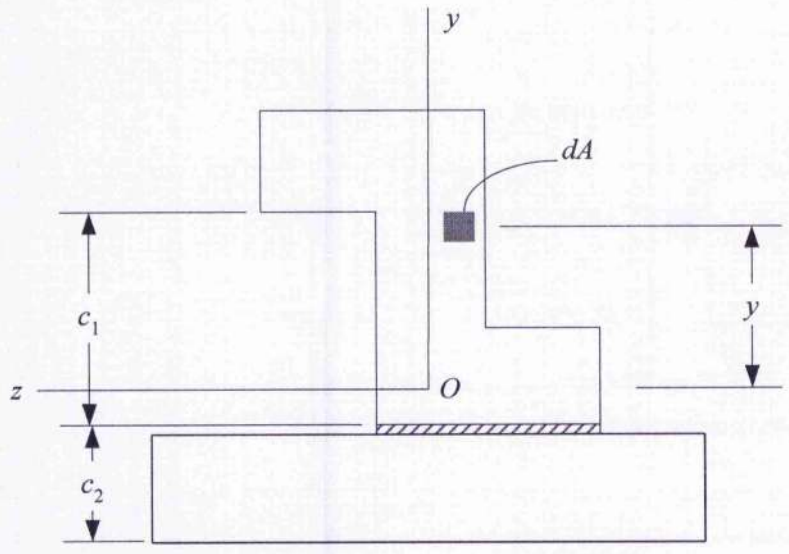

Figure B.2. Cross section of beam showing the z axis as the neutral axis of the cross section.

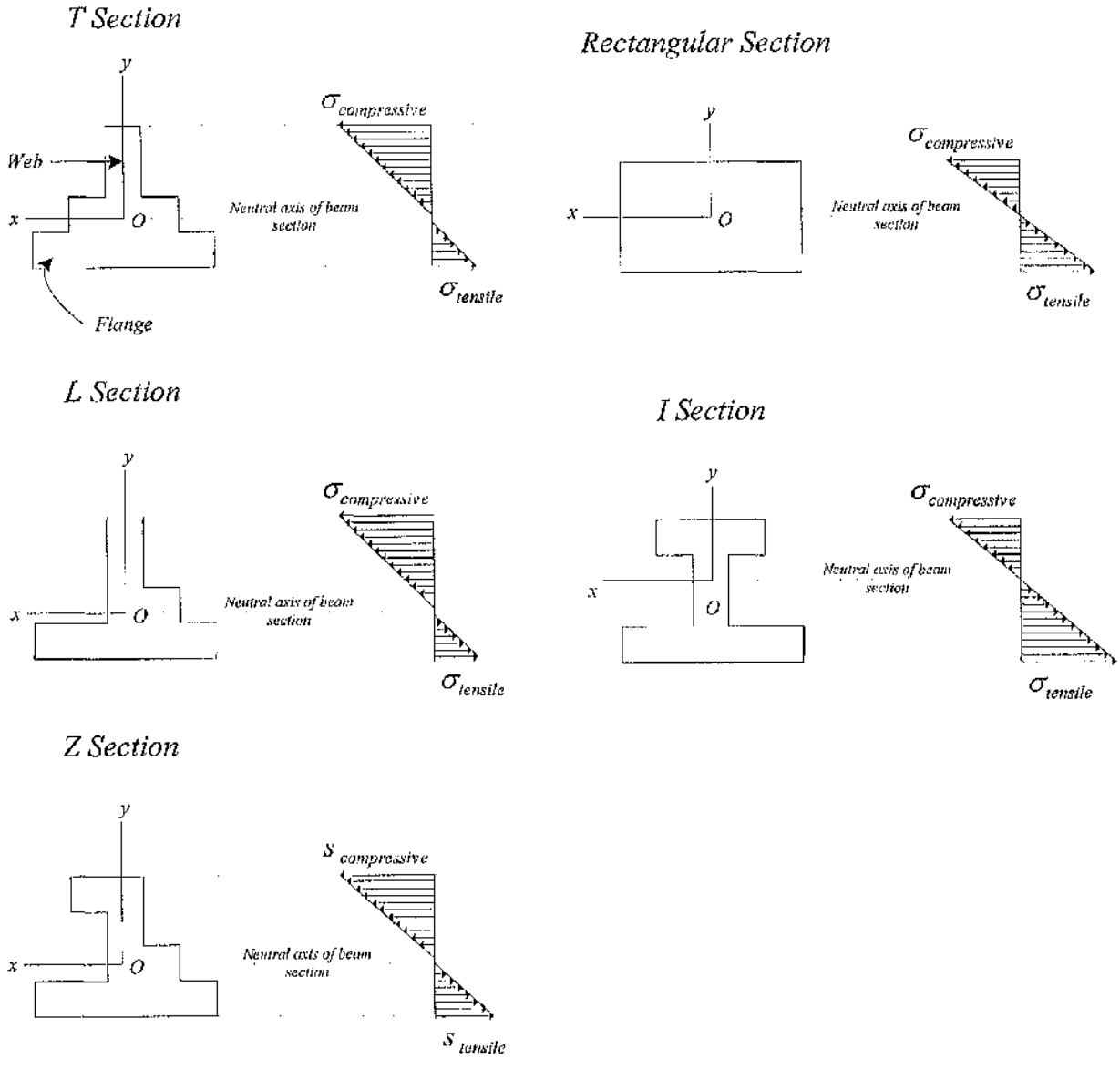

Figure B.3. Bending stress distribution of the various beam cross section.

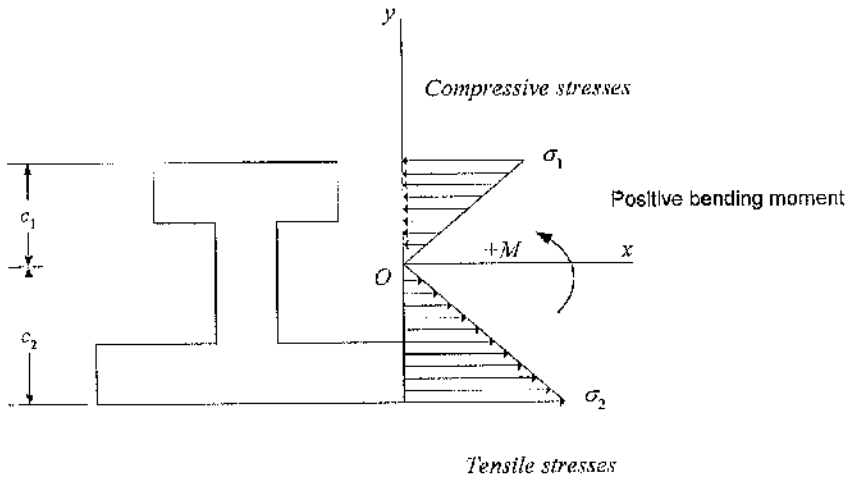

Figure B.4. Relationship between signs of bending moments and direction of normal stresses.

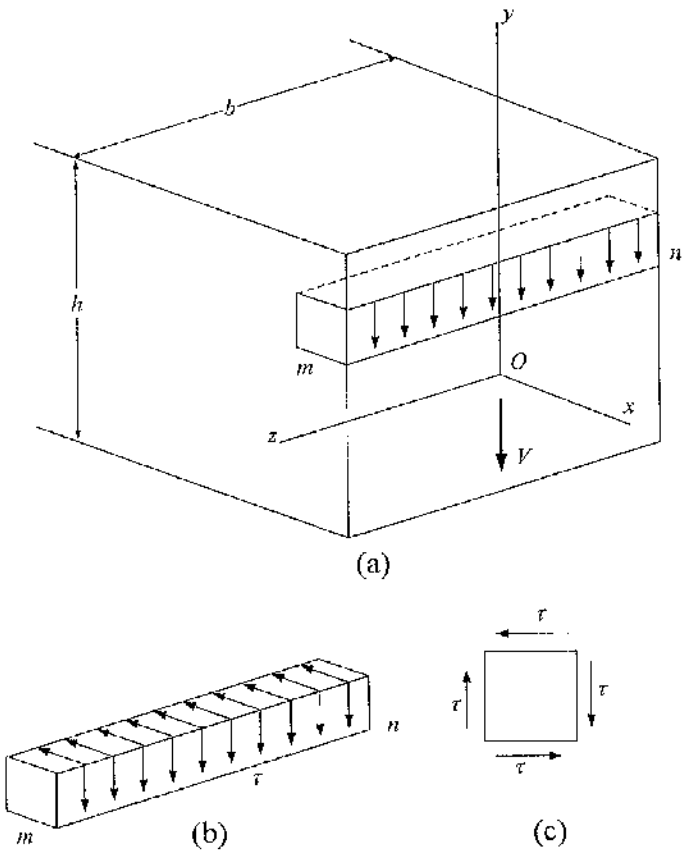

Figure B.5. Shear stresses in a beam of rectangular cross section.

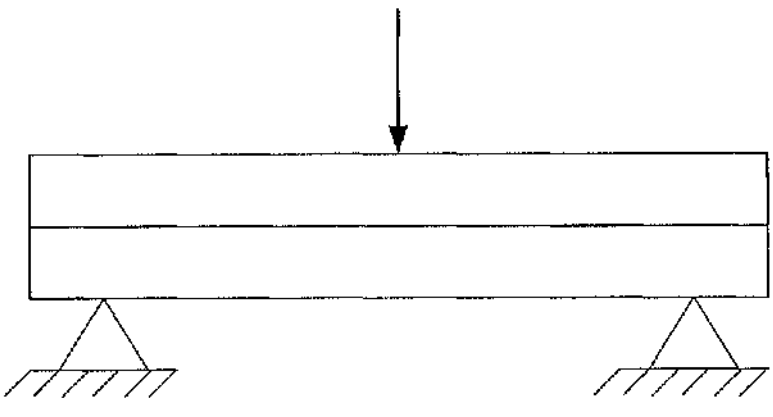

(a)

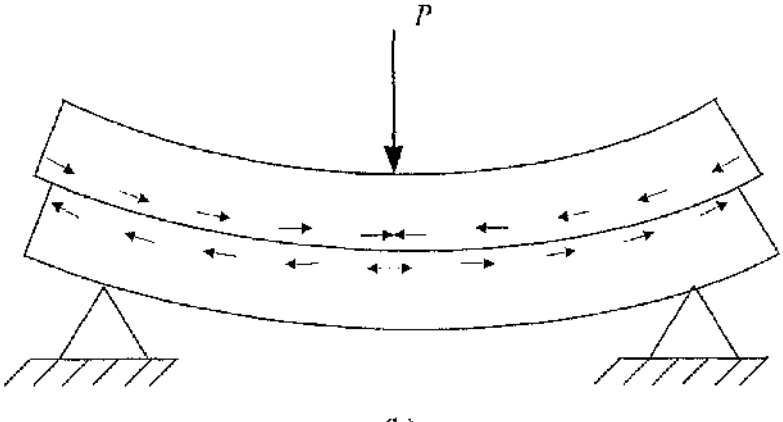

(b)

Figure B.6. Bending of two separate beams.

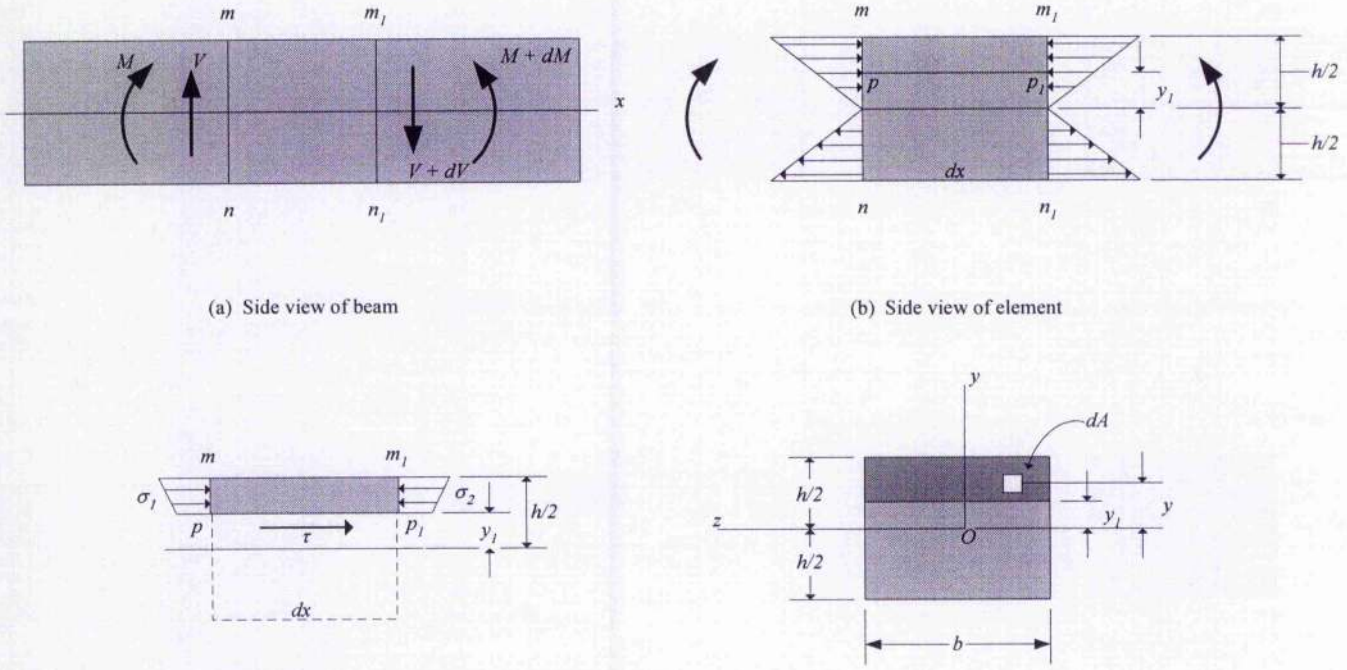

(a) Side view of beam

(b) Side view of element

(c) Side view of subelement

(d) Cross section of beam at subelement

Figure B.7. Shear stresses in a beam of rectangular cross section.

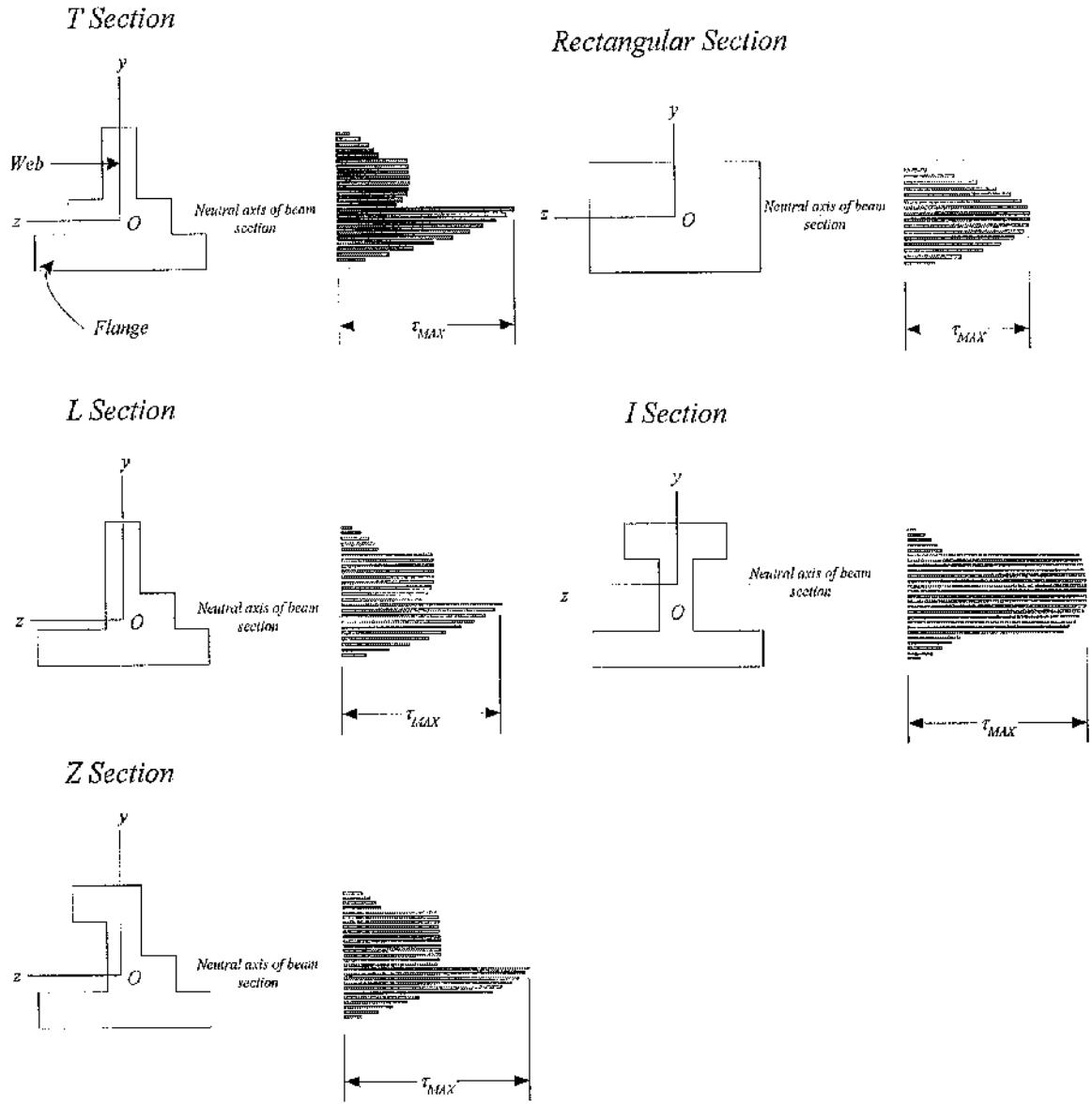

Figure B.8. Shear stresses in a rectangular beam section.

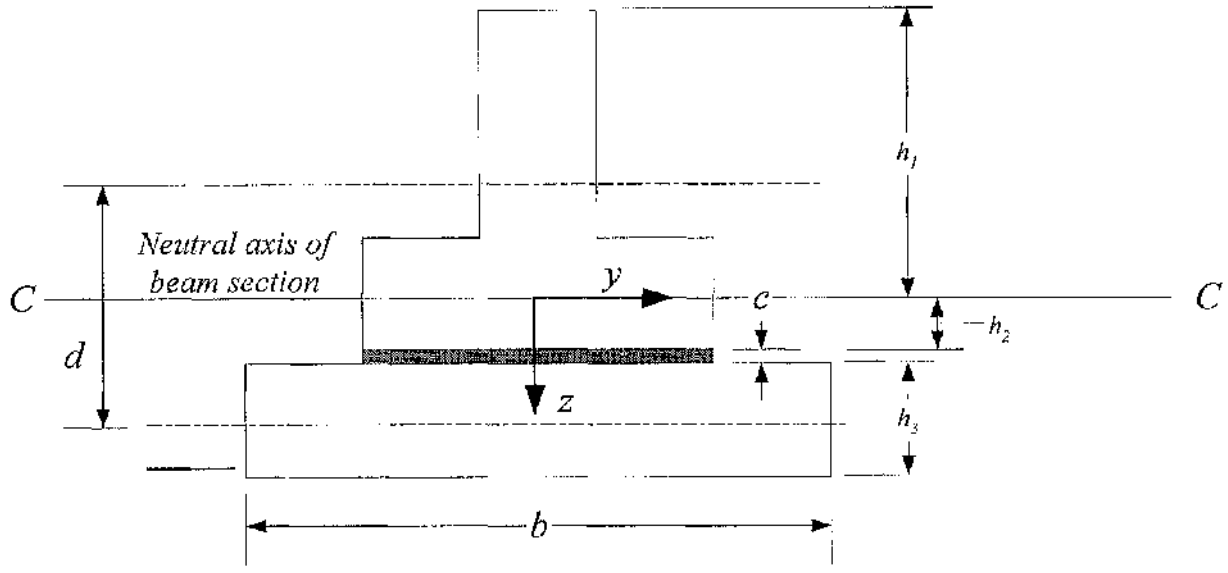

Figure B.9. Details of a T bonded/sandwich section

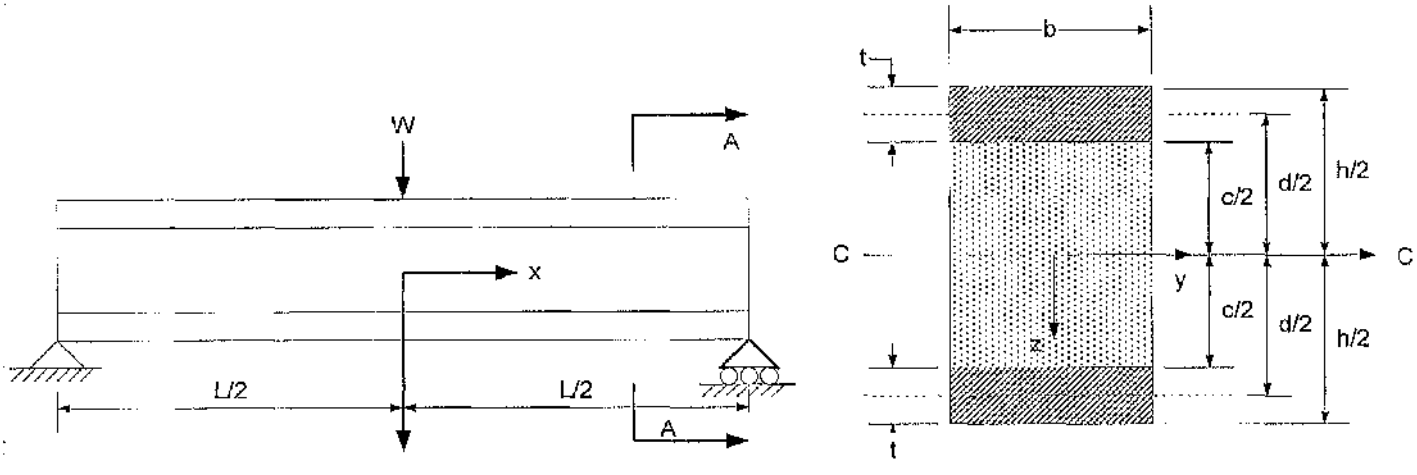

Figure B.10. Schematic of a typical sandwich beam

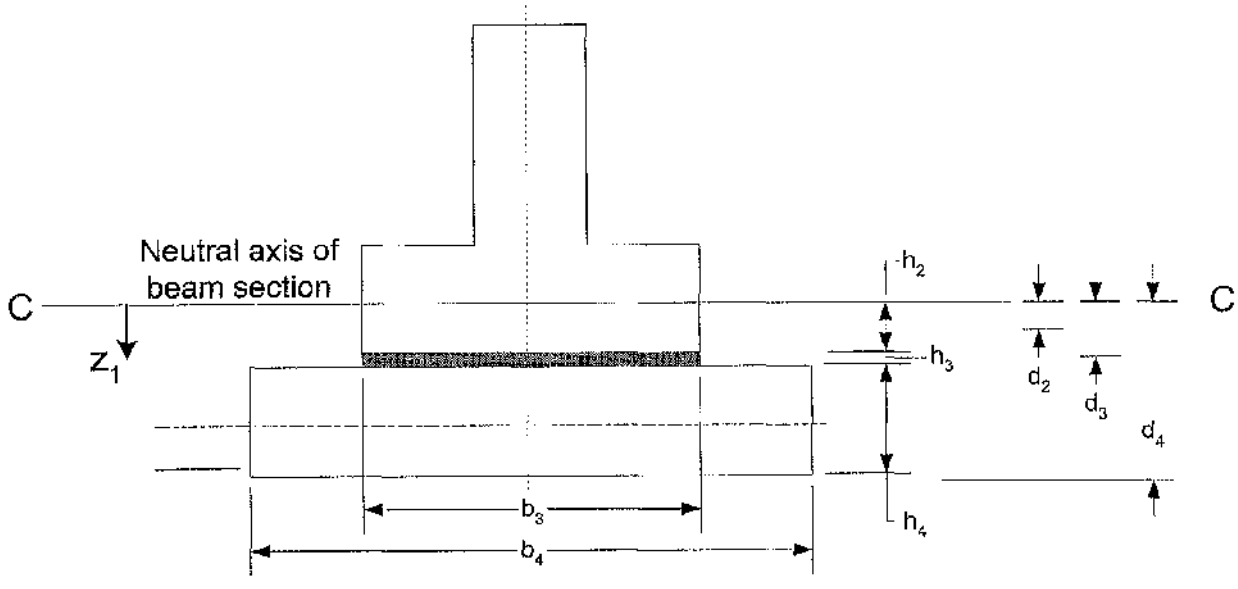

Figure B.11. Shear stress distribution and 2D schematic of the homogenous T section beam.

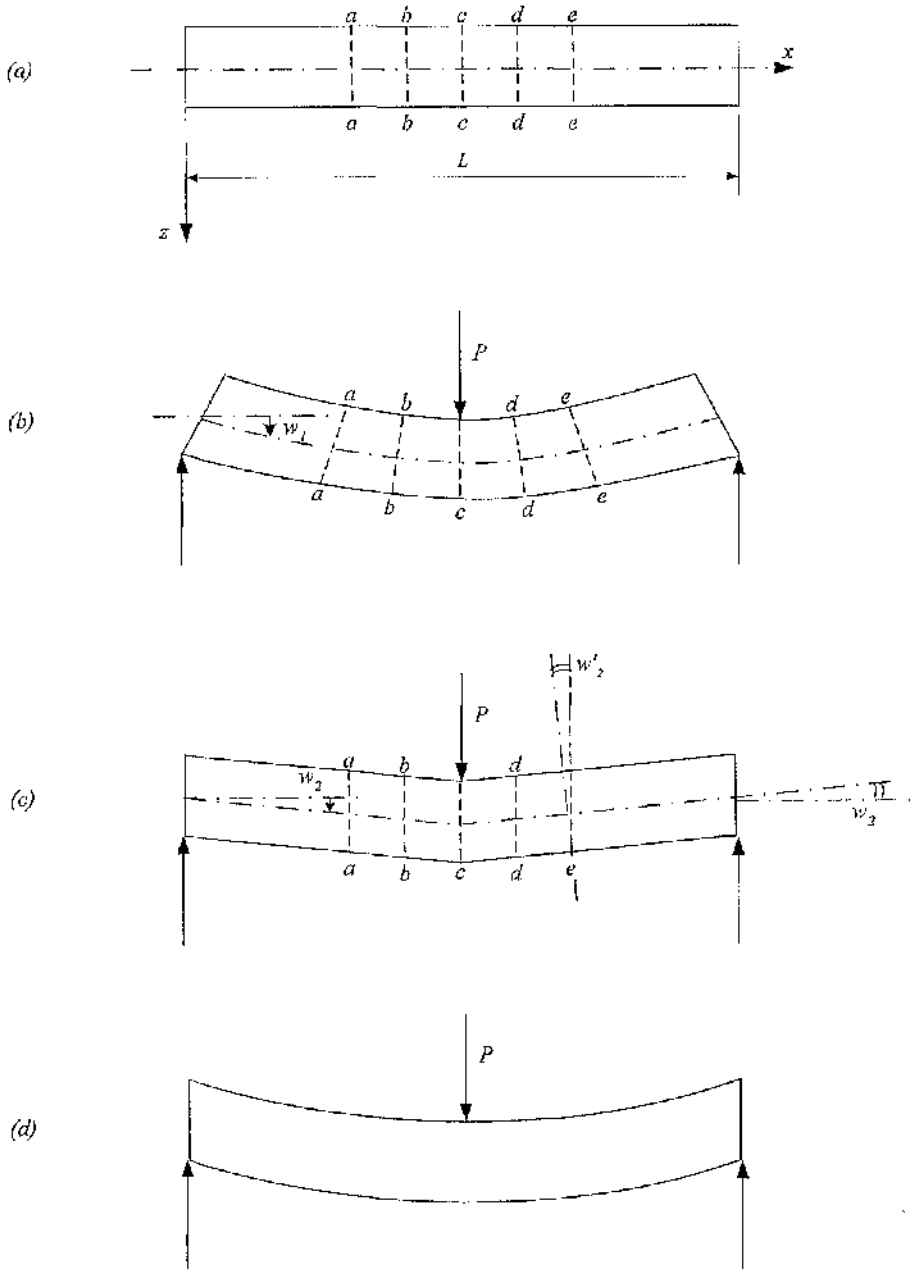

Figure B.12. Deflections of a sandwich beam under bending moment only (b) and under heavy shear forces only (c) and (d), In (c) the local stiffness of the faces are ignored, and in (d) they are taken into account. Curvature of the beam under the load has an infinite value in (c) while in (d) the value is finite. Diagram adopted from Allen [13]

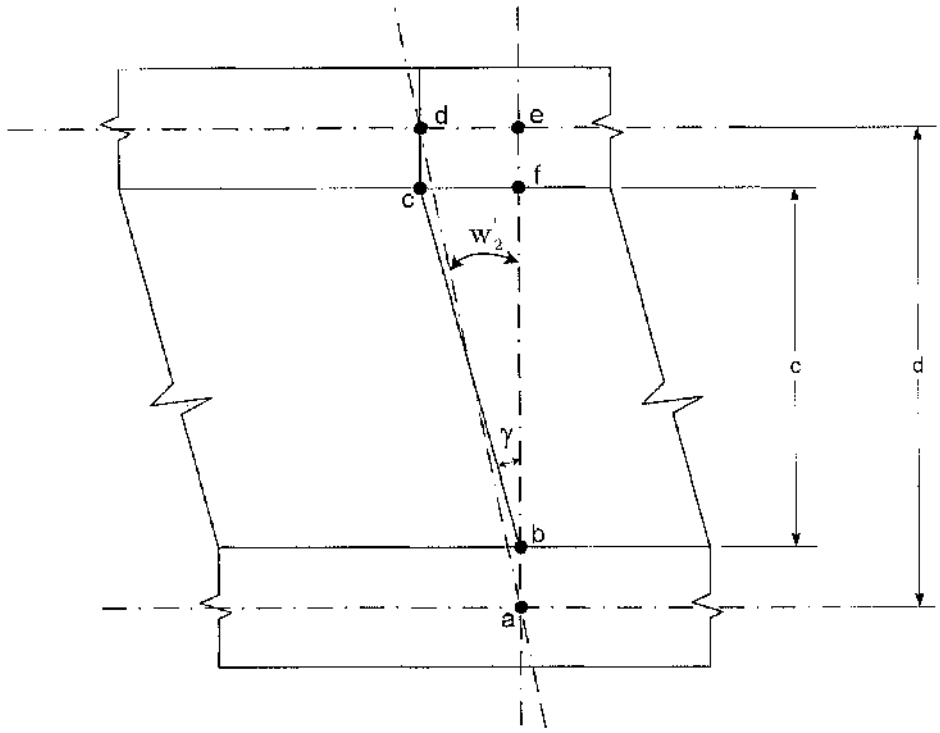

Figure B.13. Shear deformation of a beam with thick face